

**Investigation of organometallic complexes and their
application in catalysis, biological activities and crystal
engineering**

Ph.D. Thesis

by

Ajeet Singh



**DISCIPLINE OF CHEMISTRY
INDIAN INSTITUTE OF TECHNOLOGY INDORE
OCTOBER 2018**

**Investigation of organometallic complexes and their
application in catalysis, biological activities and crystal
engineering**

A THESIS

*submitted in the partial fulfillment of the
requirement for the award of the degree
of*

DOCTOR OF PHILOSOPHY

by

Ajeet Singh



**DISCIPLINE OF CHEMISTRY
INDIAN INSTITUTE OF TECHNOLOGY INDORE
OCTOBER 2018**



INDIAN INSTITUTE OF TECHNOLOGY INDORE

CANDIDATE'S DECLARATION

I hereby certify that the work which is being presented in the thesis entitled “**Investigation of organometallic complexes and their applications in catalysis, biological activities and crystal engineering**” in the partial fulfillment of the requirements for the award of the degree of **DOCTOR OF PHILOSOPHY** and submitted in the **DISCIPLINE OF CHEMISTRY, Indian Institute of Technology Indore**, is an authentic record of my own work carried out during the time period July 2013 to October 2018 under the supervision of **Prof. Pradeep Mathur** and **Dr. Shaikh M. Mobin**, Discipline of Chemistry.

The matter presented in this thesis has not been submitted by me for the award of any other degree of this or any other institute.

(Ajeet Singh)

This is to certify that the above statement made by the candidate is correct to the best of my/our knowledge.

(Prof. Pradeep Mathur)

(Dr. Shaikh M. Mobin)

AJEET SINGH has successfully given his/her Ph.D. Oral Examination held on **February 14, 2019**.

Signature of Chairperson (OEB)
Date:

Signature of External Examiner
Date:

Signature(s) of Thesis Supervisor(s)
Date:

Signature of PSPC Member #1
Date:

Signature of PSPC Member #2
Date:

Signature of Convener, DPGC
Date:

Signature of Head of Discipline
Date:

ACKNOWLEDGEMENTS

I would like to express my heartily gratitude and thanks to my supervisors Prof. Pradeep Mathur and Dr. Shaikh M. Mobin for giving me the opportunity to work in the organometallic research area. Their supervision, advice and guidance from the very early stage made the completion of this task possible. I will always remain in debt to them for their motivation, support and ways to tackle the problems.

I would also like to extend thanks to Dr. Anjan Chakraborty, Dr. Sampak Samanta and Dr. Rajneesh Misra for their valuable suggestions at the times of need.

With great happiness, I would also like to express my respect to Prof. Pradeep Mathur (Director, Indian Institute of Technology Indore) for his endless encouragement and providing me, all the possible facilities at Indian Institute of Technology Indore.

I am grateful to Dr. Amrendra K Singh (Head, Discipline of Chemistry, Indian Institute Technology Indore) for his suggestions in various aspects. I am also grateful to Dr. Sanjay K Singh, Dr. Suman Mukhopadhyay, Dr. Dharendra K Rai, Dr. Tushar Kanti Mukherjee, Dr. Apurba K Das, Dr. Satya S. Bulusu, Dr. Chelvam Venkatesh, Dr. Tridib Kumar Sarma, and Dr. Biswarup Pathak for their help during various activities.

I extend my profound thanks to my group members, Dr. Anoop Kumar Saini, Dr. Veenu Mishra, Dr. Akbar Mohammad, Dr. Sanjay K. Verma, Dr. Sandip Kumar Singh, Dr. Archana Chaudhary, Dr. Prakash Chandra, Mr. Pranav Tiwari, Mr. Vinay Sharma, Mr. Mohit Saraf, Ms. Topi Ghosh, Ms. Shagufi N Ansari, Mr. Khursheed Ahmad, Mr. Kaushik Natarajan, Ms. Pratibha kumari and Mrs. Navpreet Kaur, and Mrs. Richa Rajak for their generous support, affection and co-operation to make my work successful.

It has been a magnificent experience to work with many seniors and friends together during my Ph.D.; I would also like to thank to Dr. Pradeep K. Jaiswal, Dr. Rajendar Nasani, Dr. Bhausahab Dhokale, Dr. Bhagwati Sharma, Dr. Anvita Srivastava, Dr. Anupam Das, Dr. Abhinav Raghuvanshi for their generous co-operation and help.

I am also thankful to all my friends who helped me directly or indirectly during my Ph. D.

I am thankful to Mr. Manish Kushwaha, Mr. Kinny Pandey, Mr. Ghanashyam A. Bhavsar, Ms. Sarita Batra, and for their technical and moral support.

I wish to express love from the bottom of my heart and respect to my loving father Mr. Kishanpal Singh and to my lovable mother Mrs. Madhu Devi for their unending love with full support, perennial encouragement and patience during this period.

Lastly, I would like to express my heartfelt regards to my sister Mrs. Manju Singh, and my younger brother Mr. Surjeet Singh for their care, affection and small fights.

Ajeet Singh

*Dedicated to my beloved
Parents*

Synopsis

OBJECTIVES

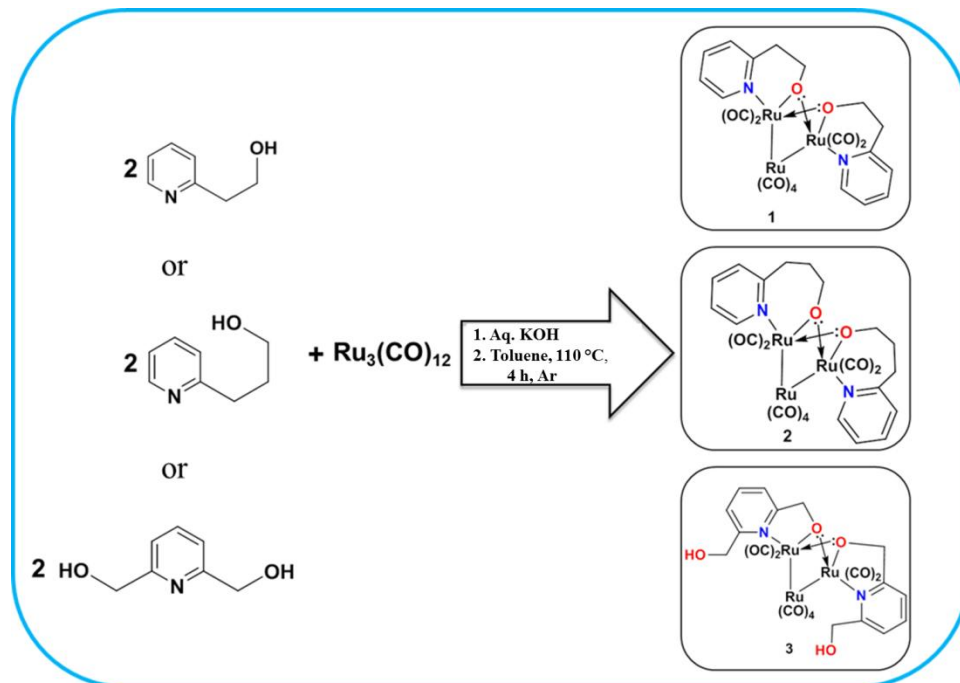
- ❖ Preparation of $\text{Ru}_3(\text{CO})_8$ -pyridine-alcohol cluster and its use for selective catalytic transformation of primary to secondary amines.
- ❖ Synthesis of tetranuclear $\text{Ru}_4(\text{CO})_8$ -substituted pyridine-methanol cluster and its use as a highly efficient electro-catalyst in water oxidation reaction.
- ❖ Synthesis of new $\text{Ru}_3(\text{CO})_8$ -picolinic-acid cluster for catalytic oxidation of alcohols to carboxylic acids in basic water medium.
- ❖ To prepare supra-molecular assemblies of triptycene – ferrocene and its derivatives and study their non-bonding interactions and packing features.
- ❖ To synthesize and examine ferrocene-substituted bis(ethynyl)-anthracene/ anthraquinone compounds for biological activities.

The thesis includes six chapters which begin with a general introduction (**Chapter 1**),

followed by catalytic properties of the newly synthesized $\text{Ru}_3(\text{CO})_{12}$ based clusters in the **Chapters 2, 3 and 4**. Furthermore, **Chapter 5** includes ferrocene anthracene/anthraquinone based complexes which are examined for their anticancer biological property. **Chapter 6** contains the report on co-crystals explored by the supra-molecular assembly of organometallic ferrocene and its derivatives with triptycene, followed by conclusions. **Chapter 7** highlights conclusions and scope for future work.

The introductory chapter (**Chapter 1**) of the thesis illustrates the brief literature of ruthenium-based catalyst, specific for N-alkylation and oxidation of alcohols to carboxylic acids, and water oxidation. We have included the background of the supramolecular chemistry of ferrocene and triptycene with different molecules. Furthermore, the background knowledge of ferrocene derivatives and anthracene/anthraquinone derivatives with their biological importance has also been discussed.

Chapter 2 mainly focuses on ruthenium-based pyridine alcohol clusters and their application for mono N-alkylation catalytic reaction of primary amines using primary alcohols to form secondary amines. After chelation effect observations,[1,2] the preparation of ruthenium-substituted pyridine-alcohols have been carried out by reacting different pyridine alcohols, i.e. 2-(2-hydroxyethyl)pyridine (hep-H), 2-(3-hydroxypropyl)pyridine (hpp-H) and 2,6-bis(hydroxymethyl)pyridine (bhmp-H₂) with Ru₃(CO)₁₂ in basic medium (**Scheme 1**). The prepared clusters **1–3** were confirmed by NMR, IR and authenticated by Single crystal x-ray diffraction (SCXRD) study.



Scheme 1. Schematic view of synthesis of **1–3**

The crystals of Clusters **1–3** were grown in dcm/toluene solvent system and confirmed by SCXRD (**Figure 1**).

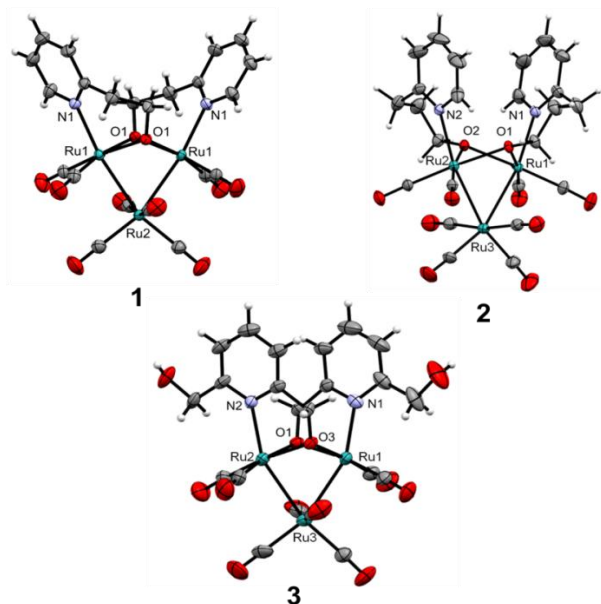
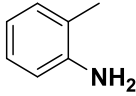
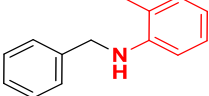
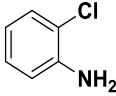
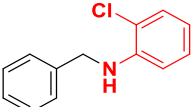
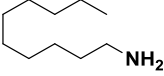
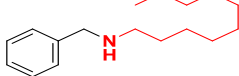
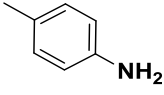
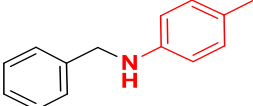
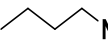
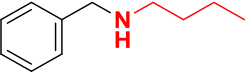
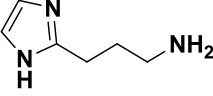
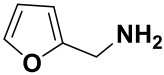
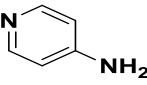
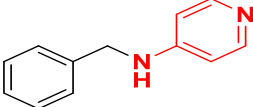
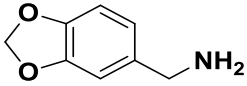
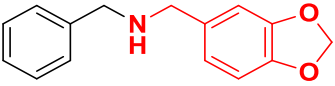


Figure 1. Perspective view of **1**, **2** and **3**

Cluster **1** was the most active catalyst for the N-alkylation reaction among **1–3**. All the catalytic reactions were performed using cluster **1** (**Table 1**).

Table 1. Direct formation of secondary amines from benzyl alcohol and various primary amines with cluster **1** as the catalyst

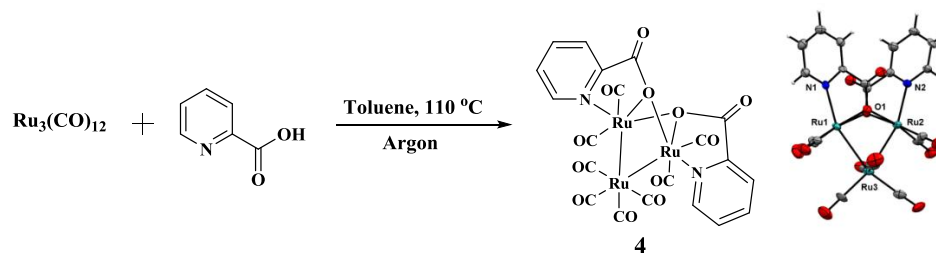
$\text{C}_6\text{H}_5\text{CH}_2\text{OH} + \text{R}_1\text{NH}_2 \xrightarrow[\text{4 \AA, mol. sieve}]{\text{Cat. 1 (0.5 mol\%), KO}^t\text{Bu (1 mmol), Toluene, 110 }^\circ\text{C, -H}_2\text{O}} \text{C}_6\text{H}_5\text{CH}_2\text{NHR}_1$				
Entry No.	RNH ₂	Conv.	C ₆ H ₅ CH ₂ NHR	GCM S Yield
1		100%		96%
2		52%		51%
3		64%		56%

4		44%		41%
5		65%		19%
6		72%		55%
7		48%		46%
8		22%		20%
9		--	-No reaction-	--
10		--	-No reaction-	--
11		73%		72%
12		>90 %		62%

Similarly, the reactions were also performed by varying the alcohol derivatives. The mono N-alkylation of primary amines with primary alcohols resulting into the selective production of secondary amines was achieved successfully using cluster **1** as a catalyst.

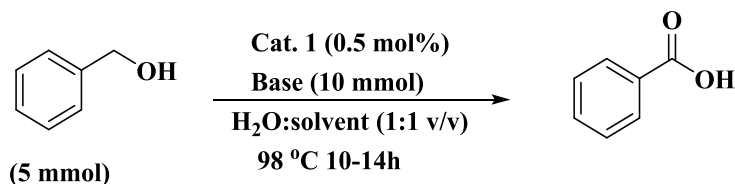
In **Chapter 3**, after the inspiration from ruthenium-substituted pyridine-alcohol clusters, synthesis of the ruthenium-substituted pyridine-carboxylic acid complexes was carried out (**Scheme 2**) by adding picolinic acid to $\text{Ru}_3(\text{CO})_{12}$ in toluene at 110 °C temperature for 4 h . The structure

of cluster **5** was also confirmed by SCXRD study. Cluster **4** is crystallized in *Pn* space group with monoclinic crystal system.



Scheme 2. Scheme for the preparation of **4** along with its crystal structure

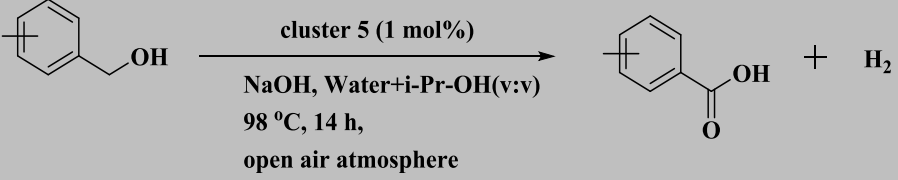
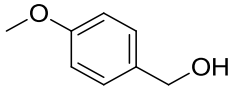
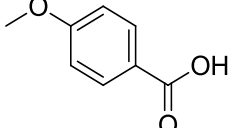
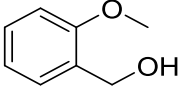
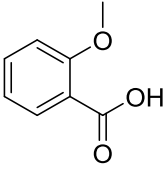
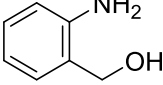
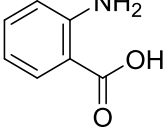
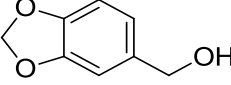
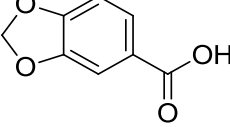
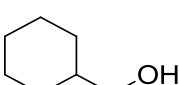
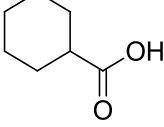
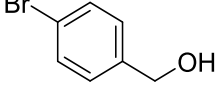
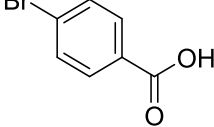
In situ, different pyridine carboxylic acid, picolinic acid, pyridine-2,6-dicarboxylic acid, iso-nicotinic acid and nicotinic acid with $\text{Ru}_3(\text{CO})_{12}$ are screened for the catalytic oxidation of alcohol to carboxylic acid using water and dioxane in the presence of NaOH.[3] Cluster **5** was found to be active and superior over other clusters. The general reaction conditions are shown in **Scheme 3**.



Scheme 3. Transformation of alcohol to carboxylic acid using cluster **4**

The cluster **4** shows selectively high yield (90%) in water and iso-propanol as the reaction medium. In the catalytic system, both water and oxygen (from the open atmosphere) are taking part in the oxidation of alcohol to carboxylic acid. Various catalytic oxidation reactions were performed to prove the activity of catalyst **4** (**Table 2**).

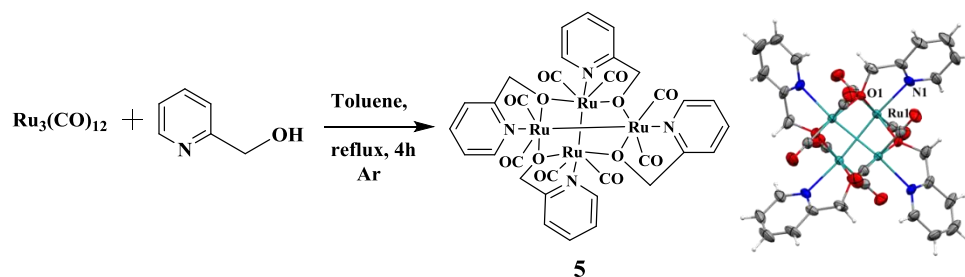
Table 2. Catalytic oxidation of various alcohols into their respective carboxylic acids using cluster **4** as the catalyst

				
Entry No.	Reactant	Product	Conversion (%)	Yield (%)
1			70	66
2			43	41
3			90	34
4			75	71
5			20	19
6			95	25

7			98	65
8			44	34
9			54	34

In short, this finding of cluster **4** may open a route to design new clusters for the transformation of alcohol to corresponding carboxylic acid derivatives

In **Chapter 4**, $\text{Ru}_4(\text{CO})_8$ -substituted pyridine-methanol complex $\text{Ru}_4(\text{CO})_8(\text{C}_5\text{H}_5\text{NCH}_2\text{O})_4$ (**5**) was synthesized by the reaction of pyridine methanol and $\text{Ru}_3(\text{CO})_{12}$ in toluene at 110 °C. After thorough characterization, the structure was also confirmed by SCXRD. Structure **5** is centro-symmetric and crystallized in $P4_2/n$ space group with tetragonal crystal system (**Scheme 4**).



Scheme 4. Synthesis of pyridine-based ruthenium carbonyl complex cluster **5** (crystal structure is shown on the right)

The organometallic compound was explored as an electrode material in a Photo-electrochemical Cell (PEC) system[4,5] for the water oxidation reaction to obtain hydrogen. The cluster **5** displays low onset potential, fast

kinetics and significant photocurrent for the oxygen evolution. The current density – voltage profile for the modified GCE with Ru4 cluster (**Figure 2**) shows that even without illumination, the complex displays catalytic activity towards water oxidation at the anodic end, as is evidenced by the current of 3.86 mA/cm² at 1 V vs. Ag/AgCl. With illumination, current increases to 4.2 mA/cm² at 1 V vs. Ag/AgCl. The maximum photocurrent observed is 0.44 mA/cm² at 0.95 V vs. Ag/AgCl.

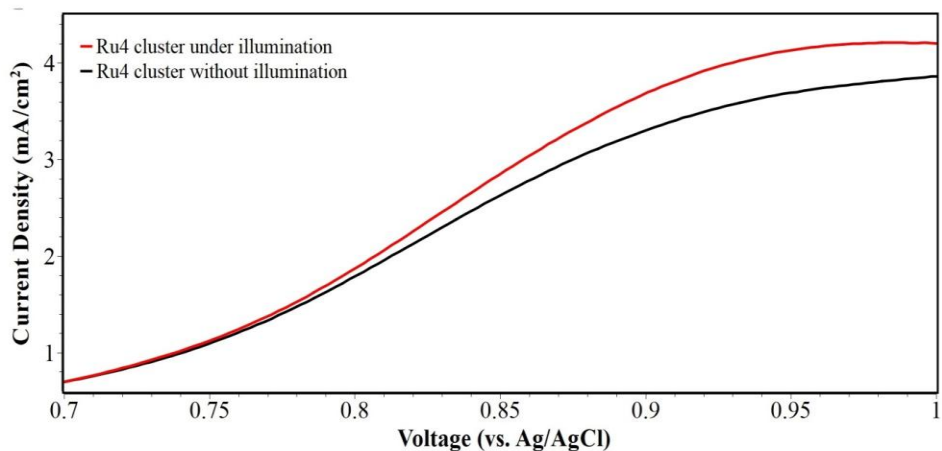
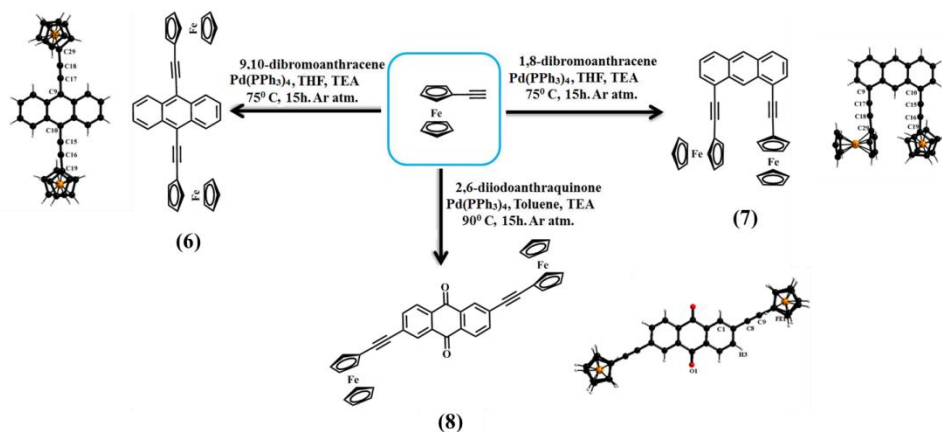


Figure 2. Current density-voltage profile for the modified Glassy Carbon Electrode with Ru4 cluster

It is proposed that this photocurrent is caused by photo-assisted MLCT transition from Ru ion to the ligand, which assists in the oxidation of water.[6] Moreover, the Faradaic Efficiency for oxygen evolution reaction is found to be 91.92 %, which is comparable to some well-known catalysts for the oxygen evolution reaction.[7,8] The study proves that the tetragonal ruthenium-pyridine-methanol cluster is a promising catalyst for water oxidation reaction.

In **Chapter 5**, three compounds (**6–8**) were synthesized, where ethynyl-ferrocene is substituted at different positions of anthracene and anthraquinone by using C-C coupling reaction employing Pd(PPh₃)₄ as a catalyst in tetrahydrofuran and toluene solvent, respectively and triethylamine as the base (**Scheme 5**).



Scheme 5. Schematic view of synthesis of **6–8**

Compounds **6–8** were characterized by NMR, Mass spectrometry and the structures are authenticated by their SCXRD study. The bioactivity[9] of **6–8** was investigated by molecular docking on various cancerous proteins, which participated in a progression of cancer. Compound **7** (1,8-diferrocenylethynylantracene) displayed the best interaction with cancer-related Aurora A protein both regarding binding energy (-10.61 kcal/mol) as well as inhibition constant (16.74 nM). Cell viability study also confirms the anticancer activity on cancerous cell lines (HeLa, A375) in which **7** has the least IC_{50} value. The normal cell line (HEK) cell viability proves the less cytotoxicity of compound **7** on normal cells. DNA/ protein binding study along with CD studies also performed to determine the interaction of **6–8** with proteins.

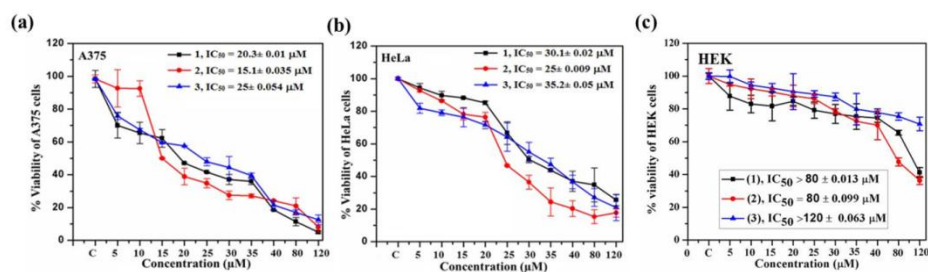
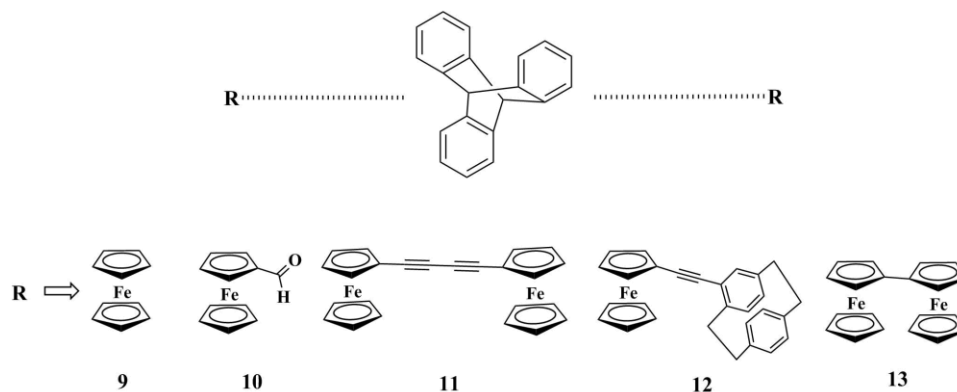


Figure 3. Cell viability studies of **6, 7** and **8** with (a) cervical cancer cell line (HeLa) (b) skin melanoma cell line (A375), (c) human embryonic kidney cell line (HEK).

The biological activities of the compounds (**6–8**), confirmed that compound **7** is found to be more effective towards anticancer activity compared to **6** and **8** from both molecular docking and cell cytotoxic assay studies.

In **Chapter 6**, crystal engineering is necessary for tuning various physical and chemical properties of material or molecules. We studied the cocrystallization of geometrically demanding triptycene (TriptH) molecule[10] with the compact ferrocene (FcH) and its derivatives featuring various level of chemical functionality and steric demands to prepare five cocrystals (**9–13**) (**Scheme 6**), which were characterized by SCXRD study (**Figure 4**).



Scheme 6. Interaction of R group with TriptH where R is FcH (**9**), Fccarboxaldehyde (**10**), Diferrocenyl diacetylene (**11**), PCP-Fc (**12**) and BiFcH (**13**) respectively

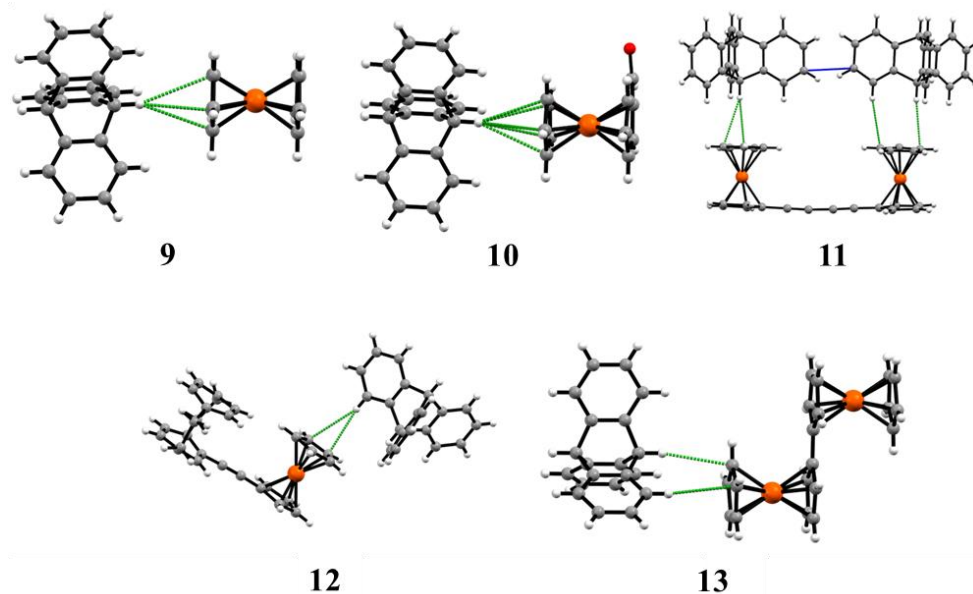


Figure 4. Cocystal structure (primary synthons) of TripH with FcH (9), Fccarboxaldehyde (10), Diferrocenyl diacetylene (11), PCP-Fc (12) and BiFcH (13) with showing the interaction between two units

The electrical conductivity property and NMR study in the solution have also been performed for **9–13** to assess the correlation between the solid-state structure and physical property and also to check the structural integrity of the co-crystal **9** in the solution. Crystal Explorer software was used to simulate the intermolecular interaction energies in the **9–13** cocrystals and their ‘energy frameworks’. Energy frameworks were entirely in line with the strongest $C_{sp^3}\text{-H}\cdots\text{Cp}$ intermolecular interactions, responsible for the 1D chain formation, and $C_{sp^2}\text{-H}\cdots\text{Ph}$ close packing, filling the space between the Phenyl lobes of TripH.

This report focuses on the structure of the triptycene-ferrocene derived cocrystals, featuring interplay between specific intermolecular $C_{sp^3}\text{-H}\cdots\pi_{cp}$ hydrogen bonding and close-packing requirements, providing a suitable model in an attempt to get a glance on early stages of crystallization.

Conclusions

Synthesis of new Ru₃ ruthenium pyridine alcohol/acid clusters and Ru₄ ruthenium pyridine methanol cluster (**1–5**) using Ru₃(CO)₁₂ with a variety of 2-pyridyl(CH₂)_nOH and picolinic acid were carried out. The catalytic application for N-alkylation of primary amine to form the secondary amine, oxidation of alcohol to carboxylic acid and water oxidation is achieved successfully. Three ferrocene-anthracene/anthraquinone based compounds **6–8** were synthesized. **6–8** were examined for their anticancer activity, in which **7** was found to be best among compounds **6–8**. In last, co-crystals **9–13** have been synthesized by triptycene and ferrocene derivatives. The electrical conductivity property and NMR study for **9** is measured. Energy calculations prove the strongest C_{sp3}-H---Cp and C_{sp2}-H---Cp intermolecular interactions, responsible for the 1D chain formation among **9–13**.

References

- [1] Park E. J., Lee J. M., Han H., Chang S. (2006), Halide Ions as a Highly Efficient Promoter in the Ru-Catalyzed Hydroesterification of Alkenes and Alkynes. *Org. Lett.*, 8, 4355-4358 doi:10.1021/ol061753e
- [2] Ko S., Na Y., Chang S. (2002), A Novel Chelation-Assisted Hydroesterification of Alkenes via Ruthenium Catalysis. *J. Am. Chem. Soc.*, 124(5), 750-751 doi:10.1021/ja017076v
- [3] Balaraman E., Khaskin E., Leitus G., Milstein D. (2013), Catalytic transformation of alcohols to carboxylic acid salts and H₂ using water as the oxygen atom source. *Nat Chem*, 5(2), 122-125 doi:10.1038/nchem.1536

- [4] Martin D. J., Reardon P. J. T., Moniz S. J. A., Tang J. (2014), Visible Light-Driven Pure Water Splitting by a Nature-Inspired Organic Semiconductor-Based System. *J. Am. Chem. Soc.*, *136*(36), 12568-12571 doi:10.1021/ja506386e
- [5] Esiner S., Willems R. E. M., Furlan A., Li W., Wienk M. M., Janssen R. A. J. (2015), Photoelectrochemical water splitting in an organic artificial leaf. *J. Mater. Chem. A*, *3*(47), 23936-23945 doi:10.1039/C5TA07325A
- [6] Kärkäs M. D., Verho O., Johnston E. V., Åkermark B. (2014), Artificial Photosynthesis: Molecular Systems for Catalytic Water Oxidation. *Chem. Rev.*, *114*(24), 11863-12001 doi:10.1021/cr400572f
- [7] Li F., Fan K., Wang L., Daniel Q., Duan L., Sun L. (2015), Immobilizing Ru(bda) Catalyst on a Photoanode via Electrochemical Polymerization for Light-Driven Water Splitting. *ACS Catalysis*, *5*(6), 3786-3790 doi:10.1021/cs502115f
- [8] Li L., Duan L., Xu Y., Gorlov M., Hagfeldt A., Sun L. (2010), A photoelectrochemical device for visible light driven water splitting by a molecular ruthenium catalyst assembled on dye-sensitized nanostructured TiO₂. *Chem. Commun.*, *46*(39), 7307-7309 doi:10.1039/C0CC01828G
- [9] Jaouen G., Vessieres A., Top S. (2015), Ferrocifen type anti cancer drugs. *Chem. Soc. Rev.*, *44*(24), 8802-8817 doi:10.1039/C5CS00486A
- [10] Marc Veen E., L. Feringa B., M. Postma P., T. Jonkman H., L. Spek A. (1999), Solid state organisation of C60 by inclusion crystallisation with triptycenes. *Chem. Commun.*(17), 1709-1710 doi:10.1039/A904457D

LIST OF PUBLICATIONS

1. **Singh A.**, Kumari P., Raghuvanshi A., Mobin S. M., Mathur P. (2018), Ferrocene-substituted bis(ethynyl)anthracene compounds as anticancer agents, *Appl. Organomet. Chem*, 32, e4071, DOI: **10.1002/aoc.4071**.
2. **Singh A.**, Mobin S. M., Mathur P. (2018), Preparation of $\text{Ru}_3(\text{CO})_8$ -pyridine-alcohol cluster and its use for selective catalytic transformation of primary to secondary amines *Dalton Trans.*, DOI: **10.1039/C8DT02972E**.
3. **Singh A.**, Singh S. K., Saini A. K., Mobin S. M., Mathur P. (2018), Facile oxidation of alcohols to carboxylic acids in basic water medium by employing ruthenium picolinate cluster as an efficient catalyst *Appl. Organomet. Chem*, DOI: **10.1002/aoc.4574**.
4. Torubaev, Y. V., Lyssenko, K. A., Barzilovich, P. Y., Saratov, G. A., Shaikh, M. M., **Singh, A.**, Mathur, P. (2018), Self-assembly of conducting cocrystals via iodine $\cdots\pi(\text{Cp})$ interactions, *CrystEngComm*, 19 (34), 5114–5121.
5. Torubaev Y. V., Skabitskiy I. V., Rusina P., Pasynskii A. A., Rai D. K., **Singh A.** (2018), Organometallic halogen bond acceptors: directionality, hybrid cocrystal precipitation, and blueshifted CO ligand vibrational band, *CrystEngComm*, 20, 2258-2266
6. Yadav S., **Singh A.**, Rashid N., Ghotia M., Roy T. K., Ingole P. P., Ray S., Mobin S. M., Dash C. (2018), Phosphine-Free Bis(Pyrrolyl)pyridine based NNN-pincer Palladium(II) Complexes as Efficient Catalysts for Suzuki-Miyaura Cross-Coupling Reactions of Aryl Bromides in Aqueous Medium, *ChemistrySelect*, DOI: **10.1002/slct.201801647**.

Publications under preparation

7. **Singh, A.**, Torubaev Y., Ansari S. N., Singh S. K., Mobin S. M., and Mathur P., Molecular Modeling of the Nucleation: A Case Study of Triptycene - Ferrocene Supra-molecular Assembly in the Solid State (unpublished).
8. **Singh, A.**, Natarajan K., Mobin S. M., and Mathur P., Tetranuclear $\text{Ru}_4(\text{CO})_8$ -substituted pyridine-methanol cluster as a highly efficient electro-catalyst in water oxidation reaction (unpublished).

TABLE OF CONTENTS

1. List of Figures	xxiv-xxxi
2. List of Tables	xxxii-xxxiv
3. Acronyms	xxxv-xxxvii
4. Nomenclature	xxxviii

Chapter 1: Introduction 1-34

1.1 Ruthenium based catalysts and their catalytic applications	1
1.2 Oxidation reactions	1
1.2.1 Oxidation	2
1.2.2 Hydrogenation	8
1.3. Ferrocene linked to biologically vital molecules as favourable anti-cancer candidates	12
1.3.1.1 Ferrocenylalkylazoles as active members for solid tumors	12
1.3.1.2 Ferrocenyl pyrazolyl as active anticancer members	12
1.3.1.3 Ferrocenyl acridine compounds targeting DNA	13
1.3.1.4 Ferrocenyl azalactone and thiomorpholide compounds targeting topoisomerase	14
1.3.1.5 Ferrocenyl nilutamide for prostate cancer cells	14
1.3.1.6 Compounds containing ferrocenyl group along with various transition metals	15
1.3.1.7 Ferrocifens, ferrocifenols and ferrocenophanes	16

for targeting breast cancer cells

1.4	Significance of triptycene and ferrocene in Supramolecules	17
1.5	References	21

Chapter 2: Preparation of $\text{Ru}_3(\text{CO})_8$ -pyridine-alcohol cluster and its use for selective catalytic transformation of primary to secondary amines **35-66**

2.1	Introduction	35
2.2	Results and Discussion	39
2.2.1	Synthesis of Ru_3 clusters 1–3	39
2.2.2	Ru_3 clusters catalyzed mono-alkylation of primary amines with alcohol	42
2.3.3	Catalytic application of clusters 1–3 for amine mono-alkylation with primary alcohols	44
2.3.4	Mercury Poisoning Study	49
2.3	Conclusion	51
2.4	Experimental	52
2.4.1	Preparation of cluster $\text{Ru}_3(\text{hep})_2(\text{CO})_8$ (1)	52
2.4.2	Preparation of cluster $\text{Ru}_3(\text{hpp})_2(\text{CO})_8$ (2)	54
2.4.3	Preparation of cluster $\text{Ru}_3(\text{bhmp-H})_2(\text{CO})_8$ (3)	56
2.4.4	Mercury Poisoning Study	58
2.5	References	61

Chapter 3: Facile oxidation of alcohols to carboxylic acids in basic water medium by employing ruthenium picolinate cluster as an efficient catalyst **67-90**

3.1	Introduction	67
3.2	Results and Discussion	70
3.2.1	Catalyst screening	70
3.2.2	Structural description of Catalyst 1	71
3.2.3	Catalytic experiments	74
3.3	Conclusion	82
3.4	Experimental	83
3.4.1	Materials and instrumentation details	83
3.4.2	Single crystal X-ray diffraction (SC-XRD)	83
3.4.3	Catalytic reaction	83
3.4.4	Analysis of products	84
3.5	References	85

Chapter 4: Tetranuclear Ru₄(CO)₈-substituted pyridine-methanol cluster as a highly efficient electro-catalyst in water oxidation reaction

91-113

4.1	Introduction	91
4.2	Results and Discussion	93
4.2.1	Structural description of 1	93
4.2.2	Linear sweep voltammetry (LSV) measurement	96
4.2.3	Electrochemical Impedance Spectroscopy analysis	99
4.2.4	Density Functional theory study	100
4.2.5	UV-Visible Spectroscopy study	100
4.3	Conclusion	103
4.4	Experimental	104
4.4.1	X-ray Crystallography measurements	104
4.4.2	Electrochemical analysis	105
4.4.3	Density functional theoretical studies	105
4.4.4	Synthesis of complex [Ru ₄ (CO) ₈ (C ₅ H ₅ NCH ₂ O) ₄] (1)	105

4.5	References	109
-----	------------	-----

**Chapter 5: Ferrocene-substituted bis(ethynyl)-anthracene
compounds as anticancer agents** **114-150**

5.1	Introduction	114
5.2	Results and Discussion	116
5.2.1	Synthesis of compounds 1–3	116
5.2.2	Molecular Structures of 1–3	117
5.2.3	Electronic absorption spectra	119
5.2.4	Density functional theoretical studies	120
5.2.5	Molecular docking	121
5.2.6	Cell cytotoxic assay	122
5.2.7	BSA binding studies	123
5.2.8	DNA binding studies	125
5.2.9	Circular Dichroism Studies	126
5.3	Conclusion	129
5.4	Experimental	130
5.4.1	X-ray Crystallography	130
5.4.2	Density functional theory	130
5.4.3	Molecular docking	131
5.4.4	MTT assay	131
5.4.5	DNA binding studies	132
5.4.6	BSA binding studies	133
5.4.7	Circular Dichroism Measurements	133
5.4.8	Synthesis of compound 1	134
5.4.9	Synthesis of compound 2	136
5.4.10	Synthesis of compound 3	138
5.5	References	144

Chapter 6: Molecular Modeling of the Nucleation: A Case Study of Triptycene - Ferrocene Supra-molecular Assembly in the Solid State **151-188**

6.1	Introduction	151
6.2	Results and Discussion	154
6.2.1	Description of the polymeric network of cocrystals 1-5	155
6.2.2	Energy calculations	164
6.2.3	2D (¹³ C/ ¹ H HSQC) NMR studies in solution phase	171
6.3	Conclusion	173
6.4	Experimental	174
6.4.1	Preparation of FcH/TripH (1)	174
6.4.2	Preparation of Cp ₂ FeCHO / TripH (2)	174
6.4.3	Preparation of CpFeC ₅ H ₄ -C≡C-C≡C-C ₅ H ₄ FeCp/ TripH (3)	175
6.4.4	Preparation of PCP-C≡C- Cp ₂ Fe/TripH (4)	175
6.4.5	Preparation of CpFeC ₅ H ₄ -C ₅ H ₄ FeCp/ TripH (5)	175
6.4.6	Computations	175
6.4.7	Electrical conductivity measurements	176
6.4.8	Crystal structure determination	176
6.5	References	179

Chapter 7: Conclusions and Scope for Future Work
189-190

LIST OF FIGURES

Chapter 1. Introduction	1
Figure 1.1. Oxidation of alcohol, alkene, and alkanes using RuO_4	2
Figure 1.2. Oxidation of alcohol to carboxylic acids and ketone	3
Figure 1.3. Oxidation of alcohol to carboxylic acids and cis-dihydroxy product	3
Figure 1.4. Oxidation of ether to ester	3
Figure 1.5. Oxidation of tertiary amine to amide	4
Figure 1.6. Oxidation of alkane to alcohol	4
Figure 1.7. Oxidation of alcohol to aldehyde	4
Figure 1.8. Oxidation of alcohol to ketone	4
Figure 1.9. Oxidation of alcohol to ketone	5
Figure 1.10. Oxidation of alcohol to ketone/aldehyde	5
Figure 1.11. Oxidation of alcohol to aldehyde/ketone	6
Figure 1.12. Demethylation of tertiary amine	6
Figure 1.13. Oxidation of cyclohexene to 6-oxoheptanoic acid and 2-hydroxy-2-methylcyclohexene	7
Figure 1.14. Oxidation of alicyclic alkane to alicyclic alcohols	7
Figure 1.15. Oxidation of alicyclic alkane to alicyclic ketone/alcohol	8
Figure 1.16. Reduction of steroidal compounds and Terminal conjugated dienes, regioselective reaction.	8
Figure 1.17. Reduction of acenathalene regioselective reaction	9
Figure 1.18. Reduction of nitro to amino group	9
Figure 1.19. Reduction of propargyl and allyl alcohols	10
Figure 1.20. Reduction using formic acid, THF and tetrahydronaphthalene	11
Figure 1.21. Ferrocenyl pyrazole complex as anticancer	12

	agents	
Figure 1.22.	Ferrocenyl pyrazole complex as anticancer agents	13
Figure 1.23.	Ferrocenyl acridine complex for DNA intercalation	13
Figure 1.24.	Azalactone-ferrocene (9) and thiomorpholide amido methyl-ferrocene (10) as inhibitors for topoisomerase II	14
Figure 1.25.	Nilutamide (11) and structurally related ferrocenyl compound	14
Figure 1.26.	Transition metal based ferrocenyl compounds as antitumor agents	15
Figure 1.27.	Ferrocifens, ferrocifenols and ferrocenophanes as antitumor agents	16
Figure 1.28.	Molecular brake shoe structure utilizing triptycene and 6,6'-dimethoxy-2,2'-bipyridine derivative	17
Figure 1.29.	Engagement and disengagement of brake using Hg^{+2} and EDTA	17
Figure 1.30.	Molecular ratchet structure utilizing triptycene and terpene derivative	18
Figure 1.31.	Supramolecular interaction present between ferrocene and Hg-Tetrafluorobenzene and Ag-Bis(trifluoromethyl)pyrazolate complex	19
Figure 1.32.	Supramolecular interaction present between ferrocene and tetracyanoethylene	20

Chapter 2. Preparation of Ru₃(CO)₈-pyridine- alcohol cluster and its use for selective catalytic transformation of primary to secondary amines	35
Chart A. Secondary amine derivatives present in various psychoactive drugs	35
Chart B. Homogeneous catalysts (i–iv) used so far for N- alkylation of primary amine	36
Scheme 2.1. Synthesis of pyridine alcohol containing ruthenium carbonyl complexes 1–3	39
Figure 2.1. Perspective view of 1, 2 and 3	40
Figure 2.2. Mercury poisoning study of Ru ₃ (hep) ₂ (CO) ₈ cluster catalyst for mono-alkylation of amine with alcohol	50
Figure 2.3. ¹ H NMR of 1	53
Figure 2.4. ¹³ C NMR of 1	54
Figure 2.5. IR of 1	54
Figure 2.6. ¹ H NMR of 2	55
Figure 2.7. ¹³ C NMR of 2	56
Figure 2.8. IR of 2	56
Figure 2.9. ¹ H NMR of 3	57
Figure 2.10. ¹³ C NMR of 3	58
Figure 2.11. IR of 3	58
Figure 2.12. Perspective view of 1a	60
Chapter 3. Facile oxidation of alcohols to carboxylic acids in basic water medium by employing ruthenium picolinate cluster as an efficient catalyst	67
Figure 3.1. Ruthenium-based active catalysts for carboxylic acid synthesis from alcohols	68
Scheme 3.1. Schematic representation for the oxidation of	71

	alcohol to carboxylic acid	
Figure 3.2.	Perspective view of cluster 1	72
Figure 3.3.	H-bonded 1-D network in 1 along c axis	73
Figure 3.4.	Plausible mechanism for catalytic oxidation of alcohol to carboxylic acid by ruthenium cluster [Ru ₃ (CO) ₈ (C ₅ H ₄ NCO ₂) ₂]	81
 Chapter 4. Tetranuclear Ru₄(CO)₈-substituted pyridine-methanol cluster as a highly efficient electro-catalyst in water oxidation reaction		92
Scheme 4.1.	Synthesis of pyridine based ruthenium carbonyl cluster 1	93
Figure 4.1.	Perspective view or molecular diagram of complex 1	94
Figure 4.2a.	Solvent accessible voids present in 1 along 'a' axis found using mercury CSD 3.8 software	94
Figure 4.2b.	Voids in c axis solvent accessible found using mercury CSD 3.8 software	95
Figure 4.3.	A PEC device, composed of an anode based on Glassy Carbon electrode along with a Nafion thin coating, a Pt cathode, and an aqueous electrolyte, for light driven water splitting	95
Figure 4.4.	Current density – voltage profile for the modified GCE with Ru ₄ cluster	96
Figure 4.5.	Hypothetical half-cell solar-to-hydrogen (HC-STH) efficiency calculations with Ru ₄ cluster	97
Figure 4.6.	EIS spectra of the glassy carbon electrodes modified with Ru ₄ cluster	99
Figure 4.7.	Comparison of theoretical and experimental UV-vis	101

Figure 4.8.	Plot b/w derivative $d[\ln(\alpha h\nu)]/d(h\nu)$ and $h\nu$ for band gap calculation	102
Figure 4.9.	^1H NMR of 1	106
Figure 4.10.	^{13}C NMR of 1	106
Figure 4.11	IR of 1	107
.		
Chapter 5.	Ferrocene-substituted bis(ethynyl)-anthracene compounds as anticancer agents	114
Scheme 5.1.	Schematic view for the synthesis of 1–3	117
Figure 5.1.	Perspective view of 1, 2 and 3 .	117
Figure 5.2.	2D network of 1 along c axis	118
Figure 5.3.	3D network of 2 along b axis	118
Figure 5.4.	3D network of 3 along tilted b axis	119
Figure 5.5.	UV–vis spectra of 1, 2 and 3	120
Figure 5.6.	HOMO and LUMO of 1, 2 and 3	121
Figure 5.7.	Molecular docking of 2 with cancer causing and viral proliferation proteins, the proteins are shown as ribbons and the interacting residues are shown as sticks, the ligand is shown as ball and stick. (A) cancer-related Aurora-A Protein Kinase (1MQ4), (B) Hepatitis C virus NS5B polymerase (2WCX)	122
Figure 5.8.	Cell viability studies of 1, 2 and 3 on cancerous as well as normal cell lines. (a) cervical cancer cell line (HeLa) (b) skin melanoma cell line (A375), (c) human embryonic kidney cell line (HEK). These cells were exposed to various concentrations of 1, 2 and 3 for 24 h and then cell viability was measured by MTT assay	123
Figure 5.9.	BSA binding of 1, 2 and 3 . Inset: Corresponding Stern–Volmer plot	124
Figure 5.10.	CD studies of 1, 2 and 3	127

Figure 5.11.	^1H NMR of 1 in CDCl_3	135
Figure 5.12.	^{13}C NMR of 1 in CDCl_3	135
Figure 5.13.	IR of 1	136
Figure 5.14.	ESI-MS of 1	136
Figure 5.15.	^1H NMR of 2 in CDCl_3	137
Figure 5.16.	^{13}C NMR of 2 in CDCl_3	137
Figure 5.17.	IR of 2	138
Figure 5.18.	ESI-MS of 2	138
Figure 5.19.	^1H NMR of 3 in CDCl_3	139
Figure 5.20.	^{13}C NMR of 3 in CDCl_3	139
Figure 5.21.	IR of 3	140
Figure 5.22.	ESI-MS of 3	140

Chapter 6. Molecular Modeling of the Nucleation: A Case Study of Triptycene - Ferrocene Supramolecular Assembly in the Solid State 151

Figure 6.1.	Cocrystal structure (primary synthons) of TripH with FcH (1), FcCHO (2), Diferrocenyl diacetylene (3), PCP-Fc (4) and BiFcH (5) with showing the interaction between two units.	154
Figure 6.2.	Fragment of the one-dimensional chain of FcH and TripH with interaction having distance C5-H11 2.964 Å, C1-H11 2.882 Å, C8-H12 3.043 Å, C9-H12 2.885 Å, and C10-H12 3.054 Å	154
Figure 6.3.	Fragment of the two-dimensional chain of FcH and TripH with C-H--- π interaction having distance H10---C28 3.126 Å and H1--- $\text{C}_{(24-29)\text{centroid}}$ 2.783 Å.	155
Figure 6.4.	Honeycomb fragment observed area of a cross-section of cocrystal 1 showing the efficient packing of FcH into the grooves of TripH	156

Figure 6.5.	Fragment of the one-dimensional chain of FcCHO and TripH with C-H _{bridgehead} --- π interaction having distance C6-H12 3.075 Å, C7-H12 3.026 Å, C8-H12 2.966 Å, C9-H12 2.975 Å, C10-H12 3.020 Å, C1-H11 3.082 Å, and C5-H11 2.927 Å	156
Figure 6.6.	Fragment of the two-dimensional chain of FcCHO and TripH with interactions having distance O1---H10 2.898 Å, O1---H23 2.713 Å, H10---C31 2.955 Å, and C20---C22 3.508 Å	157
Figure 6.7.	Note a π --- π stacking between two TripH molecules, so π --- π stacking in TripH is possible! (But not effective for TripH, itself packing), the cross-section view shows π --- π interactions with 3.508 Å (blue dotted lines).	158
Figure 6.8.	Fragment of the one-dimensional chain of Diferrocenyl diacetylene- TripH (3) with interactions having distance H49-C20 2.909 Å, H48-C22 2.801 Å, H52-C10 2.973 Å, H32-C16 2.851 Å, H32-C17 2.896 Å, H44-C1 2.925 Å, H25-C3 2.958 Å, H25-C4 2.989 Å, C42-C50 3.420 Å, and H50-C42 2.998 Å	159
Figure 6.9.	Beautiful case of closed packing and molecular recognition together in cocrystal 3	160
Figure 6.10.	Fragment of the one-dimensional chain of PCP-Fc and TripH (4) with interactions having distance C7-H20 3.043 Å, C8-H20 2.824 Å, H12-C33 3.016 Å, H12-C34 2.731 Å, H12-C35 3.098 Å, C36-H29 3.054 Å, H29-C37 3.011 Å, and H29-C38 2.878 Å	160
Figure 6.11.	Zig-zag chain arrangement of PCP-Fc and TripH (4) (No π - π stacking between TripH units)	161
Figure 6.12.	Fragment of the one-dimensional chain of Fc ₂ -	162

TripH with interaction having distance H29-C15 3.071 Å, H29-C16 2.834 Å, H14-C27 2.867 Å, H14-C28 3.086 Å, H11-C10 2.944 Å, and H23-C9 2.961 Å

Figure 6.13.	Re-appearance of natural TripH packing pattern in cocrystal 5 presents in tilted <i>ac</i> plane (Cross-sectional view)	163
Figure 6.14.	Natural packing pattern in TripH (from TRIPCN03)	163
Figure 6.15.	Trip-Trip interactions in TRIPCN03	165
Figure 6.16.	Interaction of FcH with TripH in cocrystal 1	166
Figure 6.17.	Interaction of FcCHO with TripH in cocrystal 2	167
Figure 6.18.	Interaction of Fc ₂ with TripH in cocrystal 5	168
Figure 6.19.	Energy framework in 1 , 2 (cut-off -11 kJ/mol)	169
Scheme 2.a.	TripH-C ₆₀ packing pattern expected in work	169
Scheme 2.b.	Packing pattern of aza-TripH---C ₆₀ sheets	170
Figure 6.20.	Chains and sheets C ₆₀ -TripH-o-xylene sheets in CEMNUD, Compare with TripH-FcH chains and FcC ₂ C ₂ Fc-TripH sheets	171
Figure 6.21.	2D HSQC NMR spectra of (a) triptycene, (b) ferrocene and (c) adduct triptycene-ferrocene	172

Chapter 7: Conclusions and Scope for Future Work 189

Figure 7.1.	Plausible mechanism for the N-alkylation of primary amine to secondary amine using Ru ₃ (hep) ₂ (CO) ₈ (1) catalyst	190
--------------------	---	-----

LIST OF TABLES

Chapter 2. Preparation of Ru₃(CO)₈-pyridine- alcohol cluster and its use for selective catalytic transformation of primary to secondary amines	35
Table 2.1 Crystal data and structure refinement for 1 , 2 and 3	41
Table 2.2 Comparison of cluster 1 with previous homogeneous catalysts for alkylation reaction of primary amines with primary alcohols	43
Table 2.3 Optimization of the catalytic reaction conditions for N-alkylation of 2-picolyamine using benzyl alcohol and Ru ₃ cluster catalysts.	45
Table 2.4. Direct formation of secondary amines from benzyl alcohol and various primary amines with cluster 1 as catalyst	46
Table 2.5. Direct formation of secondary amines from primary amines and varying alcohols using 1 as catalyst	49
Table 2.6. Crystal data and structure refinement for 1a	59
Chapter 3. Facile oxidation of alcohols to carboxylic acids in basic water medium by employing ruthenium picolinate cluster as an efficient catalyst	67
Table 3.1. Screening of the catalyst for the transformation of benzyl alcohol to benzoic acid in basic water and dioxane as solvent	70
Table 3.2. Crystal data and structure refinement for complex 1	72
Table 3.3. Optimization for the synthesis of benzoic acid from	75

	benzyl alcohol	
Table 3.4.	Comparative study of the benzoic acid formation from benzylic alcohol using ruthenium complexes so far	76
Table 3.5.	Synthesis of carboxylic acid derivatives from alcohols	78

Chapter 4. Tetranuclear Ru₄(CO)₈-substituted pyridine-methanol cluster as a highly efficient electro-catalyst in water oxidation reaction **91**

Table 4.1.	Comparison of photocurrents achieved on ruthenium-based complexes used as electrodes in photoelectrochemical cells	98
Table 4.2	The values for the electrochemical parameters specified in the Cole-Cole model	100
Table 4.3	Computed vertical transitions and their oscillator strengths and configurations	101
Table 4.4	Crystal data and structure refinement for 1	107

Chapter 5. Ferrocene-substituted bis(ethynyl)-anthracene compounds as anticancer agents **114**

Table 5.1.	Crystal data and structure refinement for 1–3	140
Table 5.2.	Molecular docking of 1–3 with cancer causing proteins	141
Table 5.3.	Stern-Volmer quenching constant, binding constant and number of binding site with BSA	143
Table 5.4.	IC ₅₀ values (μM) evaluated from MTT assay on A375, HeLa and HEK cells treated with 1, 2 and 3 for 24 h	143

Chapter 6. Molecular Modeling of the Nucleation: A Case Study of Triptycene - Ferrocene Supramolecular Assembly in the Solid State 151

Table 6.1.	$^{13}\text{C}/^1\text{H}$ NMR chemical shift values in solution phase of 1	172
Table 6.2.	Crystal data and structure refinement for 1-3	176
Table 6.3.	Crystal data and structure refinement for 4-5	177

ACRONYMS AND DEFINITIONS

AcOOH	Peracetic acid
A549	Adenocarcinomic human alveolar basal epithelial cells cell line
CD	Circular Dichroism
Cys-Gly	Cysteine-Glycine
C/Cys	Cysteine
CRL	Candida Rugosa Lipase
CDCl ₃	Chloroform-d
CH ₃ CN	Acetonitrile
d	Doublet
DCM	Dichloromethane
DMSO	Dimethyl Sulfoxide
DMF	Dimethyl Formamide
ER positive	Cells grow in response to the hormone estrogen
EtOH	Ethanol
Et	Ethyl
EtOAc	Ethyl Acetate
ESI-MS	Electrospray Ionization Mass Spectrometry
FTIR	Fourier Transform Infrared Spectroscopy
F/ Phe	Phenylalanine
Fmoc	Fluorenylmethyloxycarbonyl
G/Gly	Glycine
HCl	Hydrochloric Acid
H ₂ O ₂	Hydrogen peroxide
HB	Hydrogen Bonds
HepG2	Liver hepatocellular carcinoma cell line
IC50	The concentration of an inhibitor where the response (or binding) is reduced by half

L/Leu	Leucine
MDA-MR-45	Cellosaurus cell line 45
MDA-MR-231	Cellosaurus cell line 231
MTT	3-(4,5-dimethylthiazol-2-yl)-2,5-diphenyltetrazolium bromide
MeOH	Methanol
Me	Methyl
M	Molar
mM	Millimolar
NaCl	Sodium Chloride
NaOH	Sodium Hydroxide
NaHCO ₃	Sodium Hydrogen Carbonate
NMR	Nuclear Magnetic Resonance
OEP	2,3,7,8,12,13,17,18-octaethylporphyrinato
OCH ₃	Methyl ester
PPh ₃	Triphenylphosphine
PEC	Photoelectrochemical Cell
Ph	Phenyl
pH	The negative logarithm hydrogen-ion activity ($-\log_{10} [\text{H}_3\text{O}^+]$)
Ru ₃ (CO) ₁₂	Triruthenium dodecacarbonyl
RuO ₂	Ruthenium dioxide
RuO ₄	Ruthenium tetraoxide
s	Singlet
SBI	Secondary Bonding Interactions
t	Triplet
tBuOOH	tert-Butyl hydroperoxide
TPFPP	5,10,15,20-tetrakis(pentafluorophenyl) porphyrinato
THF	Tetrahydrofuran
TLC	Thin Layer Chromatography

Tyr

UV-Vis

V/Val

W/Trp

Tyrosine

UV-Visible Spectroscopy

Valine

Tryptophan

NOMENCLATURE

θ	Angle
λ	Wavelength
α	Alfa
β	Beta
\AA	Angstrom
nm	Nanometer
ω	Angular frequency
τ	Life time
δ	delta
μm	Micrometer
μL	Microlitre
π	Pi
φ	Phi
ψ	Psi
σ	Sigma
γ	Gamma
G'	Storage modulus
G''	Loss Modulus

Chapter 1

Introduction

1.1 Ruthenium based catalysts and their catalytic applications

Ruthenium complexes containing Ru – X linkage (X= H, C, N, O, P, S, arenes) has been an important catalyst in the field of homogeneous as well as heterogeneous catalysis. In the last few decades, the various pincer, hydride, phosphine ligands have been established as multi-functional building units which are used successfully in a number of crucial applications like sensors,[1,2] polymer chemistry,[3,4] photochemistry,[5,6] switches,[7] bond activation,[8] homogeneous and heterogeneous catalysis,[9] organic synthesis,[10] and as biomarkers in medicinal chemistry.[11] The variety of applications of ruthenium complexes is attractive because their electronic and steric properties can be easily tuned by changing the ligand on the metal centre.

Mainly, the focus of the present thesis is on the catalytic activity of the ruthenium carbonyl clusters. In the introduction, various catalytic applications of ruthenium complexes including oxidation, reduction of aliphatic, alicyclic and aromatic compounds along with demethylation of tertiary amines have been discussed.

1.2 Oxidation reactions

Herein, two important classes of reactions have been discussed which are as follows:

1. Oxidation
2. Hydrogenation

1.2.1 Oxidation

Herein, mainly two systems are discussed. Firstly RuO_4 followed by ruthenium complexes along with oxidants. RuO_4 is an efficient oxidant useful for oxidation of various organic compounds.[12] It shows characteristic of oxygenation, hydrogen abstraction toward different organic compounds to produce oxidized product along with RuO_2 (Figure 1.1).

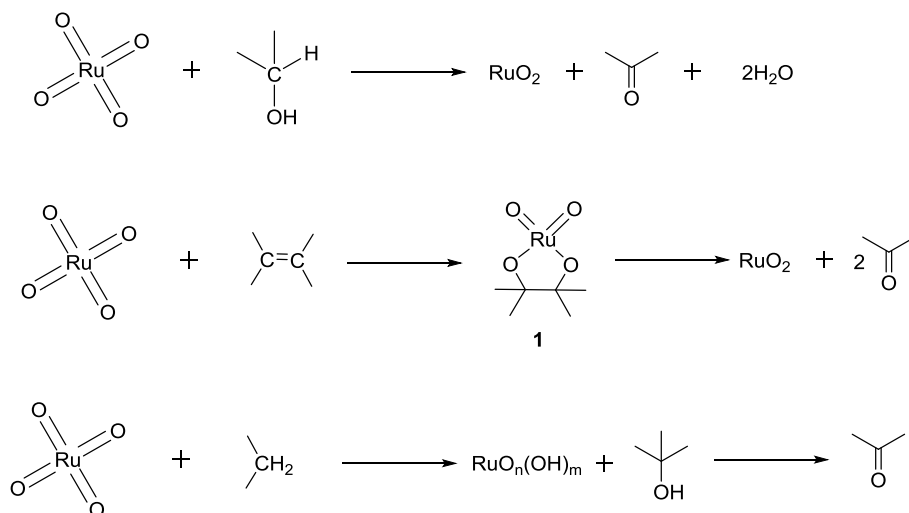


Figure 1.1 Oxidation of alcohol, alkene, and alkanes using RuO_4

The olefins reaction produces cyclized ruthenium **VI** diesters **1** that later gets converted to carbonyl compounds through C-C double bond' oxidative cleavage. Reactants containing unactivated C-H bonds like alkanes or alkanes undergo hydrogen abstraction due to which the consecutive oxygen bound to give the related hydroxy products that are generally converted to the carbonyl compounds through subsequent oxidation.

Primary and secondary alcohol oxidizes to give the corresponding carboxylic acids and ketone, respectively (Figure 1.2).[13,14]

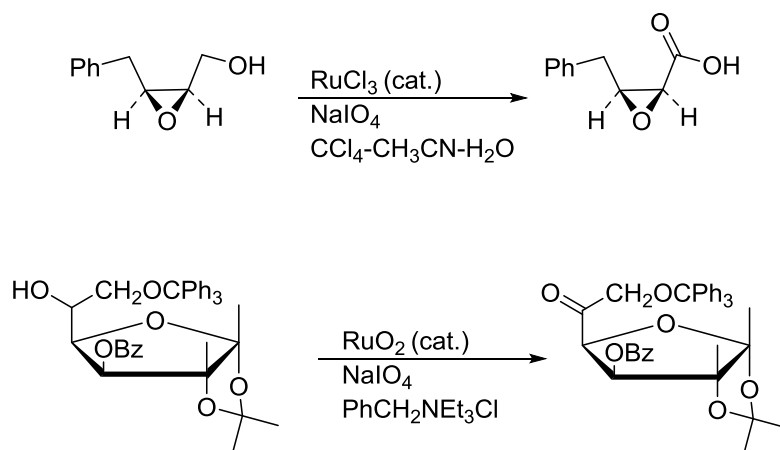


Figure 1.2 Oxidation of alcohol to carboxylic acids and ketone

Olefins give the carbonyl compounds through oxidative cleavage,[15] whereas *cis*-dihydroxylation takes if the reaction is performed for a lesser time (30 sec) at 0 °C in EtOAc-H₂O -CH₃CN (**Figure 1.3**). [16]

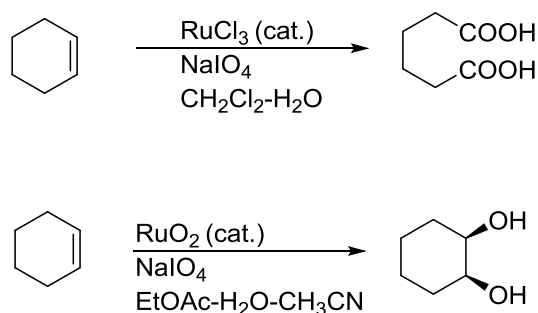


Figure 1.3 Oxidation of alcohol to carboxylic acids and *cis*-dihydroxy product

Various compounds containing heteroatom undergo methylene group oxidation at α -position, whereas ether gets oxidized to yield ester as well as lactone (**Figure 1.4**).[13]

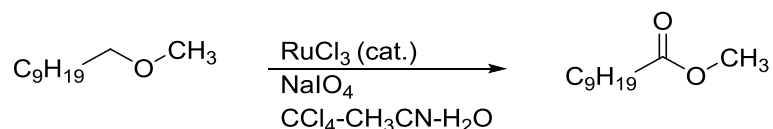


Figure 1.4 Oxidation of ether to ester

Furthermore, tertiary amines or amides oxidation also occur at α -position of heteroatom nitrogen which produces the amides or imides, respectively (**Figure 1.5**).[17]

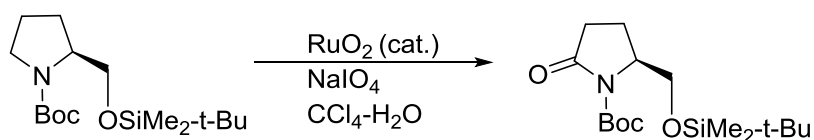


Figure 1.5 Oxidation of tertiary amine to amide

In the case of alkanes, tertiary carbon-hydrogen bonds, when oxidized with RuO_4 give the corresponding tertiary alcohols (**Figure 1.6**).[18]

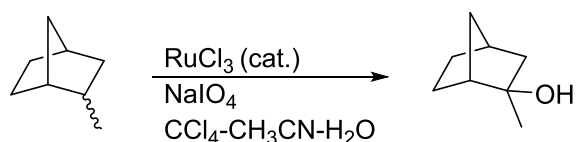


Figure 1.6 Oxidation of alkane to alcohol

Complex with ruthenium having low-valency catalyzes the oxidation of the alcohols as well as other hydroxy reactants in the presence of oxidants like AcOOH , $t\text{-BuOOH}$, [19] N -methylmorpholine N -oxide, [20] and pyridine N -oxide, [21] H_2O_2 . [21] Primary alcohols generally oxidize to produce carboxylic acids, whereas oxidation of benzyl alcohol into benzaldehyde, selectively using H_2O_2 can be achieved by reducing the reaction time (**Figure 1.7**). [22]

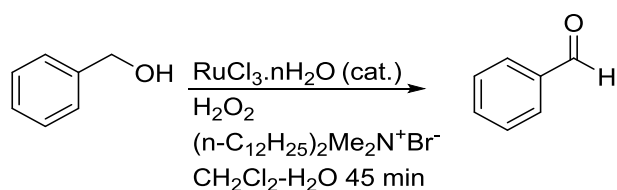


Figure 1.7 Oxidation of alcohol to aldehyde

Secondary alcohols get converted to the analogous ketones (**Figure 1.8**). [22]

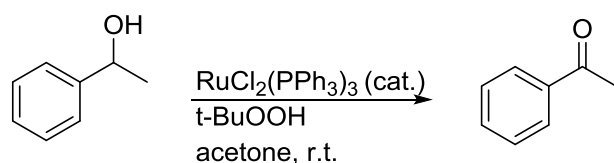


Figure 1.8 Oxidation of alcohol to ketone

Cyanohydrins produce the corresponding acyl cyanides by utilizing $\text{RuCl}_2(\text{PPh}_3)_3$ as catalyst and $t\text{-BuOOH}$ as an oxidizing agent which is

extremely useful reagent for the selective acylation of the amine reactants (**Figure 1.9**).[23]

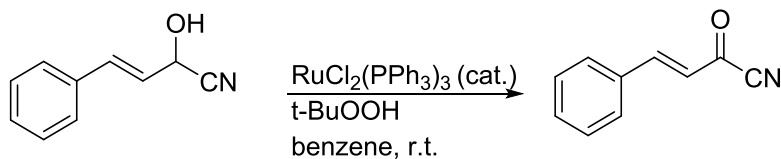


Figure 1.9 Oxidation of alcohol to ketone

Oxidation of alcohols in the air with metallic catalysts remains an appealing area for eco-friendly as well as economic reasons. Continuous research for appropriate catalyst has been done on group **viii** metal-complexes, utilizing RuCl_3 , RuO_2 , and $\text{RuCl}_2(\text{PPh}_3)_3$ as catalysts, by which alcohols like α -ketols[24] and allyl alcohols[25] can be feasibly oxidized (**Figure 1.10**).

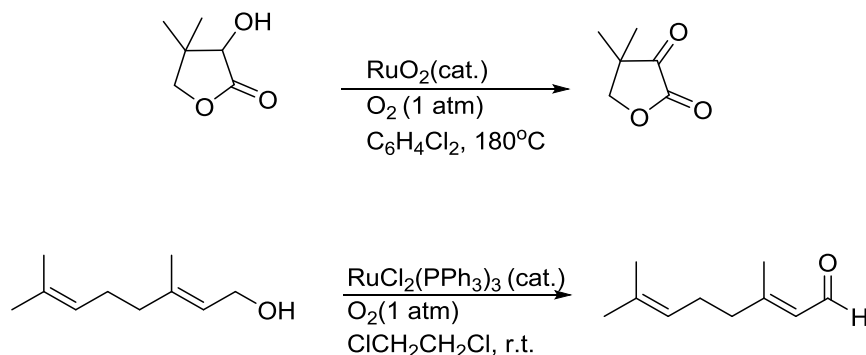


Figure 1.10 Oxidation of alcohol to ketone/aldehyde

Trinuclear ruthenium carboxylate like $\text{Ru}_3\text{O}(\text{O}_2\text{CCH}_2\text{R})_6\text{L}$ ($\text{L} = \text{PPh}_3, \text{H}_2\text{O}$) is the efficient catalyst for aerobic oxidation of alcohols.[26] This is approximately ten times more effective than RuCl_3 as well as $\text{RuCl}_2(\text{PPh}_3)_3$. Oxidation of alcohols utilizing tertiary amine N-oxide as oxidant was also done by $(n\text{-Pr}_4\text{N})(\text{RuO}_4)$, and, the same catalyst is also effective for aerobic oxidation of alcohols (**Figure 1.11**).[12]

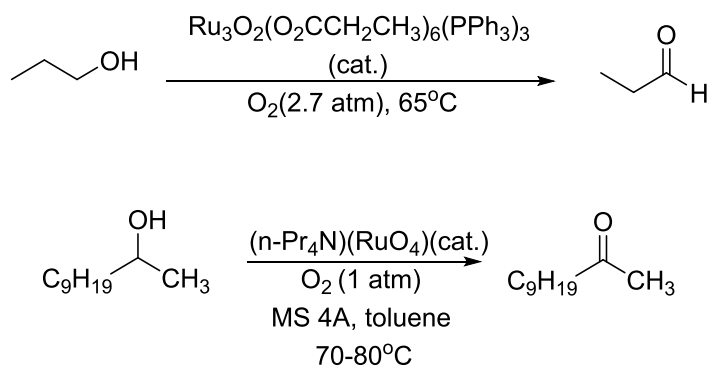


Figure 1.11 Oxidation of alcohol to aldehyde/ketone

In the case of amines, de-alkylation of tertiary amine can also be achieved using $\text{RuCl}_2(\text{PPh}_3)_3$ as a catalyst along with oxidant tert-butyl hydroperoxide which produces the peroxide intermediate. Further, hydrolysis of the obtained peroxide intermediate with an aq. HCl solution provides the corresponding de-methylated α -(tert-butylidioxy)alkylamines as a product (**Figure 1.12**).[27]

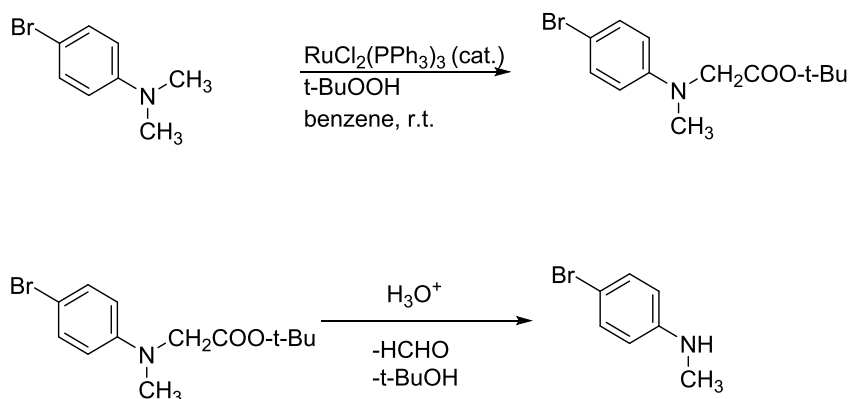


Figure 1.12 Demethylation of tertiary amine

When oxidant N-methylmorpholine N-oxide was used in place of t-BuOOH, secondary amines oxidized to imines. Aerobic oxidation of the primary amines gives analogous nitriles utilizing RuCl_3 as a catalyst in 3 atm O_2 pressure at 100 °C.[28]

Oxidations of alkenes were also explored with ruthenium RuO_4 and $\text{RuCl}_3 \cdot n\text{H}_2\text{O}$ catalysts. The difference in the oxidation using RuO_4 and $\text{RuCl}_3 \cdot n\text{H}_2\text{O}$ can be clearly observed by the catalytic oxidation reaction of 1-cyclohexene. The RuCl_3 -promoted oxidation utilizing peracetic acid as oxidant produces

hydroxymethylcyclohexene, whereas the oxidation of the same reactant in which RuO_4 is produced catalytically, yields 6-oxoheptanoic acid (**Figure 1.13**).[29]

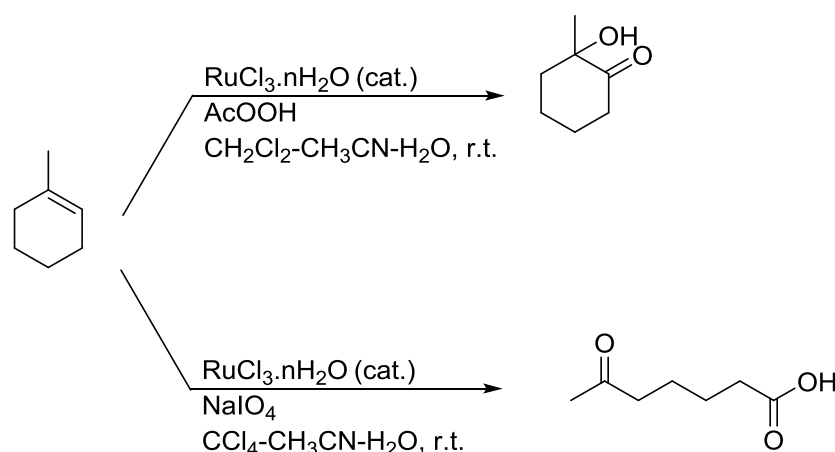


Figure 1.13 Oxidation of cyclohexene to 6-oxoheptanoic acid and 2-hydroxy-2-methylcyclohexene

The ruthenium-porphyrin complexes like $\text{Ru}(\text{OEP})(\text{PPh}_3)\text{Br}$ also displayed the catalytic activity in combination to iodosylbenzene for the conversion of alicyclic and aliphatic hydrocarbons to the analogous alcohols and ketones.[30] High catalytic activity for alkane hydroxylation was obtained utilizing ruthenium-porphyrin catalysts along with 2,4-dichloropyridine N-oxide together (**Figure 1.14**).[31]

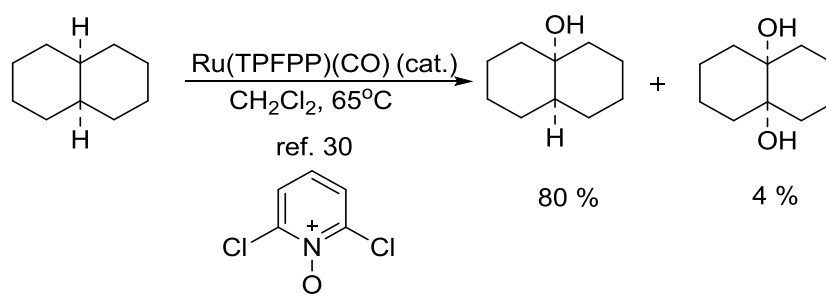
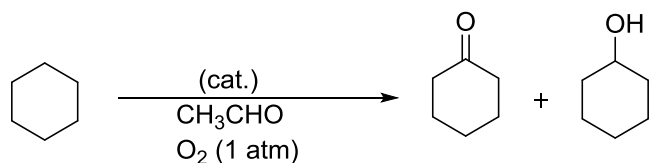


Figure 1.14 Oxidation of alicyclic alkane to alicyclic alcohols

Aerobic oxidation of the alkanes specifically oxidation like cyclohexane to cyclohexanone is significant for the industrial process. The reaction involves $\text{Ru}(\text{TPFPP})(\text{CO})$ [32] or RuCl_3 [33] -

catalyzed with molecular oxygen (1 atm) in the presence of ethanol gives the corresponding alcohols along with ketones (**Figure 1.15**).



cat. = Ru(TPFPP)(CO), RuCl₃.nH₂O

Figure 1.15 Oxidation of alicyclic alkane to alicyclic ketone/alcohol

1.2.2 Hydrogenation

Polyolefin are often hydrogenated chemoselectively using mildly reactive ruthenium complexes. RuCl₂(PPh₃)₃ and RuHCl(PPh₃)₃ are used to hydrogenated 3-oxo-1,4-diene steroidal compounds,[34] and Terminal conjugated dienes (**Figure 1.16**).[35]

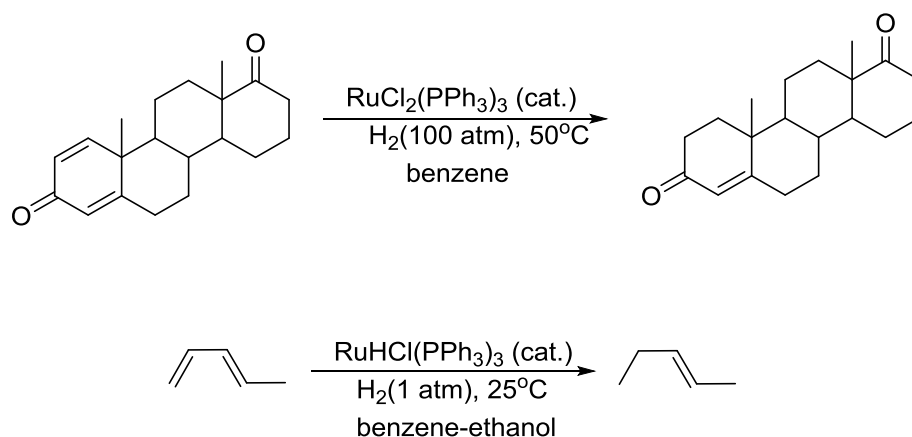


Figure 1.16 Reduction of steroidal compounds and Terminal conjugated dienes, regioselective reaction

RuCl₂(CO)(PPh₃)₃,[36] RuCl₂(PPh₃)₃,[37] and Ru(cod)(cot)[38] catalysts have been used for hydrogenation of cyclic triene to produce the cyclic monoolefin selectively.

Acenaphthylene produces 4,5-dihydroacenaphthylene[39] by regioselective hydrogenation by the utilization of $\text{Ru}_3(\text{CO})_{12}$ and H_2 . This observation is surprising, as usual hydrogenation of acenaphthylene takes place at the 1,2 position and the alkali metal hydrogenation produces 1,5-dihydroacenaphthylene (**Figure 1.17**).

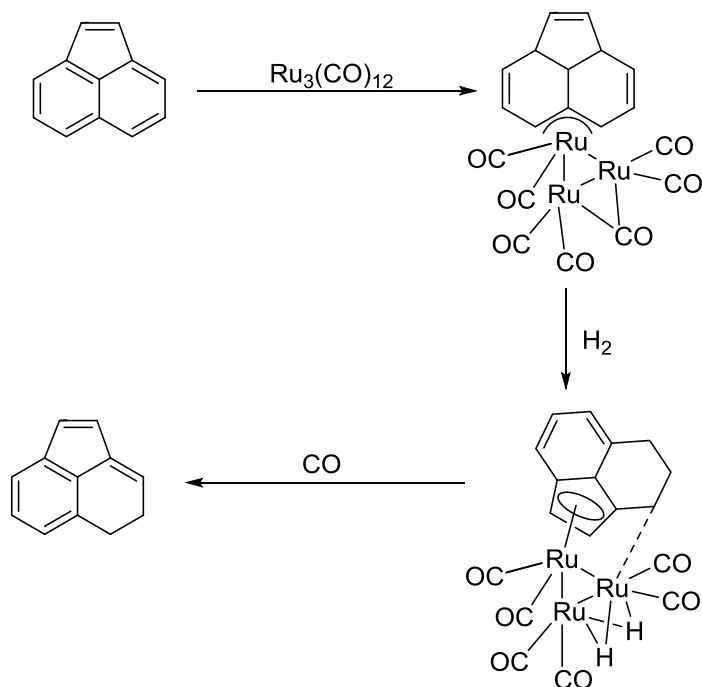


Figure 1.17 Reduction of acenaphthylene regioselective reaction

Aromatic and even aliphatic nitro compounds can also be easily transformed into the related primary amines with ruthenium catalysts in the presence of H_2 pressure. Hydrogenation of aromatic nitro compounds selectively can be achieved in the presence of acetylene moieties[40] and carbonyl by utilizing Ru-alumina catalyst and $\text{RuCl}_2(\text{PPh}_3)_3$ catalyst, respectively. Primary amines can be produced (**Figure 1.18**).

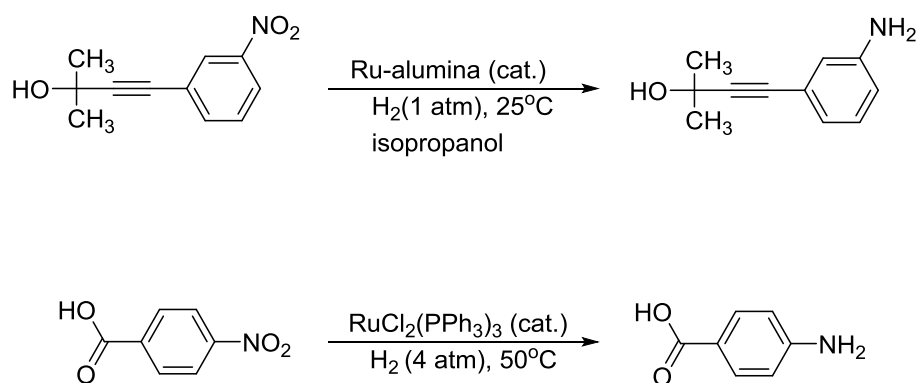


Figure 1.18 Reduction of nitro to amino group

from nitriles with very high selectivity by utilizing anionic ruthenium hydride complex catalyst.[41]

Various substrates like olefins, aldehydes, α,β -unsaturated ketones, ketones, quinolines, and imines, undergo hydrogen transfer from alcohols utilizing low valent ruthenium complex catalysts. Intramolecular transfer hydrogenation reactions occur in unsaturated alcohols such as propargyl alcohol[42] and allyl alcohol[43] to produce the α,β -unsaturated carbonyl and saturated compounds, respectively (**Figure 1.19**).

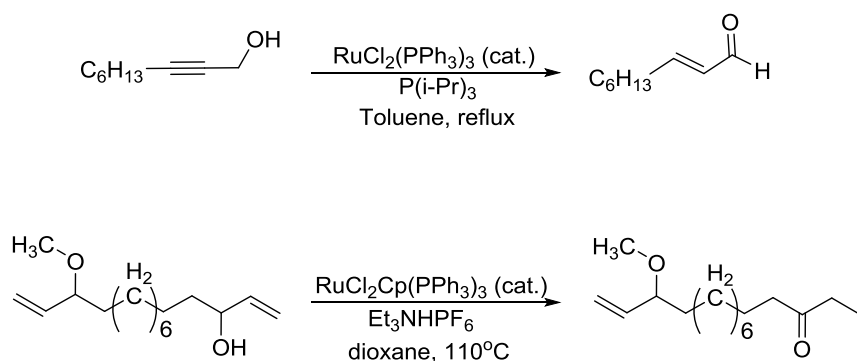


Figure 1.19 Reduction of propargyl and allyl alcohols

Alternatively, formic acid behaves as a hydrogen donor in a transfer hydrogenation reaction of aldehydes, ketones, α,β -unsaturated carbonyl reactants, and quinolines. The reaction starts with the ruthenium hydride complex formation on reacting ruthenium complex and formic acid along with the carbon dioxide exclusion.[44] Similarly, THF and tetrahydronaphthalene help in

the transfer hydrogenation reaction to carbonyl reactants which gives alcohols and the aromatic compounds (**Figure 1.20**).[45]

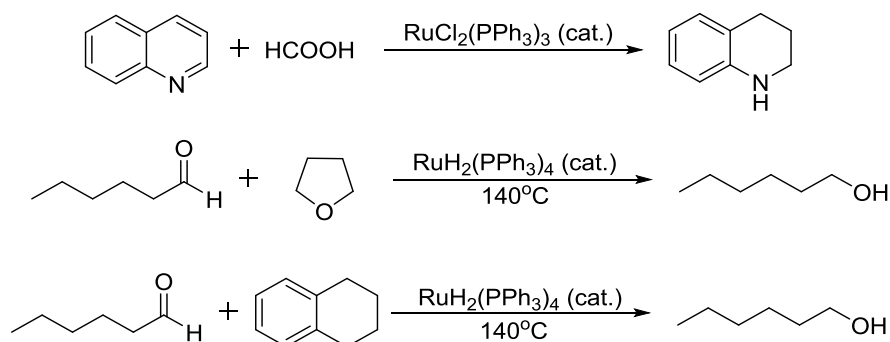


Figure 1.20 Reduction using formic acid, THF and tetrahydronaphthalene

1.3 Ferrocene based organometallic compounds and their antitumor applications

The ferrocene along with its subordinates are multitalented organometallic complexes owing to their distinctive chemical, structural as well as thermal stability along with reversible redox property. This unique character of their chemistry makes ferrocene derivatives as the excellent building blocks for several processes and their use in various fields like molecular wires, host-guest recognition, molecular sensing, material science, catalysis, charge transfer and electronic communication, as well as medicinal chemistry. The focus of these ferrocenyl derivatives for the applications associated with biological property made development in the field of bio-organometallic chemistry.[46-52]

The ferrocene use in the medicinal fields is an attractive research area. Several reports have listed ferrocene derivatives as highly appealing *in vitro* & *in vivo*, antagonistic towards several diseases which includes bacterial and fungal infections,[53,54] malaria

infection,[55] human immune-deficiency virus (HIV) infection,[56,57] and tumor or cancer.[58,59]

1.3.1. Ferrocene linked to biologically vital molecules as favourable anti-cancer candidates

1.3.1.1 Ferrocenylalkylazoles as active members for solid tumors

A variety of ferrocenylalkylazoles were synthesized, and they were in vivo studied for inhibition of tumor growth along with their toxicity level. Animals tolerated ferrocenylalkylazoles products easily in comparison with natural ferrocene or other clinical drugs.[60] The compound ferrocenyl-ethyl benzimidazole **2** and **3** (Figure 1.21) was found to be the best solid tumors, which inhibits tumor growth up to 100% followed by achieving 45% regression.

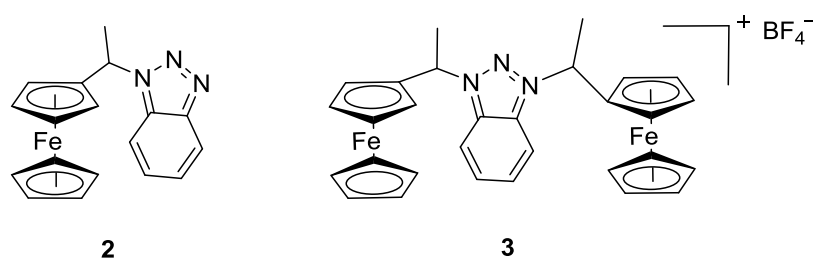


Figure 1.21 ferrocenyl pyrazole complex as anticancer agents

The reason for success is likely due to (a) the hydrophilic benzotriazolyl group can feasibly transport in aqueous media and the lipophilic ferrocenyl part maintains membrane permeability, (b) the ferrocenyl group is able to form ionic bond after oxidation along with the azolyl group which can easily form hydrogen bonds with phosphate groups on DNA cleavage points, (c) the ferrocenyl group and planar heterocycle are able to intercalate between the DNA planes, (d) the free alkyl bridge was responsible for the ligand-receptor complexes formation[60]

1.3.1.2 Ferrocenyl pyrazolyl as active anticancer members

A variety of ferrocene derivatives bearing pyrazolyl-moiety were evaluated for the inhibitory activities against A549, HepG2 and MDA-MB-45 cell lines utilizing the MTT method. Among them, compounds with R group piperidine (**3**), morpholine (**4**) and thiomorpholine (**5**) exhibited comparable antitumor biological activities in vitro against A549 and MDA-MB-45 to the positive control 5-fluorouracil (5-FU) (**Figure 1.22**).[61] All the synthesized derivatives exhibited average to effective antitumor activities against A549 cell line as compared to the known drug 5-fluorouracil.

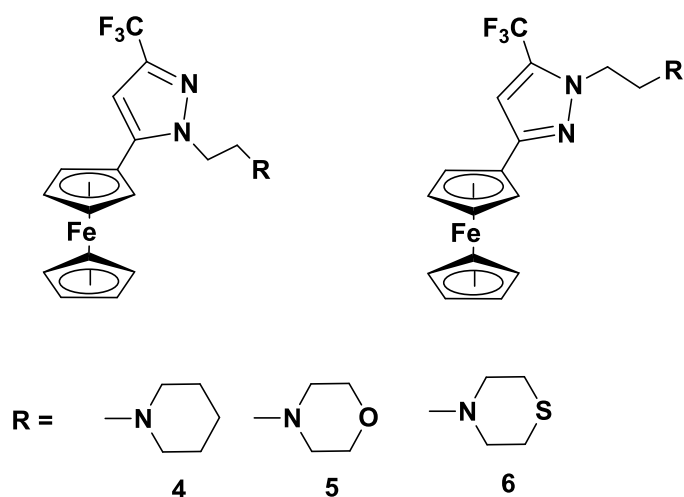


Figure 1.22 Ferrocenyl pyrazole complex as anticancer agents

1.3.1.3. Ferrocenyl acridine compounds targeting DNA

Ong's group synthesized compound **7** (**Figure 1.23**) by attaching ferrocene to acridine (a DNA intercalating agent) to compare anticancer activity with the similar ferrocenyl derivative without the acridine moiety (**8**) (**Figure 1.23**). The attachment of acridine makes the compound effective for binding with DNA but highly toxic towards cell lines.[62]

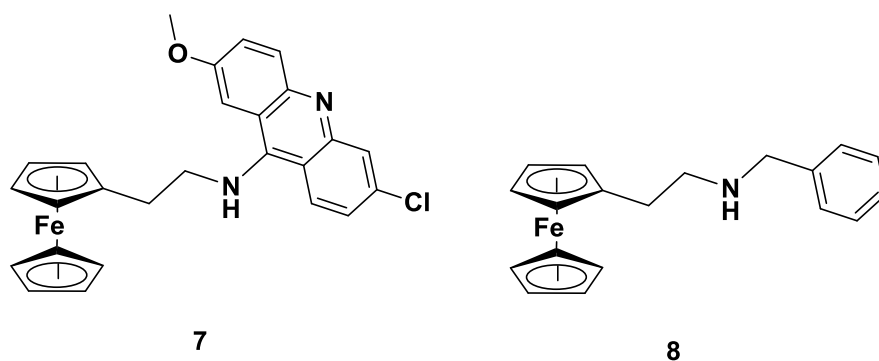


Figure 1.23 Ferrocenyl acridine complex for DNA intercalation[62]

1.3.1.4. Ferrocenyl azalactone and thiomorpholide compounds targeting topoisomerase

Topoisomerases are the class of enzymes which unwind and wind DNA to smooth DNA replication, and allow DNA control over the synthesis of different proteins. Azalactone-ferrocene (**9**) and thiomorpholide amido methyl-ferrocene (**10**) (**Figure 1.24**) were antagonists towards topoisomerase II activity which inhibited its activity resulting in neoplastic cell death.[63]

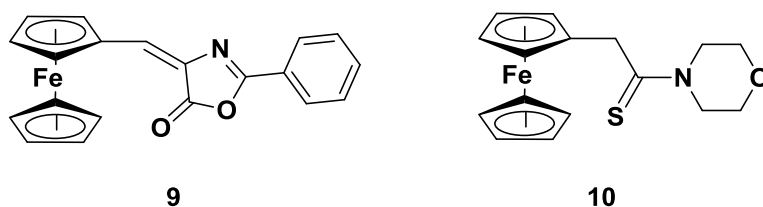


Figure 1.24 Azalactone-ferrocene (**9**) and thiomorpholide amido methyl-ferrocene (**10**) as inhibitors for topoisomerase II[63]

1.3.1.5. Ferrocenyl nilutamide for prostate cancer cells

Nilutamide (**11**) is an anti-androgen therapeutic agent for prostate cancer patients (**Figure 1.25**). A nilutamide linked to the ferrocenyl derivative drug (**12**) was made to study the anti-androgen effect.[64] It was not showing high androgen activity, but higher cytotoxic against hormone-independent prostate cancer cells was observed.

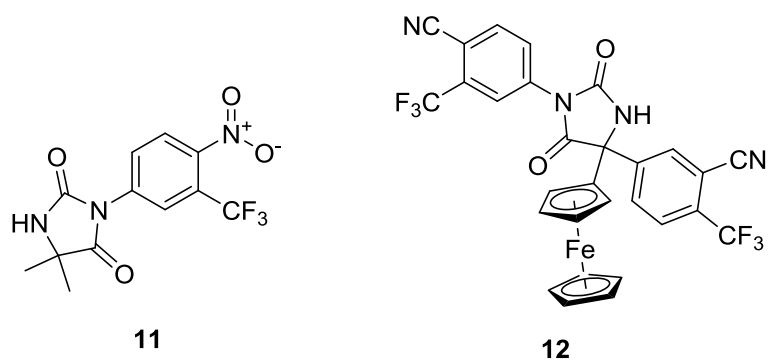


Figure 1.25 Nilutamide (**11**) and structurally related ferrocenyl compound

1.3.1.6. Compounds containing ferrocenyl group along with various transition metals

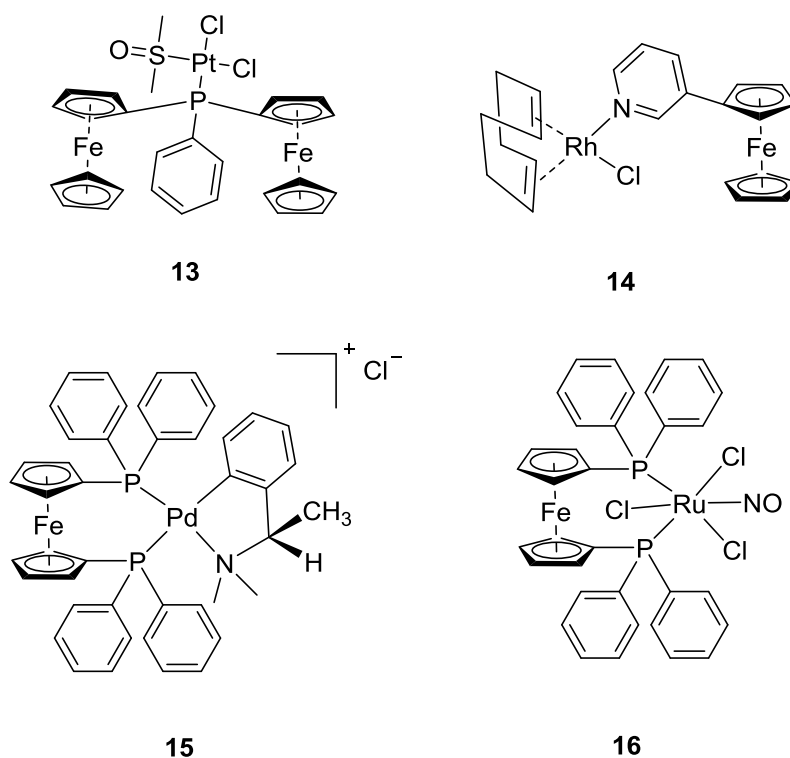


Figure 1.26 Transition metal-based ferrocenyl compounds as antitumor agents

Al-Allaf et al. synthesized $\text{cis-[Pt(Fc}_2\text{PhP)(DMSO)Cl}_2\text{]}$ (**13**) which was antitumor against leukaemia cell line P388.[65] Complex **13** showed IC_{50} values near to cisplatin and 5-fluorouracil's IC_{50} value.[65] Various metal complexes were synthesized by Rajput et al.

among which rhodium-ferrocenyl complex **14** was most active against cell line WHCO1 for growth inhibitory activity (**Figure 1.26**).^[66] The mononucleated ionic palladacycle-ferrocene complex **15** initiates the lysosomal membrane permeation along with the release of cathepsin B lysosomal enzymes to the cytosol of K562 cells.^[67] The finding was important to give the mode of action for strengthening the clinical therapy base. Von Poelhsitz et al. reported the ruthenium complex fac-[RuCl₃(NO)(dppfc)](**16**).^[68] The complex showed higher cytotoxicity on MDA-MB-231 breast tumor cells, and it was found to be six times more active than cisplatin.

1.3.1.7. Ferrocifens, ferrocifenols and ferrocenophanes for targeting breast cancer cells

The ferrocifens are probably the most promising candidates for breast cancer. Patients with ER-positive breast cancer usually prescribed with tamoxifen (**17**).^[69] It was found that on MCF-7 cells, the effect of the hydroxyferrocifens (**19**) is competitive with hydroxytamoxifen (**18**), and is slightly more effective at 0.1 mM concentration (**Figure 1.27**).

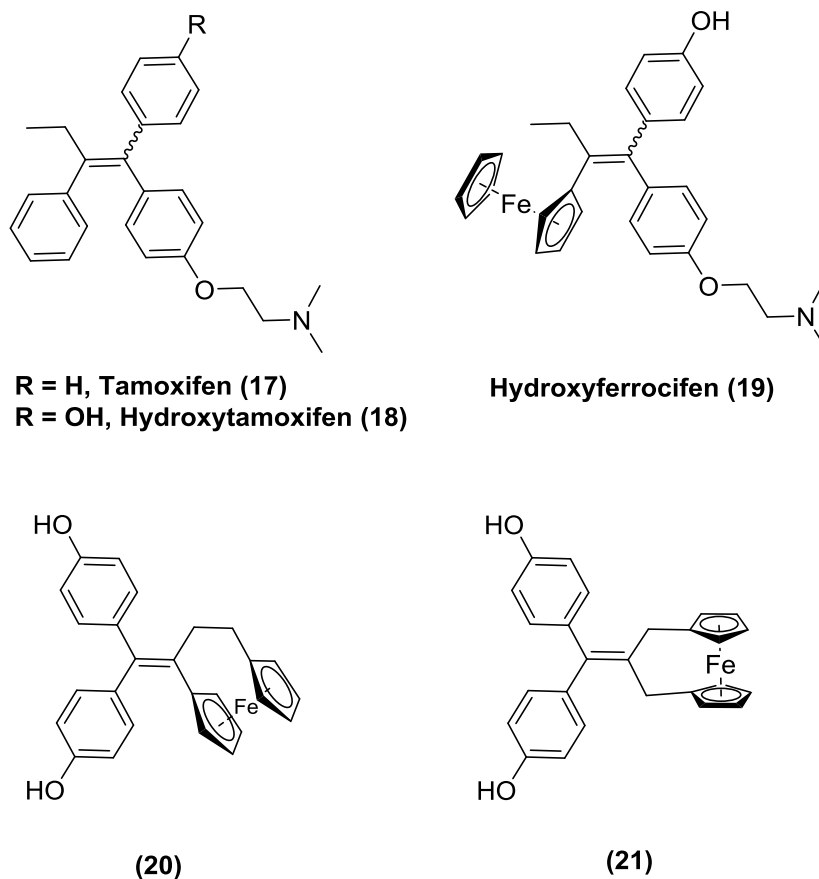


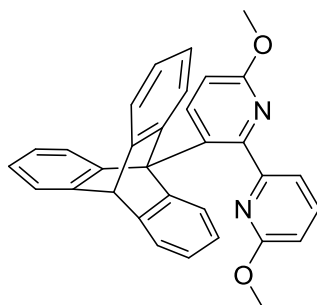
Figure 1.27 Ferrocifens, ferrocifenols and ferrocenophanes as antitumor agents

Ferrociphanes **20** and **21** showed an exceptionally high anti-proliferative effect on the MDA-MB-231 and PC-3 cells with an IC50 value of 0.09 mM.[70,71]

1.4 Importance of triptycene and ferrocene in Supramolecules

Triptycene and ferrocene were used for co-crystal formations. Triptycene has been significant due to its particular rigid fan-shaped structure. It was utilized as a tricyclic molecular brake shoe (triptycene-6,6'-dimethoxy-2,2'-bipyridine conjugate) (**22**) at the beginning (**Figure 1.28**) and then forms a molecular “ratchet” (4-

methylbenzo[*c*]phenanthrene-triptycene conjugate) (**23**), which was used to develop a molecular motor.[72]



22

Figure 1.28 Molecular brake shoe structure utilizing triptycene and 6,6'-dimethoxy-2,2'-bipyridine derivative

The addition of mercuric ion to free triptycene-6,6'-dimethoxy-2,2'-bipyridine conjugate applies the brake and slows the rotation of the triptycene. The brakes were unengaged simply by EDTA addition, which removes the mercuric ion and converts constrained to free triptycene-6,6'-dimethoxy-2,2'-bipyridine conjugate (**Figure 1.29**).

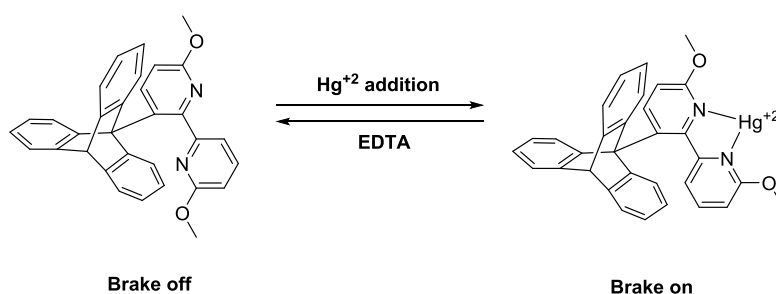
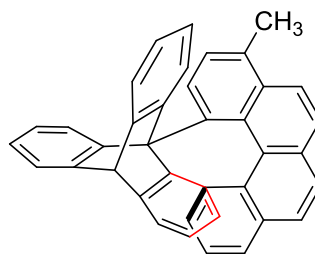


Figure 1.29 Engagement and disengagement of brake using Hg²⁺ and EDTA

Furthermore, the molecular brake molecule was modified, and the addition of 4-methylbenzo[*c*]phenanthrene to triptycene produced the molecular faucets successfully (**Figure 1.30**).



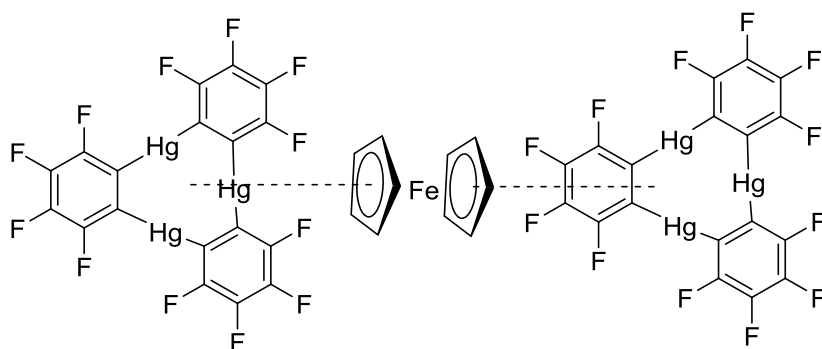
23

Figure 1.30 Molecular ratchet structure utilizing triptycene and terpene derivative

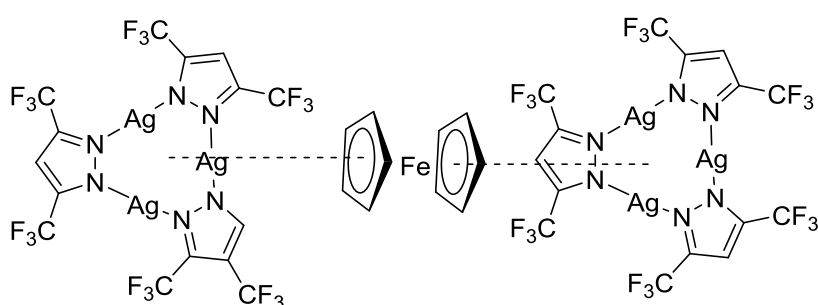
Variety of hosts, including triptycene derived tris(crown ether)s, cylindrical macro-tricyclic polyether, molecular tweezers, calixarenes, azacalixarenes, oxacalixarenes, tetra-lactam macrocycles, and other molecular cages have been obtained.

The hosts have the ability for powerful complexation with different kind of guests, preferably organic guest molecules, which produce different supramolecular identities, such as acid-base controlled [3]rotaxane-based molecular machine, ion-controlled binding and release of the guest in one complex, the chemically controlled competition for complexation, isomeric [2]rotaxanes and high order interlocked assemblies.

Ferrocene (FcH) and its derivatives have rich inclusion chemistry and attract much attention till date, due to their functionality as compact, electron rich guest molecules in host-guest supramolecular ensembles.[73] In most cases, one of the significant stabilizing interactions in the non-charge-transfer complex FcH cocrystals is a π - π interaction between cp ring of a neutral FcH molecule and aromatic hydrocarbon,[74] poly-fluorinated aromatics,[75-77] fullerenes[78,79] etc. It acts as an electron-rich unit in π_{cp} -associates with Hg (**24**)[80] and similarly with Ag (**25**), Cu-Bis(trifluoromethyl)pyrazolate complex (**Figure 1.31**).[81]



24



25

Figure 1.31 Supramolecular interaction present between ferrocene and Hg-Tetrafluorobenzene and Ag-Bis(trifluoromethyl)pyrazolate complex

Without any apparent stabilization by specific intermolecular interactions; neutral FcH molecules can also form inclusion compounds, entering the cavities of calixarenes,[82-87] cyclodextrins,[88,89] and cucurbiturils[90] filling the channels formed by thiourea[91,92] and tetracyanoethylene complex (**26**),[91] organic porous crystals[93] and MOFs (**Figure 1.32**).[94]

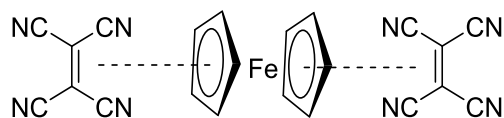


Figure 1.32 Supramolecular interaction present between ferrocene and tetracyanoethylene

1.5 References

- [1] Albrecht M., Schlupp M., Bargon J., Kotten G. v. (2001), Detection of ppm quantities of gaseous SO by organoplatinum dendritic sites immobilised on a quartz microbalance. *Chem. Commun.*(18), 1874-1875 doi:10.1039/B105660N
- [2] Schlupp M., Weil T., Berresheim A. J., Wiesler U. M., Bargon J., Müllen K. (2001), Polyphenylen-Dendrimere als empfindliche und selektive Sensorschichten. *Angew. Chem.*, 113(21), 4124-4129 doi:10.1002/1521-3757(20011105)113:21<4124::AID-ANGE4124>3.0.CO;2-2
- [3] Luconi L., Klosin J., Smith A. J., Germain S., Schulz E., Hannedouche J., Giambastiani G. (2013), Cationic Group-IV pincer-type complexes for polymerization and hydroamination catalysis. *Dalton Trans.*, 42(45), 16056-16065 doi:10.1039/C3DT51620B
- [4] Sarkar S., McGowan K. P., Kuppuswamy S., Ghiviriga I., Abboud K. A., Veige A. S. (2012), An OCO₃⁻ Trianionic Pincer Tungsten(VI) Alkylidyne: Rational Design of a Highly Active Alkyne Polymerization Catalyst. *J. Am. Chem. Soc.*, 134(10), 4509-4512 doi:10.1021/ja2117975
- [5] Prier C. K., Rankic D. A., MacMillan D. W. C. (2013), Visible Light Photoredox Catalysis with Transition Metal Complexes: Applications in Organic Synthesis. *Chem. Rev.*, 113(7), 5322-5363 doi:10.1021/cr300503r
- [6] Albrecht M., Gossage R. A., Lutz M., Spek A. L., van Kotten G. (2000), Diagnostic Organometallic and Metallodendritic Materials for SO₂ Gas Detection: Reversible Binding of Sulfur Dioxide to Arylplatinum(II) Complexes. *Chem. - Eur. J.*, 6(8), 1431-1445 doi:10.1002/(SICI)1521-3757(20000417)6:8<1431::AID-CHEM1431>3.0.CO;2-D

- [7] Albrecht M., van Koten G. (2001), Platinum Group Organometallics Based on “Pincer” Complexes: Sensors, Switches, and Catalysts. *Angew. Chem. Int. Ed.*, 40(20), 3750-3781 doi:10.1002/1521-3773(20011015)40:20<3750::AID-ANIE3750>3.0.CO;2-6
- [8] Murahashi S. I. (2005).
- [9] Copéret C., Chabanas M., Petroff Saint-Arroman R., Basset J.-M. (2003), Homogeneous and Heterogeneous Catalysis: Bridging the Gap through Surface Organometallic Chemistry. *Angew. Chem. Int. Ed.*, 42(2), 156-181 doi:10.1002/anie.200390072
- [10] Boudier A., Bromm L. O., Lotz M., Knochel P. (2000), New Applications of Polyfunctional Organometallic Compounds in Organic Synthesis. *Angew. Chem. Int. Ed.*, 39(24), 4414-4435 doi:10.1002/1521-3773(20001215)39:24<4414::AID-ANIE4414>3.0.CO;2-C
- [11] Albrecht M., Rodríguez G., Schoenmaker J., van Koten G. (2000), New Peptide Labels Containing Covalently Bonded Platinum(II) Centers as Diagnostic Biomarkers and Biosensors. *Org. Lett.*, 2(22), 3461-3464 doi:10.1021/ol006484l
- [12] Markó I. E., Giles P. R., Tsukazaki M., Chellé-Regnaut I., Urch C. J., Brown S. M. (1997), Efficient, Aerobic, Ruthenium-Catalyzed Oxidation of Alcohols into Aldehydes and Ketones. *J. Am. Chem. Soc.*, 119(51), 12661-12662 doi:10.1021/ja973227b
- [13] Carlsen P. H. J., Katsuki T., Martin V. S., Sharpless K. B. (1981), A greatly improved procedure for ruthenium tetroxide catalyzed oxidations of organic compounds. *J. Org. Chem.*, 46(19), 3936-3938 doi:10.1021/jo00332a045

- [14] Morris P. E., Kiely D. E. (1987), Ruthenium tetroxide phase-transfer-promoted oxidation of secondary alcohols to ketones. *J. Org. Chem.*, 52(6), 1149-1152 doi:10.1021/jo00382a035
- [15] Torii S., Inokuchi T., Kondo K. (1985), A facile procedure for oxidative cleavage of enolic olefins to the carbonyl compounds with ruthenium tetroxide (RuO₄). *J. Org. Chem.*, 50(24), 4980-4982 doi:10.1021/jo00224a071
- [16] Shing T. K. M., Tai V. W. F., Tam E. K. W. (1994), Practical and Rapid Vicinal Hydroxylation of Alkenes by Catalytic Ruthenium Tetraoxide. *Angew. Chem. Int. Ed. Engl.*, 33(22), 2312-2313 doi:10.1002/anie.199423121
- [17] Tanaka K.-I., Yoshifuji S., Nitta Y. (1986), A New Approach for the Total Synthesis of L- γ -Carboxyglutamic Acid : Utility of Ruthenium Tetroxide Oxidation. *Chem. Pharm. Bull.*, 34(9), 3879-3884 doi:10.1248/cpb.34.3879
- [18] Tenaglia A., Terranova E., Waegell B. (1989), Ruthenium-catalyzed C-H bond activation oxidation of bridged bicyclic and tricyclic alkanes. *Tetrahedron Lett.*, 30(39), 5271-5274 doi:10.1016/S0040-4039(01)93761-X
- [19] Tsuji Y., Ohta T., Ido T., Minbu H., Watanabe Y. (1984), Ruthenium-catalyzed oxidation of alcohols and catechols using t-butyl hydroperoxide. *J. Organomet. Chem.*, 270(3), 333-341 doi:10.1016/0022-328X(84)80381-2
- [20] Sharpless K. B., Akashi K., Oshima K. (1976), Ruthenium catalyzed oxidation of alcohols to aldehydes and ketones by amine-n-oxides. *Tetrahedron Lett.*, 17(29), 2503-2506 doi:10.1016/S0040-4039(00)78130-5
- [21] Higuchi T., Ohtake H., Hirobe M. (1991), Highly efficient oxygen transfer reactions from various heteroaromatic n-oxides to

olefins, alcohols, and sulfides catalyzed by ruthenium porphyrin. *Tetrahedron Lett.*, 32(50), 7435-7438 doi:10.1016/0040-4039(91)80127-R

[22] Barak G., Dakka J., Sasson Y. (1988), Selective oxidation of alcohols by a H₂O₂-RuCl₃ system under phase-transfer conditions. *J. Org. Chem.*, 53(15), 3553-3555 doi:10.1021/jo00250a025

[23] Murahashi S.-I., Naota T. (1993), Ruthenium-Catalyzed Oxidations for Selective Syntheses of Ketones and Acyl Cyanides. Selective Acylation of Amino Compounds with Acyl Cyanides. *Synthesis*, 1993(04), 433-440 doi:10.1055/s-1993-25877

[24] Matsumoto M., Ito S. (1984), Ruthenium-Catalyzed Aerobic Oxidation of Pantoyl Lactone to Ketopantoyl Lactone. *Synth. Commun.*, 14(7), 697-700 doi:10.1080/00397918408063756

[25] Matsumoto M., Ito S. (1981), Ruthenium-catalysed oxidation of allyl alcohols by molecular oxygen. *J. Chem. Soc., Chem. Commun.*(17), 907-908 doi:10.1039/C39810000907

[26] Bilgrien C., Davis S., Drago R. S. (1987), The selective oxidation of primary alcohols to aldehydes by oxygen employing a trinuclear ruthenium carboxylate catalyst. *J. Am. Chem. Soc.*, 109(12), 3786-3787 doi:10.1021/ja00246a049

[27] Murahashi S., Naota T., Yonemura K. (1988), Ruthenium-catalyzed cytochrome P-450 type oxidation of tertiary amines with alkyl hydroperoxides. *J. Am. Chem. Soc.*, 110(24), 8256-8258 doi:10.1021/ja00232a060

[28] Tang R., Diamond S. E., Neary N., Mares F. (1978), Homogeneous catalytic oxidation of amines and secondary alcohols by molecular oxygen. *J. Chem. Soc., Chem. Commun.*(13), 562-562 doi:10.1039/C39780000562

- [29] Menashe N., Shvo Y. (1993), Hydration of alkynes in anhydrous medium with formic acid as water donor. *J. Org. Chem.*, 58(26), 7434-7439 doi:10.1021/jo00078a023
- [30] Leung T., James B. R., Dolphin D. (1983), Catalytic oxidation of hydrocarbons using iodosylbenzene in the presence of a ruthenium(III) porphyrin complex. *Inorg. Chim. Acta*, 79, 180-181 doi:10.1016/S0020-1693(00)95214-9
- [31] Groves J. T., Bonchio M., Carofiglio T., Shalyaev K. (1996), Rapid Catalytic Oxygenation of Hydrocarbons by Ruthenium Pentafluorophenylporphyrin Complexes: Evidence for the Involvement of a Ru(III) Intermediate. *J. Am. Chem. Soc.*, 118(37), 8961-8962 doi:10.1021/ja9542092
- [32] Murahashi S.-I., Naota T., Komiya N. (1995), Metalloporphyrin-Catalyzed Oxidation of Alkanes with Molecular Oxygen in the Presence of Acetaldehyde. *Tetrahedron Lett.*, 36(44), 8059-8062 doi:10.1016/0040-4039(95)01708-P
- [33] Murahashi S., Oda Y., Naota T. (1992), Iron- and ruthenium-catalyzed oxidations of alkanes with molecular oxygen in the presence of aldehydes and acids. *J. Am. Chem. Soc.*, 114(20), 7913-7914 doi:10.1021/ja00046a048
- [34] Tsuji J., Suzuki H. (1977), Homogeneous selective hydrogenation of cyclododecatriene, cyclooctadiene, and 1,6-dienes to the corresponding monoenes catalyzed by $\text{RuCl}_2(\text{PPh}_3)_3$. *Chem. Lett.*, 6(9), 1083-1084 doi:10.1246/cl.1977.1083
- [35] Hallman P. S., Evans D., Osborn J. A., Wilkinson G. (1967), Selective catalytic homogeneous hydrogenation of terminal olefins using tris(triphenylphosphine)hydridochlororuthenium(II); hydrogen transfer in exchange and isomerisation reactions of olefins. *Chem. Commun. (London)*(7), 305-306 doi:10.1039/C19670000305

- [36] Ng F. T. T., Henry P. M. (1973), Palladium(II)-catalyzed exchange and isomerization reactions. X. Acid-catalyzed exchange of 2-cyclohexen-1-yl esters with acetic acid. *J. Org. Chem.*, 38(19), 3338-3343 doi:10.1021/jo00959a021
- [37] Tsuji J., Suzuki H. (1977), Homogeneous hydrogenation of aldehydes to alcohols catalyzed by $\text{RuCl}_2(\text{PPh}_3)_3$. *Chem. Lett.*, 6(9), 1085-1086 doi:10.1246/cl.1977.1085
- [38] Airoidi M., Deganello G., Dia G., Gennaro G. (1980), Selective, homogeneous hydrogenation of cycloheptatriene to cycloheptene catalyzed by $(\eta^4\text{-cycloocta-1,5-diene})(\eta^6\text{-cyclohepta-1,3,5-triene})\text{ruthenium}(0)$. *J. Organomet. Chem.*, 187(3), 391-403 doi:10.1016/S0022-328X(00)93432-6
- [39] Canne L. E., Bark S. J., Kent S. B. H. (1996), Extending the Applicability of Native Chemical Ligation. *J. Am. Chem. Soc.*, 118(25), 5891-5896 doi:10.1021/ja960398s
- [40] Onopchenko A., Sabourin E. T., Selwitz C. M. (1979), Selective catalytic hydrogenation of aromatic nitro groups in the presence of acetylenes. Synthesis of (3-aminophenyl)acetylene via hydrogenation of dimethylcarbinol substituted (3-nitrophenyl)acetylene over heterogeneous metallic ruthenium catalyst. *J. Org. Chem.*, 44(8), 1233-1236 doi:10.1021/jo01322a008
- [41] Grey R. A., Pez G. P., Wallo A. (1981), Anionic metal hydride catalysts. 2. Application to the hydrogenation of ketones, aldehydes, carboxylic acid esters, and nitriles. *J. Am. Chem. Soc.*, 103(25), 7536-7542 doi:10.1021/ja00415a022
- [42] Ma D., Lu X. (1989), A simple route to α,β -unsaturated aldehydes from prop-2-ynols. *J. Chem. Soc., Chem. Commun.*(14), 890-891 doi:10.1039/C39890000890

- [43] Trost B. M., Kulawiec R. J. (1993), Chemoselectivity in the ruthenium-catalyzed redox isomerization of allyl alcohols. *J. Am. Chem. Soc.*, *115*(5), 2027-2036 doi:10.1021/ja00058a059
- [44] Watanabe Y., Ohta T., Tsuji Y., Hiyoshi T., Tsuji Y. (1984), Ruthenium Catalyzed Reduction of Nitroarenes and Azaaromatic Compounds Using Formic Acid. *Bull. Chem. Soc. Jpn.*, *57*(9), 2440-2444 doi:10.1246/bcsj.57.2440
- [45] Imai H., Nishiguchi T., Fukuzumi K. (1976), Transfer hydrogenation and transfer hydrogenolysis. IX. Hydrogen transfer from organic compounds to aldehydes and ketones catalyzed by dihydridotetrakis(triphenylphosphine)ruthenium(II). *J. Org. Chem.*, *41*(4), 665-671 doi:10.1021/jo00866a016
- [46] Sun R., Wang L., Yu H., Abdin Z.-u., Chen Y., Huang J., Tong R. (2014), Molecular Recognition and Sensing Based on Ferrocene Derivatives and Ferrocene-Based Polymers. *Organometallics*, *33*(18), 4560-4573 doi:10.1021/om5000453
- [47] Heinze K., Lang H. (2013), Ferrocene—Beauty and Function. *Organometallics*, *32*(20), 5623-5625 doi:10.1021/om400962w
- [48] Takebayashi S., Shibata T. (2012), [Ir(cod)₂]BARF-Catalyzed C–H Bond Alkenylation and Alkylation of Ferrocenes. *Organometallics*, *31*(11), 4114-4117 doi:10.1021/om300348e
- [49] Skibar W., Kopacka H., Wurst K., Salzmann C., Ongania K.-H., Fabrizi de Biani F., . . . Bildstein B. (2004), α,ω -Diferrocenyl Cumulene Molecular Wires. Synthesis, Spectroscopy, Structure, and Electrochemistry. *Organometallics*, *23*(5), 1024-1041 doi:10.1021/om034233l
- [50] Fish R. H., Jaouen G. (2003), Bioorganometallic Chemistry: Structural Diversity of Organometallic Complexes with Bioligands and Molecular Recognition Studies of Several Supramolecular Hosts with

Biomolecules, Alkali-Metal Ions, and Organometallic Pharmaceuticals.

Organometallics, 22(11), 2166-2177 doi:10.1021/om0300777

[51] Dong T.-Y., Chang L.-S., Tseng I. M., Huang S.-J. (2004), Electroactive Self-Assembled Biferrocenyl Alkanethiol Monolayers on Au(111) Surface and on Gold Nanoclusters. *Langmuir*, 20(11), 4471-4479 doi:10.1021/la0303714

[52] Braga S. S., Silva A. M. S. (2013), A New Age for Iron: Antitumoral Ferrocenes. *Organometallics*, 32(20), 5626-5639 doi:10.1021/om400446y

[53] Zhang J. (2008), Preparation, characterization, crystal structure and bioactivity determination of ferrocenyl-thiazoleacylhydrazones. *Appl. Organomet. Chem.*, 22(1), 6-11 doi:10.1002/aoc.1338

[54] Biot C., François N., Maciejewski L., Brocard J., Poulain D. (2000), Synthesis and antifungal activity of a ferrocene-fluconazole analogue. *Bioorg. Med. Chem. Lett.*, 10(8), 839-841 doi:10.1016/S0960-894X(00)00120-7

[55] Fouda M. F. R., Abd-Elzaher M. M., Abdelsamaia R. A., Labib A. A. (2007), On the medicinal chemistry of ferrocene. *Appl. Organomet. Chem.*, 21(8), 613-625 doi:10.1002/aoc.1202

[56] Kerman K., Kraatz H.-B. (2009), Electrochemical probing of HIV enzymes using ferrocene-conjugated peptides on surfaces. *Analyst*, 134(12), 2400-2404 doi:10.1039/B912083A

[57] Mahmoud K. A., Luong J. H. T. (2008), Impedance Method for Detecting HIV-1 Protease and Screening For Its Inhibitors Using Ferrocene-Peptide Conjugate/Au Nanoparticle/Single-Walled Carbon Nanotube Modified Electrode. *Anal. Chem.*, 80(18), 7056-7062 doi:10.1021/ac801174r

[58] Wani W. A., Baig U., Shreaz S., Shiekh R. A., Iqbal P. F., Jameel E., . . . Ting Hun L. (2016), Recent advances in iron complexes

as potential anticancer agents. *New J. Chem.*, 40(2), 1063-1090
doi:10.1039/C5NJ01449B

[59] Meléndez E. (2012), Metallocenes as target specific drugs for cancer treatment. *Inorg. Chim. Acta*, 393, 36-52
doi:10.1016/j.ica.2012.06.007

[60] Snegur L. V., Nekrasov Y. S., Sergeeva N. S., Zhilina Z. V., Gumenyuk V. V., Starikova Z. A., . . . Babin V. N. (2008), Ferrocenylalkyl azoles: bioactivity, synthesis, structure. *Appl. Organomet. Chem.*, 22(2), 139-147 doi:10.1002/aoc.1362

[61] Huang X.-F., Wang L.-Z., Tang L., Lu Y.-X., Wang F., Song G.-Q., Ruan B.-F. (2014), Synthesis, characterization and antitumor activity of novel ferrocene derivatives containing pyrazolyl-moiety. *J. Organomet. Chem.*, 749, 157-162
doi:10.1016/j.jorganchem.2013.08.043

[62] Ong C.-W., Jeng J.-Y., Juang S.-S., Chen C.-F. (1992), A ferrocene-intercalator conjugate with a potent cytotoxicity. *Bioorg. Med. Chem. Lett.*, 2(9), 929-932 doi:10.1016/S0960-894X(00)80590-9

[63] Sai Krishna A. D., Panda G., Kondapi A. K. (2005), Mechanism of action of ferrocene derivatives on the catalytic activity of topoisomerase II α and β —Distinct mode of action of two derivatives. *Arch. Biochem. Biophys.*, 438(2), 206-216
doi:10.1016/j.abb.2005.04.014

[64] Top S., Thibaudeau C., Vessières A., Brulé E., Le Bideau F., Joerger J.-M., . . . Jaouen G. (2009), Synthesis and Structure Activity Relationship of Organometallic Steroidal Androgen Derivatives. *Organometallics*, 28(5), 1414-1424 doi:10.1021/om800698y

[65] Al-Allaf T. A. K., Rshan L. J. (1999), Heterobimetallic complexes of platinum(II) with diferrocenylphenylphosphine and their in vitro activity against P388 leukaemia. *Appl. Organomet. Chem.*,

13(1), 63-68 doi:10.1002/(SICI)1099-0739(199901)13:1<63::AID-AOC815>3.0.CO;2-1

[66] Rajput J., Moss J. R., Hutton A. T., Hendricks D. T., Arendse C. E., Imrie C. (2004), Synthesis, characterization and cytotoxicity of some palladium(II), platinum(II), rhodium(I) and iridium(I) complexes of ferrocenylpyridine and related ligands. Crystal and molecular structure of trans-dichlorobis(3-ferrocenylpyridine)palladium(II). *J. Organomet. Chem.*, 689(9), 1553-1568 doi:10.1016/j.jorganchem.2004.01.034

[67] Barbosa C. M. V., Oliveira C. R., Nascimento F. D., Smith M. C. M., Fausto D. M., Soufen M. A., . . . Caires A. C. F. (2006), Biphosphinic palladacycle complex mediates lysosomal-membrane permeabilization and cell death in K562 leukaemia cells. *Eur. J. Pharmacol.*, 542(1), 37-47 doi:10.1016/j.ejphar.2006.06.004

[68] Von Poelhsitz G., Bogado A. L., de Araujo M. P., Selistre-de-Araújo H. S., Ellena J., Castellano E. E., Batista A. A. (2007), Synthesis, characterization, X-ray structure and preliminary in vitro antitumor activity of the nitrosyl complex *fac*-[RuCl₃(NO)(dppf)], dppf=1,1'-bis(diphenylphosphine)ferrocene. *Polyhedron*, 26(16), 4707-4712 doi:10.1016/j.poly.2007.03.009

[69] Hillard E., Vessières A., Thouin L., Jaouen G., Amatore C. (2005), Ferrocene-Mediated Proton-Coupled Electron Transfer in a Series of Ferrocifen-Type Breast-Cancer Drug Candidates. *Angew. Chem.*, 118(2), 291-296 doi:10.1002/ange.200502925

[70] Görmen M., Pigeon P., Top S., Hillard E. A., Huché M., Hartinger C. G., . . . Jaouen G. (2010), Synthesis, Cytotoxicity, and COMPARE Analysis of Ferrocene and [3]Ferrocenophane Tetrasubstituted Olefin Derivatives against Human Cancer Cells. *ChemMedChem*, 5(12), 2039-2050 doi:10.1002/cmdc.201000286

- [71] Plažuk D., Vessières A., Hillard E. A., Buriez O., Labbé E., Pigeon P., . . . Jaouen G. (2009), A [3]Ferrocenophane Polyphenol Showing a Remarkable Antiproliferative Activity on Breast and Prostate Cancer Cell Lines. *J. Med. Chem.*, 52(15), 4964-4967 doi:10.1021/jm900297x
- [72] Kelly T. R. (2001), Progress toward a Rationally Designed Molecular Motor. *Acc. Chem. Res.*, 34(6), 514-522 doi:10.1021/ar000167x
- [73] Peng L., Feng A., Huo M., Yuan J. (2014), Ferrocene-based supramolecular structures and their applications in electrochemical responsive systems. *Chem. Commun.*, 50(86), 13005-13014 doi:10.1039/C4CC05192K
- [74] Atencio R., Domasevitch K. V., Zaworotko M. J. (2000), Structural Conformation and Optical and Electrochemical Properties of Imidazolyl-Substituted Naphthalenediimide and Its HgII, CdII, and CuII Halide Complexes. *Cryst. Eng.*, 2000(3), 63 doi:10.5517/cc4rph1
- [75] Day M. W. M., A.J. Grubbs, R.H. (2002), CCDC 130854: Experimental Crystal Structure Determination. *CSD Communication* doi:10.5517/cc4d53s
- [76] Clyburne J. A. C., Hamilton, T., & Jenkins, H. A. (2001), *Acta Crystallogr., Sect. C: Cryst. Struct. Commun.*, 4, 1 doi:10.5517/cc57gqk
- [77] Batsanov A. S., Collings J. C., Marder T. B. (2006), *Acta Cryst. C*, 62, m229-m231
- [78] Olmstead M. M., Hao L., Balch A. L. (1999), Organometallic C70 chemistry. Preparation and crystallographic studies of (η^2 -C70)Pd(PPh₃)₂·CH₂Cl₂ and (C70)·2{(η^5 -C₅H₅)₂Fe}. *J. Organomet. Chem.*, 578(1), 85-90 doi:10.1016/S0022-328X(98)01108-5
- [79] Crane J. D., Hitchcock P. B., Kroto H. W., Taylor R., Walton D. R. M. (1992), Preparation and characterisation of C₆₀(ferrocene)₂. *J.*

Chem. Soc., Chem. Commun.(24), 1764-1765
doi:10.1039/C39920001764

[80] Tikhonova I. A., Dolgushin F. M., Tugashov K. I., Petrovskii P. V., Antipin M. Y., Shur V. B. (2004), Binding of ferrocene by cyclic trimeric perfluoro-o-phenylenemercury. Synthesis and structure of the first double-decker sandwich complex of a sandwich. *Russ. Chem. Bull.*, 53(12), 2871-2873 doi:10.1007/s11172-005-0205-8

[81] Tsupreva V. N., Titov A. A., Filippov O. A., Bilyachenko A. N., Smol'yakov A. F., Dolgushin F. M., . . . Shubina E. S. (2011), Peculiarities of the Complexation of Copper and Silver Adducts of a 3,5-Bis(trifluoromethyl)pyrazolate Ligand with Organoiron Compounds. *Inorg. Chem.*, 50(8), 3325-3331 doi:10.1021/ic102132v

[82] MacGillivray L. R., Spinney H. A., Reid J. L., Ripmeester J. A. (2000), Entrapment of ferrocenes within supramolecular, deep-cavity resorcin[4]arenes. *Chem. Commun.*(6), 517-518
doi:10.1039/A909745G

[83] Wang Y.-J., Liu J.-L., Yang H.-M., Jia A.-Q., Zhang Q.-F. (2016), Inclusion of ferrocene within the deepened cavities formed from the hydrogen bonding self-assembly of calix[4]resorcinarenes with bis-pyridines. *J. Inclusion Phenom. Macrocyclic Chem.*, 85(1), 105-110 doi:10.1007/s10847-016-0609-0

[84] Hardie M. J. (2002), Solid State Confinement of Ferrocene by Calixarenes. *Supramol. Chem.*, 14(1), 7-10
doi:10.1080/10610270290006529

[85] Frišćić T., MacGillivray L. R. (2003), Double inclusion of ferrocene within a doubly interpenetrated three-dimensional framework based on a resorcin[4]arene. *J. Organomet. Chem.*, 666(1), 43-48 doi:10.1016/S0022-328X(02)02031-4

- [86] Mossine A. V., Kumari H., Fowler D. A., Shih A., Kline S. R., Barnes C. L., Atwood J. L. (2012), Ferrocene Species Included within a Pyrogallol[4]arene Tube. *Chem. - Eur. J.*, 18(33), 10258-10260 doi:10.1002/chem.201200263
- [87] Mossine A. V., Kumari H., Fowler D. A., Maerz A. K., Kline S. R., Barnes C. L., Atwood J. L. (2011), Ferrocene as a Hydrophobic Templating Agent with Pyrogallol[4]arenes. *Isr. J. Chem.*, 51(7), 840-842 doi:10.1002/ijch.201100068
- [88] Odagaki Y., Hirotsu K., Higuchi T., Harada A., Takahashi S. (1990), X-Ray structure of the α -cyclodextrin-ferrocene (2 : 1) inclusion compound. *J. Chem. Soc., Perkin Trans. 1*(4), 1230-1231 doi:10.1039/P19900001230
- [89] Liu Y., Zhong R.-Q., Zhang H.-Y., Song H.-B. (2005), A unique tetramer of 4 : 5 β -cyclodextrin-ferrocene in the solid state. *Chem. Commun.*(17), 2211-2213 doi:10.1039/B418220K
- [90] Jeon W. S., Moon K., Park S. H., Chun H., Ko Y. H., Lee J. Y., . . . Kim K. (2005), Complexation of Ferrocene Derivatives by the Cucurbit[7]uril Host: A Comparative Study of the Cucurbituril and Cyclodextrin Host Families. *J. Am. Chem. Soc.*, 127(37), 12984-12989 doi:10.1021/ja052912c
- [91] Adman E., Rosenblum M., Sullivan S., Margulis T. N. (1967), Structure of the ferrocene-tetracyanoethylene complex. *J. Am. Chem. Soc.*, 89(17), 4540-4542 doi:10.1021/ja00993a062
- [92] Hough E., Nicholson D. G. (1978), X-Ray crystallographic studies on ferrocene included in a thiourea host lattice. *J. Chem. Soc., Dalton Trans.*(1), 15-18 doi:10.1039/DT9780000015
- [93] Wei W., Wang G., Zhang Y., Jiang F., Wu M., Hong M. (2011), A Versatile Tripodal Host with Cylindrical Conformation:

Solvatomorphism, Inclusion Behavior, and Separation of Guests.
Chem. - Eur. J., 17(7), 2189-2198 doi:10.1002/chem.201002246

[94] Jiang J.-J., Yan C., Pan M., Wang Z., Deng H.-Y., He J.-R., . . .
Su C.-Y. (2012), Structural Conformation and Optical and
Electrochemical Properties of Imidazolyl-Substituted
Naphthalenediimide and Its HgII, CdII, and CuII Halide Complexes.
Eur. J. Inorg. Chem., 2012(8), 1171-1179 doi:10.1002/ejic.201101181

Chapter 2

Preparation of $\text{Ru}_3(\text{CO})_8$ -pyridine-alcohol cluster and its use for selective catalytic transformation of primary to secondary amines

2.1 Introduction

Pyridines based ruthenium complexes and clusters have attracted much attention over the last few decades as innovative catalysts for selective transformations and functionalization of specific substrates.[1-8] Park and Ko et al. have reported the influence of the size of the alkyl formate chain in a 2-alkylformate ligand with $\text{Ru}_3(\text{CO})_{12}$ as the catalyst for the hydroesterification reactions of alkenes without decarbonylation in case of 2-pyridyl methylformate.[9,10] Ko et al. also introduced chelating N-(pyridin-2-yl)formamide with $\text{Ru}_3(\text{CO})_{12}$ as an efficient catalyst for the hydroamidation reaction of alkenes.[11]

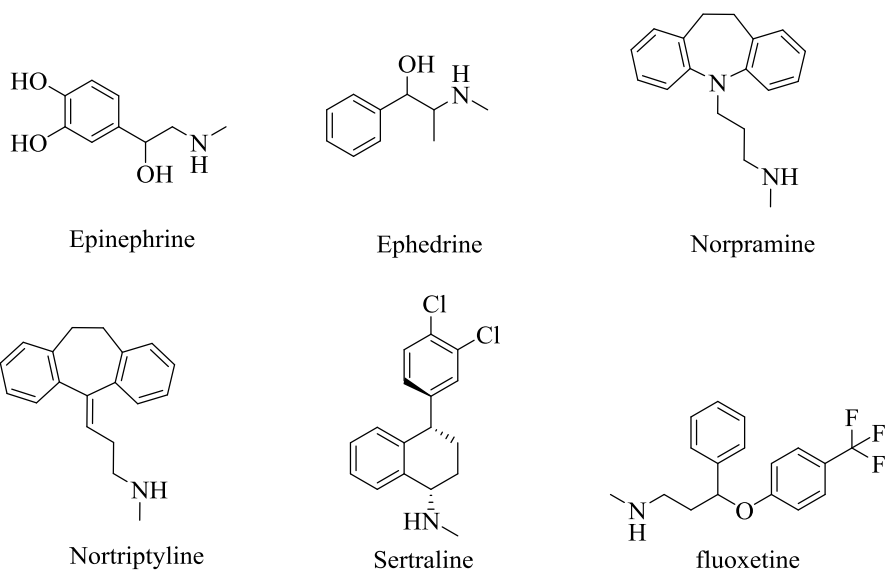


Chart A. Secondary amine derivatives present in various psychoactive drugs

Preparation of secondary amines as scaffolds present in various psychoactive drugs[12-14] poses a challenge (**Chart A**), as alkylation of

a primary amine, in general, yields a mixture of secondary and tertiary amines.[15-19] Therefore, we undertook to study the selective N-alkylation of primary amines.

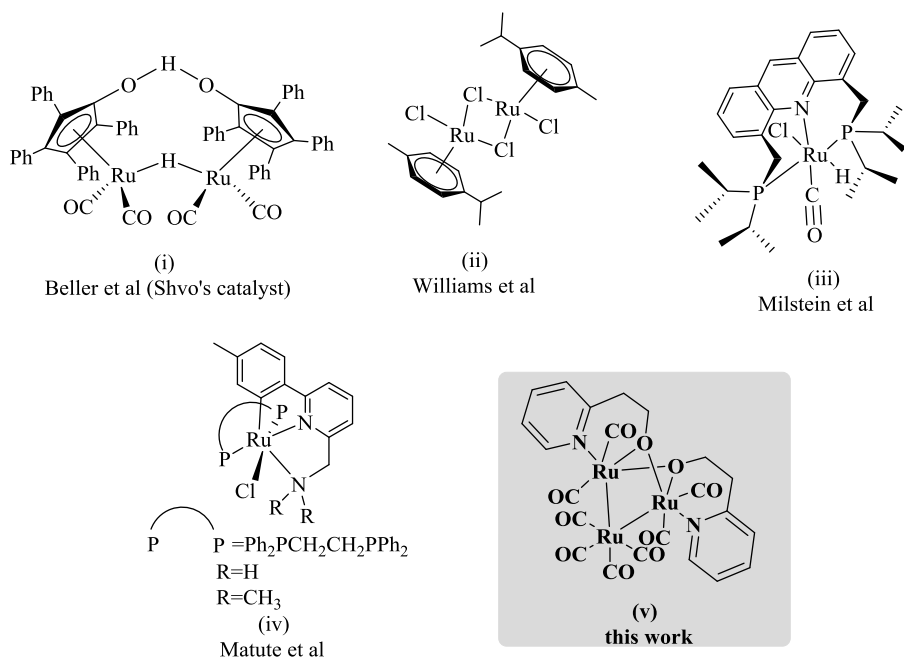


Chart B. Homogeneous catalysts (i–iv) used so far for N-alkylation of primary amine

Grigg[20] and Watanabe[21] have reported N-alkylation using homogeneous catalysts RhH(PPh₃)₄ and RuCl₂(PPh₃)₃, respectively. Yamaguchi[22] and Kempe[23,24] used [Cp*IrCl₂]₂, and [IrCl(PN)COD], respectively to perform N-mono and N,N-di alkylation reactions. Hollmann et al. utilized Shvo's ruthenium catalyst (**Chart B, i**) for alkylation of indoles[25] whereas Williams employed a ruthenium-dimer catalyst (**Chart B, ii**) for N-alkylation of primary amines.[26] Milstein and co-workers contributed to N-alkylation of the primary amine preparation from ammonia and primary alcohol using PNP pincer ruthenium complex (**Chart B, iii**) at high temperature (130–180 °C).[27] Matute and co-workers also reported N-alkylation of primary amines using Ru-CNN pincer complex (**Chart B, iv**)[28] whereas Ramachandran et al. made use of mononuclear phosphine-ruthenium complex for N-alkylation of primary amines.[29,30]

The earlier reported ruthenium catalysts for the N-alkylation of primary amine involve ruthenium-hydride, phosphine, or pincer ruthenium catalyst. Either the synthesis of those catalysts requires sophisticated conditions or the catalyst loading for the N-alkylation reaction is relatively high. In contrast, we report a facile preparation of ruthenium carbonyl clusters involving chelation of simple pyridine alcohol as ligands, with the catalyst loading as low as 0.5mol % which is much lower than previously reported other catalyst loading. Additionally, the cluster catalyst is found to be active for a variety of aromatic and aliphatic amines.

Kim et al. had shown that *in situ* addition of various pyridine alcohols viz. 2-hydroxypyridine, 2-(2-hydroxyethyl)pyridine, 2-(3-hydroxypropyl)pyridine and 2,6-bis(hydroxymethyl)pyridine along with $\text{Ru}_3(\text{CO})_{12}$ and sodium formate catalyzed the hydroesterification reaction of alkenes at 170 °C, in which the 2-(hydroxymethyl)pyridine ligand offers better catalyst activity than other pyridine alcohols.[4] This proved that the chelating functional pyridine alcohols have a positive influence on $\text{Ru}_3(\text{CO})_{12}$ to promote as a catalytic hydroesterification reaction of alkenes.

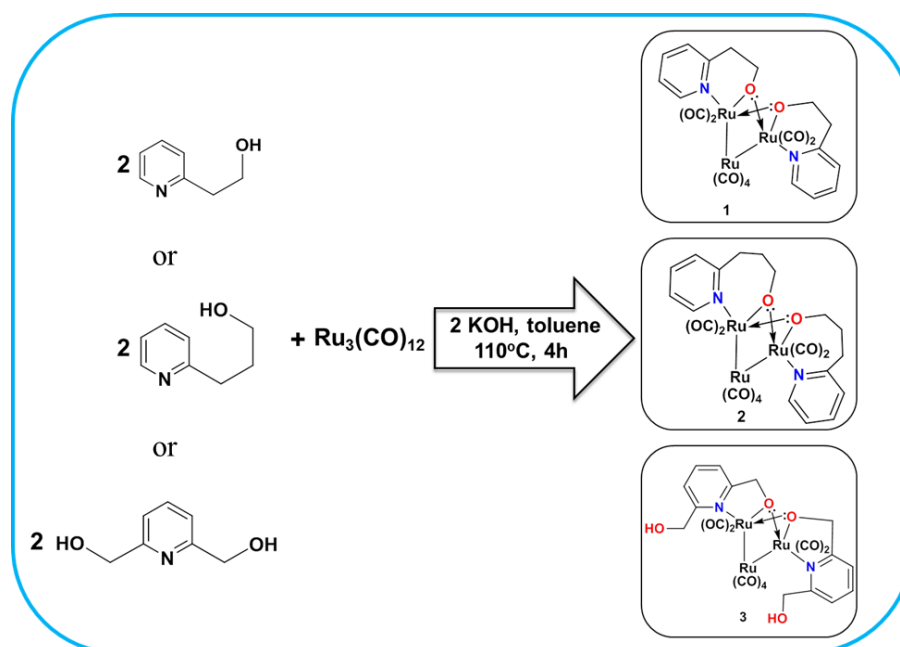
The chelation effect observations of pyridine-alcohol ligands motivated us to explore the structural modifications of the triruthenium unit by varying the nature and length of the side chain of the functional pyridine-alcohol ligands. Thus, the coordination of 2-(2-hydroxyethyl)pyridine (hep-H), 2-(3-hydroxypropyl)pyridine (hpp-H) and 2,6-bis(hydroxymethyl)pyridine (bhmp-H₂) with the $\text{Ru}_3(\text{CO})_{12}$ precursor have been studied. We report that two of these ligands can be incorporated into the trinuclear structure to afford the ruthenium cluster complexes $\text{Ru}_3(\text{hep})_2(\text{CO})_8$ (**1**), $\text{Ru}_3(\text{hpp})_2(\text{CO})_8$ (**2**), and $\text{Ru}_3(\text{bhmp-H})_2(\text{CO})_8$ (**3**). The compound **1** and its analogues have been reported by Doorn et al.,[31] Herein, we report for the first time the crystal structures of **1–3** which have the similar mode of ligand binding as reported by them.

We also report that the clusters **1–3** catalyze the mono N-alkylation of primary amines with alcohols via a hydrogen transfer reaction resulting in the selective production of secondary amines and show the influence of the nature of the chelating ligand in the Ru₃ clusters as catalysts.

2.2 Results and Discussion

2.2.1 Synthesis of Ru₃ clusters 1–3

The reaction of Ru₃(CO)₁₂ with pyridine-alcohol, { 2-(2-hydroxyethyl)pyridine (hep-H) (for cluster **1**) and 2-(3-hydroxypropyl)pyridine (hpp-H) (for cluster **2**) has been carried out in 1:2 molar ratio in toluene (25 mL) at 110 °C for 4h using 2 equivalent of KOH (Scheme 2.1).



Scheme 2.1. Synthesis of pyridine alcohol containing ruthenium carbonyl complexes **1–3**

On varying the ratio, 1:4 and 1:6 of Ru₃(CO)₁₂: ligand the same products, **1** and **2** were obtained in good yield. We investigated whether 2,6-bis(hydroxymethyl)pyridine (bhmp-H₂) would change the nature of the resulting cluster by maintaining the above synthetic conditions. Surprisingly, we obtained cluster **3**, similar to **1** and **2**, but with two pendant CH₂OH arms. Fine crystals of **1–3** were obtained from toluene, and the new clusters have been characterized by infrared and ¹H, and ¹³C NMR spectroscopy, mass spectrometry, and CHN analysis. Their molecular structures were established by single crystal X-ray diffraction studies. Infrared and ¹³C NMR spectra of **1–3** confirmed the presence of only terminal carbonyls. Mass spectra of all three compounds showed the

respective molecular ion peaks and additional ones corresponding to successive loss of carbonyl groups (**Figure 2.4–2.11**).

The molecular structures of **1–3** are shown in **Figure 2.1**, and their structural parameters are presented in **Table 2.1**. The distance between two neighbouring unbonded Ru1 and Ru2 atoms in **1–3** are in the range of 3.030 Å – 3.045 Å which is larger than the bonded Ru-Ru distances (2.775 Å – 2.815 Å).[32] In **3**, the two free -OH groups are oriented away from the Ru₃ unit; other structural features are unexceptional. Along with **1–3**, the other toluene solvated form of cluster **1** is also analyzed and named as Cluster **1a** (**Figure 2.12**).

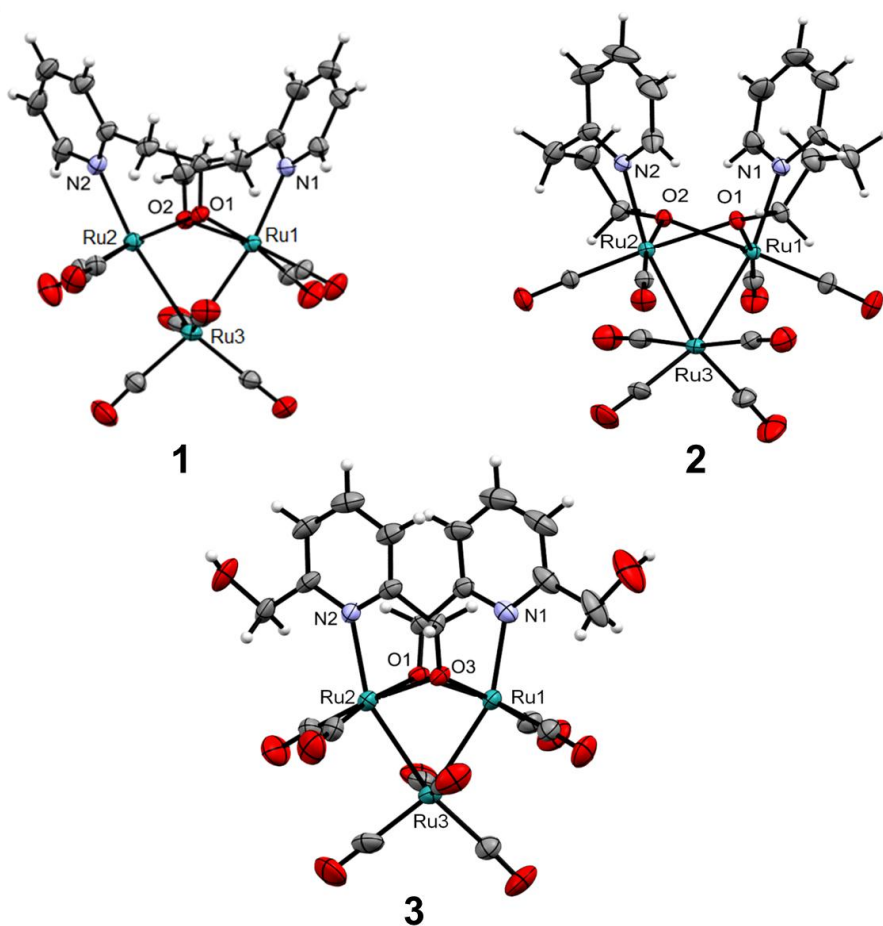


Figure 2.1 Perspective view of **1**, **2** and **3**

Table 2.1 Crystal data and structure refinement^{[33],[34]} for **1**, **2** and **3**

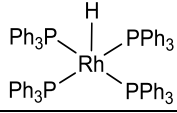
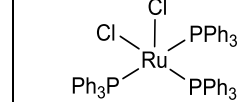
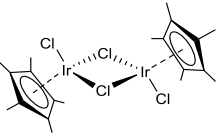
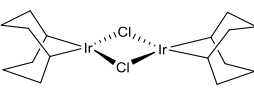
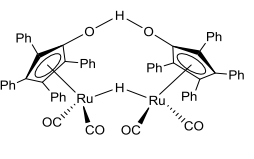
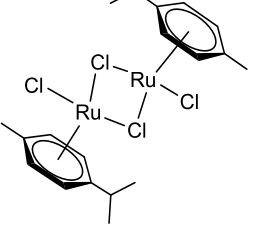
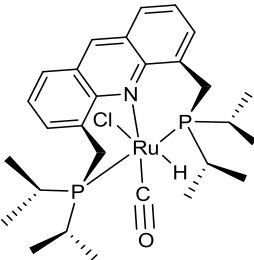
Identification code	1	2	3
Empirical formula	C ₂₂ H ₁₆ N ₂ O ₁₀ Ru ₃	C ₂₄ H ₂₀ N ₂ O ₁₀ Ru ₃	C ₂₂ H ₁₆ N ₂ O ₁₂ Ru ₃
Formula weight	771.58	799.63	803.58
Temperature/K	293	293(2)	293(2)
Crystal system	monoclinic	Triclinic	monoclinic
Space group	<i>P2₁/n</i>	<i>P</i> $\bar{1}$	<i>P2₁/n</i>
a/Å	10.5526(2)	9.9410(6)	10.5934(7)
b/Å	14.8131(3)	9.9539(8)	13.4587(9)
c/Å	16.8846(2)	14.4372(10)	18.7560(11)
α /°	90	89.273(6)	90
β /°	93.161(2)	76.892(6)	97.916(7)
γ /°	90	81.270(6)	90
Volume/Å ³	2635.33(10)	1374.89(17)	2648.6(3)
Z	4	2	4
ρ_{calc} Mg/m ³	1.945	1.932	2.015
μ /mm ⁻¹	1.753	1.683	1.754
F(000)	1496.0	780	1560.0
Crystal size/mm ³	0.34 × 0.32 × 0.28	0.34 × 0.32 × 0.3	0.32 × 0.30 × 0.28
Radiation	Mo K α (λ = 0.71073)	MoK α (λ = 0.71073)	MoK α (λ = 0.71073)
2 θ range for data collection/°	3.004 to 29.007	3.182 to 32.247	3.027 to 32.156
Index ranges	-13 ≤ h ≤ 14, -19 ≤ k ≤ 20, -22 ≤ l ≤ 22	-14 ≤ h ≤ 14, -12 ≤ k ≤ 14, -21 ≤ l ≤ 17	-15 ≤ h ≤ 15, -18 ≤ k ≤ 20, -28 ≤ l ≤ 27
Reflections collected	30798	16236	35820
Refinement method	Full-matrix least-squares on F ²	Full-matrix least-squares on F ²	Full-matrix least- squares on F ²
Independent reflections	6385 [R _{int} = 0.0365, R _{sigma} = 0.0236]	8893 [R _{int} = 0.0271, R _{sigma} = 0.0380]	8800 [R _{int} = 0.1548, R _{sigma} = 0.1626]
Data/restraints/parameters	6385/0/334	8893/40/439	8800/0/354
Goodness-of-fit on F ²	1.059	1.147	1.002
Final R indexes [I ≥ 2 σ (I)]	R ₁ = 0.0264, wR ₂ = 0.658	R ₁ = 0.0379, wR ₂ = 0.0838	R ₁ = 0.0650, wR ₂ = 0.1071
Final R indexes [all]	R ₁ = 0.0314,	R ₁ = 0.0504,	R ₁ = 0.1830,

data]	wR ₂ = 0.0696	wR ₂ = 0.0932	wR ₂ = 0.1519
Largest diff. peak/hole / e Å ⁻³	0.561/-0.698	1.185/-1.019	1.068/-1.188
CCDC No.	1852237	1539166	1541897

2.2.2. Ru₃ clusters catalyzed mono-alkylation of primary amines with alcohol

A search of the literature reveals the presence of several hydride/pincer complexes of rhodium, iridium, and ruthenium along with their phosphine complexes for catalysis of mono-alkylation of amines with alcohols (**Table 2.2**). Grigg et al. used Rh catalyst (5 mol %) to achieve the N-methylation of pyrrolidine. Aminoarenes were converted to secondary and tertiary amines by the reaction around 180 °C with primary alcohols in the presence of dichlorotris(triphenylphosphine)-ruthenium (1 mol %). Fujita et al. utilized [Cp*IrCl₂]₂ (1.0 mol % Ir catalyst) for N-alkylation reaction. Blank and Yamaguchi also utilized the Ir catalysts for the N-alkylation of amines using primary alcohols. Hollman et al. used 1 mol % ruthenium catalyst and performed the N-alkylation reaction at 150 °C. Hamid et al. utilized ruthenium catalyst (0.5–2.5 mol %) for excellent N-alkylation of amines in reflux toluene. Gunanathan and Milstein performed the outstanding direct primary amine synthesis utilizing ruthenium PNP catalyst using only 0.1 mol % of the catalyst. Ramachandran et al. used mononuclear phosphine-ruthenium complex for the N-alkylation reaction, but they used 1.0 mol % or KOH in their reaction. Our catalyst is comparable to many catalysts reported so far (**Table 2.2**) as, the catalytic reaction used a smaller amount of catalyst (0.5 mol %), the catalyzed reaction is performed at a relatively low temperature (110 °C). The synthetic procedure for cluster **1–3**, is relatively uncomplicated and requires shorter time and to the best of our knowledge, this is the first example of the use of ruthenium carbonyl clusters **1–3** for catalysis of mono-alkylation of amines with primary alcohols.

Table 2.2. Comparison of cluster **1** with previous homogeneous catalysts for alkylation reaction of primary amines with primary alcohols

$\text{R}_1\text{CH}_2\text{OH} + \text{R}_2\text{CH}_2\text{NH}_2 \xrightarrow[\text{toluene, reflux, } -\text{H}_2\text{O}]{\text{Catalyst base}} \text{R}_1\text{CH}_2\text{N}(\text{H})\text{CH}_2\text{R}_2$					
Entry No.	Catalyst or pre-catalyst	Substrates R ₁ OH and R ₂ NH ₂	Reaction parameters	Yield (%)	Ref.
1		pyrrolidine + MeOH	Reflux, 4 h, 70 °C	98%	[20]
2		Aniline + EtOH	180 °C, 5 h.	74%	[21]
3		NH ₄ BF ₄ + RCH ₂ OH Aniline + benzyl alcohol	NaHCO ₃ , 140 °C, 17h NaHCO ₃ , 110 °C, 17h	75% 94%	[22], [35]
4		o-amino pyridine + benzyl alcohol	KO ^t Bu, 70 °C, 17h (2 mol % catalyst)	97%	[24]
5		Hexyl amine, aryl amine	2-methyl- butan-ol, 150 °C (1 mol % catalyst)	98%	[25]
6		^t BuNH ₂ , benzyl alcohol	5 mol % dppf, toluene, 110 °C, 24h (2.5 mol % catalyst)	94%	[26]
7		Benzyl alcohol, NH ₃	toluene, 110 °C, 24h (0.1 mol % catalyst)	83%	[27]

8	<p>$P = Ph_2PCH_2CH_2PPh_2$ $R = H$ $R = CH_3$</p>	Benzyl alcohol, NH_3	KO^tBu , toluene, $110\text{ }^\circ C$, 24h (1 mol % catalyst)	92%	[28]
9		2-amino benzothiazole, benzyl alcohol	KOH , toluene, $110\text{ }^\circ C$, 12h (0.5 mol % catalyst)	96%	[29]
10	<p>1</p>	2-amino pyridine, benzyl alcohol	KO^tBu , toluene, $110\text{ }^\circ C$, 24h (0.5 mol % catalyst)	96%	Present work

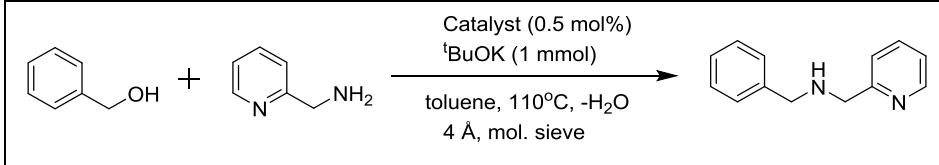
2.2.3 Catalytic application of clusters 1–3 for amine mono-alkylation with primary alcohols

Clusters **1–3** and $Ru_3(CO)_{12}$ were evaluated as catalysts for the transformation of primary amine 2-picolyamine to a secondary amine in the model reaction (**Table 2.3**). Typically, the reaction was performed using 1.0 mmol of benzyl alcohol and 2-picolyamine as reactants, low loading (0.5 mol %) of catalyst **1–3** and 1.0 mmol potassium tert-butoxide as a base, 4 Å mol. sieve, and stirred in 600 μL of toluene.

In the absence of ruthenium catalyst and base, the amine alkylation was not observed (**Table 2.3**, entries 1, 2). The optimization of reaction conditions was performed at room temperature, $55\text{ }^\circ C$, $75\text{ }^\circ C$ and $110\text{ }^\circ C$. The reaction was not observed below $110\text{ }^\circ C$. The effect of time on the reaction was observed, and within 24 h at $110\text{ }^\circ C$, the reaction was completed with catalyst **1** (entries 3–6). Among all the ruthenium-based clusters, **1–3**, similar catalytic activity was obtained, but the most active catalyst was cluster **1**, likely due to the six-membered ring formed by the

coordination of 2-(2-hydroxyethyl)pyridine ligand to $\text{Ru}_3(\text{CO})_8$ (entries 6–8). The precursor $\text{Ru}_3(\text{CO})_{12}$ in the absence of pyridine-alcohol shows a much lower conversion (entry 9) thus, demonstrating the importance of the chelating ligand ($\text{N} \curvearrowright \text{O}$).

Table 2.3. Optimization of the catalytic reaction conditions for N-alkylation of 2-picolylamine using benzyl alcohol and Ru_3 cluster catalysts.

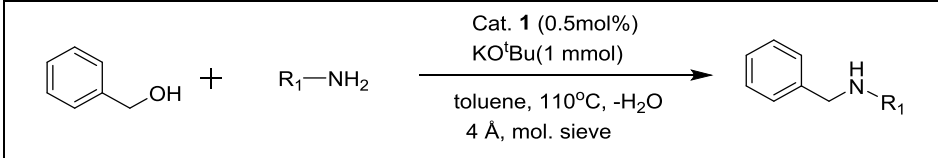
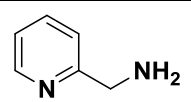
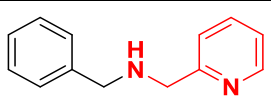
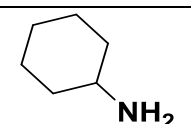
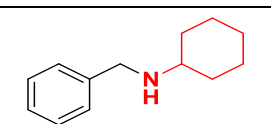
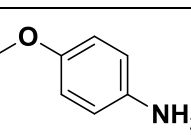
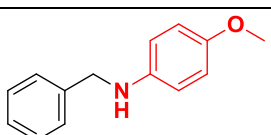
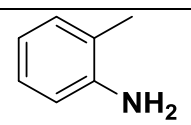
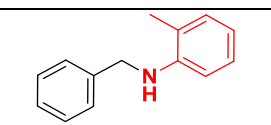
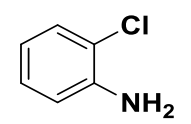
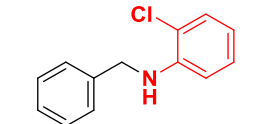
					
Entry	Catalyst	Base	Time (h)	Conv.	Yield
1	NA	^t BuOK	24	0	0
2	Cat.1	NA	24	0	0
3	Cat. 1	^t BuOK	6	79	74
4	Cat. 1	^t BuOK	12	85	80
5	Cat. 1	^t BuOK	18	92	88
6	Cat. 1	^t BuOK	24	100	96
7	Cat. 2	^t BuOK	24	90	85
8	Cat. 3	^t BuOK	24	95	90
9	$\text{Ru}_3(\text{CO})_{12}$	^t BuOK	24	70	54

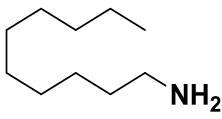
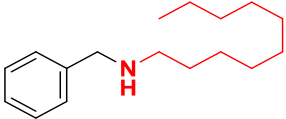
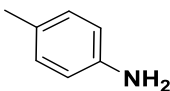
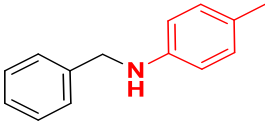
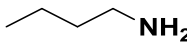
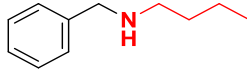
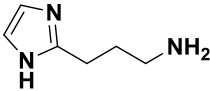
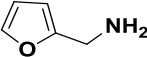
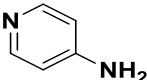
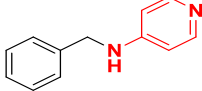
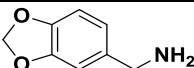
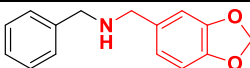
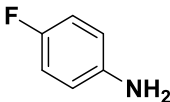
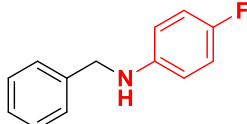
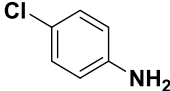
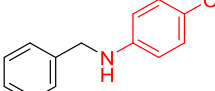
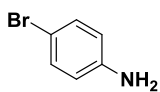
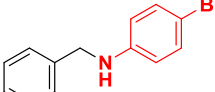
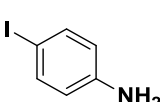
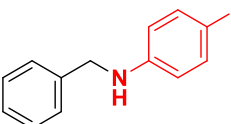
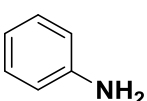
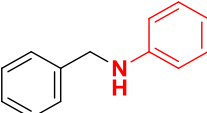
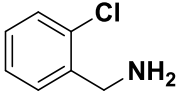
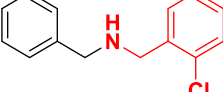
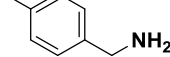
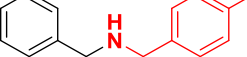
Under the optimized conditions (entry 6) {cat.1 (0.5 mol %), benzyl alcohol (1.0 mmol), 2-picolylamine (1.0 mmol), and 1.0 mmol potassium tert-butoxide in toluene (500 μL) charged with 4 Å, mol. sieves were heated in a closed tube}; the desired secondary amine was obtained in high yield (96%).

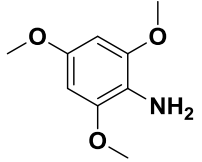
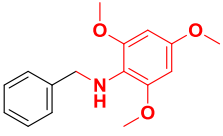
Encouraged by this catalytic transformation, the mono-alkylation of various primary amines bearing electron donating or electron withdrawing substituents were explored (**Table 2.4**). Higher yields were observed with *para* electron donating substituents on the aniline ring whereas the *ortho*-substituted aniline was less reactive likely due to the steric hindrance (**Table 2.4**, entries 3, 4 and 7). With halogen substituents on pyridine ring, the conversion was observed, but the desired product

yields were low. The catalyst was active even with aliphatic amines (entries 2, 6 and 8) but for heterocycles containing the imidazole and furan rings (entries 9–10), the mono-alkylation was not observed. 4-aminopyridine and piperonylamine also gave excellent yields for the mono-alkylation of primary amines (entries 11–12). In the case of halo-aniline, the para-fluoro aniline gave the highest yield followed by chloro, bromo and iodo aniline (entries 13–16). Aniline, (2-chlorophenyl)methanamine, and p-tolylmethanamine, also gave the desired product in good yield, and at last reactant with maximum substitution like trimethoxyaniline mono-alkylation also produced the secondary amine product in better yield (entries 17–20).

Table 2.4. Direct formation of secondary amines from benzyl alcohol and various primary amines with cluster **1** as catalyst

				
Entry	RNH ₂	Conv.	C ₆ H ₅ CH ₂ NHR	Yield
1		100%		96%
2		52%		51%
3		64%		56%
4		44%		41%
5		65%		19%

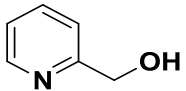
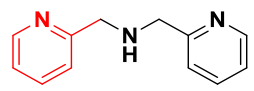
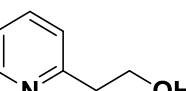
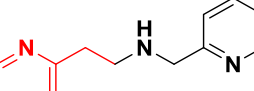
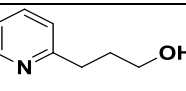
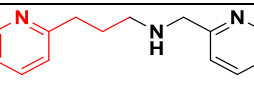
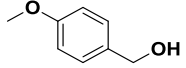
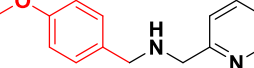
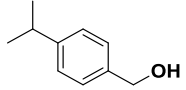
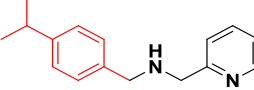
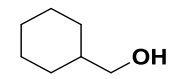
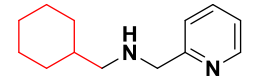
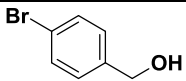
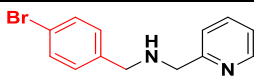
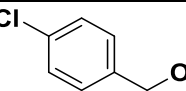
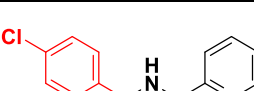
6		72%		55%
7		48%		46%
8		22%		20%
9		--	-no reaction-	--
10		--	- no reaction -	
11		73%		70%
12		>90%		62%
13		79%		72%
14		64%		62%
15		55%		50%
16		52%		38%
17		72%		68%
18		58%		50%
19		70%		47%

20		74%		60%
----	---	-----	---	-----

Complex **1** (0.5 mol %), benzyl alcohol (1.0 mmol), primary amine (1.0 mmol), and toluene (500 μ L) charged with 4 Å, mol. sieves, were heated in a closed tube. Conversion of alcohol and yield of products were determined by GC-MS. Isolated yields (1, 4, 7, 11, 20) were analyzed by ^1H and ^{13}C NMR along with GC-MS.

Catalyst **1** showed significant results even when pyridine alcohols, pyridin-2-ylmethanol, pyridin-2-ylethanol, and pyridin-2-ylpropanol were screened (**Table 2.5**, entries 1–3). The three synthesized dipyridyl secondary amines are the precursors of significant NNN-pincer ligands. Presence of functional groups on benzyl alcohol substrates did not prevent the catalytic secondary amine formation (**Table 2.5**, entries 5, 6). Halo-benzyl alcohol also gave the expected product, but the less stable bromo derivative gave lower yield in the reaction (**Table 2.5**, entries 7, 8). A plausible mechanism has also been proposed which is shown in Appendix A section. Mechanism shows that the catalytic reaction proceeds by the initial deprotonation of primary alcohols using potassium tert-butoxide along with the simultaneous decoordination of carbonyl to produce ruthenium alkoxide species **A**. Furthermore, **A** undergoes β hydride shift to produce aldehyde and ruthenium hydride species **B**. The produced aldehyde reacts with the primary amine to form Schiff base which is reduced by **B** to generate ruthenium amide species **C**. Primary alcohol again attacks **C** to regenerate **A** along with the secondary amine product.

Table 2.5. Direct formation of secondary amines from primary amines and varying alcohols using **1** as catalyst

$\text{R}_2\text{CH}_2\text{OH} + \text{pyridin-2-ylmethanamine} \xrightarrow[\text{toluene, 110}^\circ\text{C, -H}_2\text{O, 4 \AA, mol. sieve}]{\text{Cat. 1 (0.5mol\%), } ^t\text{BuOK (1 mmol)}} \text{pyridin-2-ylmethanamine-N(R}_2\text{)}$				
Entry	$\text{R}_2\text{CH}_2\text{OH}$	Conv.	$\text{C}_5\text{H}_4\text{NCH}_2\text{NHCH}_2\text{R}$ 2	Yield
1		52%		41%
2		82%		75%
3		90%		54%
4		75%		64%
5		90%		78%
6		67%		50%
7		80%		8%
8		73%		55%

Complex **1** (0.5 mol %), primary alcohol (1.0 mmol), pyridin-2-ylmethanamine (1.0 mmol), and toluene (500 μL) charged with 4 \AA mol. sieves were heated in a closed tube. Conversion of alcohols and yield of products were analyzed by GC-MS. Isolated yields (1, 5) were analyzed by ^1H and ^{13}C NMR along with GC-MS.

2.2.4 Mercury Poisoning Study

We have also investigated the influence of mercury(0)[36] on the mono-alkylation of primary amines using alcohol in the presence of **1**. The yield

of the mono-alkylation does not reduce significantly when mercury(0) is introduced in the reaction mixture (from 96% to 84%). The failure of Hg(0) to halt the reaction suggests that the reaction involves the homogenous ruthenium pyridine alcohol cluster catalyst. **Figure 2.2** displays condition 1 as the optimized reaction condition and condition 2 as the reaction condition in the presence of Hg(0) with the respective yields.

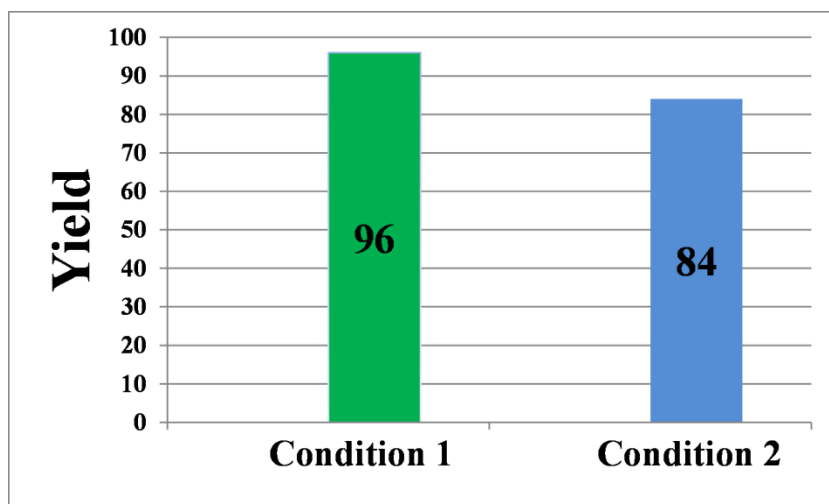


Figure 2.2 Mercury poisoning study of $\text{Ru}_3(\text{hep})_2(\text{CO})_8$ cluster catalyst for mono-alkylation of amine with alcohol

2.3 Conclusion

The above results show that pyridine alcohols react with $\text{Ru}_3(\text{CO})_{12}$ to form clusters $\text{Ru}_3(\text{hep})_2(\text{CO})_8$ (**1**), $\text{Ru}_3(\text{hpp})_2(\text{CO})_8$ (**2**), and $\text{Ru}_3(\text{bhmp-H})_2(\text{CO})_8$ (**3**). They all contain a trans py-Ru-Ru-py arrangement, and the chelating ligands offer 2 oxygen atom bridging the non-bonded Ru(1) and Ru(2) sites. The catalytic transformation highlights the high efficiency and versatility of the clusters $\text{Ru}_3(\text{N} \curvearrowright \text{O})_2(\text{CO})_8$ catalyst (L= hep, hpp, bhmp-H). Cluster **1** was the most efficient catalyst for the N-alkylation reactions of primary amines. The catalytic transformations are entirely selective leading to excellent yields of secondary amine. This work has created simple Ru₃ catalysts, with pyridine alcohol chelating ligands, which do not contain pincer or hydride ligands, and excellent catalytic activity for mono-alkylation for primary amines is achieved successfully. Other catalytic transformations like hydrogen production from renewable alcohols, oxidation of alcohols into carboxylates, usually performed by pincer metal catalysts, can be explored by employing these Ru₃ **1–3** clusters.

2.4 Experimental

All reactions were done under an inert gas atmosphere. Ruthenium carbonyl, pyridine alcohols, and other alcohols along with amine derivatives were purchased from Aldrich and TCI chemicals. Reagents used for purification and crystallization were purchased either from Rankem or Merck and distilled before use. NMR spectra were recorded in deuterated acetone (CD_3COCD_3) on a Bruker Avance (III) spectrometer (400 MHz). Single crystal x-ray diffraction studies of complexes **1–3** were carried out using an Agilent Technologies Supernova CCD system. The mass chromatograms were recorded on a Bruker-Daltonics-microTOF-QII mass spectrometer. Elemental analysis was performed by using a Thermo Scientific FLASH 200 instrument. GC Samples were analyzed in Shimadzu QP2010 Ultra. The parameters used in the column oven program were as follows: 40 °C (hold 5 min.) \rightarrow 20 °C/min. \rightarrow 280 °C (hold 13 min.) along with injection temperature of 280 °C, the interface temperature was 300 °C, and the ion source temperature was 220 °C.

2.4.1 Preparation of cluster $\text{Ru}_3(\text{hep})_2(\text{CO})_8$ (**1**).

Pyridin-2-yl-ethanol (113 μL , 1 mmol) and KOH (42 mg, 1.05 mmol), were placed into a round bottom flask using water (1 mL) as a solvent, and the reaction mixture was stirred for 1 hour at room temperature. After 1 hour, water was evaporated, and residual water was removed using a high vacuum pump. $\text{Ru}_3(\text{CO})_{12}$ (0.320 g, 0.5 mmol) was added along with 25 mL of dry toluene into the same flask and refluxed at 110 °C for 3 hours, the yellow colored solution was cooled and evaporated by rotavapor, and the resulting precipitate was washed with hexane five times and once with a small quantity of diethyl ether. Later, the precipitate was dissolved in acetone-dichloromethane mixture; filtered using celite and the filtered solvent was evaporated. The residue was recrystallized in toluene solvent. The yellow coloured crystalline solid was obtained. The identity of the complex was determined by using ^1H

and ^{13}C NMR, mass spectrometry, CHN elemental analysis and a single-crystal XRD study. Yield: 62% (0.240 g), ^1H NMR (400 MHz, acetone- d_6 , 25 °C, ppm): δ 8.97 (d, 1H), 7.94 (t, 1H), 7.50 (t, 1H), 7.41 (d, 1H), 4.08 (tt, 1H), 3.04 (m, 2H), 2.68 (t, 1H); ^{13}C NMR (100 MHz, acetone- d_6 , 25 °C, ppm): δ 205.4, 205.2, 203.9, 196.1, 162.7, 155.2, 139.8, 127.1, 124.6, 65.5, 43.6; Elem. Anal. Calcd: C, 34.25; H, 2.09; N, 3.63; Found: C, 34.29; H, 1.95; N, 3.64; Selected IR on (KBr, cm^{-1}): 2950(w), 2915(w), 2847(s), 2060(s), 1985(s), 1914(s), 1603(w), 1079(s); ESI-MS (m/z) 687.55.

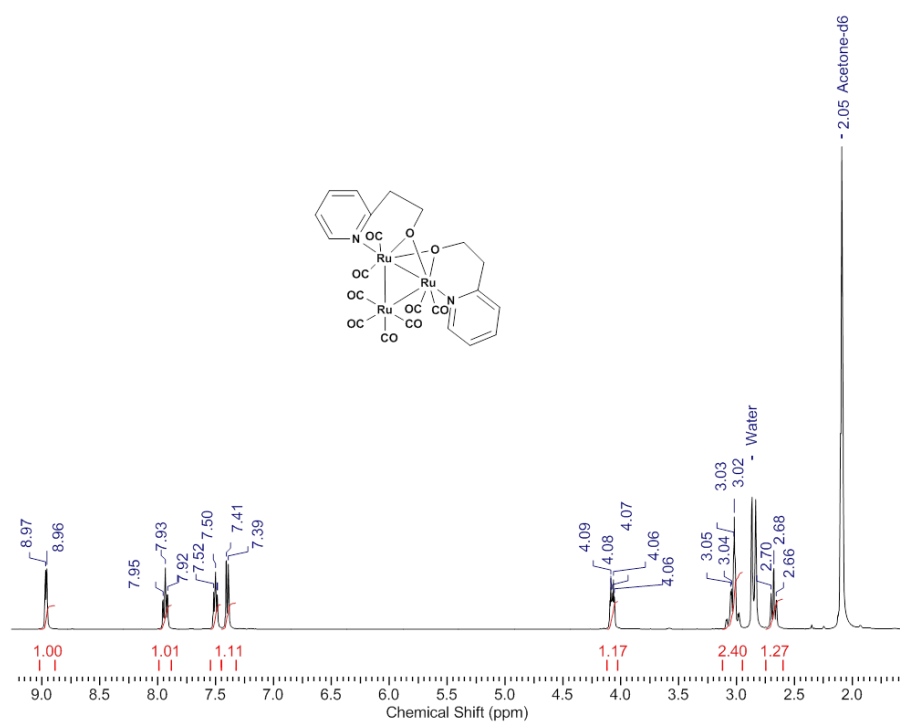


Figure 2.3 ^1H NMR of **1**

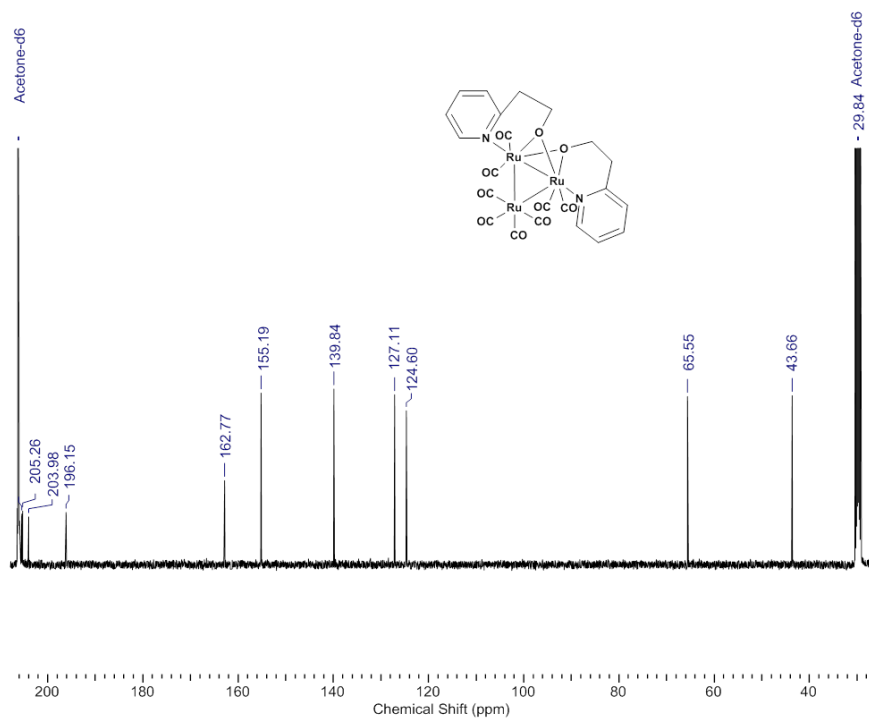
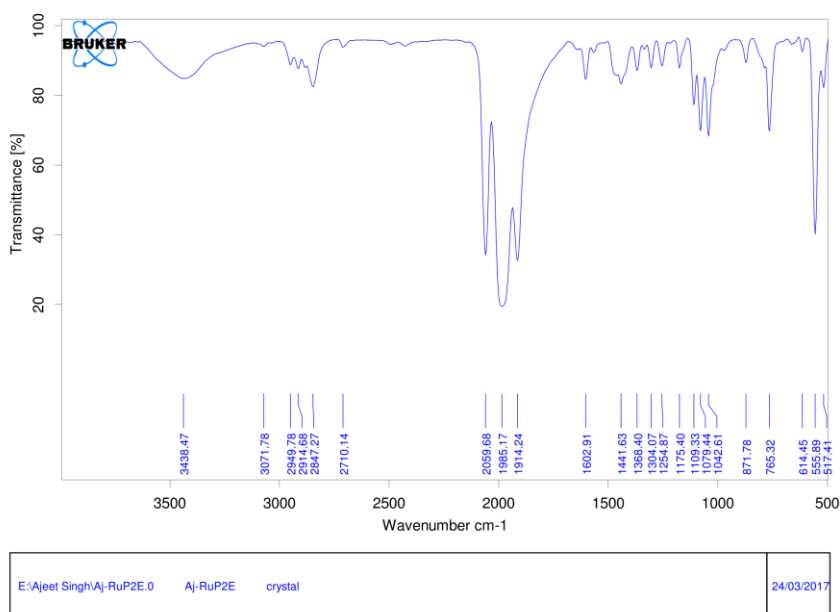


Figure 2.4 ^{13}C NMR of **1**



Page 1/1

Figure 2.5 IR of **1**

2.4.2. Preparation of cluster $\text{Ru}_3(\text{hpp})_2(\text{CO})_8$ (**2**)

Using same conditions as those for $\text{Ru}_3(\text{hep})_2(\text{CO})_8$ (**1**) preparation, the $\text{Ru}_3(\text{hpp})_2(\text{CO})_8$ (**2**) complex was prepared by using the 2-pyridin-2-yl-propanol (129 μL , 1 mmol) with KOH (41 mg, 1.03 mmol) and $\text{Ru}_3(\text{CO})_{12}$ (0.320 g, 0.5 mmol) into 25 mL of toluene as the solvent.

After recrystallization, red coloured complex **2** was obtained. Yield: 54%, ^1H NMR (400 MHz, acetone- d_6 , 25 °C, ppm): δ 8.78 (d, 1H), 7.79 (t, 1H), 7.32 (dd, 2H), 4.28 (t, 1H), 3.90 (d, 1H), 3.36 (t, 1H), 3.12 (dd, 1H), 1.95 (t, 1H), 1.55 (q, 1H); ^{13}C NMR (100 MHz, acetone- d_6 , 25 °C, ppm): δ 206.2, 205.8, 203.4, 195.7, 166.8, 154.0, 139.8, 127.9, 123.8, 74.8, 38.1, 35.9; Elem. Anal. Calcd: C, 36.05; H, 2.52; N, 3.50; Found: C, 36.99; H, 2.43; N, 3.61; Selected IR on (KBr, cm^{-1}): 2943(w), 2912(w), 2840(s), 2066(s), 1987(s), 1914(s), 1602(w), 1085(s); ESI-MS (m/z) 542.61

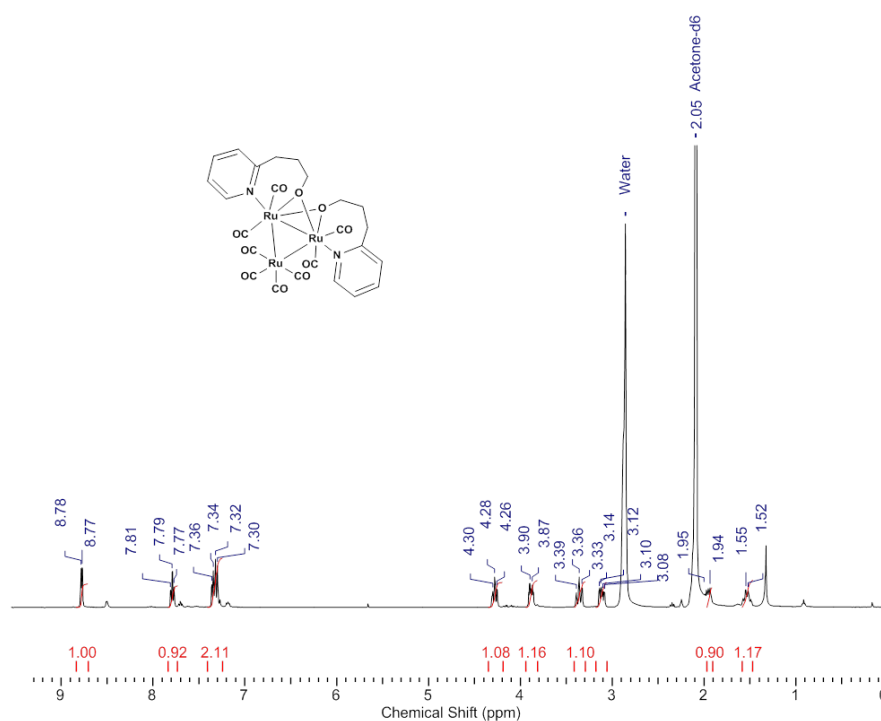


Figure 2.6 ^1H NMR of **2**

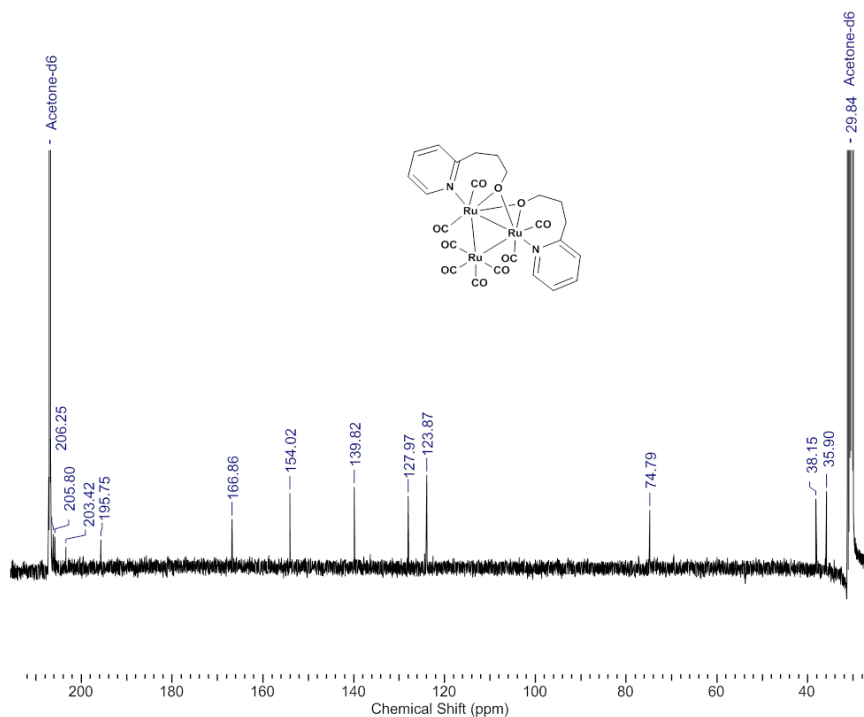
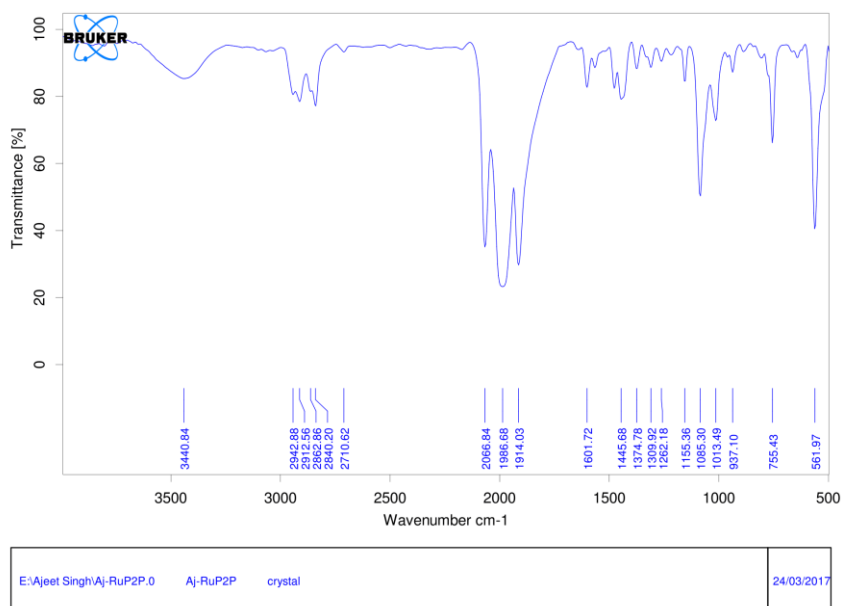


Figure 2.7 ^{13}C NMR of **2**



Page 1/1

Figure 2.8 IR of **2**

2.4.3 Preparation of cluster $\text{Ru}_3(\text{bhmp-H})_2(\text{CO})_8$ (**3**)

Using same conditions as those for $\text{Ru}_3(\text{hep})_2(\text{CO})_8$ (**1**) preparation, the $\text{Ru}_3(\text{bhmp-H})_2(\text{CO})_8$ (**3**) complex was prepared by using

the (6-hydroxymethyl-pyridin-2-yl)-methanol (0.139 g, 1 mmol) with KOH (40 mg, 1 mmol) and Ru₃(CO)₁₂ (0.320 g, 0.5 mmol) with 25 mL of toluene as the solvent. After recrystallization, yellow crystalline solid was obtained. Yield: 58%, ¹H NMR (400 MHz, acetone-d₆, 25 °C, ppm): δ 7.76 (d, 2H), 6.73 (t, 1H), 5.16 (m, 2H), 5.01 (m, 2H), 4.27 (d, 1H); ¹³C NMR (100 MHz, acetone-d₆, 25 °C, ppm): δ 207.7, 204.5, 203.6, 193.9, 167.4, 162.9, 138.7, 121.0, 117.3, 78.5, 68.0; Elem. Anal. Calcd: C, 32.88; H, 2.01; N, 3.49. Found: C, 33.29; H, 2.06; N, 3.45; Selected IR on (KBr, cm⁻¹): 3408(br), 2925(w), 2855(w), 2076(s), 1993(s), 1910(s), 1604(w), 1078(s); ESI-MS (m/z) 750.20

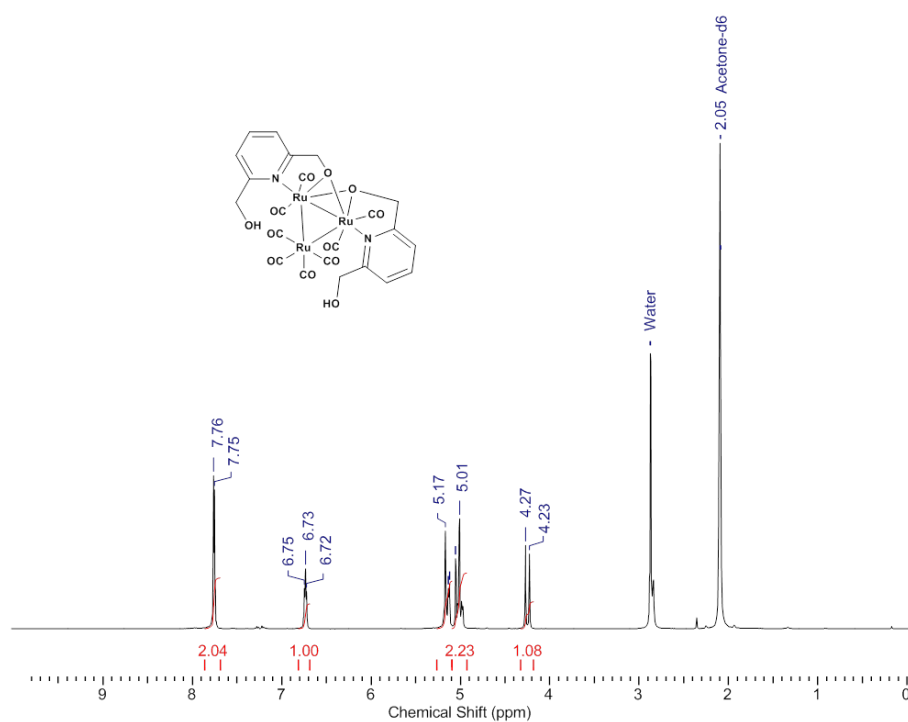


Figure 2.9 ¹H NMR of **3**

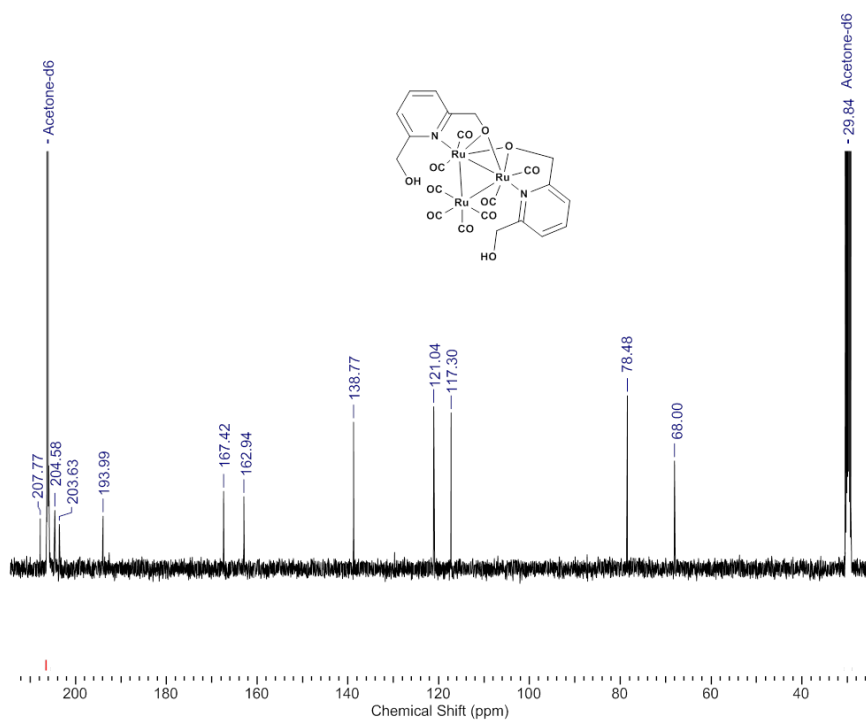


Figure 2.10 ^{13}C NMR of 3

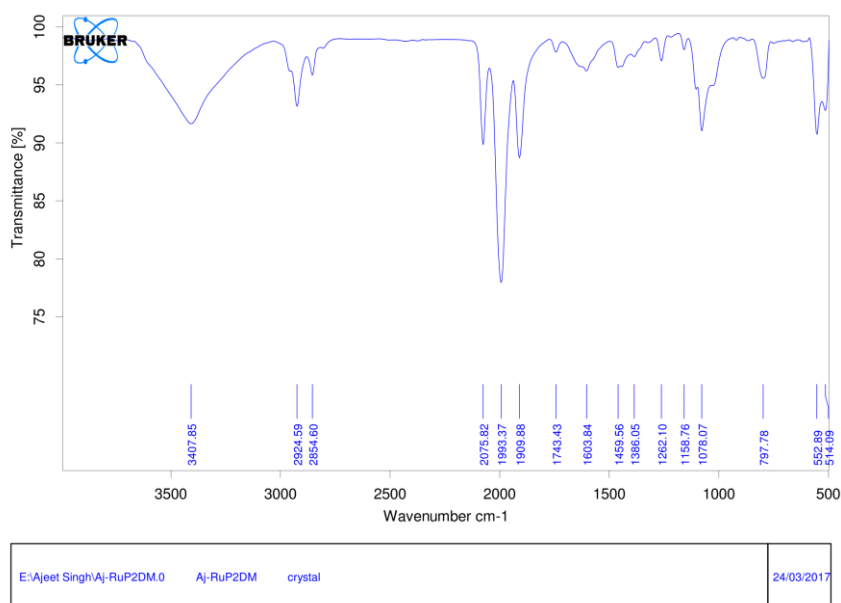


Figure 2.11 IR of 3

2.4.4 Mercury Poisoning Study

Mercury Poisoning experiment for the mono-alkylation of primary amine was performed in a 25-mL tube capped with a glass stopper. In a sealed tube, an 8 x 4 mm oval-shaped stirring bar, 4 Å mol. sieves, 1mmol of

picolylamine, 1mmol of benzyl alcohol, mercury (1mmol), and catalyst (4 mg) along with the KO^tBu (1mmol) along with 1mL of toluene was added and flushed with N₂. The reaction was carried out at 110°C for 24h. As the reaction was completed, the un-reacted drops of mercury were present in the reaction mixture. Then after washing out the reaction mixture, mercury was quenched. Furthermore, the yield was calculated.

Other Figures and Tables

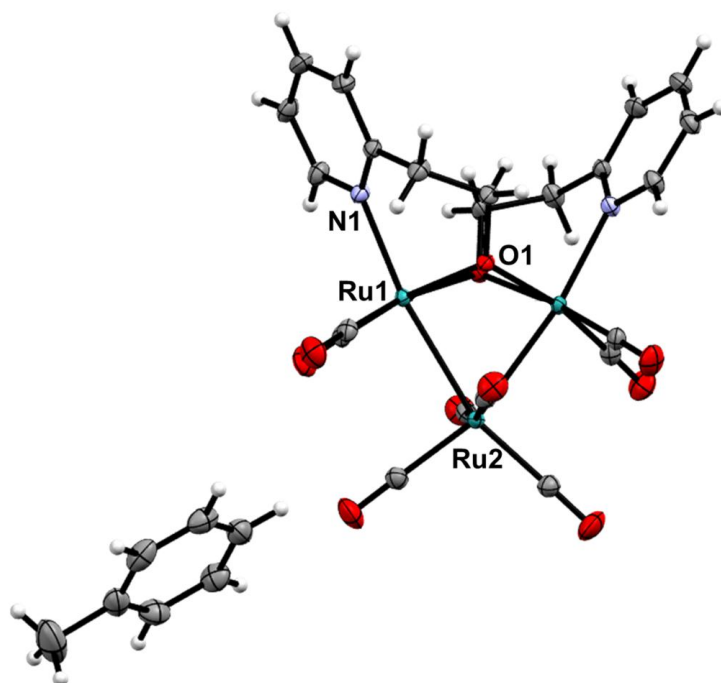


Figure 2.12 Perspective view of **1a**

Table 2.6 Crystal data and structure refinement for **1a**

Identification code	1a
Empirical formula	C ₃₆ H ₃₂ N ₂ O ₁₀ Ru ₃
Formula weight	955.84
Temperature/K	293
Crystal system	monoclinic
Space group	<i>I</i> ₂ / <i>a</i>
a/Å	18.6183(4)
b/Å	11.77089(19)
c/Å	17.3349(2)
α/°	90
β/°	107.9232(17)
γ/°	90

Volume/Å³	3614.65(11)
Z	4
ρ_{calc} Mg/m³	1.756
μ/mm⁻¹	1.297
F(000)	1896
Crystal size/mm³	0.31 × 0.3 × 0.29
Radiation	Mo Kα (λ = 0.71073)
2θ range for data collection/°	2.944 to 32.347
Index ranges	-23 ≤ h ≤ 26, -16 ≤ k ≤ 16, -24 ≤ l ≤ 25
Reflections collected	12688
Refinement method	Full-matrix least-squares on F ²
Independent reflections	5279 [R _{int} = 0.0219, R _{sigma} = 0.0226]
Data/restraints/parameters	5279/0/232
Goodness-of-fit on F²	1.052
Final R indexes [I ≥ 2σ (I)]	R1 = 0.0255, wR2 = 0.0650
Final R indexes [all data]	R1 = 0.0268, wR2 = 0.0661
Largest diff. peak/hole / e Å⁻³	0.939/-1.421
CCDC No.	1539165

2.5 Reference

- [1] Kim D. S., Park W. J., Jun C. H. (2017), Metal–Organic Cooperative Catalysis in C–H and C–C Bond Activation. *Chem. Rev.*, *117*(13), 8977-9015 doi:10.1021/acs.chemrev.6b00554
- [2] Mack J. B. C., Gipson J. D., Du Bois J., Sigman M. S. (2017), Ruthenium-Catalyzed C–H Hydroxylation in Aqueous Acid Enables Selective Functionalization of Amine Derivatives. *J. Am. Chem. Soc.*, *139*(28), 9503-9506 doi:10.1021/jacs.7b05469
- [3] Wang X., Chen W., Zhang L., Yao T., Liu W., Lin Y., . . . Li Y. (2017), Uncoordinated Amine Groups of Metal–Organic Frameworks to Anchor Single Ru Sites as Chemoselective Catalysts toward the Hydrogenation of Quinoline. *J. Am. Chem. Soc.*, *139*(28), 9419-9422 doi:10.1021/jacs.7b01686
- [4] Kim D.-S., Park W.-J., Lee C.-H., Jun C.-H. (2014), Hydroesterification of Alkenes with Sodium Formate and Alcohols Promoted by Cooperative Catalysis of Ru₃(CO)₁₂ and 2-Pyridinemethanol. *J. Org. Chem.*, *79*(24), 12191-12196 doi:10.1021/jo501828j
- [5] Wieder N. L., Carroll P. J., Berry D. H. (2011), Structure and Reactivity of Acetylene Complexes of Bis(imino)pyridine Ruthenium(0). *Organometallics*, *30*(8), 2125-2136 doi:10.1021/om100953g
- [6] Wenzel A. G., Blake G., VanderVelde D. G., Grubbs R. H. (2011), Characterization and Dynamics of Substituted Ruthenacyclobutanes Relevant to the Olefin Cross-Metathesis Reaction. *J. Am. Chem. Soc.*, *133*(16), 6429-6439 doi:10.1021/ja2009746
- [7] Kuai C., Wang L., Cui H., Shen J., Feng Y., Cui X. (2016), Efficient and Selective Synthesis of (E)-Enamides via Ru(II)-

- Catalyzed Hydroamidation of Internal Alkynes. *ACS Catalysis*, 6(1), 186-190 doi:10.1021/acscatal.5b01791
- [8] Arndt M., Salih K. S. M., Fromm A., Goossen L. J., Menges F., Niedner-Schatteburg G. (2011), Mechanistic Investigation of the Ru-Catalyzed Hydroamidation of Terminal Alkynes. *J. Am. Chem. Soc.*, 133(19), 7428-7449 doi:10.1021/ja111389r
- [9] Ko S., Na Y., Chang S. (2002), A Novel Chelation-Assisted Hydroesterification of Alkenes via Ruthenium Catalysis. *J. Am. Chem. Soc.*, 124(5), 750-751 doi:10.1021/ja017076v
- [10] Park E. J., Lee J. M., Han H., Chang S. (2006), Halide Ions as a Highly Efficient Promoter in the Ru-Catalyzed Hydroesterification of Alkenes and Alkynes. *Org. Lett.*, 8(19), 4355-4358 doi:10.1021/ol061753e
- [11] Ko S., Han H., Chang S. (2003), Ru-Catalyzed Hydroamidation of Alkenes and Cooperative Aminocarboxylation Procedure with Chelating Formamide. *Org. Lett.*, 5(15), 2687-2690 doi:10.1021/ol034862r
- [12] Sahn J. J., Hodges T. R., Chan J. Z., Martin S. F. (2016), Norbenzomorphan Framework as a Novel Scaffold for Generating Sigma 2 Receptor/PGRMC1 Subtype-Selective Ligands. *ChemMedChem*, 11(6), 556-561 doi:10.1002/cmdc.201500551
- [13] Sitte H. H., Freissmuth M. (2015), Amphetamines, new psychoactive drugs and the monoamine transporter cycle. *Trends Pharmacol. Sci.*, 36(1), 41-50 doi:10.1016/j.tips.2014.11.006
- [14] Granger B. A., Kaneda K., Martin S. F. (2012), Libraries of 2,3,4,6,7,11b-Hexahydro-1H-pyrido[2,1-a]isoquinolin-2-amine Derivatives via a Multicomponent Assembly Process/1,3-Dipolar Cycloaddition Strategy. *ACS Comb. Sci.*, 14(1), 75-79 doi:10.1021/co2001636

- [15] Figliolia R., Baldino S., Nedden H. G., Zanotti-Gerosa A., Baratta W. (2017), Mild N-Alkylation of Amines with Alcohols Catalyzed by the Acetate Ru(OAc)₂(CO)(DiPPF) Complex. *Chem. - Eur. J.*, 23(58), 14416-14419 doi:10.1002/chem.201702996
- [16] Akhtar W. M., Cheong C. B., Frost J. R., Christensen K. E., Stevenson N. G., Donohoe T. J. (2017), Hydrogen Borrowing Catalysis with Secondary Alcohols: A New Route for the Generation of β -Branched Carbonyl Compounds. *J. Am. Chem. Soc.*, 139(7), 2577-2580 doi:10.1021/jacs.6b12840
- [17] Yu X. J., He H. Y., Yang L., Fu H. Y., Zheng X. L., Chen H., Li R. X. (2017), Hemilabile N-heterocyclic carbene (NHC)-nitrogen-phosphine mediated Ru (II)-catalyzed N-alkylation of aromatic amine with alcohol efficiently. *Catal. Commun.*, 95, 54-57 doi:10.1016/j.catcom.2017.03.007
- [18] Ahn J. M., Ratani T. S., Hannoun K. I., Fu G. C., Peters J. C. (2017), Photoinduced, Copper-Catalyzed Alkylation of Amines: A Mechanistic Study of the Cross-Coupling of Carbazole with Alkyl Bromides. *J. Am. Chem. Soc.*, 139(36), 12716-12723 doi:10.1021/jacs.7b07052
- [19] Midya S., Mondal A., Begum A., Balaraman E., Djukic J. P., Agbossou-Niedercorn F., Michon C. (2017), A Simple Cobalt(II) Chloride Catalyzed N-Alkylation of Amines with Alcohols. *Synthesis*, 49(17), 3957-3961 doi:10.1055/s-0036-1589064
- [20] Grigg R., Mitchell T. R. B., Sutthivaiyakit S., Tongpenyai N. (1981), Transition metal-catalysed N-alkylation of amines by alcohols. *J. Chem. Soc., Chem. Commun.*(12), 611-612 doi:10.1039/C39810000611
- [21] Watanabe Y., Tsuji Y., Ige H., Ohsugi Y., Ohta T. (1984), Ruthenium-catalyzed N-alkylation and N-benzoylation of

- aminoarenes with alcohols. *J. Org. Chem.*, 49(18), 3359-3363
doi:10.1021/jo00192a021
- [22] Fujita K. i., Enoki Y., Yamaguchi R. (2008), Cp*Ir-catalyzed N-alkylation of amines with alcohols. A versatile and atom economical method for the synthesis of amines. *Tetrahedron*, 64(8), 1943-1954 doi:10.1016/j.tet.2007.11.083
- [23] Blank B., Michlik S., Kempe R. (2009), Synthesis of Selectively Mono-N-Arylated Aliphatic Diamines via Iridium-Catalyzed Amine Alkylation. *Adv. Synth. Catal.*, 351(17), 2903-2911 doi:10.1002/adsc.200900548
- [24] Blank B., Michlik S., Kempe R. (2009), Selective Iridium-Catalyzed Alkylation of (Hetero)Aromatic Amines and Diamines with Alcohols under Mild Reaction Conditions. *Chem. - Eur. J.*, 15(15), 3790-3799 doi:10.1002/chem.200802318
- [25] Hollmann D., Bähn S., Tillack A., Beller M. (2007), Eine allgemeine rutheniumkatalysierte Synthese von aromatischen Aminen. *Angew. Chem.*, 119(43), 8440-8444 doi:10.1002/ange.200703119
- [26] Hamid M. H. S. A., Allen C. L., Lamb G. W., Maxwell A. C., Maytum H. C., Watson A. J. A., Williams J. M. J. (2009), Ruthenium-Catalyzed N-Alkylation of Amines and Sulfonamides Using Borrowing Hydrogen Methodology. *J. Am. Chem. Soc.*, 131(5), 1766-1774 doi:10.1021/ja807323a
- [27] Gunanathan C., Milstein D. (2008), Selective Synthesis of Primary Amines Directly from Alcohols and Ammonia. *Angew. Chem. Int. Ed.*, 47(45), 8661-8664 doi:10.1002/anie.200803229
- [28] Agrawal S., Lenormand M., Martín-Matute B. (2012), Selective Alkylation of (Hetero)Aromatic Amines with Alcohols Catalyzed by a Ruthenium Pincer Complex. *Org. Lett.*, 14(6), 1456-1459 doi:10.1021/ol3001969

- [29] Ramachandran R., Prakash G., Nirmala M., Viswanathamurthi P., Malecki J. G. (2015), Ruthenium(II) carbonyl complexes designed with arsine and PNO/PNS ligands as catalysts for N-alkylation of amines via hydrogen autotransfer process. *J. Organomet. Chem.*, 791, 130-140 doi:10.1016/j.jorganchem.2015.05.054
- [30] Ramachandran R., Prakash G., Selvamurugan S., Viswanathamurthi P., Malecki J. G., Linert W., Gusev A. (2015), Ruthenium(ii) complexes containing a phosphine-functionalized thiosemicarbazone ligand: synthesis, structures and catalytic C-N bond formation reactions via N-alkylation. *RSC Advances*, 5(15), 11405-11422 doi:10.1039/C4RA14797A
- [31] Van Doorn J. A., Van Leeuwen P. W. N. M. (1981), Reactions between 8-quinolinol (and related ligands) and triruthenium dodecacarbonyl; x-ray crystal structure determination of $\text{Ru}_3(\text{CO})_8(\text{C}_9\text{H}_6\text{NO})_2$. *J. Organomet. Chem.*, 222(2), 299-309 doi:10.1016/S0022-328X(00)89158-5
- [32] Mason R., Rae A. I. M. (1968), The crystal structure of ruthenium carbonyl, $\text{Ru}_3(\text{CO})_{12}$. *J. Chem. Soc. (A)*, 1, 778-779
- [33] Sheldrick G. M. (2015), Crystal structure refinement with SHELXL. *Acta Crystallogr., Sect. C: Struct. Chem.*, 71(Pt 1), 3-8 doi:10.1107/S2053229614024218
- [34] Dolomanov O. V., Bourhis L. J., Gildea R. J., Howard J. A. K., Puschmann H. (2009), OLEX2: a complete structure solution, refinement and analysis program. *J. Appl. Crystallogr.*, 42(2), 339-341 doi:10.1107/S0021889808042726
- [35] Yamaguchi R., Kawagoe S., Asai C., Fujita K.-i. (2008), Selective Synthesis of Secondary and Tertiary Amines by Cp*Iridium-Catalyzed Multialkylation of Ammonium Salts with Alcohols. *Org. Lett.*, 10(2), 181-184 doi:10.1021/ol702522k

- [36] Whitesides G. M., Hackett M., Brainard R. L., Lavalleye J. P. P. M., Sowinski A. F., Izumi A. N., . . . Staudt E. M. (1985), Suppression of unwanted heterogeneous platinum(0)-catalyzed reactions by poisoning with mercury(0) in systems involving competing homogeneous reactions of soluble organoplatinum compounds: thermal decomposition of bis(triethylphosphine)-3,3,4,4-tetramethylplatinacyclopentane. *Organometallics*, 4(10), 1819-1830 doi:10.1021/om00129a023

Chapter 3

Facile oxidation of alcohols to carboxylic acids in basic water medium by employing ruthenium picolinate cluster as an efficient catalyst

3.1 Introduction

Benzoic acid and its derivatives are important precursors for the synthesis of useful organic compounds.[1-4] Several hundred thousand tons of benzoic acid for industrial applications are produced every year.[5,6] Benzoic acid is a main component in the food preservatives[7] mostly because of its antifungal[8,9] and antimicrobial activities.[9] Its derivatives are also useful for the production of plasticizer,[10] alkyd resins[11,12] or polymers.[13,14]

In the past few decades, the use of transition metal complexes contributed tremendously to catalytic organic synthesis.[15-21] Oxidations of alcohols to carboxylic acids require various oxidants in large quantity like KMnO_4 , iodosobenzene, *t*-BuOOH, chromium oxide and thus produce copious waste.[22] Whereas, the catalytic synthesis of carboxylic acid derivatives from alcohols was initially performed with ruthenium-hydride complexes, polyoxometallates or PNN pincer complexes.[23-26]

Rhodium-catalyzed oxidation of alcohol to a carboxylate at high pH and, using ketone as a hydrogen acceptor under mild conditions was reported by Grützmacher et al.[27] Heterogeneous copper system[28] with NaOH at 320°C with high pressure has also been used for catalytic oxidation of alcohol to carboxylates.[29] For the oxidation of alcohols to the carboxylic acids, a new clean and atom economy approach has been introduced by Milstein's group using water as the oxygen donor in the presence of a base and using the PNN pincer ruthenium-hydride catalyst.[30] The reaction takes place with

dehydrogenation of alcohol to give coordinated aldehyde to which water addition allows to the formation of the carboxylic acid.[30] Prechtl's group also contributed to the carboxylic acid formation from alcohols using PNP pincer ruthenium-hydride catalyst (**Figure 3.1, cat. ii b**),[31] Beller's group could convert renewable glycerol into 2-oxopropanoic acid using ruthenium-hydride PNP pincer complex (**Figure 3.1, cat. ii a**).[32] By contrast, Möller's group used simple ruthenium(II)-NHCarbene complex to perform this transformation (**Figure 3.1, cat. iii**).[33] Peng's group used ruthenium complex containing new 2,6-bis(benzimidazole-2-yl)pyridine pincer ligand for this catalytic transformation (**Figure 1, cat. iv**),[34] whereas Gauvin's group[35] have shown that recyclable PNP-ruthenium-hydride catalysts, prepared *in-situ* by addition of PNP ligand to $[\text{Ru}(\text{H})(\text{X})(\text{CO})(\text{PPh}_3)_3]$ ($\text{X} = \text{H}, \text{Cl}$), was efficient for the oxidation of primary alcohols into carboxylate (**Figure 3.1, cat. ii c**).[35] Recently Bera's group reported that this oxidation reaction could be efficiently performed by non-pincer, ruthenium-hydride complex (**Figure 3.1, cat. v**).[36]

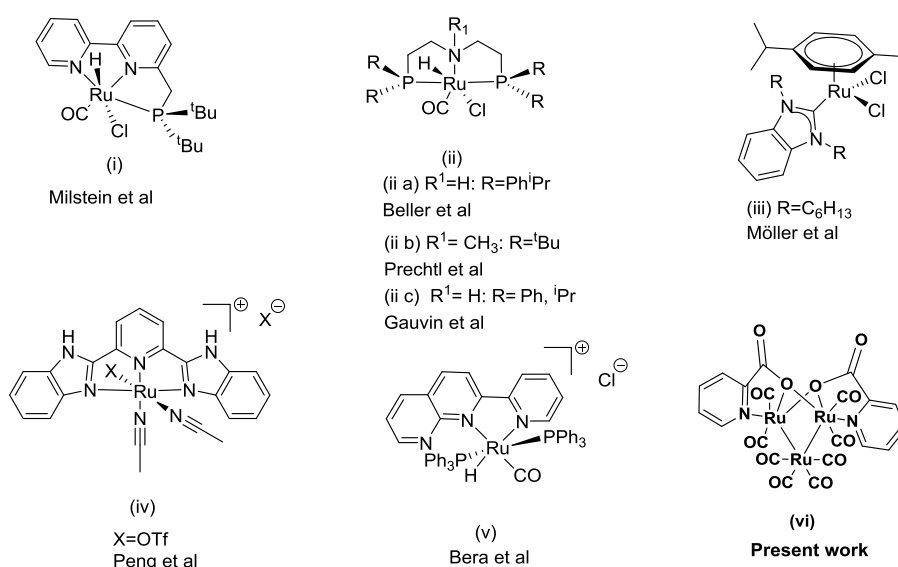


Figure 3.1. Ruthenium-based active catalysts for carboxylic acid synthesis from alcohols

Most of the above mentioned efficient ruthenium catalysts for the transformation of alcohol to carboxylate into basic water involve

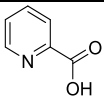
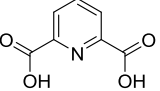
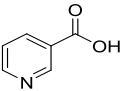
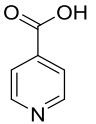
ruthenium-hydride or pincer ruthenium catalysts. In this report, we describe the preparation of a new ruthenium carbonyl cluster $[\text{Ru}_3(\text{CO})_8(\text{C}_5\text{H}_4\text{NCO}_2)_2]$ (**1**) containing two simple chelating pyridine-carboxylate ligands, (**Figure 3.1**, cat. vi) as an efficient catalyst, without pincer ligand for the transformation of a variety of alcohols into carboxylic acids in basic water-isopropanol medium with good yields.

3.2 Results and discussion

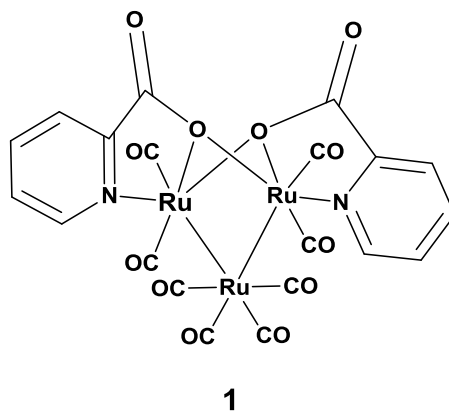
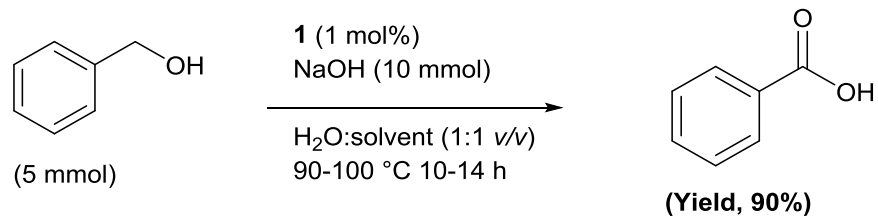
3.2.1 Catalyst screening

The oxidation of benzyl alcohol into carboxylic acid using a catalyst arising in situ from $\text{Ru}_3(\text{CO})_{12}$ and a pyridine derivative containing a carboxylate group picolinic acid (1a), pyridine-2,6-dicarboxylic acid (1b), nicotinic acid (1c) and iso-nicotinic acid (1d) to get the adducts **1–4**, respectively (**Table 3.1**). It was found that adduct/cluster **1** and adduct **2** were active in the catalytic transformation of alcohols to carboxylic acids using NaOH in an open atmosphere for 14 h at bath temperature, 98 °C in water-solvent (**Scheme 3.1**) likely due to their appropriate 5-membered chelation to $\text{Ru}_3(\text{CO})_{12}$ which is not possible with nicotinic and iso-nicotinic acid ligands. The chelation environment is confirmed by the structure of cluster **1**. It was authenticated by single crystal X-ray studies.

Table 3.1. Screening of the catalyst for the transformation of benzyl alcohol to benzoic acid in basic water and dioxane as solvent

Entry No.	Component 1	Component 2	Adduct/Cluster	Catalytic oxidation reaction
1	$\text{Ru}_3(\text{CO})_{12}$		1	-R-
2	$\text{Ru}_3(\text{CO})_{12}$		2	-R-
3	$\text{Ru}_3(\text{CO})_{12}$		3	-NR-
4	$\text{Ru}_3(\text{CO})_{12}$		4	-NR-
5	$\text{Ru}_3(\text{CO})_{12}$	—		-NR-

R= Reaction successful NR= No reaction Reaction conditions: benzyl alcohol (5 mmol), base (10 mmol), catalyst (1 mol%), H_2O (500 μL), solvent (500 μL) were stirred at bath temperature 98 °C in an oil bath in open atmosphere.



Scheme 3.1. Schematic representation for the oxidation of alcohol to carboxylic acid

3.2.2 Structural description of Catalyst 1

The cluster **1** was obtained by the reaction of $\text{Ru}_3(\text{CO})_{12}$ with simple chelation of picolinic acid in toluene at 110°C for an hour. The molecular structure of **1** revealed the binding modes of picolinic acid ligand to $\text{Ru}_3(\text{CO})_{12}$ and the crystal structure is shown in **Figure 3.2**. The detailed structural parameters of complex **1** are shown in **Table 3.2**.

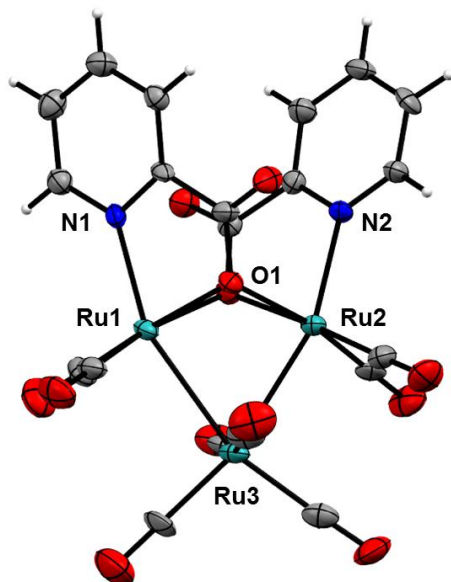


Figure 3.2 Perspective view of cluster **1**

Table 3.2 Crystal data and structure refinement for complex **1**

Identification code	Complex 1
Empirical formula	C ₁₀ H ₄ NO ₆ Ru _{1.5}
Formula weight	385.75
Temperature/K	293(2)
Crystal system	Monoclinic
Space group	<i>Pn</i>
a/Å	9.45480(10)
b/Å	11.71470(10)
c/Å	11.03310(10)
α/°	90
β/°	98.2050(10)
γ/°	90
Volume/Å³	1209.52(2)
Z	4
ρ_{calc}/cm³	2.118
μ/mm⁻¹	15.593
F(000)	740
Crystal size/mm³	0.34 × 0.33 × 0.29
Radiation	Cu Kα (λ = 1.54184)
2θ range for data collection/°	7.546 to 142.5
Index ranges	-8 ≤ h ≤ 11, -14 ≤ k ≤ 14, -13 ≤ l ≤ 13
Reflections collected	6597
Independent reflections	3023 [R _{int} = 0.0467, R _{sigma} = 0.0271]
Data/restraints/parameters	3023/2/334
Goodness-of-fit on F²	1.091

Final R indexes [$I \geq 2\sigma(I)$]	$R_1 = 0.0487$, $wR_2 = 0.1282$
Final R indexes [all data]	$R_1 = 0.0494$, $wR_2 = 0.1343$
Largest diff. peak/hole / $e \text{ \AA}^{-3}$	1.52/-1.43
CCDC No.	1576762

Structure of **1** is symmetric and crystallized in Pn space group with monoclinic crystal system. In this structure, the asymmetric unit consists of one picolinate ligand attached to one ruthenium atom by the nitrogen atom and one oxygen atom. The oxygen of the picolinate ligand is bridging the two ruthenium atoms, each adopting a distorted octahedral $RuC_2N_1O_2$ coordination sphere (see **Figure 3.2**). The unique O–Ru–O *cis* bite angle is 76.33° , and similarly, the other O–Ru–O bite angle is 76.88° , the *trans* N–Ru–Ru angle is 158.93° in complex **1**. Two carbonyls are attached to each ruthenium atom bearing picolinate ligand. Overall two picolinate and eight carbonyl ligands are attached to three ruthenium atoms. The complex **1** has a glide plane perpendicular to $[0, 1, 0]$ with glide component $[1/2, 0, 1/2]$. The order of the glide plane is 2. The distance between 2 ruthenium atoms (Ru1 and Ru2) is 3.068 \AA which is more than the traditional $Ru_3(CO)_{12}$ crystal structure (2.848 \AA).^[37] The Ru1 and Ru2 are bonded to Ru3 with 2.778 and 2.764 \AA , respectively. The ruthenium atoms Ru1 and Ru2 are attached to two oxygen atoms sharing the electron pair, i.e. lone pair (2.207 \AA) and a bond pair (2.148 \AA). Nitrogen donates its lone pair to Ru1 and Ru2 atom with the bond length of 2.514 \AA .

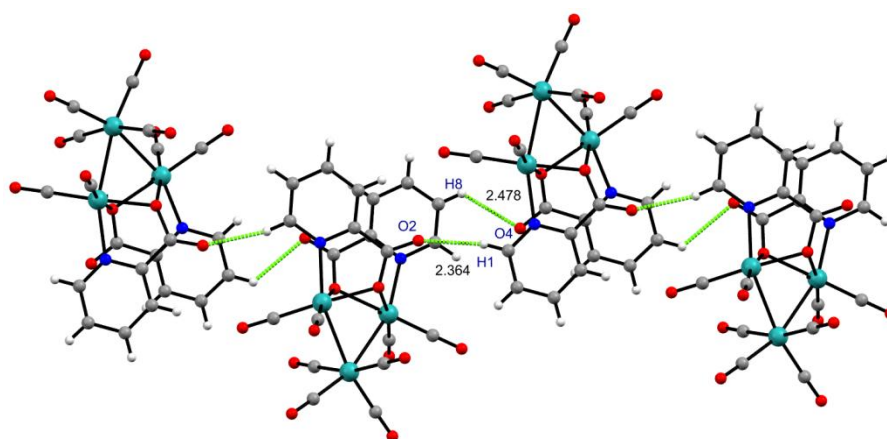


Figure 3.3 H-bonded 1-D network in **1** along *c* axis

The complex **1** forms the 1-D polymeric chain using C-H...O interaction, i.e. H4...O5 with distance 2.705 Å, and H1...O2 and H8...O4 with the distances 2.364 and 2.478 Å, respectively (**Figure 3.3**). 1-D chain extends to 2-D network *via* π - π interaction between C6-C10 with distance 3.354 Å.

3.2.3 Catalytic experiments

The oxidation reaction of benzyl alcohol (**Scheme 3.1**) using 1 mol% of catalyst **1** was evaluated in water in the presence of different solvents between 75°C–100°C. Using dioxane, DMF with water, a side product hydrobenzoin was obtained along with benzoic acid in the inert (argon) atmosphere (**Table 3.3**, entries no. 1 and 4) whereas, the same byproduct was obtained at the lower temperature of standard condition (**Table 3.3**, entry no. 13). Using alcohols, chloroform and acetonitrile with water in inert atmosphere gave only benzoic acid, but in lower yields (**Table 3.3**, entries no. 2, 3, 5, 6). Neat solvents like DMF and t-butanol gave a lower yield in the inert and open environment, respectively (**Table 3.3**, entry no. 7). Using neat water in an argon atmosphere, without any other solvent, and without a base, the reaction did not give any oxidized product (**Table 3.3**, entry no. 8) as the catalyst **1** is not soluble in the neat water. In general, when the reactions were performed either in water and alcohol medium (inert atmosphere) or neat alcohol medium in the open atmosphere, both lead to a lower yield of the product. In contrast, when the reaction was performed in the iso-propanol and water (1:1) as the medium in open air atmosphere, a higher yield (90%) of benzoic acid was observed at 98 °C (**Table 3.3**, entry no. 11). This significant result proves the importance of cluster **1** in catalyzing the alcohol to carboxylic acid into basic water in the open atmosphere. Several alcohols along with the water as reaction medium were also studied and iso-propanol appears as the most suitable solvent for this reaction (**Table 3.3**, entries no. 10–13).

Table 3.3. Optimization for the synthesis of benzoic acid from benzyl alcohol

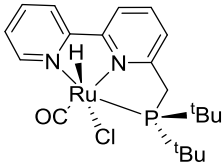
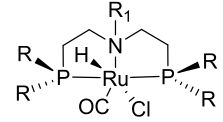
Entry No.	Solvent	Reaction atmosphere	Base (10 mmol)	Time (h)	Conv. (%)	Yield (%)	
						benzoic acid	hydrobenzoin
1	Dioxane	H ₂ O/Ar	NaOH	14	65	21	42
2	Methanol	H ₂ O/Ar	NaOH	14	19	19	0
3	Iso-propanol	H ₂ O/Ar	NaOH	10	2	1	0
4	DMF	H ₂ O/Ar	NaOH	24	74	9	35
5	Chloroform	H ₂ O/Ar	NaOH	12	17	7	0
6	Acetonitrile	H ₂ O/Ar	NaOH	12	24	10	0
7	DMF	Ar	NaOH	24	7	0	0
8	Water	Ar	NaOH	12	0	0	0
9	Methanol	H ₂ O/O ₂	NaOH	12	69	69	0
10	Ethanol	H ₂ O/O ₂	NaOH	12	82	81	0
11	Iso-propanol	H₂O/O₂	NaOH	12	90	90	0
12	t-butanol	H ₂ O/O ₂	NaOH	12	40	27	0
13	Iso-propanol ^a	H ₂ O/O ₂	NaOH	24	34	2	32

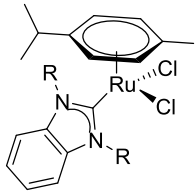
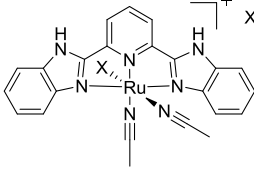
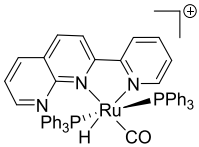
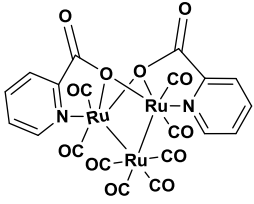
Reaction conditions: benzyl alcohol (5 mmol), base (10 mmol), catalyst **1** (1 mol%), H₂O (500 μL), solvent (500 μL) were stirred at bath temperature 98 °C in an oil bath in open atmosphere. Products were analyzed using GC-MS and ¹H NMR; a=room temperature (25 °C)

We evaluated different bases in the oxidation reaction; K_2CO_3 , KOH, and NaOH, the most efficient bases were found to be KOH and NaOH as the base is effective for the de-protonation in alcohol/solvent medium. Interestingly, at room temperature, hydrobenzoin was formed in high quantity, and as the temperature was increased (at 60 °C), the formation of benzoic acid was enhanced. The optimization studies of the temperature proved that the reaction was even possible at RT, 60 °C, 75 °C but with the lower conversion of benzyl alcohol to benzoic acid. This study proves that the catalyst **1** is also active even at the lower temperature.

Previous examples of the synthesis of benzoic acid from alcohol as reviewed earlier are summarized in **Table 3.4**.

Table 3.4. Comparative study of the benzoic acid formation from benzylic alcohol using ruthenium complexes so far

$\text{R-CH}_2\text{-OH} \xrightarrow[\text{base, solvent, temp., time}]{\text{catalyst}} \text{R-COOH} + \text{H}_2$ <p style="text-align: center;">Alcohol Acid</p>					
Entry No.	Catalyst or pre-catalyst	Substrate	Reaction parameters	Yield (%)	Ref. (s)
1		Alcohol	Catalyst, NaOH, water (reflux), 18 h, argon.	84%	[30]
2	 <p> $R_1 = \text{H}; R = \text{Ph}^i\text{Pr}$ $R_1 = \text{CH}_3; R = ^i\text{Bu}$ $R_1 = \text{H}; R = \text{Ph}, ^i\text{Pr}$ </p>	Alcohol	1) Catalyst, NaOH, 120 °C, 20 h 2) Catalyst, KOH, 125 °C, 20 h	1) 67% 2) 92%	[31,32,35]

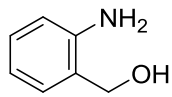
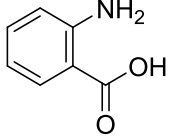
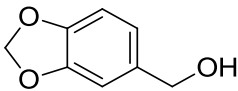
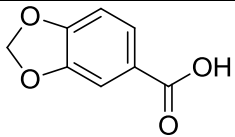
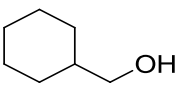
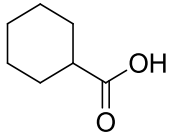
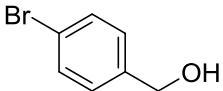
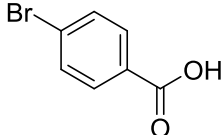
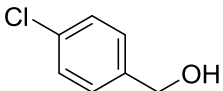
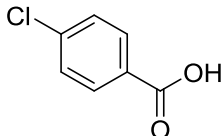
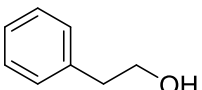
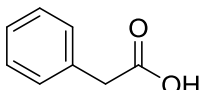
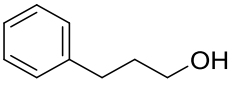
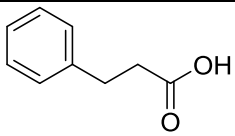
3	 $R = C_6H_{13}$	Alcohol	Catalyst, NaOH, water (reflux), 24 h	92%	[33]
4	 $X = OTf$	Benzyl alcohol	Catalyst, CsOH, water (reflux), 24 h (argon)	82%	[34]
5		Benzyl alcohol	Catalyst, water, NaOH, 110 °C, (6h–24h)	100 %	[36]
6		Benzyl alcohol	Catalyst, NaOH, water, iso-propanol, 98 °C, 12 h	90%	Our work

So far the reported catalysts (**Table 3.4**, entries no. 1–5) are either ruthenium hydride or ruthenium pincer complex precursors which require much efforts and sensitive environment to synthesize them. Also, the catalytic oxidation also needs a higher temperature. However, **1** is easily obtained by the simple chelation of picolinic acid ligand to $Ru_3(CO)_{12}$ by refluxing them in toluene for an hour. Moreover, the reaction conditions for catalytic oxidation are also comparatively mild.

The substrate scope of the oxidation reaction is presented in **Table 3.5**. The catalytic oxidation is more favorable in substituents with electron donating inductive effect (**Table 3.5**, entries no. 1 and 4). Para substituted benzyl alcohols are more easily oxidized than the ortho substituted benzyl alcohols likely because they are not creating any steric hindrance like ortho substituted benzyl alcohols. The reaction was also performed with cyclic aliphatic compound; however, inferior yield was obtained (**Table 3.5**, entry no. 5). The p-chloro substituted benzyl alcohol gave the higher yield over p-bromo substituted benzyl alcohol because of stronger C-Cl bond over C-Br bond, as benzoic acid is the other byproduct along with p-halobenzoic acid. To prove the efficiency of catalyst **1** to aliphatic alcohol derivatives, 2-phenylethan-1-ol and 2-phenylpropan-1-ol were also explored and desired carboxylic acids were formed. So, the catalyst was also found to be active over aliphatic derivatives. Furthermore, when pyridyl ring substituted compounds were used instead of benzyl substituents, the oxidation reaction did not occur, which is attributed to pyridine ring interaction with ruthenium and deactivation of the catalyst **1**.

Table 3.5. Synthesis of carboxylic acid derivatives from alcohols

Entry No.	Reactant	Product	Conversion (%)	Yield by GCMS (%)
1			70	66
2			43	41

3			90	34
4			75	71
5			20	19
6			95	25
7			98	65
8			44	34
9			54	34

Yields measured by GCMS, as consolidated in **Table 3.5**, are the average of 3 reactions with $\pm 5\%$ error observed.

Reaction conditions: alcohol (5 mmol), NaOH (10 mmol), catalyst **1** (1 mol%) were heated in an open atmosphere at bath temperature of 98 °C. The reaction time is 14 h. Derivatives of benzoic acid were obtained by 2M HCl acid treatment of the reaction mixture. Products were analyzed using GC-MS and ^1H , ^{13}C NMR.

Several attempts were made to isolate the intermediate by following different procedures [30,36,38,39] by reacting catalyst and benzyl alcohol in aqueous methanol as well as in CHCl_3 .

Unfortunately, the intermediate could not be isolated successfully. The role of the picolinic acid anion is most likely to assist removal of CO and subsequent addition of PhCH_2O^- ligand. We have also checked the ruthenium pyridine alcohol cluster for the catalytic transformation of primary alcohols to the carboxylic acid, but we only found the conversion of primary alcohols to aldehyde, with very less trace of carboxylic acid.

The plausible oxidation mechanism is based on the Milstein mechanism for pincer-ruthenium(II) catalyst,[30] and here the catalytic transformation takes place at one of Ru centers bridged by two picolinate ligands as $\text{Ru}_3(\text{CO})_{12}$ itself does not catalyze the alcohol oxidation. After CO elimination, it involves the initial coordination of the deprotonated alcohol (PhCH_2O^-) to one of the two bridged Ru atoms (**Figure 3.4, 1a**). This is followed, after CO decoordination, by hydride beta-elimination from the Ru-OCH₂Ph species to give the coordinated aldehyde $\text{HRu}(\text{O}=\text{CHPh})$ [30,36](**1b**). Further reaction with water gives a gem-diolate complex and H₂ elimination (**1c**). Beta hydride elimination gives the final carboxylic acid product, and the RuH(CO) species (**1d**) can deprotonate PhCH₂OH to give **1a**.

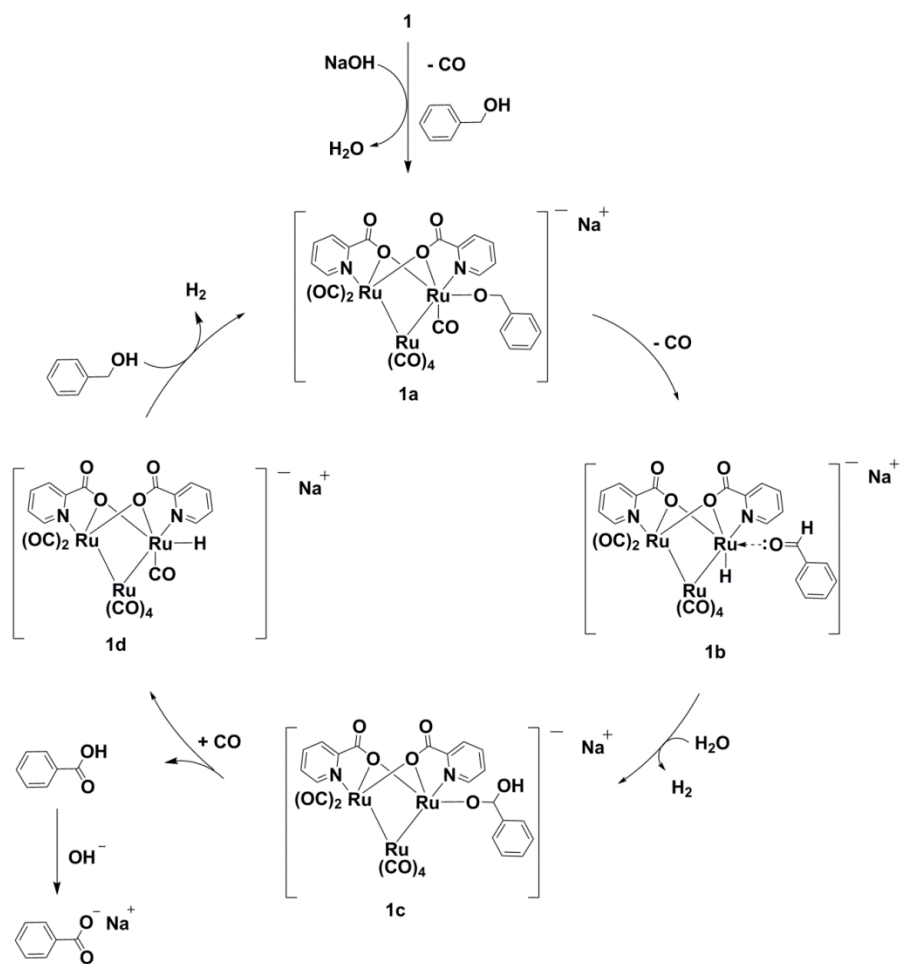


Figure 3.4 Plausible mechanism for catalytic oxidation of alcohol to carboxylic acid by ruthenium cluster $[\text{Ru}_3(\text{CO})_8(\text{C}_5\text{H}_4\text{NCO}_2)_2]$.

3.3 Conclusions

In summary, a new $\text{Ru}_3(\text{CO})_{12}$ based pyridine-acid $[\text{Ru}_3(\text{CO})_8(\text{C}_5\text{H}_4\text{NCO}_2)_2]$ cluster was synthesized by facile addition of picolinic acid to $\text{Ru}_3(\text{CO})_{12}$ and characterized by single crystal XRD. The complex/catalyst **1** was evaluated for the catalytic oxidation of alcohol to carboxylic acid (yield, 90%) using basic water in the open atmosphere. The crystal structure of complex **1** revealed the C-H...O and π ... π interactions. The catalyst **1** is comparable with previously reported ruthenium hydride or ruthenium pincer complexes as it converts the primary alcohol to carboxylic acid at a relatively lower temperature (98 °C) in water in open environment (**Scheme 1**). Moreover, cluster **1** shows selectively high yield (90%) in water and iso-propanol as the reaction medium. In the catalytic system, both water and oxygen (from the open atmosphere) are taking part in the oxidation of alcohol to the carboxylic acid. These findings may open a route to design new clusters for the transformation of alcohol to corresponding carboxylic acid derivatives.

3.4 Experimental section

3.4.1 Materials and instrumentation details

$\text{Ru}_3(\text{CO})_{12}$, picolinic acid and alcohol derivatives were purchased from Aldrich and TCI chemicals. Reagents used for purification and crystallization of products were purchased from Rankem and Merck and used as received. NMR spectra were recorded in CDCl_3 on a Bruker Avance (III) spectrometer (400 MHz). X-ray structural study of complex **1** was carried out using Agilent Technologies Supernova CCD system. Samples were analyzed in Shimadzu QP2010 Ultra equipped with Rtx-5MS column (length 30 meters, internal diameter 0.25 mm). The column oven program was used as 40 °C (hold 5 min.) \rightarrow 20 °C/min. \rightarrow 280 °C (hold 13 min.) along with injection temperature 280 °C, interface temperature was 300 °C, and ion source temperature was 220 °C.

3.4.2 Single crystal X-ray diffraction (SC-XRD)

Graphite-monochromated Cu $K\alpha$ ($\lambda_\alpha = 1.54184 \text{ \AA}$) source at 25 °C was used to collect data. The standard phi-omega scan technique was used to collect data. The interpretation of the collected data was done by CrysAlisPro CCD software. The SHELXS-97 direct method was used to produce the crystal structures, and refinement was done by the full matrix least squares method on F^2 . [40] Olex-1.2 software was also used. [41] All the C–H... π interactions, [42] molecular drawings, and mean plane analyses were obtained by Diamond (ver. 3.1d) and Mercury (ver. 3.1). The crystals structure and their refinement data are shown in **Figure 3.2** and **Table 3.2**, respectively.

3.4.3 Catalytic reaction

5 mmol benzyl alcohol, 10 mmol NaOH were mixed in 500 μL of water and 500 μL of iso-propanol solvent media. 1 mol% of catalyst **1** was added. The reaction was performed at bath temperature of 98 °C, i.e. in the atmospheric oxygen environment. After 14 h, the solvent was evaporated, and a white precipitate was observed. 5 mL of 2M HCl was added to the reaction mixture and stirred for 5 min. Then 5

mL ethyl acetate was added and extraction was done using 5 x 3 mL ethyl acetate. Then after brine wash, the recovered mixture was passed through a small column of sodium sulphate. After evaporation of the solvent, white solid benzoic acid was obtained. The solid was recrystallized using methanol, and the NMR data show the benzoic acid formation. The yield of the benzoic acid was 90% which was similar to the result observed using GC-MS.

3.4.4 Analysis of products

After completion of reactions, the solvent was evaporated, and products were isolated. Synthesized products were characterized using GC-MS, ^1H and ^{13}C NMR. Crystallographic data for complex **1** has been deposited with the Cambridge Crystallographic Data Centre, CCDC No. 1576762 in CIF format.

3.5 References

- [1] Sun H., Xu S., Li Z., Xu J., Liu J., Wang X., . . . Guo K. (2017), A preorganized dual H-bond donor promotes benzoic acid active in the polymerization of δ -valerolactone. *Polym. Chem.*, 8(36), 5570-5579 doi:10.1039/C7PY01192J
- [2] Pfennig T., Carraher J. M., Chemburkar A., Johnson R. L., Anderson A. T., Tessonier J.-P., . . . Shanks B. H. (2017), A new selective route towards benzoic acid and derivatives from biomass-derived coumalic acid. *Green Chem.*, 19 4879-4888 doi:10.1039/C7GC02041D
- [3] Liu R., Hu R. J., Zhang P., Skolnick P., Cook J. M. (1996), Synthesis and Pharmacological Properties of Novel 8-Substituted Imidazobenzodiazepines: High-Affinity, Selective Probes for α 5-Containing GABAA Receptors. *J. Med. Chem.*, 39(9), 1928-1934 doi:10.1021/jm950887n
- [4] Mirallai S. I., Koutentis P. A. (2015), The Conversion of 4-Anilinoquinazoline- and 3-Aryl-4-imino-3,4-dihydroquinazoline-2-carbonitriles into Benzo[4,5]imidazo[1,2-c]quinazoline-6-carbonitriles via Oxidative and Nonoxidative C–N Couplings. *J. Org. Chem.*, 80(16), 8329-8340 doi:10.1021/acs.joc.5b01514
- [5] program F. (1998), FINAL PROGRAM. *Chemical & Engineering News Archive*, 76(9), 53-140 doi:10.1021/cen-v076n009.p053
- [6] Mahmoud E., Yu J., Gorte R. J., Lobo R. F. (2015), Diels–Alder and Dehydration Reactions of Biomass-Derived Furan and Acrylic Acid for the Synthesis of Benzoic Acid. *ACS Catalysis*, 5(11), 6946-6955 doi:10.1021/acscatal.5b01892

- [7] Chen L., Huang X. (2017), Preparation and application of a poly (ionic liquid)-based molecularly imprinted polymer for multiple monolithic fiber solid-phase microextraction of phenolic acids in fruit juice and beer samples. *Analyst* doi:10.1039/C7AN01186E
- [8] Berne S., Kovačič L., Sova M., Kraševc N., Gobec S., Križaj I., Komel R. (2015), Benzoic acid derivatives with improved antifungal activity: Design, synthesis, structure–activity relationship (SAR) and CYP53 docking studies. *Biorg. Med. Chem.*, 23(15), 4264-4276 doi:10.1016/j.bmc.2015.06.042
- [9] López A., Ming D. S., Towers G. H. N. (2002), Antifungal Activity of Benzoic Acid Derivatives from *Piper lanceaefolium*. *J. Nat. Prod.*, 65(1), 62-64 doi:10.1021/np010410g
- [10] Materials E. P. (2015), Emerald's benzoic acid investment supports demand for non-phthalate plasticizers. *Additives for Polymers*, 2015(6), 7 - 8 doi:10.1016/S0306-3747(15)30071-3
- [11] William M. Kraft V., and Hyman M. Metz, Fair Lawn, NJ. (1956), Benzoic acid-modified alkyd resins and their production. *US patent 2915488*
- [12] Raymond L. Heinrich B., Tex., and David A. Berry and Richard J. Dick, Columbus, Ohio. (1958), Modification of alkyd resins with 4-biphenyl benzoic acid. *US patent 2982747*
- [13] Han T., Zhao Z., Deng H., Kwok R. T. K., Lam J. W. Y., Tang B. Z. (2017), Iridium-catalyzed polymerization of benzoic acids and internal diynes: a new route for constructing high molecular weight polynaphthalenes without the constraint of monomer stoichiometry. *Polym. Chem.*, 8(8), 1393-1403 doi:10.1039/C6PY02165D

- [14] Shibasaki Y., Abe Y., Sato N., Fujimori A., Oishi Y. (2010), Direct condensation polymerization of N-alkylated p-aminobenzoic acid and packing of rigid-rod main chains with flexible side chains. *Polym. J.*, 42(1), 72-80 doi:10.1038/pj.2009.306
- [15] DuBois M. R. (1989), Catalytic applications of transition-metal complexes with sulfide ligands. *Chem. Rev.*, 89(1), 1-9 doi:10.1021/cr00091a001
- [16] Chen P. P.-Y., Yang R. B.-G., Lee J. C.-M., Chan S. I. (2007), Facile O-atom insertion into C C and C H bonds by a trinuclear copper complex designed to harness a singlet oxene. *PNAS*, 104(37), 14570-14575 doi:10.1073/pnas.0707119104
- [17] Sorokin A. B. (2013), Phthalocyanine Metal Complexes in Catalysis. *Chem. Rev.*, 113(10), 8152-8191 doi:10.1021/cr4000072
- [18] Midya S. P., Sahoo M. K., Landge V. G., Rajamohanan P. R., Balaraman E. (2015), Reversed reactivity of anilines with alkynes in the rhodium-catalysed C-H activation/carbonylation tandem. *Nat. Commun.*, 6, 8591 doi:10.1038/ncomms9591
- [19] Twilton J., Le C., Zhang P., Shaw M. H., Evans R. W., MacMillan D. W. C. (2017), The merger of transition metal and photocatalysis. *Nat. Rev. Chem.*, 1(7) doi:10.1038/s41570-017-0052
- [20] Yang W., Wei L., Yan T., Cai M. (2017), Highly efficient heterogeneous aerobic oxidative C-C coupling from Csp³-H bonds by a magnetic nanoparticle-immobilized bipy-gold(iii) catalyst. *Catal. Sci. Technol.*, 7(8), 1744-1755 doi:10.1039/C6CY02567F
- [21] Balaraman E., Nandakumar A., Jaiswal G., Sahoo M. K. (2017), Iron-catalyzed dehydrogenation reactions and their

- applications in sustainable energy and catalysis. *Catal. Sci. Technol.*, 7(15), 3177-3195 doi:10.1039/C7CY00879A
- [22] Hu P., Ben-David Y., Milstein D. (2016), General Synthesis of Amino Acid Salts from Amino Alcohols and Basic Water Liberating H₂. *J. Am. Chem. Soc.*, 138(19), 6143-6146 doi:10.1021/jacs.6b03488
- [23] Rozenel S. S., Arnold J. (2012), Bimetallic Ruthenium PNP Pincer Complex As a Platform to Model Proposed Intermediates in Dinitrogen Reduction to Ammonia. *Inorg. Chem.*, 51(18), 9730-9739 doi:10.1021/ic3010322
- [24] Zbieg J. R., Yamaguchi E., McInturff E. L., Krische M. J. (2012), Enantioselective C-H Crotylation of Primary Alcohols via Hydrohydroxyalkylation of Butadiene. *Science*, 336(6079), 324
- [25] Gunanathan C., Milstein D. (2014), Bond Activation and Catalysis by Ruthenium Pincer Complexes. *Chem. Rev.*, 114(24), 12024-12087 doi:10.1021/cr5002782
- [26] Wylie W. N. O., Kang X., Luo Y., Hou Z. (2014), PNP-Ligated Heterometallic Rare-Earth/Ruthenium Hydride Complexes Bearing Phosphinophenyl and Phosphinomethyl Bridging Ligands. *Organometallics*, 33(4), 1030-1043 doi:10.1021/om401216v
- [27] Zweifel T., Naubron J.-V., Grützmacher H. (2009), Catalyzed Dehydrogenative Coupling of Primary Alcohols with Water, Methanol, or Amines. *Angew. Chem. Int. Ed.*, 48(3), 559-563 doi:10.1002/anie.200804757
- [28] Thaddeus S. F., Moench W. L. (2003). Process for the preparation of carboxylic acid salts from primary alcohols. In: US patent 6,646,160.

- [29] Reid E. E., Worthington H., Larchar A. W. (1939), The Action of Caustic Alkali and of Alkaline Salts on Alcohols. *J. Am. Chem. Soc.*, *61*(1), 99-101 doi:10.1021/ja01870a032
- [30] Balaraman E., Khaskin E., Leitus G., Milstein D. (2013), Catalytic transformation of alcohols to carboxylic acid salts and H₂ using water as the oxygen atom source. *Nat Chem*, *5*(2), 122-125 doi:10.1038/nchem.1536
- [31] Choi J. H., Heim L. E., Ahrens M., Prechtl M. H. (2014), Selective conversion of alcohols in water to carboxylic acids by in situ generated ruthenium trans dihydrido carbonyl PNP complexes. *Dalton Trans.*, *43*(46), 17248-17254 doi:10.1039/c4dt01634c
- [32] Li Y., Nielsen M., Li B., Dixneuf P. H., Junge H., Beller M. (2015), Ruthenium-catalyzed hydrogen generation from glycerol and selective synthesis of lactic acid. *Green Chem.*, *17*(1), 193-198 doi:10.1039/c4gc01707b
- [33] Malineni J., Keul H., Moller M. (2015), A green and sustainable phosphine-free NHC-ruthenium catalyst for selective oxidation of alcohols to carboxylic acids in water. *Dalton Trans.*, *44*(39), 17409-17414 doi:10.1039/c5dt01358e
- [34] Dai Z., Luo Q., Meng X., Li R., Zhang J., Peng T. (2017), Ru(II) complexes bearing 2,6-bis(benzimidazole-2-yl)pyridine ligands: A new class of catalysts for efficient dehydrogenation of primary alcohols to carboxylic acids and H₂ in the alcohol/CsOH system. *J. Organomet. Chem.*, *830*, 11-18 doi:10.1016/j.jorganchem.2016.11.038
- [35] Zhang L., Nguyen D. H., Raffa G., Trivelli X., Capet F., Desset S., . . . Gauvin R. M. (2016), Catalytic Conversion of Alcohols into Carboxylic Acid Salts in Water: Scope, Recycling, and Mechanistic Insights. *ChemSusChem*, *9*(12), 1413-1423 doi:10.1002/cssc.201600243

- [36] Sarbajna A., Dutta I., Daw P., Dinda S., Rahaman S. M. W., Sarkar A., Bera J. K. (2017), Catalytic Conversion of Alcohols to Carboxylic Acid Salts and Hydrogen with Alkaline Water. *ACS Catalysis*, 7(4), 2786-2790 doi:10.1021/acscatal.6b03259
- [37] Mason R., Rae A. I. M. (1968), The crystal structure of ruthenium carbonyl, Ru₃(CO)₁₂. *J. Chem. SOC. (A)*, 1, 778-779
- [38] Ghafouri M., Moghadam M., Mehrani K., Daneshvar A. (2017), Supported ruthenium hydride catalysts for direct conversion of alcohols to carboxylic acids using styrene oxide as oxidant. *Appl. Organomet. Chem.*, DOI: 10.1002/aoc.4048 doi:10.1002/aoc.4048
- [39] Santilli C., Makarov I. S., Fristrup P., Madsen R. (2016), Dehydrogenative Synthesis of Carboxylic Acids from Primary Alcohols and Hydroxide Catalyzed by a Ruthenium N-Heterocyclic Carbene Complex. *J. Org. Chem.*, 81(20), 9931-9938 doi:10.1021/acs.joc.6b02105
- [40] Sheldrick G. M. (2015), Crystal structure refinement with SHELXL. *Acta Crystallogr., Sect. C: Struct. Chem.*, 71(Pt 1), 3-8 doi:10.1107/S2053229614024218
- [41] Dolomanov O. V., Bourhis L. J., Gildea R. J., Howard J. A. K., Puschmann H. (2009), OLEX2: a complete structure solution, refinement and analysis program. *J. Appl. Crystallogr.*, 42(2), 339-341 doi:10.1107/S0021889808042726
- [42] Chaudhary A., Mohammad A., Mobin S. M. (2017), Recent Advances in Single-Crystal-to-Single-Crystal Transformation at the Discrete Molecular Level. *Cryst. Growth Des.*, 17(5), 2893-2910 doi:10.1021/acs.cgd.7b00154

Chapter 4

Tetranuclear $\text{Ru}_4(\text{CO})_8$ -substituted pyridine-methanol cluster as a highly efficient electro-catalyst in water oxidation reaction

4.1 Introduction

In recent times, there is an urgent need for sustainable and low-cost sources of energy, owing to the vastly expanding demand and concerns about environmental damage due to conventional sources of energy.[1] Although some sources exist as sources for renewable energy, one of the most promising sources is solar energy, with theoretically unlimited input in the form of solar radiation, and having a very low adverse impact towards the environment.[2] Hydrogen has been gaining attention as one of the most promising candidates for a future source of energy and fuel,[3] with its main advantages primarily being in overwhelming abundance, a much more environmentally friendly method of generation and usage for practical applications.[4] However, even without considering the future potential as an input for fuel cells, hydrogen is currently used in abundance today in the manufacture of ammonia, refining of petroleum and methanol manufacture. The most significant advantage of using hydrogen is that the by-products of its use are generally water, which may be recycled to generate more hydrogen. Today, hydrogen is commercially generated via use of electrolyzers, which utilise an electrical input to split water into H_2 and O_2 , as the reaction cannot occur spontaneously due to being thermodynamically unfavourable. Furthermore, due to various factors, the external energy required to generate hydrogen from water efficiently exceeds the theoretical redox potential of 1.23 V vs. RHE. In practice, commercial electrolyzers employ a voltage of 1.6 V or more to split water and generate hydrogen and oxygen at a rate that is commercially feasible for industrial purposes with an estimated cost of 3–15 euros per kilogram of

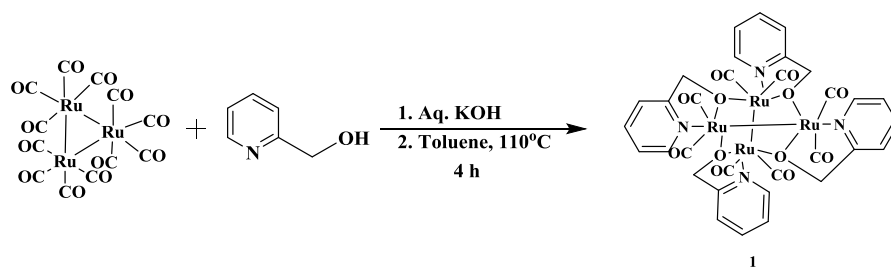
H₂ produced.[5] Other methods include thermochemical conversion of water into hydrogen and oxygen, which involves high-temperature processes, which are not only corrosive but also require the burning of fuels at large scale to generate such heat. In recent times, the use of solar energy as the “input” for an electrolyzer is an idea that has active support from research communities around the world. The prospects of obtaining clean, pure hydrogen using solar radiation as an energy source invite a hope for very sustainable production in the future. However, most of the traditional research on materials to be used as electrodes for photo-electrochemical cells has focused on inorganic compounds,[6] with only a few groups focusing on organic or organometallic materials for use as electrodes in a PEC system.[7-10]

Such materials have the potential advantages of tunable charge-transfer properties along with a synthesis method that would sidestep challenges associated with the provision of high power or temperature. Furthermore, organic synthesis can be easily scaled up to massive production levels, facilitating fast time to market.

Herein, we describe a novel compound which displays low onset potential, fast kinetics and significant photocurrent for the oxygen evolution (anodic) reaction in a photo-electrochemical cell.

4.2 Results and Discussion

The reaction of $\text{Ru}_3(\text{CO})_{12}$ with pyridine-methanol was carried out in 1:2 molar ratio in basic toluene (25 mL) at 110°C for 4 h (**Scheme 4.1**). Compound **1** has been characterized by ^1H , ^{13}C NMR, mass spectrometry, CHN and authenticated by single crystal XRD. ^1H NMR (400 MHz, acetone- d_6) spectra of Cluster **1** show corresponding peak for substituted pyridine (characteristic signal near 7–9 ppm showing 4 proton signals) and alkyl chain (**Figure 4.9**) and ^{13}C NMR (100.635 MHz, acetone- d_6) spectrum of **1** shows the typical peak of carbonyl near 200 MHz with acetone and reference peak of acetone are 29.8 and 207 (**Figure 4.10**). All H signals shift downfield on coordination with $\text{Ru}_3(\text{CO})_{12}$ in ^1H NMR. All carbon peaks are also shifted downfield after coordination to $\text{Ru}_3(\text{CO})_{12}$ in ^{13}C NMR. We performed ^1H NMR from 0 to -60 ppm and did not find any peak. This rule out the possibility of hydride presence on ruthenium atom which shares two rutheniums in complex **1**. The IR spectra of **1** showed three noticeable band corresponds to $\nu_{\text{C}=\text{O}}$ stretching mode (**Figure 4.11**).^[11] The LCMS spectrum of **1** shows the m/z peaks at 796.83. Furthermore, cluster **1** has also been authenticated by single crystal X-ray studies.



Scheme 4.1 Synthesis of pyridine-based ruthenium carbonyl cluster **1**

4.2.1 Structural description of **1**

XRD analysis revealed the binding modes of pyridine alcohol ligand to $\text{Ru}_3(\text{CO})_{12}$ and its crystal structures is shown in **Figure 4.1**.

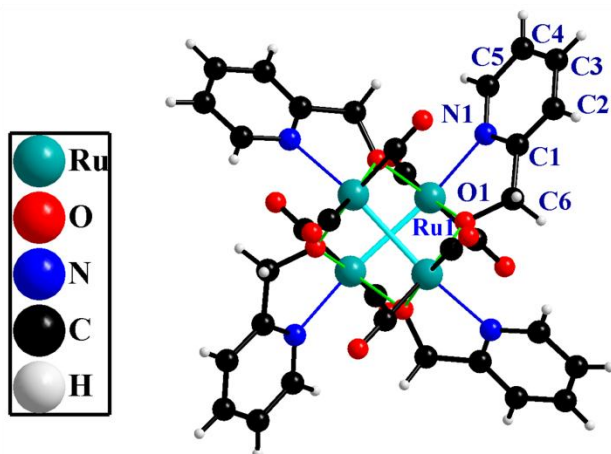


Figure 4.1 Perspective view or molecular diagram of complex **1**

Structure **1** is centrosymmetric and crystallized in $P4_2/n$ space group with tetragonal crystal system. In this crisscross structure, each oxygen atom of the pyridin-2-yl-methanolate ligand shares two ruthenium atoms, each adopting a distorted octahedral $Ru_1C_2N_1O_2$ coordination sphere (see **Figure 4.1**). The bond length of bonded Ru-Ru is 2.758 Å in **1** is shorter as compared to traditional $Ru_3(CO)_{12}$ with a mean Ru–Ru bond length of 2.848 Å.¹² Cluster **1** has the voids in crystal unit cells which are big enough to hold a spherical probe of 1.2 Å radius. The horizontal and vertical view of the voids is shown in **Figure 4.2a–4.2b**. The presence of such solvent accessible voids allows us to optimize mechanical properties by providing porosity via additive manufacturing.

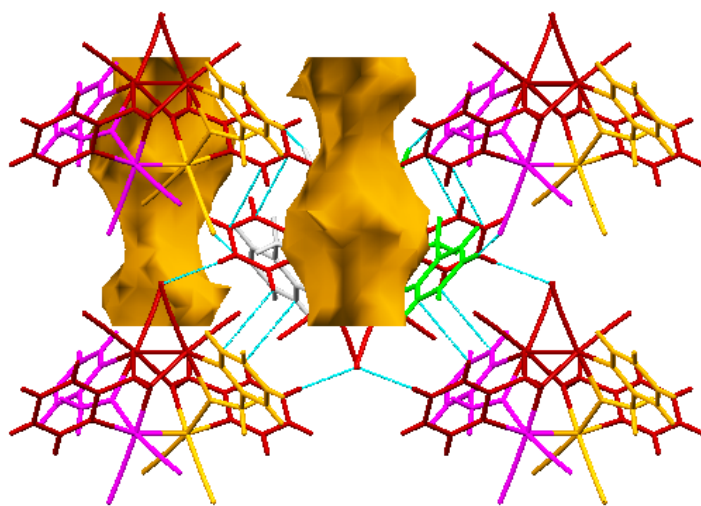


Figure 4.2a Solvent accessible voids present in **1** along ‘a’ axis found using mercury CSD 3.8 software

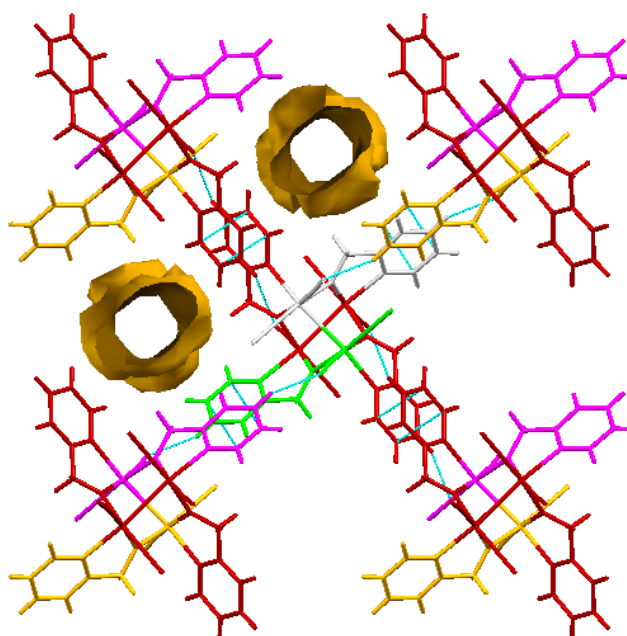


Figure 4.2b Voids in c axis solvent accessible found using mercury CSD 3.8 software

A three-electrode PEC cell was set up with the photoanode comprising of **1** deposited on Glassy carbon electrode as the working electrode, Ag/AgCl as the reference electrode, and Pt wire as the counter electrode as shown in **Figure 4.3**.

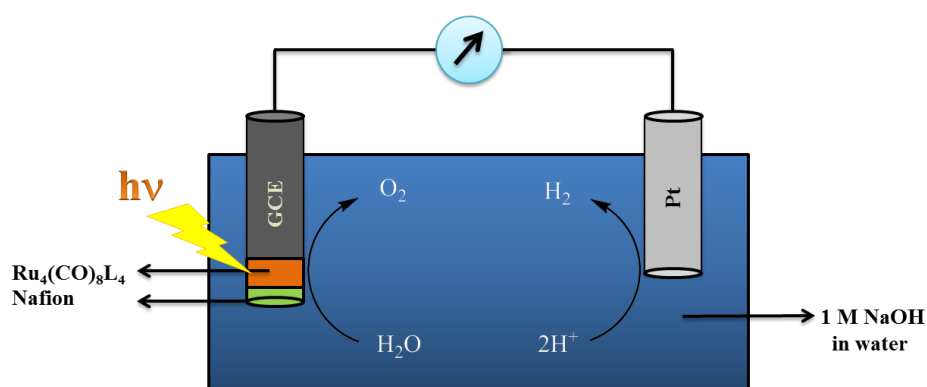


Figure 4.3. A PEC device, composed of an anode based on Glassy Carbon electrode along with a Nafion thin coating, a Pt cathode, and an aqueous electrolyte, for light-driven water splitting

4.2.2 Linear sweep voltammetry (LSV) measurement

Linear sweep voltammetry (LSV) experiments were performed and current density-voltage profile graph is plotted as shown in **Figure 4.4**.

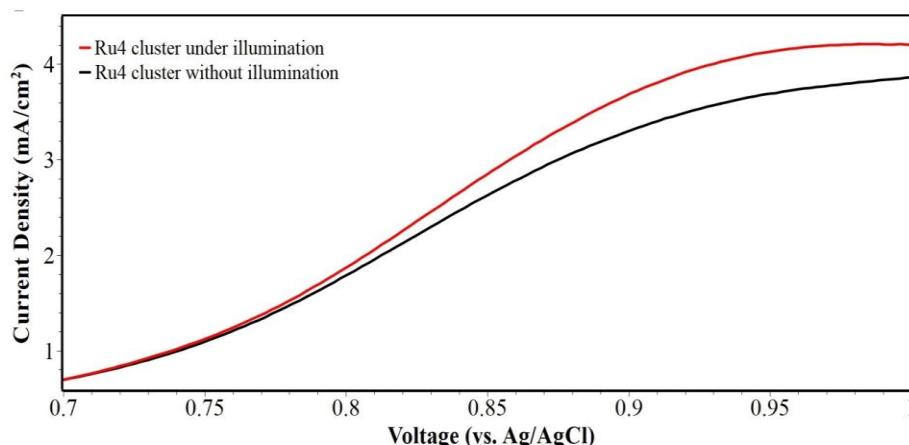


Figure 4.4 Current density-voltage profile for the modified GCE with Ru4 cluster

For Cluster **1**, without light illumination, the current rapidly increased with the rise of applied potential from 0.75 to 0.95 V (vs. Ag/AgCl), and reached a constant plateau at $E > 0.20$ V with a current density of 3.86 mA cm^{-2} ; this value is competitive when considering previously reported results.

For comparison, the Cluster **1** electrode was also studied under illumination (**Figure 4.3**), and it was found that it behaves similarly to dark conditions with a current of 4.2 mA/cm^2 at 1 V. The maximum photocurrent observed is 0.44 mA/cm^2 at about 0.95 V vs. Ag/AgCl. These values are significantly higher in comparison to the current densities under light conditions, indicating that the working electrodes are photoactive.

It is proposed that this photocurrent is caused by photo-assisted MLCT transition from Ru ion to the ligand, which assists in the oxidation of water.[12]

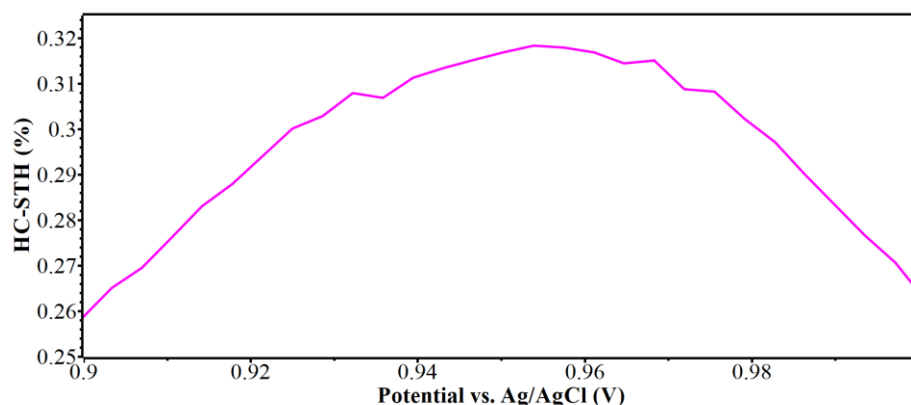


Figure 4.5 Hypothetical half-cell solar-to-hydrogen (HC-STH) efficiency calculations with Ru4 cluster

The Hypothetical half-cell solar-to-hydrogen (HC-STH) efficiency (**Figure 4.5**) in percentage for the oxygen evolution was calculated in accordance with the formula suggested by Hisatomi et al.[13]:

$$HC - STH \% = \frac{j(E_{O_2/H_2O} - E_{RHE}) \times 100}{P_{sun}}$$

Substituting for $E(O_2/H_2O)$, which is 1.23 V (vs. Ag/AgCl) and $E(RHE)$, which is 1.9568 V vs. RHE and 0.9568 V vs. Ag/AgCl, we get the value of HC-STH as 0.3185% at 0.9568 V vs. Ag/AgCl. This value is comparable to studies on ZnO electrodes,[14] $Sm_2Ti_2O_5$ electrodes,[15] and (Ag, Cu)GaSe₂ electrodes modified with CdS and CuGa₃Se[16] performed by other groups. Moreover, the Faradaic Efficiency for oxygen evolution reaction is found to be 91.92%, which is comparable to contemporary reports for the oxygen evolution reaction.[17] A representative table comparing the results achieved in this work with other recent work on Ruthenium-based complexes is provided in **Table 4.1**.

Table 4.1 Comparison of photocurrents achieved on ruthenium-based complexes used as electrodes in photoelectrochemical cells

Material for active electrode	Preparation Method	Substrate	Electrolyte	Maximum Stable photocurrent	Ref.
FTO/TiO ₂ (PS [Ru(bpy) ₂ (4,4'-((OH) ₂ PO) ₂ -bpy) ₂] ⁺ Br ₂ + binuclear Ruthenium Catalyst)	Chemical Bath Deposition	FTO	0.1 M Na ₂ SO ₄ (pH 6.4)	0.5 mA cm ⁻²	[18]
FTO/TiO ₂ (PS [Ru(bpy) ₂ (4,4'-((OH) ₂ PO) ₂ -bpy) ²⁺] ⁺ Br ₂ + mononuclear Ruthenium Catalyst)	Chemical Bath Deposition	FTO	0.1 M Na ₂ SO ₄ (pH 6.4)	0.45 mA cm ⁻²	[19]
Poly-[Ru(bda)(vpy) ₂] ₂ @Fe ₂ O ₃	Microwave assisted one pot self-assembly + Electro polymerization on pre-coated substrate	FTO	0.05 mM phosphate buffer	0.40 mA cm ⁻²	[20]
RuP modified graphitic C ₃ N ₄ (g-C ₃ N ₄)	Thermal treatment of urea (g-C ₃ N ₄) + Wet Chemical Synthesis (RuP-modified g-C ₃ N ₄)	FTO	0.5 M Na ₂ SO ₄	< 0.4 μA cm ⁻²	[21]
Ru-based catalyst-porphyrin dyad@TiO ₂ /FTO	Screen printing/doctor blade (TiO ₂), chemical bath deposition (Ru based catalyst/porphyrin dyad)	FTO	20 mM phosphate buffer at pH 7.5 with 0.1 M TBAPF ₆	0.13 mA cm ⁻²	[22]
FTO/SnO ₂ /tetra(4-carboxyphenyl)-porphyrinato-tin (IV) : Ru(II)(bda)(4-picoline) 3-N-(pyridin-4-ylmethylene) : 2-(3,5-di-tert-butyl-2-hydroxy phenyl)-1H-benzimidazol-5(6)-carboxylic acid}	Screen printing (SnO ₂ on FTO), Chemical bath deposition for rest	FTO	Phosphate Buffer (pH 6.86)	0.125 mA cm ⁻²	[23]
Tetranuclear Ru₄(CO)₈-substituted pyridine-methanol cluster	Drop casting on Glassy carbon electrode surface	Glassy Carbon Electrode	1 M NaOH	0.44 mA cm⁻²	Present Work

4.2.3 Electrochemical Impedance Spectroscopy analysis

The EIS spectra of the glassy carbon electrodes modified with Ru4 cluster are shown in (Figure 4.6). The EIS spectra were modelled based on an empirical Cole-Cole model for complex impedances[24] comprising of series resistance, and a parallel combination of a resistor and capacitor. The circuit diagram equation:

$$Z(\omega) = \left(\frac{1}{R_0} + j\omega CPE \right)^{-1} + R_{ser}$$

Where R_0 represents the ionic resistance of the material while CPE is a reference to constant phase element, which is a frequency dependent capacitive element, while ω is an angular frequency of. The impedance of a CPE is described as

$$Z_{CPE} = A^{-1} \cdot (j\omega)^{-n}$$

Where n is a distributing factor for the impedance and has a value between 0 and 1. If $n=1$, the element is an ideal capacitor, and if $n=0$, the element is an ideal resistor. A is a constant fitting parameter for any given circuit.

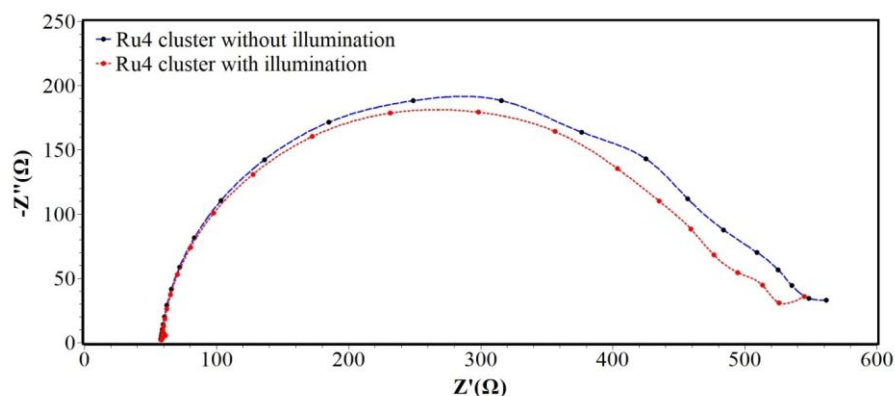


Figure 4.6 EIS spectra of the glassy carbon electrodes modified with Ru4 cluster

The values for the electrochemical parameters specified in the above model are shown in (Table 4.2) for the Ru4 cluster complex with and without illumination at 0.8 V vs. Ag/AgCl. It can be observed that under illumination, there is a reduction in the ionic resistance of the material, which confirms with the higher current values observed earlier

in this report.[19,25] The value of n is 0.7, indicating that the capacitive component is more dominant in the material.

Table 4.2 The values for the electrochemical parameters specified in the Cole-Cole model

Quantity (unit)	Without Illumination	With Illumination
R_{ser} (ohm)	1.7348×10^{-11}	1.6632×10^{-11}
CPE (F)	3.09244×10^{-2}	3.09244×10^{-2}
n	0.7	0.7
R_o (ohm)	4.38×10^2	4.16×10^2

4.2.4 Density Functional theory

To understand geometry optimization, energy, and electronic communication in compounds **1**, DFT calculations have been done¹³. The bond distances calculated for the optimized structures in **1** are similar to those obtained by their x-ray crystal structures. For complex **1**, the HOMO is localized on the ruthenium atoms with attached carbonyls, while LUMO is on the ligand unit. However, In **1**, the electron density is spread symmetrical but half, i.e. two out of four ligands in its LUMO. Most of the electron density lies on the ruthenium atoms part. And the electrostatic potential separation is present in **1** i.e. $-7.155 e^{-2}$ to $7.155 e^{-2}$.

4.2.5 UV-Visible Spectroscopy study

Based on the TD-DFT calculations of excitation energies and oscillator strengths, we calculated a theoretical UV-Vis spectrum of **1**, and then compared it to the experimental UV-Vis spectrum for **1**, as a solvent in both the cases. Based on the results of the excitation energies, it is found that the most likely absorptions that cause a jump from HOMO energy levels to LUMO energy levels correspond to an energy input of 2.822 eV (Table 4.3).

Table 4.3. Computed vertical transitions and their oscillator strengths and configurations

Complexes	Acetone		
	$\lambda_{\text{max}}[\text{nm}]$	f	Configuration
1	439.34 nm	0.0205	HOMO-1 \rightarrow LUMO+1 (-0.16557) HOMO \rightarrow LUMO (-0.35343)
	439.34 nm	0.0205	HOMO-1 \rightarrow LUMO+1 (0.16557) HOMO \rightarrow LUMO (0.53689)

The UV Vis spectrum thus constructed has an absorption maximum of approximately 440 nm,[26,27] and is supported by the experimental UV spectra observed for **1** which shows distinct absorption at around 430 nm. The theoretical and experimental UV-Vis Spectra are presented in **Figure 4.7**, and to find the band gap, we used Tauc's relations to plot the derivative $d[\ln(\alpha h\nu)]/d(h\nu)$,[28] the maxima of the discontinuity would give us the value of the band gap (**Figure 4.8**). We thus found out the optical band gap to be 2.85 eV, which is very close to the 2.822 eV previously calculated as being the major absorption energy.

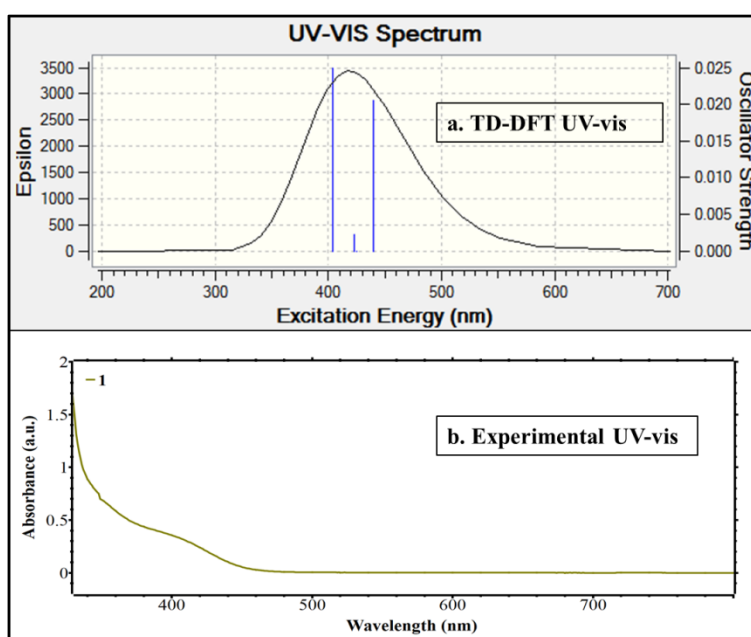


Figure 4.7 Comparison of theoretical and experimental UV-vis

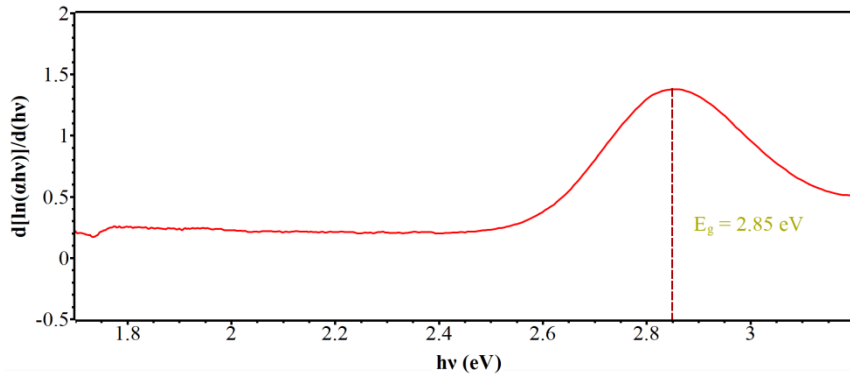


Figure 4.8 Plot b/w derivative $d[\ln(\alpha hv)]/d(hv)$ and $h\nu$ for band gap calculation

4.3 Conclusion

The visible light-driven water splitting is successfully demonstrated in a PEC device by using complex **1** as a catalyst for water oxidation as the anode, and a platinum electrode as the cathode for proton reduction. Through this study, we found that the tetragonal ruthenium structure will meet the demand of new catalyst demand with the lowering of onset potential of complex **1** for water oxidation, and produced the maximum 4.26 mA cm^{-2} . The activity of the catalyst in the anode considered due to its MLCT charge transfer. We are currently optimizing this system by developing more active catalysts, a more suitable photosensitizer, and new supporting materials.

4.4 Experimental

All reactions were done under an inert gas atmosphere. Ruthenium carbonyl and all pyridine alcohol derivatives were purchased from Aldrich and TCI chemicals. Reagents used for purification and crystallization were purchased either from Rankem or Merck and distilled prior to use. NMR spectra were recorded in deuterated acetone (CD_3COCD_3) on a Bruker Advance (III) spectrometer (400MHz). Coupling constants, J values, are reported in Hertz (Hz), and the splitting patterns are designated as s, singlet; d, doublet; t, triplet; m, multiplet; br., broad. IR spectra were recorded with a Bio-Rad FTS 3000 MX instrument on KBr pellets. X-ray structural studies of complexes **1–4** were carried out using the Agilent Technologies Supernova CCD system. The mass spectra were recorded on Bruker-Daltonics-microTOF-QII mass spectrometer. TG analysis was carried out on Mettler Toledo instrument Elemental analysis was carried out using a Thermo Scientific FLASH 200 elemental analyzer.

4.4.1 X-ray Crystallography

Data were collected at 293 K using graphite-monochromated Mo $K\alpha$ ($\lambda_\alpha = 0.71073 \text{ \AA}$). The data collection strategy was interpreted by employing the CrysAlisPro CCD software. The collection of data was done by the standard phi-omega scan techniques. The data were scaled and reduced employing CrysAlisPro RED. The direct methods using SHELXS-97 was used to solve the crystal structures and refined by the full matrix least squares method with SHELXL-97, refining on F^2 .^[29] Olex-1.2 was also used for structure solutions.[30] The H-atoms were placed at geometrically constrained positions and refined using isotropic temperature factors, generally $1.2 \times U_{eq}$ of their parent atoms. All remaining non-hydrogen atoms were refined anisotropically. All the C–H $\cdots\pi$ interactions,[31] molecular drawings,[32] and mean plane analyses were obtained by Diamond (ver. 3.1d)[33] and Mercury (ver. 3.1) .[34] The crystals and their refinement data are shown in **Table 4.4**.

4.4.2 Electrochemical analysis

Electrochemical measurements were performed in an Autolab Electrochemical Workstation (PGSTAT 204, with NOVA 1.10) in a standard 3-electrode cell, with Platinum as a counter electrode, Ag/AgCl as a reference electrode and glassy carbon electrode modified with (Ru₄ cluster) as the working electrode. An aqueous solution of 1 M NaOH (pH = 13.6) was used as the electrolyte, and a 1000 W/m² calibrated Xenon lamp was utilised as the light source for measuring photocurrents. The results obtained were normalised to conform to the standard unit of mA cm⁻¹. Linear sweep voltammetry was carried out between 0 and 1 V vs. Ag/AgCl with a scan rate of 10 mV/s. The Nyquist plots were obtained at 0.8 V vs. Ag/AgCl under darkness and under illumination, with a frequency range of 1 Hz to 100000 Hz. The potential of the Ag/AgCl reference electrode was found to be +480 mV with respect to a standard ferrocyanide/ferrocenium couple.

4.4.3 Density functional theoretical studies

To explore the electronic structure and optimize the structure of **1**, and calculating the band gap; DFT calculations were performed by using the Gaussian09 program.[35] All calculation was done at the B3LYP[36,37] level of theory employing the LanL2DZ basis set for Ru and 6-31G* basis set for the remaining atoms. The geometries were optimized without imposing symmetry or any other restraints.

4.4.4 Synthesis of complex [Ru₄(CO)₈(C₅H₅NCH₂O)₄] (**1**)

Ru₃(CO)₁₂ (0.320 g, 0.5 mmol) and Pyridin-2-yl-methanol (300 μl, 3.09 mmol) were put into a two-neck round bottom flask along with toluene (40 ml) as a solvent, and this reaction mixture was stirred for 15 minutes at room temperature and then at 110°C or reflux for 4 hours. After 4 hours, the brown colored solution obtained which was cooled and evaporated using a rotavapor and the resulting precipitate was washed with hexane five times to remove any un-reacted Ru₃(CO)₁₂ left and once with very less quantity of diethyl ether. The precipitate was then dissolved in dichloromethane solution, filtered and was crystallized from

a dichloromethane/hexane (20:1) solvent mixture. The product is purified by re-crystallization in toluene. Yield: 70% (0.372 g). ^1H NMR (400 MHz, acetone- d_6): δ (ppm) = 9.66 (t, 1H), 8.67 (d, 1H), 8.24 (d, 2H), 6.44 (dd, 1H), 5.88 (dd, 1H), 3.59 (s, 1H), 3.11 (d, 1H); ^{13}C NMR (100 MHz, acetone- d_6): δ (ppm) = 206.8, 204.9, 166.4, 150.55, 138.3, 129.7, 129.0, 123.6, 120.5, 79.7. HRMS (ESI): m/z calculated for $[\text{Ru}_4(\text{CO})_8(\text{C}_5\text{H}_5\text{NCH}_2\text{O})_4] - \text{Cl}$: 307.649 $[\text{M}^+]$, found 305.255 $[\text{M}^+]$, Anal. Calcd: C, 36.23; H, 2.28; N, 5.28. Found: C, 41.98; H, 3.79; N, 4.08.

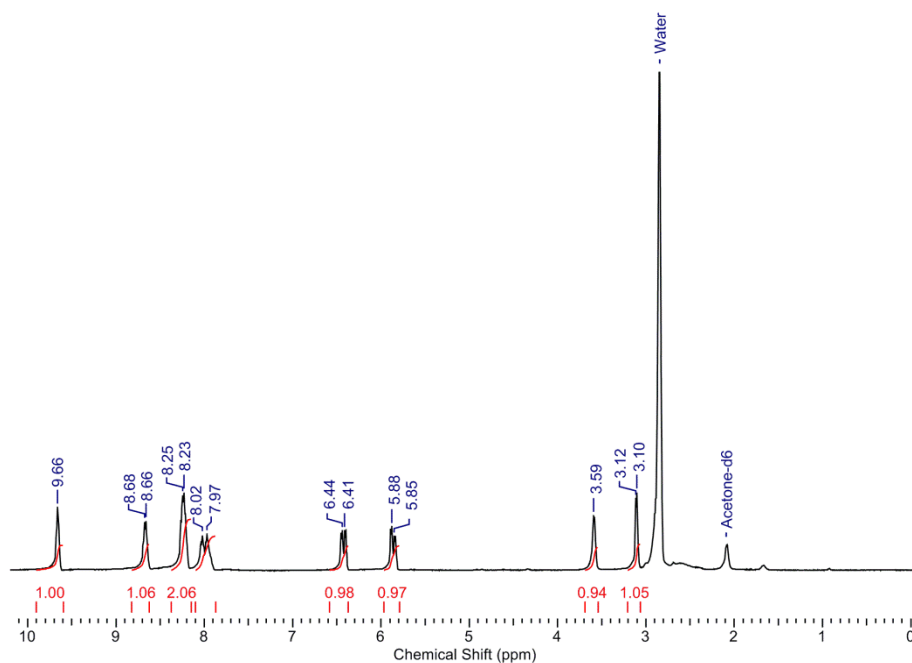


Figure 4.9 ^1H NMR of 1

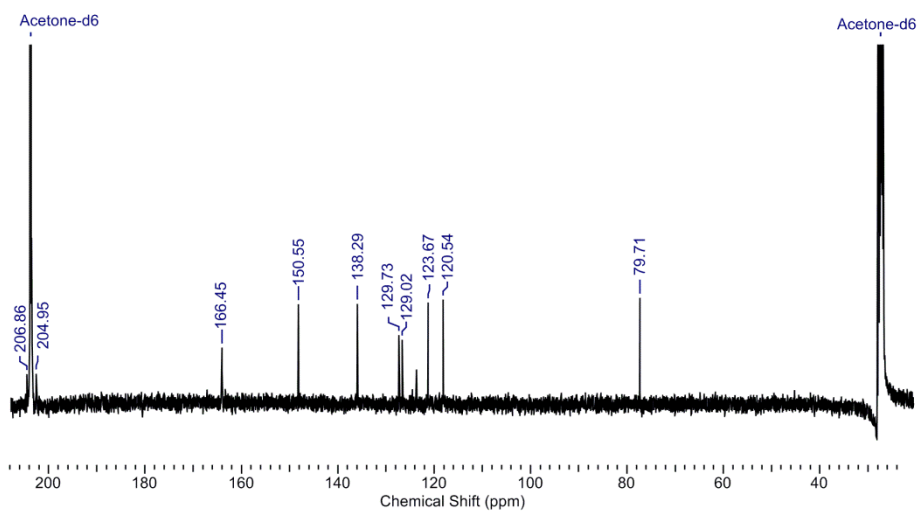


Figure 4.10 ^{13}C NMR of 1

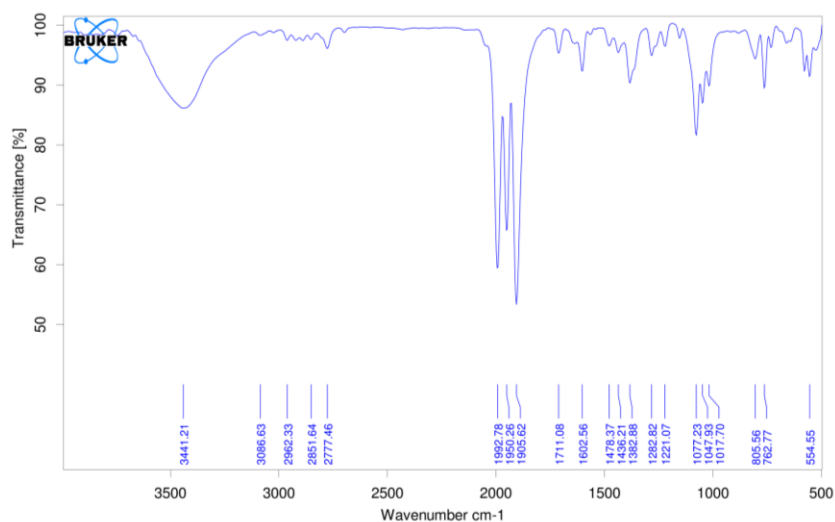


Figure 4.11 IR of **1**

Table 4.4 Crystal data and structure refinement for **1**.

Identification code	1
Empirical formula	C ₃₂ H ₂₄ N ₄ O ₁₂ Ru ₄
Formula weight	1060.83
Temperature/K	293
Crystal system	tetragonal
Space group	<i>P4₂/n</i>
a/Å	14.9432(3)
b/Å	14.9432(3)
c/Å	10.2658(3)
α/°	90
β/°	90
γ/°	90
Volume/Å ³	2292.35(11)
Z	2
ρ _{calc} /g/cm ³	1.537
μ/mm ⁻¹	1.345
F(000)	1032.0
Crystal size/mm ³	0.35 × 0.31 × 0.28
Radiation	MoKα (λ = 0.71073)
2θ range for data collection/°	6.744 to 49.984
Index ranges	-17 ≤ h ≤ 13, -17 ≤ k ≤ 17, -12 ≤ l ≤ 10
Reflections collected	4928
Independent reflections	1833 [R _{int} = 0.0250, R _{sigma} = 0.0247]
Data/restraints/parameters	1833/0/118
Goodness-of-fit on F ²	1.193
Final R indexes [I ≥ 2σ (I)]	R ₁ = 0.0426, wR ₂ = 0.1263

Final R indexes [all data]	$R_1 = 0.0468$, $wR_2 = 0.1303$
Largest diff. peak/hole / $e \text{ \AA}^{-3}$	1.06/-0.39
CCDC No.	1539164

4.5 References

- [1] Khoo H. H., Tan R. B. H. (2006), Environmental Impact Evaluation of Conventional Fossil Fuel Production (Oil and Natural Gas) and Enhanced Resource Recovery with Potential CO₂ Sequestration. *Energy Fuels*, 20(5), 1914-1924 doi:10.1021/ef060075+
- [2] Lewis N. S., Nocera D. G. (2006), Powering the planet: Chemical challenges in solar energy utilization. *PNAS*, 103(43), 15729 doi:10.1073/pnas.0603395103
- [3] Lim T., Ju S. (2017), Thermochemical hydrogen generation of indium oxide thin films. *AIP Advances*, 7(3), 035207 doi:10.1063/1.4978489
- [4] Momirlan M., Veziroglu T. N. (2005), The properties of hydrogen as fuel tomorrow in sustainable energy system for a cleaner planet. *Int. J. Hydrogen Energy*, 30(7), 795-802 doi:10.1016/j.ijhydene.2004.10.011
- [5] Ursua A., Gandia L. M., Sanchis P. (2012), Hydrogen Production From Water Electrolysis: Current Status and Future Trends. *Proceedings of the IEEE*, 100(2), 410-426 doi:10.1109/JPROC.2011.2156750
- [6] Chen S., Thind S. S., Chen A. (2016), Nanostructured materials for water splitting - state of the art and future needs: A mini-review. *Electrochem. Commun.*, 63, 10-17 doi:10.1016/j.elecom.2015.12.003
- [7] Martin D. J., Reardon P. J. T., Moniz S. J. A., Tang J. (2014), Visible Light-Driven Pure Water Splitting by a Nature-Inspired Organic Semiconductor-Based System. *J. Am. Chem. Soc.*, 136(36), 12568-12571 doi:10.1021/ja506386e
- [8] Esiner S., Willems R. E. M., Furlan A., Li W., Wienk M. M., Janssen R. A. J. (2015), Photoelectrochemical water splitting in

- an organic artificial leaf. *J. Mater. Chem. A*, 3(47), 23936-23945
doi:10.1039/C5TA07325A
- [9] You B., Jiang N., Sheng M., Gul S., Yano J., Sun Y. (2015), High-Performance Overall Water Splitting Electrocatalysts Derived from Cobalt-Based Metal–Organic Frameworks. *Chem. Mater.*, 27(22), 7636-7642 doi:10.1021/acs.chemmater.5b02877
- [10] Sherman B. D., Xie Y., Sheridan M. V., Wang D., Shaffer D. W., Meyer T. J., Concepcion J. J. (2017), Light-Driven Water Splitting by a Covalently Linked Ruthenium-Based Chromophore–Catalyst Assembly. *ACS Energy Letters*, 2(1), 124-128 doi:10.1021/acseenergylett.6b00661
- [11] Mason R., Rae A. I. M. (1968), The crystal structure of ruthenium carbonyl, $\text{Ru}_3(\text{CO})_{12}$. *J. Chem. Soc. (A)*, 1, 778-779
- [12] Walsh D., Patureau P., Walton J., Potticary J., Hall S. R., Weller M. T. (2016), Visible light promoted photocatalytic water oxidation: effect of fluctuating light intensity upon reaction efficiency. *RSC Advances*, 6(99), 97363-97366
doi:10.1039/C6RA22906A
- [13] Hisatomi T., Kubota J., Domen K. (2014), Recent advances in semiconductors for photocatalytic and photoelectrochemical water splitting. *Chem. Soc. Rev.*, 43(22), 7520-7535
doi:10.1039/C3CS60378D
- [14] Lu Y.-J., Liu C.-F., Hu C.-C., Kuo J.-H., Boddula R. (2017), Fabrication and characterization of ZnO nanowires array electrodes with high photocurrent densities: Effects of the seed layer calcination time. *Mater. Chem. Phys.*, 189, 56-63
doi:10.1016/j.matchemphys.2016.12.058
- [15] Ma G., Kuang Y., Murthy D. H. K., Hisatomi T., Seo J., Chen S., . . . Domen K. (2018), Plate-like $\text{Sm}_2\text{Ti}_2\text{S}_2\text{O}_5$ Particles Prepared by a Flux-Assisted One-Step Synthesis for the Evolution of O_2

- from Aqueous Solutions by Both Photocatalytic and Photoelectrochemical Reactions. *J. Phys. Chem. C*, 122(25), 13492-13499 doi:10.1021/acs.jpcc.7b12087
- [16] Zhang L., Minegishi T., Nakabayashi M., Suzuki Y., Seki K., Shibata N., . . . Domen K. (2015), Durable hydrogen evolution from water driven by sunlight using (Ag,Cu)GaSe₂ photocathodes modified with CdS and CuGa₃Se₅. *Chem. Sci.*, 6(2), 894-901 doi:10.1039/C4SC02346C
- [17] Chen L., Dong X., Wang Y., Xia Y. (2016), Separating hydrogen and oxygen evolution in alkaline water electrolysis using nickel hydroxide. *Nat. Commun.*, 7, 11741 doi:10.1038/ncomms11741
- [18] Zhang L., Gao Y., Ding X., Yu Z., Sun L. (2014), High-Performance Photoelectrochemical Cells Based on a Binuclear Ruthenium Catalyst for Visible-Light-Driven Water Oxidation. *ChemSusChem*, 7(10), 2801-2804 doi:10.1002/cssc.201402561
- [19] Li F., Fan K., Wang L., Daniel Q., Duan L., Sun L. (2015), Immobilizing Ru(bda) Catalyst on a Photoanode via Electrochemical Polymerization for Light-Driven Water Splitting. *ACS Catalysis*, 5(6), 3786-3790 doi:10.1021/cs502115f
- [20] Fan K., Li F., Wang L., Daniel Q., Chen H., Gabrielsson E., . . . Sun L. (2015), Immobilization of a Molecular Ruthenium Catalyst on Hematite Nanorod Arrays for Water Oxidation with Stable Photocurrent. *ChemSusChem*, 8(19), 3242-3247 doi:10.1002/cssc.201500730
- [21] Wang J., Chen J., Wang P., Hou J., Wang C., Ao Y. (2018), Robust photocatalytic hydrogen evolution over amorphous ruthenium phosphide quantum dots modified g-C₃N₄ nanosheet. *Appl. Catal., B*, 239, 578-585 doi:10.1016/j.apcatb.2018.08.048
- [22] Yamamoto M., Wang L., Li F., Fukushima T., Tanaka K., Sun L., Imahori H. (2016), Visible light-driven water oxidation using a

- covalently-linked molecular catalyst–sensitizer dyad assembled on a TiO₂ electrode. *Chem. Sci.*, 7(2), 1430-1439 doi:10.1039/C5SC03669K
- [23] Na Y., Miao S., Zhou L., Wei P., Cao Y. (2018), Bio-inspired model of photosystem II: supramolecular assembly of an electron mediator into an SnO₂ photoanode co-sensitized by a porphyrin photosensitizer and ruthenium molecular catalyst. *Sustainable Energy & Fuels*, 2(3), 545-548 doi:10.1039/C7SE00515F
- [24] Sandifer J. R., Buck R. P. (1974), Impedance characteristics of ion selective glass electrodes. *J. Electroanal. Chem. Interfacial Electrochem.*, 56(3), 385-398 doi:10.1016/S0022-0728(74)80039-2
- [25] Yuan G., Zhu C., Liu Y., Fang Y., Cui Y. (2010), Water clusters induced assembly of chiral organic microstructures showing reversible phase transformations and luminescence switching. *Chem. Commun.*, 46(13), 2307-2309 doi:10.1039/B923259A
- [26] Arul N. S., Mangalaraj D., Ramachandran R., Grace A. N., Han J. I. (2015), Fabrication of CeO₂/Fe₂O₃ composite nanospindles for enhanced visible light driven photocatalysts and supercapacitor electrodes. *J. Mater. Chem. A*, 3(29), 15248-15258 doi:10.1039/C5TA02630J
- [27] Soma H., Uchino T. (2017), Blue and Orange Photoluminescence and Surface Band-Gap Narrowing in Lithium-Doped MgO Microcrystals. *J. Phys. Chem. C*, 121(3), 1884-1892 doi:10.1021/acs.jpcc.6b12177
- [28] Dalouji V., Ebrahimi P., Binaei N., Tanhaee E., Nezafat N. B., Dejam L., Solaymani S. (2018), The Optical Properties of Aluminum-Doped Zinc Oxide Thin Films (AZO): New Methods for Estimating Gap States. *J. Supercond. Novel Magn.* doi:10.1007/s10948-018-4828-z

- [29] Sheldrick G. M. (2015), Crystal structure refinement with SHELXL. *Acta Crystallogr., Sect. C: Struct. Chem.*, 71(Pt 1), 3-8 doi:10.1107/S2053229614024218
- [30] Dolomanov O. V., Bourhis L. J., Gildea R. J., Howard J. A. K., Puschmann H. (2009), OLEX2: a complete structure solution, refinement and analysis program. *J. Appl. Crystallogr.*, 42(2), 339-341 doi:10.1107/S0021889808042726
- [31] Torubaev Y. V., Lyssenko K. A., Barzilovich P. Y., Saratov G. A., Shaikh M. M., Singh A., Mathur P. (2017), Self-assembly of conducting cocrystals via iodine $\cdots\pi$ (Cp) interactions. *CrystEngComm*, 19(34), 5114-5121 doi:10.1039/C7CE00857K
- [32] Singh A., Kumari P., Raghuvanshi A., Mobin S. M., Mathur P. (2018), Ferrocene-substituted bis(ethynyl)anthracene compounds as anticancer agents. *Appl. Organomet. Chem.*, 32(2), DOI: 10.1002/aoc.4071 doi:10.1002/aoc.4071
- [33] H. Putz. K. B. G., Kreuzherrenstr. 102, 53227 Bonn, Germany,. Diamond - Crystal and Molecular Structure Visualization.
- [34] C. F. Macrae, P. R. Edgington, P. McCabe, E. Pidcock, G. P. Shields, R. Taylor, . . . Streek J. v. d. (2006), *J. Appl. Cryst.*, , 39, 453-457 doi:10.1107/S002188980600731X
- [35] Frisch M. J., Trucks G. W., Schlegel H. B., Scuseria G. E., Robb M. A., Cheeseman J. R., . . . Petersson G. A. (2009), 09, Revision D. 01, Gaussian. *Inc.*, Wallingford, CT
- [36] Becke A. D. (1993), Density-functional thermochemistry. III. The role of exact exchange. *J. Chem. Phys.*, 98(7), 5648-5652 doi:10.1063/1.464913
- [37] Lee C., Yang W., Parr R. G. (1988), Development of the Colle-Salvetti correlation-energy formula into a functional of the electron density. *Phys. Rev. B*, 37(2), 785-789 doi:10.1103/PhysRevB.37.785

Chapter 5

Ferrocene-substituted bis(ethynyl)-anthracene compounds as anticancer agents

5.1 Introduction

The varying structures and properties of ferrocene-based compounds in various biological systems drive the arduous search of the scientists to perceive the unrevealed concepts of its functionality, that display interesting cytotoxic[1,2], antimalarial,[3-5] antifungal[6] and DNA-cleaving activity.[7] Furthermore, interactions of ferrocene-based compounds with proteins and DNA are the recent focus research areas because of its adequate potential for the development of new therapeutic products which can show anti-cancer property and transportation viability all over the physiological system through the protein binding.

Several ferrocene compounds have been so far examined and screened as the important candidate for pharmaceuticals.[7-12] From the anthracene point of view, azonafide is a class of drugs well known.[13] The idea was to club both to get combined and improved biological activity of the resulting compounds. Though, few reports are revealing the crucial biological activity of ferrocene bonded to mono-aromatic ring compounds,[10-12] however, the role of ferrocene bonded to poly-aromatic systems like anthracene is not reported in medicinal biochemistry. Detailed study of the interactions of the ferrocene-based compounds against different serum albumins is needed to understand the metallic-pharmaceutical pharmacokinetics and structure-activity relationships since they bind towards several compounds.[14] The nature of the interaction between different ferrocenyl compounds and proteins, which have been observed until now is confined in nature, and it requires more research for generalization.[13,15-17]

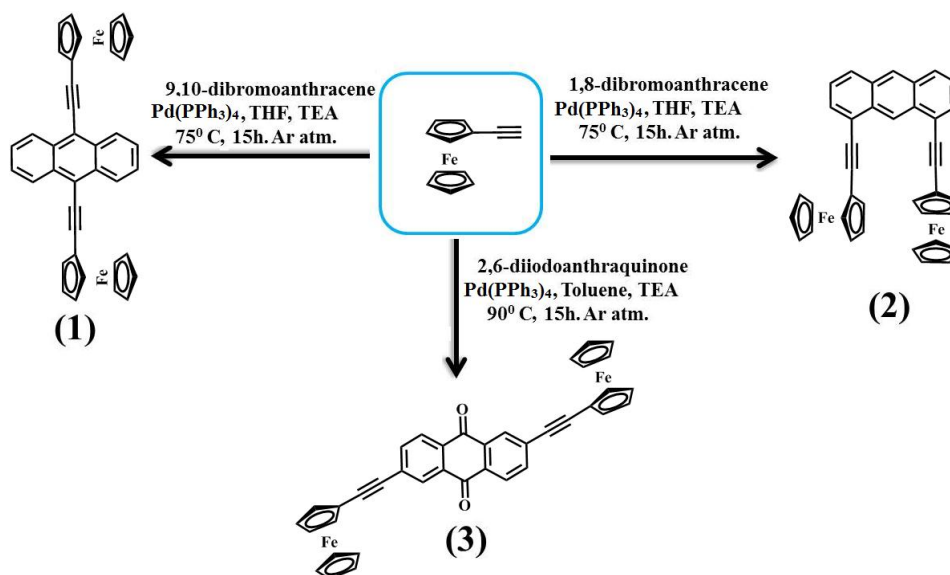
Herein we report the synthesis of 9,10-Bis-ferrocenylethynyl-anthracene (**1**), 1,8-Bis-ferrocenylethynyl-anthracene (**2**), and 2,6-Bis-

ferrocenylethynyl-anthraquinone (**3**) by C-C cross-coupling reaction and their structural, spectroscopic and biological activities.

5.2 Results and Discussion

5.2.1 Synthesis of compounds 1–3

The reaction of dibromo-anthracene with ethynyl-ferrocene in a 1:2 molar ratio in THF/TEA using Pd(PPh₃)₄ as a catalyst led to the formation of C-C cross-coupled products **1–2**. The compound **3** was also prepared similarly by replacing dibromo-anthracene with diiodo-anthraquinone in toluene (**Scheme 5.1**). Toluene was used instead of THF because of poor solubility of the diiodo-anthraquinone in THF. Compound **1** was earlier synthesized by N. Chawdhury et al.[18], but crystal structure was not analyzed[18]. Compounds **1**, **2** and **3** have been characterized by ¹H, ¹³C NMR, HRMS and authenticated by single crystal XRD. ¹H NMR (400 MHz, CDCl₃) spectra of all the compounds show corresponding peaks for ferrocene (characteristic signal near 4 ppm showing two singlets for C₅H₅ and C₅H₄) and anthracene. The ¹³C NMR (100.635 MHz, CDCl₃) spectrum of **1** and **3** shows the typical peak of ferrocene near 25.16MHz whereas it is shifted in the case of **2** (δ 94.2) may be due to the one side distribution of electron density of ferrocene. The IR spectra of **1–3** showed a remarkable band ~2200 cm⁻¹ corresponds to ν_{C≡C} stretching mode. 1672.05 cm⁻¹ is ν_{C=O} stretching frequency observed in **3** as the characteristic peak of anthraquinone as compared to free anthraquinone (1675 cm⁻¹). There is not much effect of ferrocene electron density on ν_{C=O} stretching frequency. The out of plane C-H vibration B_{2u} modes are present as 1620.14 cm⁻¹, 1632.20 cm⁻¹ and 1591.35 cm⁻¹ in **1**, **2** and **3**, respectively. Around 1575cm⁻¹, there should be a band of ν_{C=C} stretching frequency, but this band is overlapped by the out of plane vibrations in **1–3**. The out of plane C-H bending mode is observed in **1–3** as 1051.76 cm⁻¹, 1020.30 cm⁻¹ and 1035.59 cm⁻¹, respectively. The =C-H stretch peaks were 3091.93 cm⁻¹, 3095.05 cm⁻¹ and 3103.71cm⁻¹ for **1–3** respectively (Fig. S17–S19). The HRMS spectra of **1**, **2** and **3** show the molecular ion peaks at 594.07, 594.08 and 624.1, respectively. Further, the compounds have also been confirmed by single crystal X-ray structures.



Scheme 5.1 Schematic view for the synthesis of **1–3**

5.2.2 Molecular Structures of **1–3**

1–3 has been crystallized in a centrosymmetric monoclinic system (**Figure 5.1**). The ferrocene units are found to be staggered in **1–3**. The small deviation from linearity was observed in **1**; the C10-C15-C16 angle is of 177.09° and the C9-C17-C18 angle is of 178.63° , consequently, the $\text{C}\equiv\text{C}$ - bond deviates 2.91° and 1.57° out of the anthracene plane, similarly, compound **2** and **3**, the $\text{C}\equiv\text{C}$ - bond are also slightly deviated from linearity. In **1**, the two ferrocenes are on the same side of the anthracene plane whereas, in **3**, they are on opposite side. In the case of **2**, as the two ferrocenes are on 1 and 8-position, they align themselves perpendicular to each other to minimize the steric crowding.

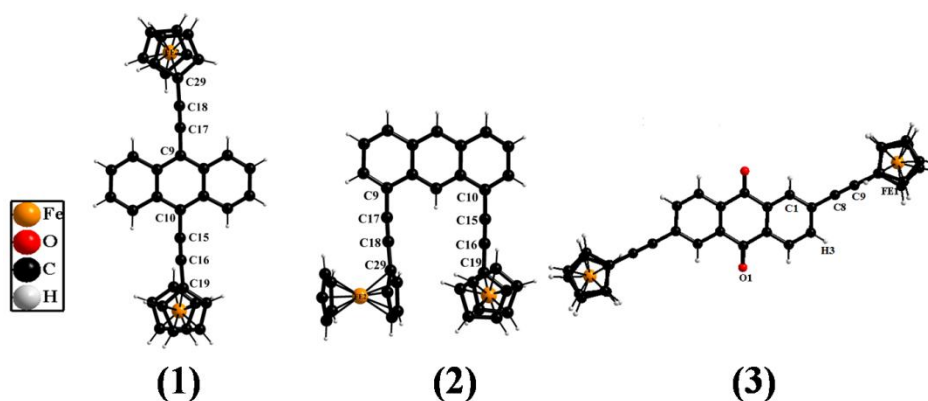


Figure 5.1 Perspective view of **1, 2** and **3**.

The packing diagram of **1–3** shows the presence of intermolecular C–H \cdots π interaction which forms a 1D polymeric chain. Each 1D-polymeric chain is extended *via* C–H \cdots π interactions between two adjoining layers, give rise to the formation of a 2D network (**Figure 5.2**).

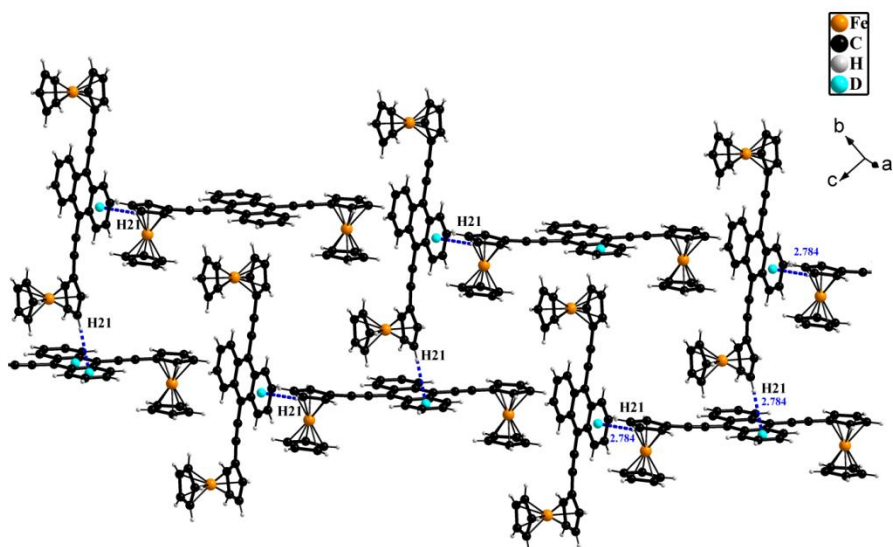


Figure 5.2 2D network of **1** along c axis

2 and **3** are forming a 3D network using the C–H \cdots π and $\pi\cdots\pi$ interactions, respectively (**Figure 5.3, 5.4**).

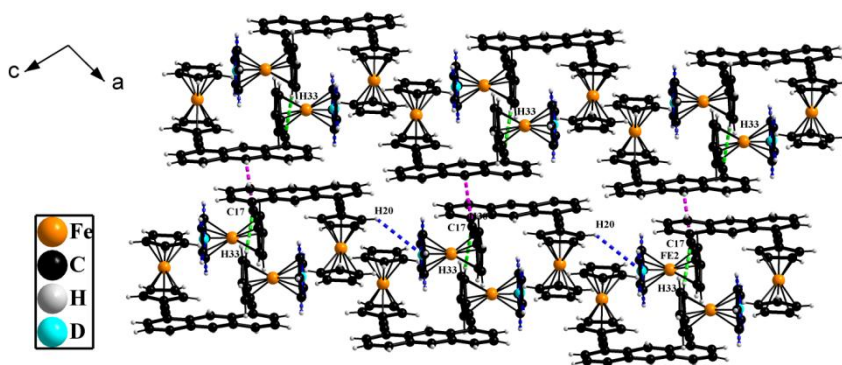


Figure 5.3 3D network of **2** along b axis

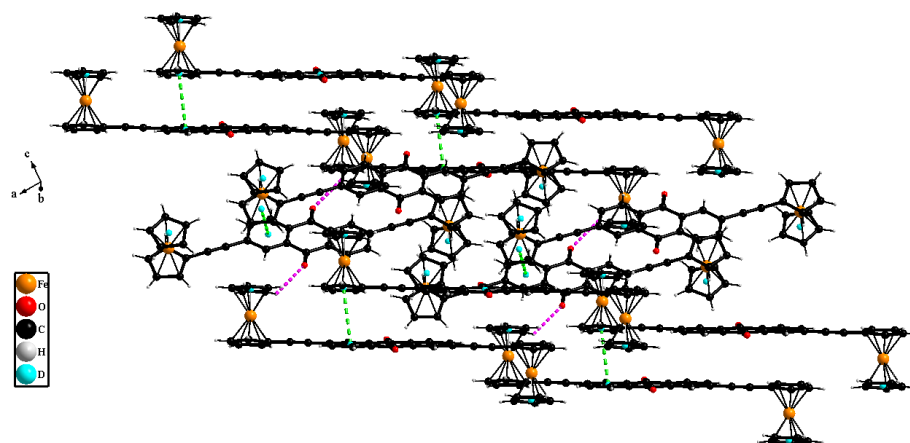


Figure 5.4 3D network of **3** along tilted b axis

5.2.3 Electronic absorption spectra

The electronic absorption spectra of compounds **1–3** have been recorded in chloroform at room temperature (RT) (**Figure 5.5**). The absorption spectra of **1**, **2** and **3** in chloroform show two dominating absorption peaks. **1** shows absorptions at 443 nm, 513 nm, compound **2** at 390 nm, 413 nm and compound **3** at 360 nm, 515 nm wavelength which corresponds to the π - π^* and metal-to-ligand charge transfer (MLCT) process transition.[19] Similar to our previously reported compounds,[20] the absorption maxima of 9,10-substituted anthracene compound **1** was found to be red-shifted, which suggests more perturbation of the 9,10-substituents on the anthracene ring.

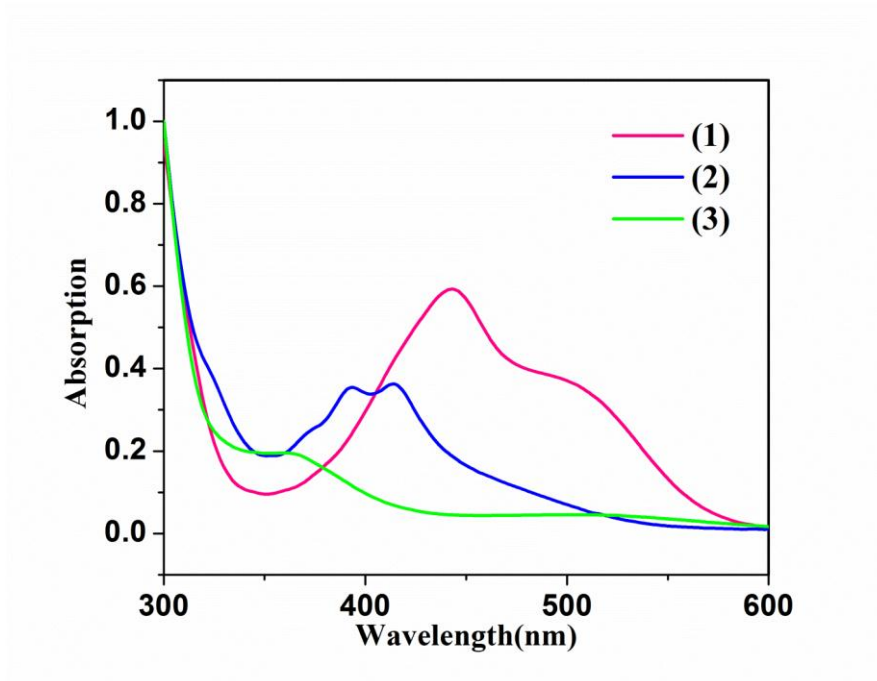


Figure 5.5 UV-vis spectra of **1**, **2** and **3**

5.2.4 Density functional theoretical studies

To understand geometry optimization, energy, and electronic communication in compounds **1–3**, DFT calculations have been done. The bond distances calculated for the optimized structures in **1–3** are similar to those obtained by their x-ray crystal structures. The frontier molecular orbitals (FMO) of **1–3** are shown in **Figure 5.6**. For compounds **1** and **2**, the highest-occupied molecular orbitals (HOMOs) are of π -type, and the lowest-unoccupied molecular orbitals (LUMOs) are of π^* -type, and both are delocalized on the anthracene unit. However, in **3**, HOMO is localized on the ferrocene unit, while LUMO is on the anthraquinone unit. This study reveals a particular donor-acceptor system, accompanied by the charge transfer process, where, ferrocenyl moiety behaves as donor and anthraquinone part behaves as an acceptor.

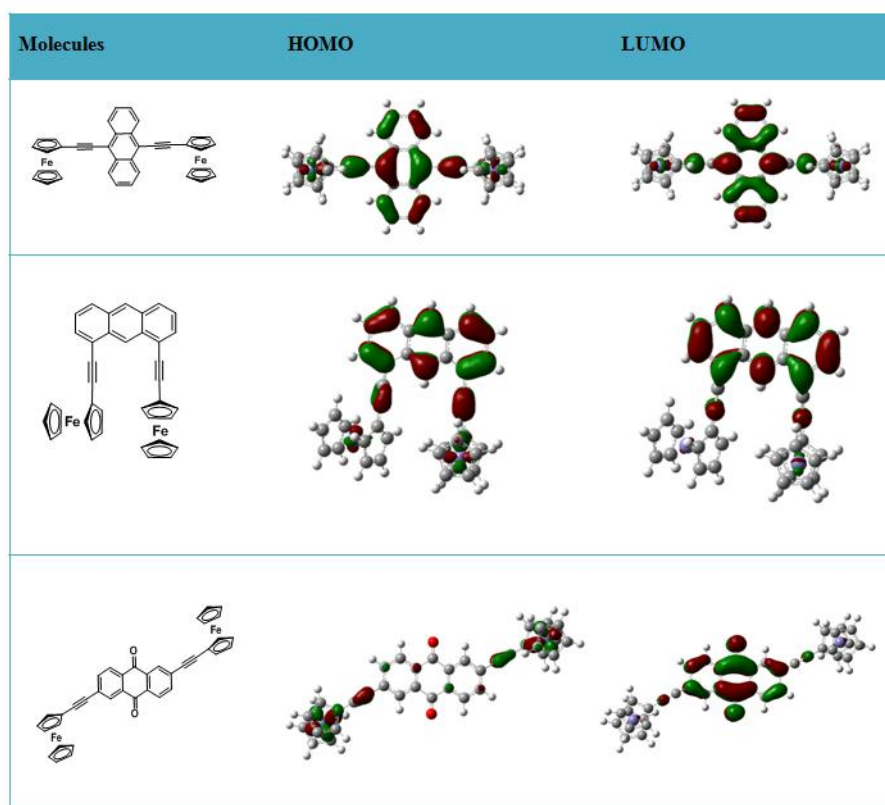


Figure 5.6 HOMO and LUMO of **1**, **2** and **3**

5.2.5 Molecular docking

To understand the binding affinity[21] and mode of interaction of proteins towards the compounds **1–3**, molecular docking was done with 3 cancer-causing proteins. Based on parameters of inhibition constant, binding energy, van der Waal's interactions and intermolecular energy between different proteins; several observations were made i.e. **2** strongly binds with cancer-related Aurora-A Protein Kinase (**1MQ4**)[22] with the interacting residues Gly140, Leu139, Lys141, Val147, Gly142, Ala160, Tyr212, Lys162, Ala213, Thr217, Gly216, Tyr219, Arg220, Leu263, Glu260, Asp274 (**Figure 5.7, Table 5.2**) as compared to **1** and **3**.

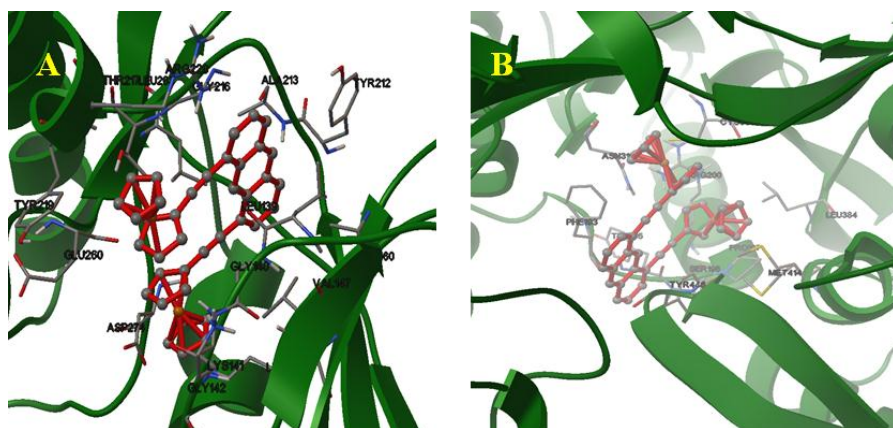


Figure 5.7 Molecular docking of **2** with cancer-causing and viral proliferation proteins, the proteins are shown as ribbons, and the interacting residues are shown as sticks, the ligand is shown as ball and stick. (A) cancer-related Aurora-A Protein Kinase (**1MQ4**), (B) Hepatitis C virus NS5B polymerase (**2WCX**)

In all cases, **1** and **2** are surrounded by both hydrophobic and charged amino acids of protein as shown in **Table 5.2**, respectively. The compound **3** is mostly surrounded by hydrophobic and aromatic amino acids. Benzyl group of phenylalanine 181 and 406 stabilized by cyclopentadienyl ring and anthraquinone of **3** by $\pi \cdots \pi$ stacking interaction. Inhibition constant of the compound **2** toward cancer-related Aurora-A Protein Kinase is better than that of earlier reported compound[23] thus it makes **2** a potential candidate for further testing it as an anticancer drug.

5.2.6 Cell cytotoxic assay

The MTT assay determines the cell proliferation rate. When the metabolic events leading to apoptosis or necrosis, MTT assay can be employed to measure the reduction in the cell viability. The yellow tetrazolium MTT is reduced to purple coloured formazan by metabolically active cells, by the action of dehydrogenase enzymes.[24] Here, this assay is used to examine the anti-proliferative effect[25] for **1–3** on human melanoma cancer (A375), cervical carcinoma (HeLa) and normal human embryonic kidney (HEK) cells lines. The cytotoxicity of the compounds **1–3** is found to be concentration dependent, i.e. average cell viability ratio decreases by

increasing the concentrations of the compounds. The IC₅₀ values of **1**, **2** and **3** subsequent to 24h of treatment are found to be 20.3 μM, 15.1 μM, 25 μM, respectively, on A375 and 30.1 μM, 25 μM, 35.2 μM, respectively, on HeLa cells lines and > 80± 0.013 μM, 80± 0.099 μM, >120 ± 0.063 μM respectively on HEK cell line as shown in **Figure 5.8** and **Table 5.4**. This suggests that the compounds are less toxic to normal cell line in nature as compared to cancerous cell line. The *in-vitro* cytotoxicity assay confirms that compound **2** exhibits higher cytotoxicity with the tumor cell lines selected and it may act as a potential chemotherapeutic agent against cancer.

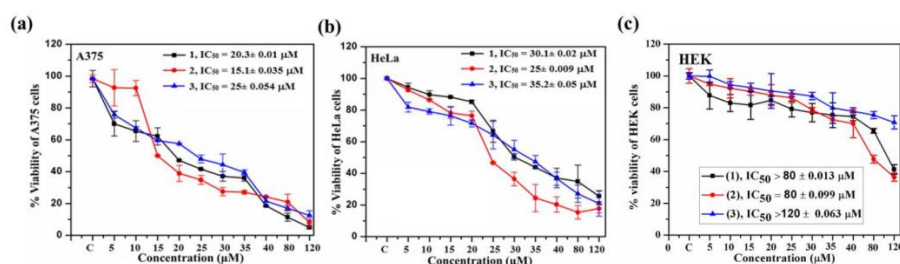


Figure 5.8 Cell viability studies of **1**, **2** and **3** on cancerous as well as normal cell lines. (a) cervical cancer cell line (HeLa) (b) skin melanoma cell line (A375), (c) human embryonic kidney cell line (HEK). These cells were exposed to various concentrations of **1**, **2** and **3** for 24 h and then cell viability was measured by MTT assay

5.2.7 BSA binding studies

The plasma proteins present in blood are necessary for the transportation of drugs all over the blood inside the body. If the molecules bind to them, the transportation of the drug will be affected. The interaction of organometallic compounds with proteins is generally examined by the intrinsic fluorescence intensity. The interaction of the compounds with BSA has been well studied by fluorescence quenching. The three amino acids which are responsible for the fluorescence property in BSA are tryptophan, tyrosine and phenylalanine residues. The quenching may happen because of various reasons, such as the formation

of ground-state complex, excited state reactions, molecular rearrangement, energy transfer and collision.[26]^[26]

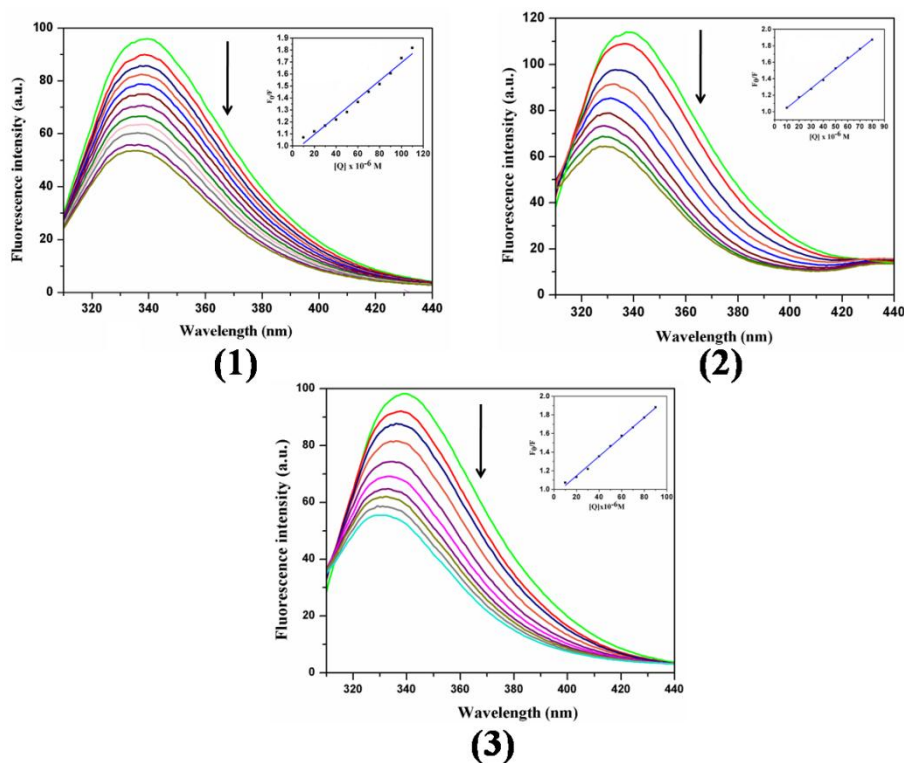


Figure 5.9 BSA binding of **1**, **2** and **3**. Inset: Corresponding Stern–Volmer plot

To overcome the inner filter effect, we dilute the sample from 5 μ M to 1 μ M. When we plotted the normalization graph, we found there is no shift in maxima wavelength. This suggests that in such concentration, we did not observe the inner filter effect. The spectra of **1**, **2** and **3**–BSA clearly shows the remarkable decrease in the intensity of the fluorescence accompanied by a noticeable blue shift at 340 nm. The blue shift indicates that after the addition of compounds, the polarity around the fluorescence chromophore (such as tryptophan, tyrosine) of BSA decreases due to which the hydrophobicity increases and the peptides strand become less extended. The result suggests that the conformation of protein slightly changes.[27,28] At 340 nm, the intensity of the fluorescent spectral band quenched up to 40% of its initial value (**Figure 5.9**).

The maximum wavelength of emission is shifted to higher energy

which shows the transfer of energy from the indole moiety present in the tryptophan towards **1–3** attached to the specific protein. The fluorescence quenching data were understood by the Stern–Volmer equation[29].

The Stern-Volmer quenching rate constant (K_{SV}) values obtained are $1.00 \times 10^3 \text{ M}^{-1}$ for **1**, $1.19 \times 10^4 \text{ M}^{-1}$ for **2** and $1.00 \times 10^4 \text{ M}^{-1}$ for **3** which is on the higher value indicates a firm binding between **1**, **2** and **3** and BSA (**Figure 5.9**). The value of bimolecular quenching rate constant (K_q) of **1**, **2** and **3** is found to be $1 \times 10^{11} \text{ M}^{-1} \text{ s}^{-1}$, $1.19 \times 10^{12} \text{ M}^{-1} \text{ s}^{-1}$, and $1 \times 10^{12} \text{ M}^{-1} \text{ s}^{-1}$ respectively shows the static quenching. The varying concentrations of **1**, **2** and **3** show linearity in Stern–Volmer plot. This shows one stable ground state complex formation in BSA-**1**, **2** and **3** systems.[30]

To find out the number of binding sites and value of binding constant, the Scatchard equation is used. The result obtained is the higher binding constant ($5.6 \times 10^6 \text{ M}^{-1}$) and “n” value (1.37) for **2**-BSA as compared to **1**-BSA ($4.01 \times 10^6 \text{ M}^{-1}$, 1.05) and **3**-BSA ($4.8 \times 10^6 \text{ M}^{-1}$, 1.19). These are also comparatively the higher value about many compounds reported so far[31-33] (**Table 5.3**). A possible justification for the higher values is that the compound **2** is more electron releasing than **1** and **3** due to its exposed orientation and the presence of electron donating cis-ferrocenyl group, the comparatively higher electron density on anthracene ring may inspire more interaction with the electron withdrawing domain of the protein.

Moreover, molecular docking of **1–3** is also performed with BSA. This result also shows that compound **2** strongly binds with BSA as compared to **1** and **3** regarding binding energy and inhibition constant i.e., $-9.29 \text{ KcalMol}^{-1}$ and 154.9 nM respectively. The interacting residues with **2** are Ser109, Pro110, Asp111, Arg144, His145, Pro146, Ala193, Arg196, Glu424, Ser428, Arg458. The hydrophobic amino acid like proline, tryptophan, leucine, isoleucine interacts with **1–3**.

5.2.8 DNA binding studies

DNA is considered as a vital target to mediate necrosis or apoptosis to the cells. Therefore, CT-DNA and compounds **1**, **2** and **3** interactions can be

understood by UV-Vis titration experiments. The binding to DNA leads to changes in the UV/Vis spectra of complexes. This may be due to the change in the DNA conformation after binding with **1–3**. Hypochromism with the negligible shift at 254nm is observed, upon addition of **1**. But in the case of **2** and **3**, hypochromism with the blue shift at absorption maxima is observed at 258nm and 254nm, respectively. The hyperchromic effect with blue shift suggests that **1–3** bind to DNA by partial intercalation, external contact or may be due to electrostatic binding.[34] The intrinsic binding constants K_b are found to be $1.216 \times 10^3 M^{-1}$, $3.51 \times 10^3 M^{-1}$ and $5.27 \times 10^2 M^{-1}$, respectively for **1–3**. From the binding constant, it is inferred that compound **2** binds more strongly with CT-DNA as compared to **1** and **3**.

The CT-DNA and compounds **1**, **2** and **3** interaction can be understood by the steady state competitive binding experiment employing **1–3** as the quenchers. Ethidium bromide (EB) is used the fluorescent probe. The EB emits intense fluorescent light upon interaction with the DNA because of intercalation of EB between DNA base pairs. When the compounds **1**, **2** and **3** intercalate into DNA, the binding sites in DNA for EB decreases, therefore quenching of the fluorescent intensity is observed. This fluorescence intensities reduction reveals that the compounds **1**, **2** and **3** displace the EB molecules from the binding sites of DNA.

The phenomenon is more clearly visible in **2** as compared to **1** and **3**. Furthermore, K_q values for compounds **1–3** are $5.6 \times 10^3 M^{-1}$, $6.0 \times 10^3 M^{-1}$, $5.6 \times 10^3 M^{-1}$ respectively, which are obtained from the classical Stern–Volmer equation.[35] The binding constant (K_b) of **1**, **2** and **3** with Ct DNA obtained from double logarithm equation $\log[F_0-F/F]$ vs $\log[Q]$ are 3.34×10^6 , 3.72×10^6 and $4.62 \times 10^6 M^{-1}$, respectively, reflecting favourable binding of the compound **3** and DNA after displacing EB molecules attached to the DNA as compared to the compounds **1** and **2**.

5.2.9 Circular Dichroism Studies

Conformational changes in protein helix perturbation in BSA upon **1**, **2** and **3** interaction is noticeable using circular dichroism spectroscopic

results. In the BSA CD spectrum, there are two major characteristic bands at 208 nm (negative) and 222 nm (negative) indicating negative cotton effect because of the $n \rightarrow \pi^*$ transition in the peptide linkage of the α -helical structure (**Figure 5.10**).

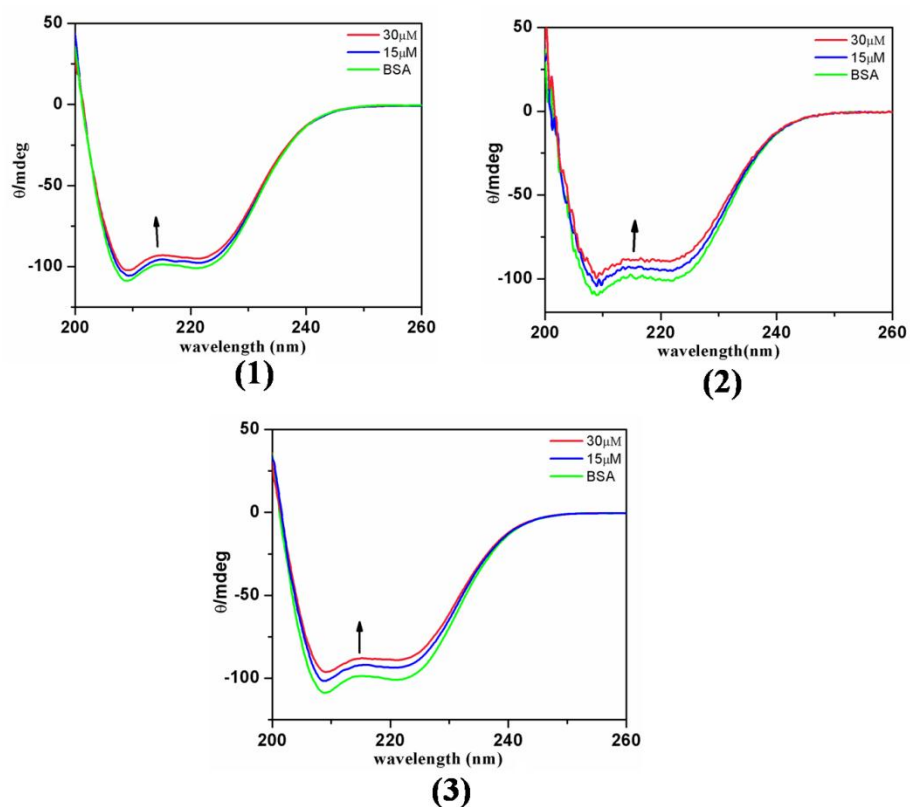


Figure 5.10 CD studies of **1**, **2** and **3**

The conformational changes of the protein could be traced by the changes in the intensity and position of these spectral bands in CD spectra. Upon the interaction of **1**, **2** and **3** with BSA, these bands show the appreciable increase in intensity, which indicate that BSA binds to **1**, **2** and **3** and leave its native conformation.[36]

All these bands which are observed shows increase in intensity with the compounds **1**, **2** and **3** that can be assigned to the local perturbation of native conformation of BSA α and β -helix. The reason envisaged that the hydrophobic domains in the protein chain have the hydrophobic interaction with the compounds. The perturbed amino acids of protein assume a confirmation that facilitates its binding to the compounds **1–3**. Interestingly **1**, binds with BSA as a β form is not seen at a lower concentration. The composition of the peptide's secondary

structure is approximated by the Circular Dichroism spectra analysis using Yang's reference.[37]

5.3 Conclusion

We have synthesized two bis-ferrocenylethynyl-anthracene (**1** and **2**) and a 2,6-bis-ferrocenylethynyl-anthraquinone **3** compounds with substitutions on different positions of anthracene and anthraquinone ring. The biological activities of the compounds (**1–3**), confirmed that compound **2** is found to be more effective towards anticancer activity compared to **1** and **3** from both molecular docking and cell cytotoxic assay studies. Cytotoxic activities further confirm the binding of the compounds to DNA, which consequently leads to cell death.

5.4 Experimental

All experiments were done under an inert atmosphere. All reaction solvents were distilled prior to use; freshly dried tetrahydrofuran (THF) and triethylamine were used. Column chromatography was carried out using silica gel (230-400 mesh) as specified. All reagents were purchased either from Rankem or Sigma-Aldrich and used without further purification. NMR spectra were recorded in deuterated chloroform (CDCl_3) on a Bruker Avance (III) instrument. IR spectra were recorded with a Bio-Rad FTS 3000 MX instrument on KBr pellets. The mass spectra were recorded on Bruker-Daltonics, microTOF-QII mass spectrometer. All UV data were measured at RT at the 10^{-4}M concentration in chloroform on a Varian UV-vis spectrophotometer (model: Cary 100).

5.4.1 X-ray Crystallography

Data were collected at 293 K using graphite-monochromated Mo $K\alpha$ ($\lambda_\alpha = 0.71073 \text{ \AA}$). The data collection strategy was interpreted by employing the CrysAlisPro CCD software. The collection of data was done by the standard phi-omega scan techniques. The data were scaled and reduced employing CrysAlisPro RED. The direct methods using SHELXS-97 was used to solve the crystal structures and refined by the full matrix least squares method with SHELXL-97, refining on F^2 .^[38] The H-atoms were placed at geometrically constrained positions and refined using isotropic temperature factors, generally $1.2 \times U_{eq}$ of their parent atoms. All remaining non-hydrogen atoms were refined anisotropically. All the C–H $\cdots\pi$ interactions, molecular drawings, Mercury (ver. 3.1). The crystals and their refinement data are shown in **Table 5.1**.

5.4.2 Density functional theory

In order to explore the electronic structure and optimize the structure of the Bis-ferrocenylethynyl-anthracene (**1-2**) and Bis-ferrocenylethynyl-anthraquinone (**3**); DFT calculations were performed by using the Gaussian09 program.^[38]^[39] All calculation was done at

B3LYP[39,40] level of theory employing the Lan12DZ basis set for Fe and 6-31G* basis set for the remaining atoms. The geometries were optimized without imposing symmetry or any other restraints.

5.4.3 Molecular docking

On the basis of the literature survey, three different protein structural data were downloaded from the Protein Data Bank. The examined proteins were cancer-related Aurora-A Protein Kinase, Ephrin A2 (ephA2) Receptor Protein Kinase (cancer-associated protein kinases), Cancer-related (FAK) Focal Adhesion Kinase and Bovine Serum Albumin (**4F5S**).

AutoDock 4.2[41] employing the Lamarckian genetic algorithm (LGA) was used for the docking of ligands with proteins. The coordinates of **1–3** were utilized from crystal structures as a .cif file and saved as the .PDB format using Mercury software. The water molecules and co-crystallized inhibitors were omitted from all the protein structure. Polar hydrogen atoms, Gastegier and Kollman charges were given. All other bonds had rotational freedom. MGL AutoDock Tool (ADT) was used to generate the grid parameter file of each protein. A grid-box was made to cover the entire protein domain. The center of the protein structure was considered as the center of the grid-box. The value of 0.375 was used as the spacing between grid points for all protein structure. After finalization of grid map, autodock was run. The population size of GA was 150 and the maximum number of energy evaluations and generations were 2500000 and 27000, respectively. A maximum number of top individuals that survived automatically was set to 1 having the mutation, and the crossover rate was 0.02 and 0.8, respectively. The parameters were the same for all target proteins. The docking calculation resulted in 10 different conformations. The best conformation was selected based on the lowest binding energy and inhibitory constant.

5.4.4 MTT assay

The MTT assay was performed to examine the effect of **1–3** on cell viability. Human melanoma cancer cell line (A375), cervical cancer

cell lines (HeLa) and normal human embryonic kidney (HEK) cells were used in our study. Minimum essential medium (MEM, Himedia) supplemented with 10% FBS and 1% antibiotics Penicillin/ Streptomycin; 10,000 Uml⁻¹ was used for the culture of both A375 and HeLa cells. Dulbecco's Modified Eagle Medium (DMEM) was used for the culture of HEK. To perform cell viability assay, 8000 cells well⁻¹ in 100 µL complete media which were seeded in triplicates into 96 well plates and cell adhesion was done after the incubation for 24 hours in 5% CO₂ atmosphere at 37 °C. After cell adhesion, the compounds **1–3** were completely dissolved in 0.1% DMSO at different concentration, and 10 µL of the above solution was added to each well to give final concentration with the range from 5–120 µM. 0.1% DMSO was added as the control. Cell viability assay was assessed using standard 3-(4,5-dimethylthiazole-2-yl)-2,5-diphenyl tetrazolium bromide (MTT).[42] After 24 hours of incubation, 100µL MTT (0.5mg/ml) was added to each well and incubated for another 4 hours. The medium was then removed and 100 µL DMSO was added and was shaken for 10 min. in order to dissolve formazan crystals. Absorbance at the 570 nm wavelength was measured with Synergy H1 Biotek microplate reader. The cell viability data were calculated as % cell viability = (mean OD of treated cells (control)/ mean OD of untreated cells (control)) × 100. IC₅₀ (half maximal inhibitory concentration values) were obtained using the relative viability over **1–3** concentration graph.

5.4.5 DNA binding studies

The CT- DNA binding studies were performed by UV/Vis and fluorescence spectroscopic methods. In UV/Vis titration experiment, compounds were dissolved in 50µM Tris–HCl buffer: THF (7:3) v/v. The concentration of CT-DNA was determined by measuring absorption intensity at 260nm by employing ϵ_{260} of DNA as 6600 dm³mol⁻¹ cm⁻¹. [43] The concentration of compound was kept constant 1 × 10⁻⁵ M and the concentration of DNA varies from 0 to 100 µM. The binding constants (K_b) were determined using the equation:

$$[\text{DNA}]/(\varepsilon_a - \varepsilon_f) = [\text{DNA}]/(\varepsilon_b - \varepsilon_f) + 1/K_b(\varepsilon_b - \varepsilon_f)$$

Where [DNA] is the concentration of DNA, ε_a , ε_f and ε_b correspond to the apparent extinction coefficient, the extinction coefficient of the unbound compound and the extinction coefficient of a fully bounded compound, respectively. A plot of $[\text{DNA}]/(\varepsilon_a - \varepsilon_f)$ vs. [DNA] gives the binding constant K_b as the ratio of the slope to the intercept.[34,44]

Further DNA binding for the compounds **1–3** was measured by a fluorescence spectral technique; ethidium bromide (EB) displacement assay from EB bound CT-DNA in Tris-HCl buffer at biological pH 7.4 was done, as EB was used as it was non-emissive in Tris-HCl buffer solution (pH 7.4) because of fluorescence quenching of the independent EB by the solvent. Absorption titration was carried out by keeping the CT-DNA and EB concentration fixed at 10 μM and 20 μM respectively while changing the **1–3** concentration varying from 0 to 130 μM . Furthermore, the fluorescence intensity change at 605 nm (520 nm excitation) of EB (20 μM) attached to DNA was measured in respect of the concentration of the **1–3** (0 to 130 μM).

5.4.6 BSA binding studies

The interaction of the compounds **1–3** with bovine serum albumin (BSA) was studied through tryptophan emission quenching experiment. Emission intensity of BSA at $\lambda = 340$ nm. The solution of the compounds **1–3** was gradually added to the solution of BSA (5 μM) in 50 μM Tris-HCl buffer (pH 7.4) and the emission signals which were showing quenching recorded at 340 nm ($\lambda_{\text{ex}} = 295$ nm).

5.4.7 Circular dichroism measurements

The circular dichroism (CD) spectroscopy of BSA in the presence of **1–3** was done by using JASCO 720 spectro-polarimeter equipped with a Peltier temperature control device at 298 K under the continuous flow of nitrogen purging. All the experiments were performed in a 1mm path length quartz cell. Three successive scans were recorded at a scan speed of 50 nm cm^{-1} , and their average was considered to get the CD spectra of

Bovine serum albumins. The results were obtained by the deduction of Tris-HCl (blank). The information of the change in the secondary structure of BSA has been achieved by the far UV-CD spectra (200–260 nm). First, the spectra of free BSA (10 μ M) were recorded, and then the CD spectral changes were observed by monitoring the binding of BSA while adding 15 μ M and 30 μ M of **1–3** successively.

5.4.8 Synthesis of compound **1**

To a stirred solution of the 9,10-Dibromo-anthracene (0.20 mmol), and ethynyl-ferrocene (0.45 mmol) in 40 mL of THF and 40 mL of TEA (1:1, v/v), Pd(PPh₃)₄ (32 mg, 0.028 mmol) was added under an inert atmosphere at RT. The reaction mixture was stirred for 15h at 75 °C and checked by TLC. The reaction solvent was then dried under reduced pressure, the crude mixture was dissolved in DCM and passed through celite and again dried. Further, the separation was carried out by SiO₂ chromatography with DCM/hexane (2:3, v/v) to obtain 9,10-Bis-ferrocenylethynyl-anthracene (**1**) as red colored solid. Brown red crystals were obtained in DCM: Hexane (4:1) in 5 days. Characterization data: ¹H NMR (400 MHz, CDCl₃): δ 4.37 (s, 10H, C₅H₅), 4.42 (s, 4H, C₅H₄), 4.77 (s, 4H, C₅H₄), 7.64 (4H, non-terminal ant.-H), 8.63 (4H, terminal ant.-H). ¹³C NMR (100.635 MHz, CDCl₃): 14.2; 22.8; 31.9; 50.8; 68.9; 70.9; 72.4; 80.2; 121.1; 155.5; 191.1; IR (KBr, cm⁻¹): 3091.93, 3060.15, 2957.68, 2201.23, 1620.14, 1412.41, 1390.11, 915.36, 820.06, 762.24, 638.30; λ_{max} = 443, 513 nm; HRMS (m/z): [M] calculated for C₃₈H₂₆Fe₂, 594.07; found, 594.07.

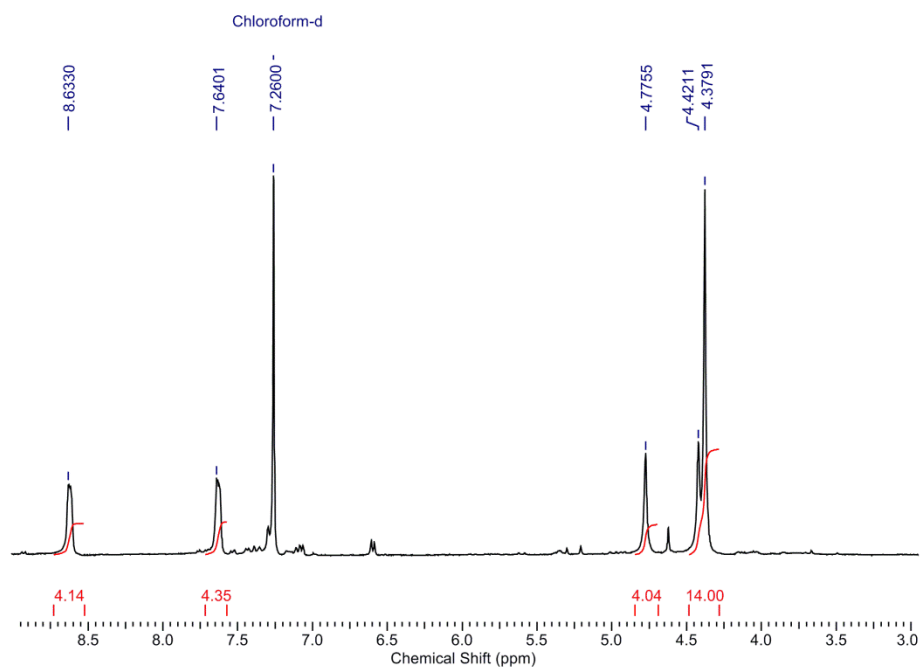


Figure 5.11 ^1H NMR of **1** in CDCl_3

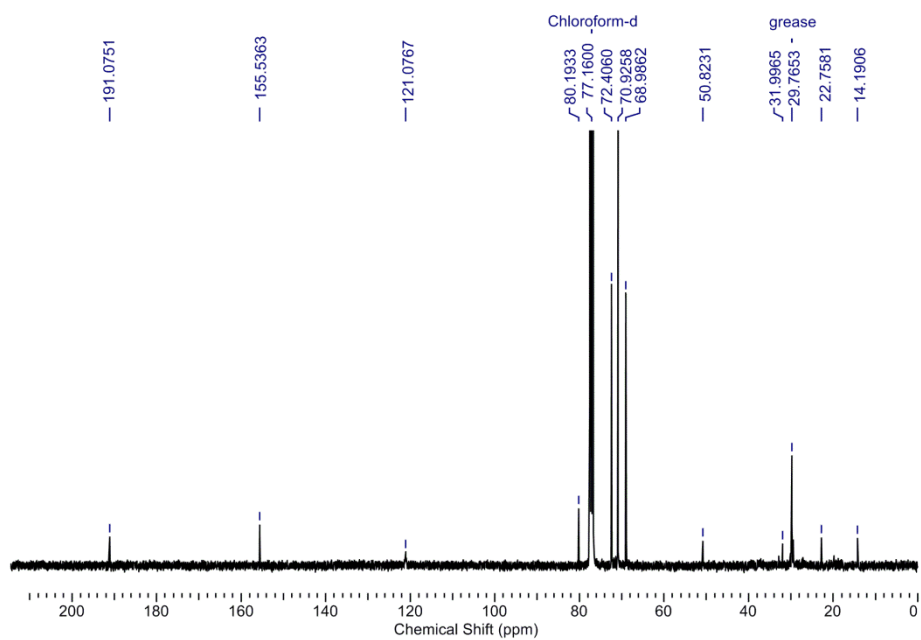


Figure 5.12 ^{13}C NMR of **1** in CDCl_3

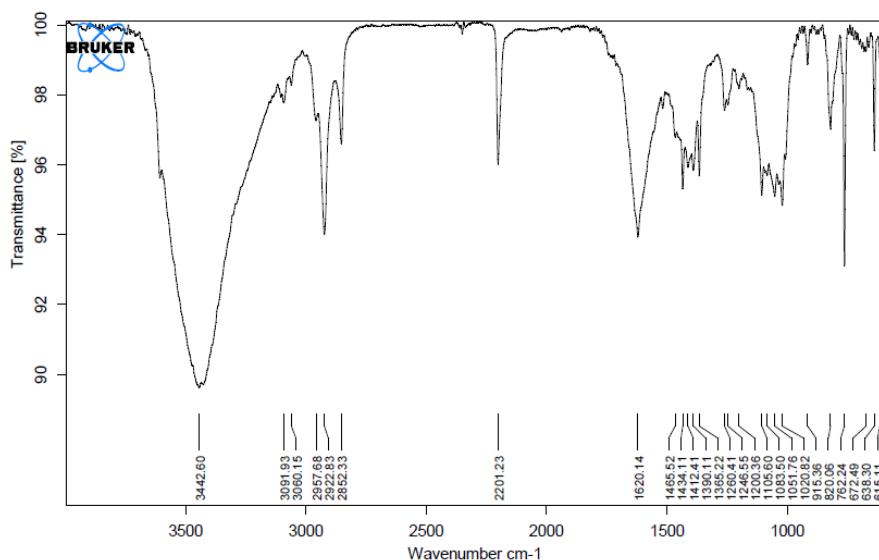


Figure 5.13 IR of **1**

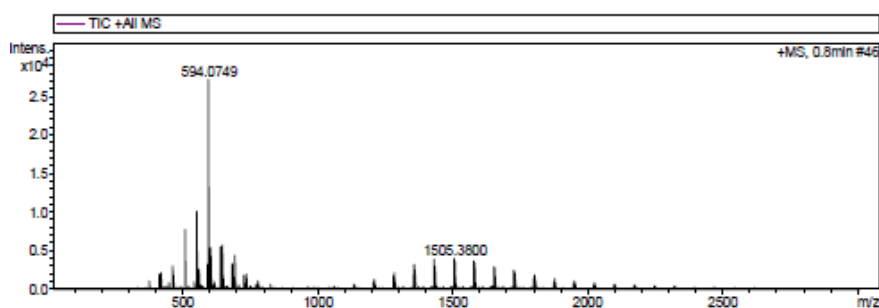


Figure 5.14 ESI-MS of **1**

5.4.9 Synthesis of compound **2**

To a stirred solution of the 1,8-Dibromo-anthracene (0.20 mmol) and ethynyl-ferrocene (0.45 mmol) in 40 mL of THF and 40 mL of TEA, Pd(PPh₃)₄ (40 mg, 0.035 mmol) was added under an inert atmosphere at RT. Further, the procedure followed is as same as **1**. 1,8-Bis-ferrocenylethynyl-anthracene (**2**) was obtained as red solid. Dark red crystals were obtained in DCM: Hexane (4:1) in 5 days. Characterization data: ¹H NMR (400 MHz, CDCl₃): δ 4.25 (s, 10H, C₅H₅), δ 4.25 (s, 4H, C₅H₄), 4.63 (s, 4H, C₅H₄), 7.46 (t, J = 8Hz, 2H, pos. 3,6), 7.77 (d, J = 8Hz, 2H, pos. 2,7), 7.99 (d, J = 8Hz, pos. 4,5), 8.45 (s, 1H, pos.10), 9.46 (s, 1H, pos.9). ¹³C NMR (100.635 MHz, CDCl₃): 65.3; 68.9; 70.1; 71.9 84.2; 94.1; 122.2; 124.2; 125.2; 128; 129.9; 131.6; IR (KBr, cm⁻¹): 3095.05, 3047.58, 2924.17, 2205.48 1632.20, 1319.20 1104.03, 1020.30,

880.67, 745.64, 524.60; $\lambda_{\text{max}} = 390, 413 \text{ nm}$; HRMS (m/z): [M] calculated for $\text{C}_{38}\text{H}_{26}\text{Fe}_2$, 594.07; found, 594.08.

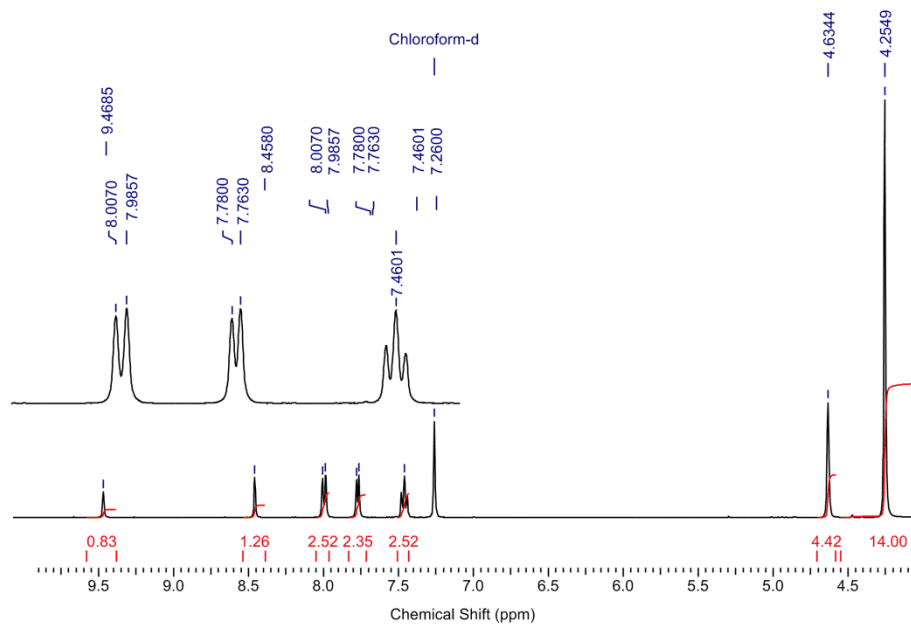


Figure 5.15 ^1H NMR of **2**

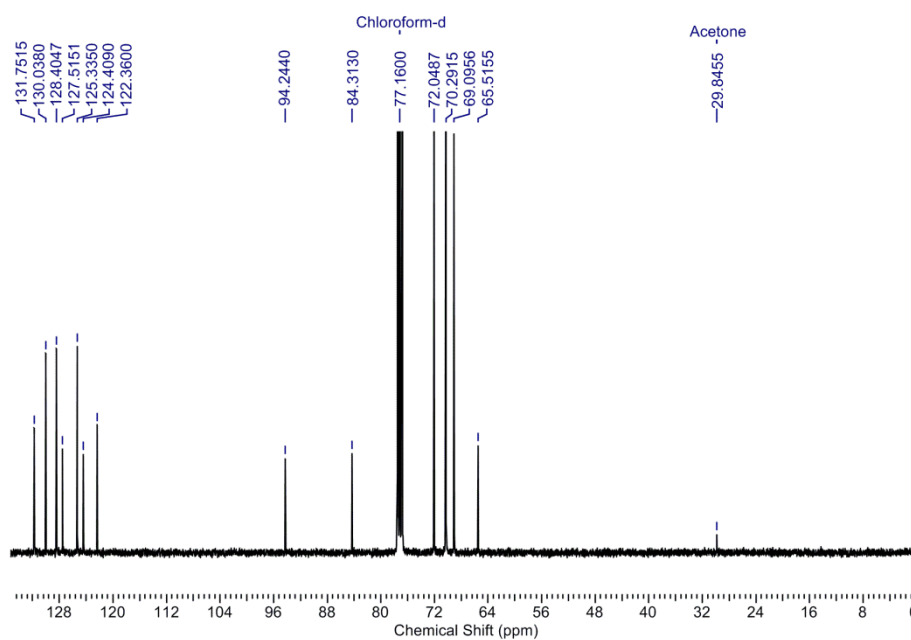


Figure 5.16 ^{13}C NMR of **2**

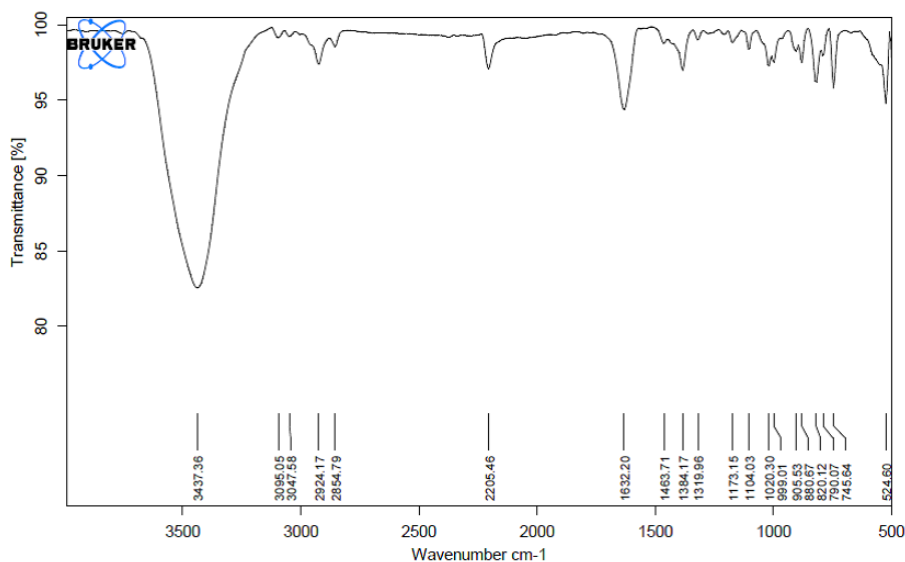


Figure 5.17 IR of 2

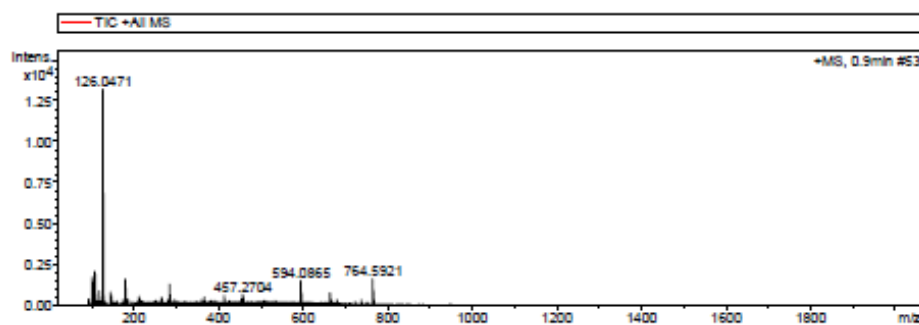


Figure 5.18 ESI-MS of 2

5.4.10 Synthesis of compound 3

To a stirred solution of the 2,6-Diiodoanthraquinone (0.20 mmol), and ethynyl-ferrocene (0.45 mmol) in 40 mL of Toluene and 40 mL of TEA (1:1, v/v), Pd(PPh₃)₄ (40 mg, 0.035 mmol) were added under an inert atmosphere at RT. The reaction mixture was stirred for 15h at 90 °C. Further, the procedure followed is as same as **1**. 2,6-Bis-ferrocenylethynyl-anthraquinone (**3**) was obtained as red colored solids. Red crystals were obtained in DCM/Hexane (4:1) in 8 days. Characterization data: ¹H NMR (400 MHz, CDCl₃): δ 4.28 (s, 10H, C₅H₅), 4.33 (s, 4H, C₅H₄), 4.57 (s, 4H, C₅H₄), 7.84 (d, J = 8Hz, 2H, pos. 3,7), 8.27 (d, J = 8Hz, 2H, pos. 4,8), 8.32 (s, pos. 1), 8.37 (s, pos. 5). ¹³C NMR (100.635 MHz, CDCl₃):14.2; 24.9; 25.9; 31.5, 62.2; 70.3; 10.7; 113.9; 135.3; 14.4; 153.6; IR (KBr, cm⁻¹): 3103.71, 2924.45, 2853.69,

2204.61, 1672.05, 1591.35, 1413.30, 1312.29, 1281.13, 1106.65, 1035.59, 919.19, 822.83, 743.02, 710.67; $\lambda_{\text{max}} = 360, 515 \text{ nm}$; HRMS (m/z): [M] calculated for $\text{C}_{38}\text{H}_{26}\text{Fe}_2$, 624.04; found, 663.45.

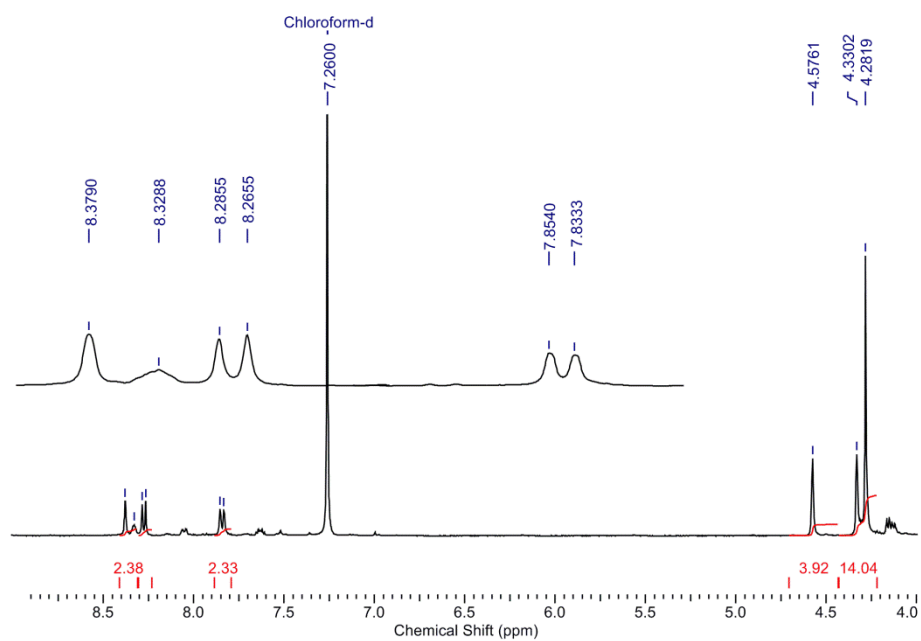


Figure 5.19 ^1H NMR of **3** in CDCl_3

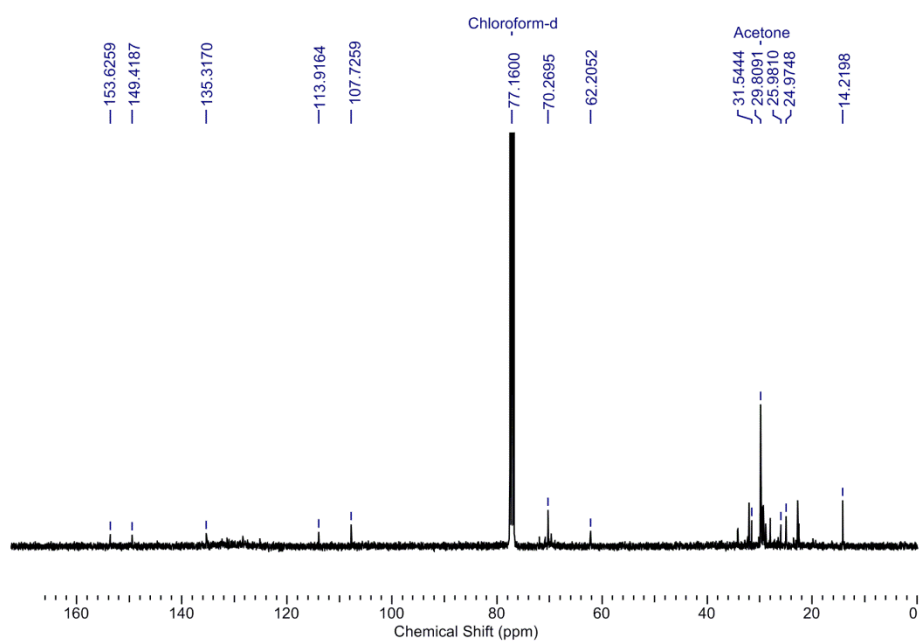


Figure 5.20 ^{13}C NMR of **3** in CDCl_3

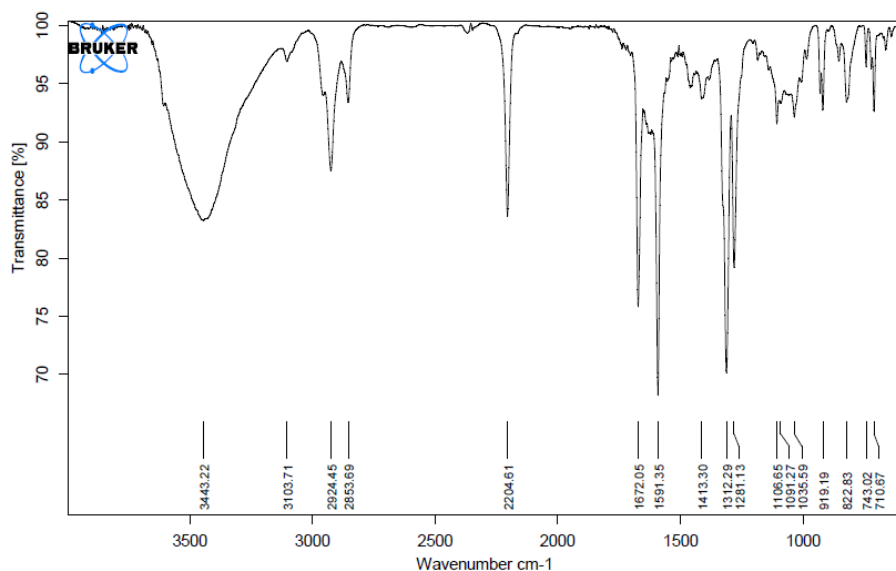


Figure 5.21 IR of **3** in CDCl_3

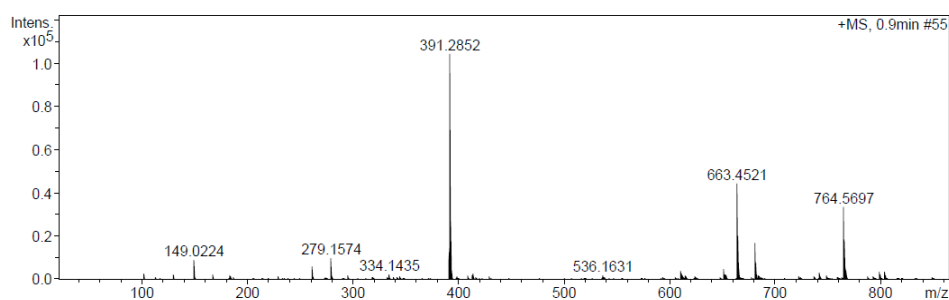


Figure 5.22 ESI-MS of **3**

Table 5.1 Crystal data and structure refinement for **1–3**

Identification code	1	2	3
Empirical formula	$\text{C}_{38}\text{H}_{26}\text{Fe}_2$	$\text{C}_{76}\text{H}_{52}\text{Fe}_4$	$\text{C}_{38}\text{H}_{24}\text{Fe}_2\text{O}_2$
Formula weight	594.29	1188.57	624.27
Temperature/K	293(2)	293(2)	300.0
Crystal system	Monoclinic	Monoclinic	Monoclinic
Space group	$P2_1/c$	$P2_1/n$	$P2_1/n$
a/Å	11.1693(5)	15.0626(5)	6.7940(3)
b/Å	17.3199(6)	11.3239(4)	18.4075(9)
c/Å	14.4292(6)	16.9711(7)	10.8529(8)
$\alpha/^\circ$	90	90	90
$\beta/^\circ$	96.725(5)	104.276(4)	99.160(5)
$\gamma/^\circ$	90	90	90
Volume/Å³	2772.2(2)	2805.32(18)	1339.96(13)
Z	4	2	2
$\rho_{\text{calc}}/\text{g/cm}^3$	1.424	1.407	1.547
μ/mm^{-1}	1.073	1.060	1.119
F(000)	1224.0	1224.0	640.0

Crystal size/mm³	0.23 × 0.18 × 0.13	0.330 × 0.220 × 0.180	0.32 × 0.27 × 0.23
Radiation	MoK α (λ = 0.71073)	MoK α (λ = 0.71073)	MoK α (λ = 0.71073)
2θ range for data collection/°	5.96 to 49.99	6.12 to 64.34	5.84 to 49.99
Index ranges	-13 ≤ h ≤ 13, -20 ≤ k ≤ 20, -17 ≤ l ≤ 17	-21 ≤ h ≤ 19, -16 ≤ k ≤ 11, -24 ≤ l ≤ 25	-7 ≤ h ≤ 8, -21 ≤ k ≤ 21, -12 ≤ l ≤ 12
Reflections collected	21315	38077	10009
Independent reflections	4878 [R _{int} = 0.0760, R _{sigma} = 0.0587]	9338 [R _{int} = 0.0327, R _{sigma} = 0.0249]	2351 [R _{int} = 0.0291, R _{sigma} = 0.0205]
Data/restraints/parameters	4878/0/362	9338/0/362	2351/0/190
Goodness-of-fit on F²	1.118	1.039	1.099
Final R indexes [I ≥ 2σ (I)]	R ₁ = 0.0803, wR ₂ = 0.2080	R ₁ = 0.0446, wR ₂ = 0.1162	R ₁ = 0.0420, wR ₂ = 0.1110
Final R indexes [all data]	R ₁ = 0.1256, wR ₂ = 0.2587	R ₁ = 0.0607, wR ₂ = 0.1279	R ₁ = 0.0485, wR ₂ = 0.1176
Largest diff. peak/hole/e Å⁻³	1.18/-1.00	0.53/-0.40	0.46/-0.20
CCDC No.	1503798	1503799	1503800

Table 5.2 Molecular docking of 1–3 with cancer causing proteins

Ligand	Protein (PDB Id)	Binding energy (Kcal/Mol)	Inhibition constant	Interacting residues
1	cancer- related Aurora-A Protein Kinase (1MQ4)	-8.83	338.17nM	GLY142, LYS143, PHE144, VAL147, LYS162, LEU164, GLN177, LEU210, LYS258, ASN261, LEU263, ALA273, ASP274, TRP277, CYS290
	Cancer- associated protein kinases Ephrin A2 (ephA2) Receptor Protein	-7.81	1.88 μ M	ILE619, ALA621, GLY622, GLU623, PHE624, GLU663, TYR694, GLU696, ASN697, GLY698, ASP757, GLY759

	Kinase (1MQB)			
	Cancer-related (FAK) Focal Adhesion Kinase (1MP8)	-7.19	5.32 μ M	ILE420, GLY429, GLY431, GLN432, PHE433, VAL436, ALA452, LYS454, GLU471, ASN551, LEU553,ASP564
2	cancer-related Aurora-A Protein Kinase (1MQ4)	-10.61	16.74nM	LEU139, GLY140, LYS141, GLY142, VAL147, ALA160, LYS162, TYR212, ALA213, GLY216, THR217, TYR219, ARG220, GLU260, LEU263, ASP274
	cancer-associated protein kinases Ephrin A2 (ephA2) Receptor Protein Kinase (1MQB)	-8.6	424.47 nM	ILE619, GLY620, ALA621, ALA644, LYS646, THR692, GLU693, TYR694, MET695, ALA699, ARG743, ASN744, LEU746, SER756, ASP757
	cancer-related (FAK) Focal Adhesion Kinase (1MP8)	-7.9	1.63 μ M	ILE428, GLU430, GLY431, GLN432, ALA452, ILE454, GLU471, VAL484, MET499, GLU506, ARG550, ASP564
3	cancer-related Aurora-A Protein Kinase (1MQ4)	-9.01	250.47nM	LEU139, LYS143, VAL147, LYS162, VAL174, GLN177, ALA213, GLY216, THR217, GLU260, ASN261, LEU263, ASP274, TRP277, THR288, LEU289, CYS290
	cancer-associated protein kinases	-7.94	1.52 μ M	THR21, LYS23, HIS45, CYS45, PRO47, GLN56, PHE61, LYS112,

	Ephrin A2 (ephA2) Receptor Protein Kinase (1MQB)			LYS115, GLU116, ASN119
	cancer- related (FAK) Focal Adhesion Kinase (1MP8)	-7.24	4.9 μ M	ILE428, GLY431, GLN432, ALA452, LYS454, GLN470, GLU471, LEU501, CYS502, GLY505, GLU506, ASP564

Table 5.3 Stern-Volmer quenching constant, binding constant and number of binding site with BSA

Compounds	$K_{sv}(M^{-1})$	$K_q(M^{-1} S^{-1})$	$K_b(M^{-1})$	n
1	1.00×10^3	1.0×10^{11}	4.01×10^6	1.05
2	1.19×10^4	1.19×10^{12}	5.6×10^6	1.37
3	1.00×10^4	1.0×10^{12}	4.8×10^6	1.19

Table 5.4 IC₅₀ values (μ M) evaluated from MTT assay on A375, HeLa and HEK cells treated with **1**, **2** and **3** for 24 h

Compounds	A375	HeLa	HEK
1	20.3 \pm 0.01	30.1 \pm 0.02	> 80 \pm 0.013
2	15.1 \pm 0.035	25 \pm 0.009	80 \pm 0.099
3	25.0 \pm 0.054	35.2 \pm 0.05	> 120 \pm 0.063

Mean (\pm SD), n=3

5.5 References

- [1] Tabbì G., Cassino C., Cavigliolo G., Colangelo D., Ghiglia A., Viano I., Osella D. (2002), Water Stability and Cytotoxic Activity Relationship of a Series of Ferrocenium Derivatives. ESR Insights on the Radical Production during the Degradation Process *J. Med. Chem.*, 45(26), 5786-5796 doi:10.1021/jm021003k
- [2] Dyson P. J., Sava G. (2006), Metal-based antitumour drugs in the post genomic era. *Dalton Trans.*(16), 1929-1933 doi:10.1039/B601840H
- [3] Zhou B., Li J., Feng B.-J., Ouyang Y., Liu Y.-N., Zhou F. (2012), Syntheses and in vitro antitumor activities of ferrocene-conjugated Arg-Gly-Asp peptides. *J. Inorg. Biochem.*, 116, 19-25 doi:10.1016/j.jinorgbio.2012.06.014
- [4] Huang X.-F., Wang L.-Z., Tang L., Lu Y.-X., Wang F., Song G.-Q., Ruan B.-F. (2014), Synthesis, characterization and antitumor activity of novel ferrocene derivatives containing pyrazolyl-moiety. *J. Organomet. Chem.*, 749, 157-162 doi:10.1016/j.jorganchem.2013.08.043
- [5] Roux C., Biot C. (2012), Ferrocene-based antimalarials. *Future Med. Chem.*, 4(6), 783-797 doi:10.4155/fmc.12.26
- [6] Biot C., François N., Maciejewski L., Brocard J., Poulain D. (2000), Synthesis and antifungal activity of a ferrocene-fluconazole analogue. *Bioorg. Med. Chem. Lett.*, 10(8), 839-841 doi:10.1016/S0960-894X(00)00120-7
- [7] Dive D., Biot C. (2008), Ferrocene Conjugates of Chloroquine and other Antimalarials: the Development of Ferroquine, a New Antimalarial. *ChemMedChem*, 3(3), 383-391 doi:10.1002/cmdc.200700127

- [8] Rubbiani R., Blacque O., Gasser G. (2016), Sedaxicenes: potential new antifungal ferrocene-based agents? *Dalton Trans.*, 45(15), 6619-6626 doi:10.1039/C5DT04231C
- [9] Babin V. N., Belousov Y. A., Borisov V. I., Gumenyuk V. V., Nekrasov Y. S., Ostrovskaya L. A., . . . Snegur L. V. (2014), Ferrocenes as potential anticancer drugs. Facts and hypotheses. *Russ. Chem. Bull.*, 63(11), 2405-2422 doi:10.1007/s11172-014-0756-7
- [10] Núñez M. C., Pavani M. G., Díaz-Gavilán M., Rodríguez-Serrano F., Gómez-Vidal J. A., Marchal J. A., . . . Campos J. M. (2006), Synthesis and anticancer activity studies of novel 1-(2,3-dihydro-5H-1,4-benzodioxepin-3-yl)uracil and (6'-substituted)-7- or 9-(2,3-dihydro-5H-1,4-benzodioxepin-3-yl)-7H- or 9H-purines. *Tetrahedron*, 62(50), 11724-11733 doi:10.1016/j.tet.2006.09.039
- [11] Pedotti S., Patti A., Dedola S., Barberis A., Fabbri D., Dettori M. A., . . . Delogu G. (2016), Synthesis of new ferrocenyl dehydrozingerone derivatives and their effects on viability of PC12 cells. *Polyhedron*, 117, 80-89 doi:10.1016/j.poly.2016.05.039
- [12] Ornelas C. (2011), Application of ferrocene and its derivatives in cancer research. 35(10), 1973-1985 doi:10.1039/C1NJ20172G
- [13] Piao W.-H., Wong R., Bai X.-F., Huang J., Campagnolo D. I., Dorr R. T., . . . Shi F.-D. (2007), Therapeutic Effect of Anthracene-Based Anticancer Agent Ethonafide in an Animal Model of Multiple Sclerosis. *J. Immunol.*, 179(11), 7415
- [14] Lee P., Wu X. (2015), Review: Modifications of Human Serum Albumin and Their Binding Effect. *Curr Pharm Des*, 21(14), 1862-1865

- [15] Freeman C. L., Swords R., Giles F. J. (2012), Amonafide: a future in treatment of resistant and secondary acute myeloid leukemia? *Expert Rev. Hematol.*, 5(1), 17-26 doi:10.1586/ehm.11.68
- [16] Kaur S., Dhoun S., Depotter G., Kaur P., Clays K., Singh K. (2015), Synthesis, linear and nonlinear optical properties of thermally stable ferrocene-diketopyrrolopyrrole dyads. *RSC Advances*, 5(103), 84643-84656 doi:10.1039/C5RA17977G
- [17] Hudson R. D. A., Asselberghs I., Clays K., Cuffe L. P., Gallagher J. F., Manning A. R., . . . Wostyn K. (2001), The linear and nonlinear optical properties of organometallic chromophores derived from ferrocene, $[\text{Fe}_2(\eta^5\text{-C}_5\text{H}_5)_2(\text{CO})_2(\mu\text{-CO})(\mu\text{-C} \cdot \text{CH}_3)]^+[\text{BF}_4]^-$ and terthienyl spacers. Crystal structure of 2-[(E)-2-ferrocenylethenyl]-5-(2-thienyl)thiophene. *J. Organomet. Chem.*, 637–639, 435-444 doi:10.1016/S0022-328X(01)00947-0
- [18] Chawdhury N., Long N. J., Mahon M. F., Ooi L.-l., Raithby P. R., Rooke S., . . . Younus M. (2004), Synthesis and characterisation of aromatic ethynyl-bridged ferrocenes. *J. Organomet. Chem.*, 689(4), 840-847 doi:10.1016/j.jorganchem.2003.11.035
- [19] Caballero A., Tormos R., Espinosa A., Velasco M. D., Tárraga A., Miranda M. A., Molina P. (2004), Selective Fluorescence Sensing of Li^+ in an Aqueous Environment by a Ferrocene–Anthracene-Linked Dyad. *Org. Lett.*, 6(24), 4599-4602 doi:10.1021/ol047972m
- [20] Mishra V., Raghuvanshi A., Saini A. K., Mobin S. M. (2016), Anthracene derived dinuclear gold(I) diacetylide complexes: Synthesis, photophysical properties and supramolecular interactions. *J. Organomet. Chem.*, 813, 103-109 doi:10.1016/j.jorganchem.2016.04.013
- [21] Saini A. K., Kumari P., Sharma V., Mathur P., Mobin S. M. (2016), Varying structural motifs in the salen based metal complexes of Co(ii), Ni(ii) and Cu(ii): synthesis, crystal

structures, molecular dynamics and biological activities. *Dalton Trans.*, 45(47), 19096-19108 doi:10.1039/C6DT03573F

- [22] Robertazzi A., Vargiu A. V., Magistrato A., Ruggerone P., Carloni P., de Hoog P., Reedijk J. (2009), Copper–1,10-Phenanthroline Complexes Binding to DNA: Structural Predictions from Molecular Simulations. *J. Phys. Chem. B*, 113(31), 10881-10890 doi:10.1021/jp901210g
- [23] Zhou S.-F., Ding Y.-H., Zhou Z.-W., Ha C.-F., Zhang X.-Y., Pan S.-T., . . . Qiu J.-X. (2015), Alisertib, an Aurora kinase A inhibitor, induces apoptosis and autophagy but inhibits epithelial to mesenchymal transition in human epithelial ovarian cancer cells. *Drug Des., Dev. Ther.*, 425 doi:10.2147/DDDT.S74062
- [24] Zheng L.-W., Wu L.-L., Zhao B.-X., Dong W.-L., Miao J.-Y. (2009), Synthesis of novel substituted pyrazole-5-carbohydrazide hydrazone derivatives and discovery of a potent apoptosis inducer in A549 lung cancer cells. *Biorg. Med. Chem.*, 17(5), 1957-1962 doi:10.1016/j.bmc.2009.01.037
- [25] Jaouen G., Vessieres A., Top S. (2015), Ferrocifen type anti cancer drugs. *Chem. Soc. Rev.*, 44(24), 8802-8817 doi:10.1039/C5CS00486A
- [26] *Principles of Fluorescence Spectroscopy*. (2006). (J. R. Lakowicz Ed.). Boston, MA: Springer US.
- [27] Suryawanshi V. D., Walekar L. S., Gore A. H., Anbhule P. V., Kolekar G. B. (2016), Spectroscopic analysis on the binding interaction of biologically active pyrimidine derivative with bovine serum albumin. *Journal of Pharmaceutical Analysis*, 6(1), 56-63 doi:10.1016/j.jpha.2015.07.001
- [28] Cheng Z., Liu R., jiang X. (2013), Spectroscopic studies on the interaction between tetrandrine and two serum albumins by

- chemometrics methods. *Spectrochim. Acta, Part A*, 115, 92-105
doi:10.1016/j.saa.2013.06.007
- [29] van de Weert M., Stella L. (2011), Fluorescence quenching and ligand binding: A critical discussion of a popular methodology. *J. Mol. Struct.*, 998(1), 144-150 doi:10.1016/j.molstruc.2011.05.023
- [30] Ray A., Koley Seth B., Pal U., Basu S. (2012), Nickel(II)-Schiff base complex recognizing domain II of bovine and human serum albumin: Spectroscopic and docking studies. *Spectrochim. Acta, Part A*, 92, 164-174 doi:10.1016/j.saa.2012.02.060
- [31] Kuznetsova I. M., Sulatskaya A. I., Povarova O. I., Turoverov K. K. (2012), Reevaluation of ANS Binding to Human and Bovine Serum Albumins: Key Role of Equilibrium Microdialysis in Ligand – Receptor Binding Characterization. *PLOS ONE*, 7(7), e40845 doi:10.1371/journal.pone.0040845
- [32] Liu E. H., Qi L.-W., Li P. (2010), Structural Relationship and Binding Mechanisms of Five Flavonoids with Bovine Serum Albumin. *Molecules*, 15(12), 9092-9103 doi:10.3390/molecules15129092
- [33] Möller M., Denicola A. (2002), Study of protein-ligand binding by fluorescence. *Biochem. Mol. Biol. Educ.*, 30(5), 309-312 doi:10.1002/bmb.2002.494030050089
- [34] Patra A., Saha Santu K., Sen Tamal K., Carrella L., Musie Ghezai T., Khuda-Bukhsh Anisur R., Bera M. (2014), Water-Soluble Heteronuclear $[\text{NaCu}^{\text{II}}_6]$ Metallomacrocyclic Sandwich Complexes: Synthesis, Structure, Properties and In Vitro Biological Studies. *Eur. J. Inorg. Chem.*, 2014(30), 5217-5232 doi:10.1002/ejic.201402582
- [35] Das M., Nasani R., Saha M., Mobin S. M., Mukhopadhyay S. (2015), Nickel(II) complexes with a flexible piperazinyl moiety: studies on DNA and protein binding and catecholase like

- properties. *Dalton Trans.*, 44(5), 2299-2310
doi:10.1039/C4DT02675F
- [36] Lees J. G., Miles A. J., Wien F., Wallace B. A. (2006), A reference database for circular dichroism spectroscopy covering fold and secondary structure space. *Bioinformatics*, 22(16), 1955-1962 doi:10.1093/bioinformatics/btl327
- [37] Sheldrick G. M. (2015), Crystal structure refinement with SHELXL. *Acta Crystallogr., Sect. C: Struct. Chem.*, 71(Pt 1), 3-8 doi:10.1107/S2053229614024218
- [38] Frisch M. J., Trucks G. W., Schlegel H. B., Scuseria G. E., Robb M. A., Cheeseman J. R., . . . Petersson G. A. (2009), 09, Revision D. 01, Gaussian. *Inc., Wallingford, CT*
- [39] Becke A. D. (1993), Density-functional thermochemistry. III. The role of exact exchange. *J. Chem. Phys.*, 98(7), 5648-5652 doi:10.1063/1.464913
- [40] Lee C., Yang W., Parr R. G. (1988), Development of the Colle-Salvetti correlation-energy formula into a functional of the electron density. *Phys. Rev. B*, 37(2), 785-789 doi:10.1103/PhysRevB.37.785
- [41] Morris G. M., Goodsell D. S., Halliday R. S., Huey R., Hart W. E., Belew R. K., Olson A. J. (1998), Automated docking using a Lamarckian genetic algorithm and an empirical binding free energy function. *J. Comput. Chem.*, 19(14), 1639-1662 doi:10.1002/(SICI)1096-987X(19981115)19:14<1639::AID-JCC10>3.0.CO;2-B
- [42] Patel N., Oudemans P. V., Hillman B. I., Kobayashi D. Y. (2013), Use of the tetrazolium salt MTT to measure cell viability effects of the bacterial antagonist *Lysobacter enzymogenes* on the filamentous fungus *Cryphonectria parasitica*. *Antonie van*

Leeuwenhoek, 103(6), 1271-1280 doi:10.1007/s10482-013-9907-3

- [43] Bhattacharyya S., Sarkar A., Dey S. K., Jose G. P., Mukherjee A., Sengupta T. K. (2013), Copper(ii) complex of methionine conjugated bis-pyrazole based ligand promotes dual pathway for DNA cleavage. *Dalton Trans.*, 42(32), 11709-11719 doi:10.1039/C3DT51296G
- [44] Sundaravadivel E., Vedavalli S., Kandaswamy M., Varghese B., Madankumar P. (2014), DNA/BSA binding, DNA cleavage and electrochemical properties of new multidentate copper(ii) complexes. *RSC Advances*, 4(77), 40763-40775 doi:10.1039/C4RA03554B

Chapter 6

Molecular Modeling of the Nucleation: A Case Study of Triptycene - Ferrocene Supra-molecular Assembly in the Solid State

6.1 Introduction

The complex interplay between close packing requirements and molecular recognition in the formation of crystal structures is the actual problem of crystal engineering.[1]. Opinions on the nature of the dominant driving force of the process of crystal formation are quite polarized.[1-5] The concept of supramolecular synthons suggested by Desiraju[6] released the tension[7] between kinetic and geometry not only by considering both the chemical recognition patterns and their statistical occurrence in the molecular crystal structures, but further distinguished the synthons as the strong synthons (more “chemical”) and the weak synthons (more influenced by geometry). This concept allowed considering a crystallization process as a chemically meaningful strong-to-weak synthon sequence, so that chemical (*i.e.* kinetic) factors are responsible for the supra-molecular self-assembly at the early stages of crystallization, while the close packing requirements gradually come into power later. The use of hetero-synthons can be particularly helpful in the model study of the crystallization process and its practical implementation.

Hydrogen,[8] halogen,[9] other directional and specific secondary bonding interactions (SBI) [10-12] allow rationalizing the supra-molecular and crystal self-assembly as a chemically reasonable, kinetically controlled event, which makes crystal engineering possible.[9] These interactions are responsible for tuning structure-

depended physical properties[13] like mechanical properties,[14] electronic properties[15] and photo-optical properties.[16]

Triptycene (TripH) derivatives are intensively applied in supramolecular chemistry,[17] “molecular machines”,[18] and materials science.[19] For example, derivatives of TripH have been incorporated in the polymer networks which showed increased transition temperatures (T_g) property and, also increased the ductility of film samples.[20,21] The geometrically challenging three-bladed propeller-shaped structure of TripH is not fit for efficient packing in the solid state form. The only known crystal form of TripH (TRIPCN01-07), reveals an “inefficient” close packing which is stabilized only by hydrogen bonds (HB) and there is the absence of π -- π stacking or any directional intermolecular interactions.

Ferrocene (FcH) and its derivatives have rich inclusion chemistry and attract much attention till date, due to their functionality as compact, electron rich guest molecules in host-guest supramolecular ensembles.[22] In most cases, one of the significant stabilizing interactions in the non-charge-transfer complex (CT) FcH cocrystals is a π -- π interaction between cp ring of a neutral FcH molecule and aromatic hydrocarbon,[23] poly-fluorinated aromatics,[24-26] fullerenes[27,28] etc. It acts as an electron-rich unit in π_{cp} - associates with Hg [29]and Ag, Cu- *anti*-crown-ethers.[30]

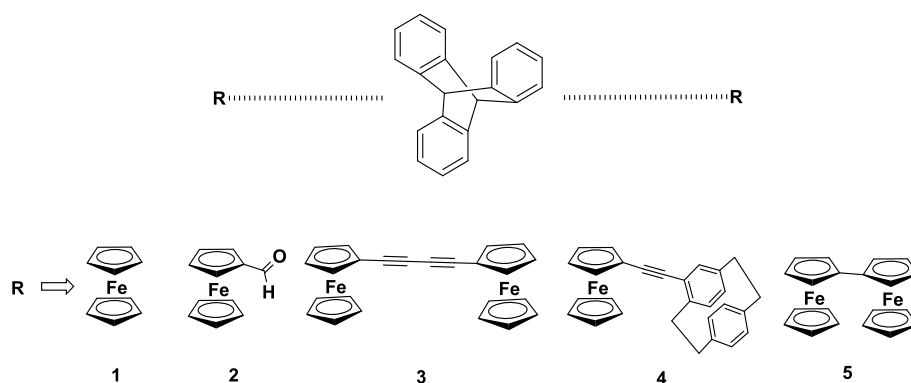
Without any apparent stabilization by specific intermolecular interactions; neutral FcH molecules can also form inclusion compounds, entering the cavities of calixarenes,[31-36] cyclodextrins,[37,38] and cucurbiturils[39] filling the channels formed by thiourea[40,41] and organic porous crystals[42] and MOFs.[43]

With the above concept in mind, considering the importance of TripH and FcH, we studied the cocrystallization of the geometrically demanding TripH molecule with the compact FcH[44] and its derivatives, along with energy calculations, featuring various levels of chemical functionality and steric demands to prepare five cocrystals

(**1–5**), which were characterized by single-crystal X-ray diffraction. The electrical conductivity measurement and NMR study in the solution have also been performed for **1–5** to assess the correlation between the solid-state structure and physical property and to check the structural integrity of the cocrystal **1** in the solution.

6.2 Results and Discussion

The preparation of TripH-based cocrystals (**1–5**) has been carried out by slow evaporation of equimolar mixture in the DCM/hexane or chloroform/hexane (**Scheme 6.1**). The best solvent system to grow crystals **1–5** was chloroform (bp 61°C) and hexane (bp 69 °C) 1:1 mixture which provides the minimal difference in boiling point and their polarity is suitable to dissolve both the precursors together.



Scheme 6.1 Interaction of R group with TripH where R is FcH (1), FcCHO (2), Diferrocenyl diacetylene (3), PCP-Fc (4) and BiFcH (5) respectively

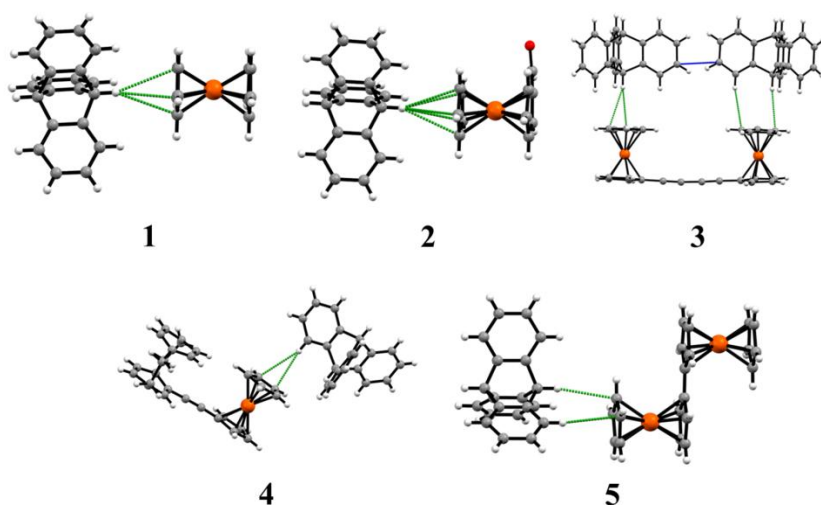


Figure 6.1. Cocrystal structure (primary synthons) of TripH with FcH (1), FcCHO (2), Diferrocenyl diacetylene (3), PCP-Fc (4) and BiFcH (5) with showing the interaction between two units.

Crystal **1–3** are crystallized in triclinic crystal system with $P-1$ space group whereas **4** and **5** are crystallized in monoclinic crystal system with $P2_1/c$ and $P2_1/n$ space group respectively (**Table 6.1** and **6.2**). We succeeded in growing of cocrystals **2–5** only after series of trials under different conditions in chloroform/hexane or dcm/hexane, while **1** forms readily as shiny orange crystals in chloroform/hexane mixture (**Figure 6.1**). To check the possibility of other crystal forms in FcH-TripH system; ratio of FcH and TripH was varied as 1:1, 1:2, 1:3, 2:1, 3:1, 3:1 but in all experiments, we found the same crystal of 1:1 composition for **1**.

6.2.1 Description of the polymeric network of cocrystals 1–5

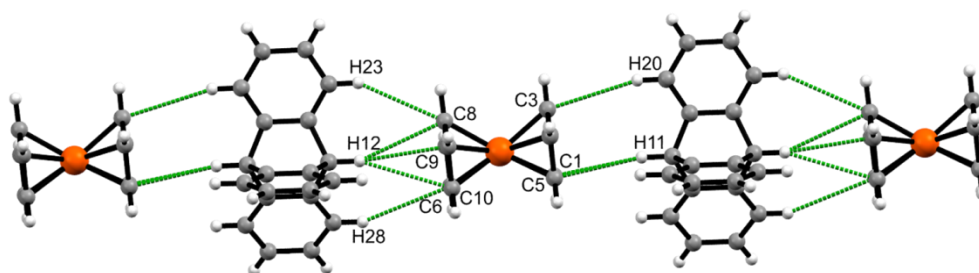


Figure 6.2. Fragment of the one-dimensional chain of FcH and TripH with interaction having distance C5-H11 2.964 Å, C1-H11 2.882 Å, C8-H12 3.043 Å, C9-H12 2.885 Å, and C10-H12 3.054 Å

In cocrystal **1**, the FcH and TripH form the 1D chain with C-H_{bridgehead}---□□ interactions as shown in **Figure 6.2** with the distance range of 2.882–3.054 Å. The FcH and TripH molecules are organized in chains of a one-dimensional strand in approximate ac -plane to obtain a close packing in chain form. The shortest TripH---TripH separation in two adjacent layers is 2.289 Å along ab axis. Four FcH molecules surround the TripH along the diagonal to ac plane. The FcH in adjacent is layer is 6.54 Å apart (**Figure 6.3**).

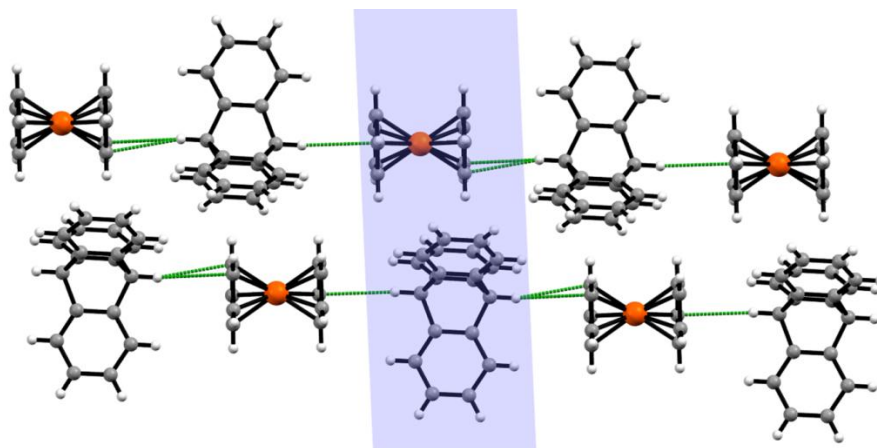


Figure 6.3. Fragment of the two-dimensional chain of FcH and TripH with C-H... π interaction having distance H10...C28 3.126 Å and H1...C_{(24-29)centroid} 2.783 Å.

The 2D-chains alignment shown in **Figure 6.3** arrange as honeycomb network in *ac* plane, when observed through cross-section (**Figure 6.4**).

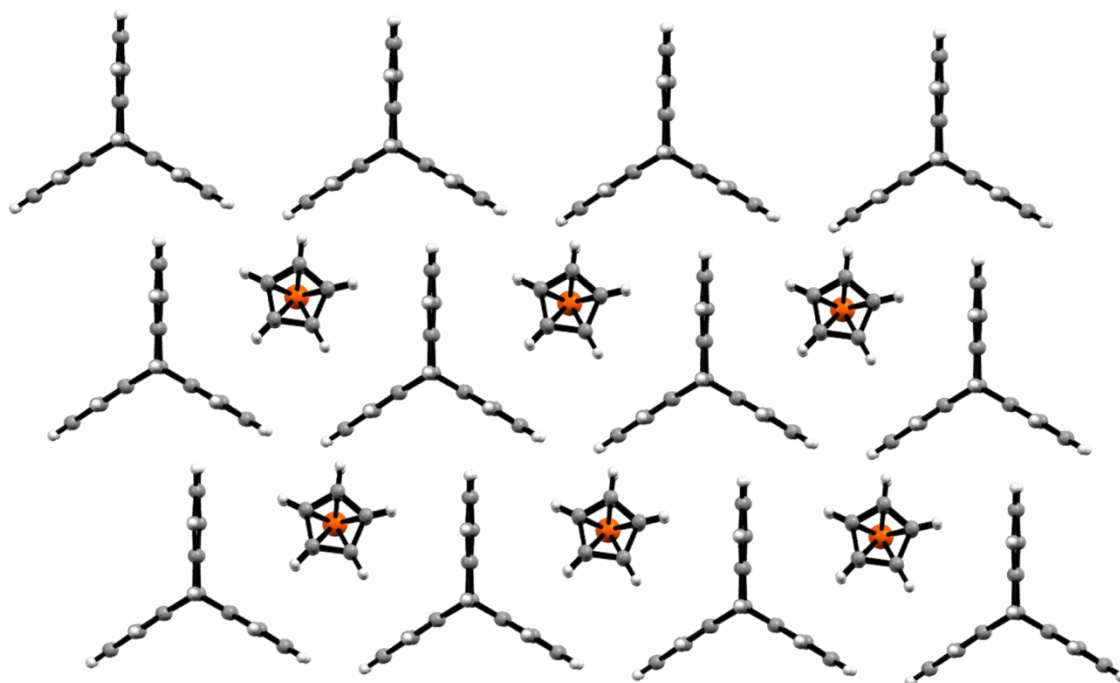


Figure 6.4. Honeycomb fragment observed area of a cross-section of cocrystal **1** showing the efficient packing of FcH into the grooves of TripH

As the rigid fan-shape becomes a favourable shape to allow the supramolecular assembly with ferrocene; its molecular arrangement might allow variation in the packing arrangement, if introduced with the other ferrocene derivatives. Further, the FcCHO and TripH molecules are also organized in chains of one-dimensional strands in approximate *ac*-plane to obtain a close packing in the form of the chain (see **Figure 6.5**).

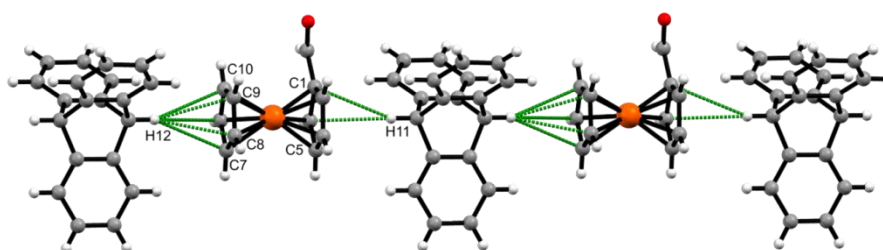


Figure 6.5. Fragment of the one-dimensional chain of FcCHO and TripH with C-H_{bridgehead}... π interaction having distance C6-H12 3.075 Å, C7-H12 3.026 Å, C8-H12 2.966 Å, C9-H12 2.975 Å, C10-H12 3.020 Å, C1-H11 3.082 Å, and C5-H11 2.927 Å

Now, the shortest TripH...TripH separation increased to 2.421 Å in two adjacent layers along *ab* axis. The FcCHO in the adjoining layer is only 2.53 Å apart which gives rise to intermolecular associations among them, and the C-H_{bridgehead}... π stabilized interaction in the FcCHO-TripH chain remains significant (see **Figure 6.6**).

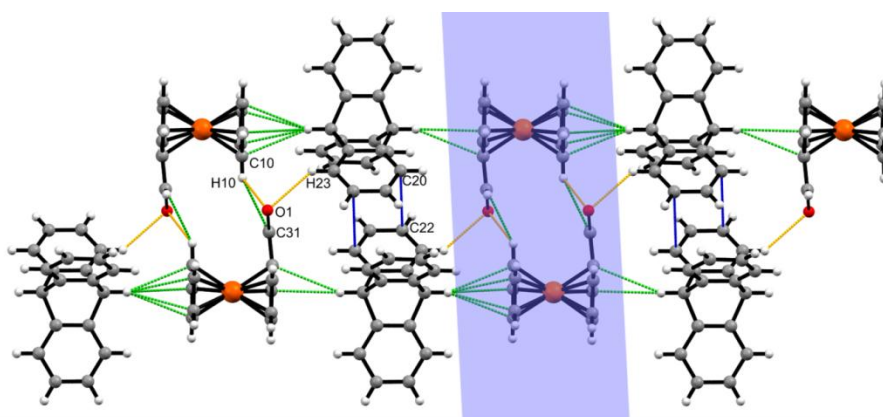


Figure 6.6. Fragment of the two-dimensional chain of FcCHO and TripH with interactions having distance O1---H10 2.898 Å, O1---H23 2.713 Å, H10---C31 2.955 Å, and C20---C22 3.508 Å

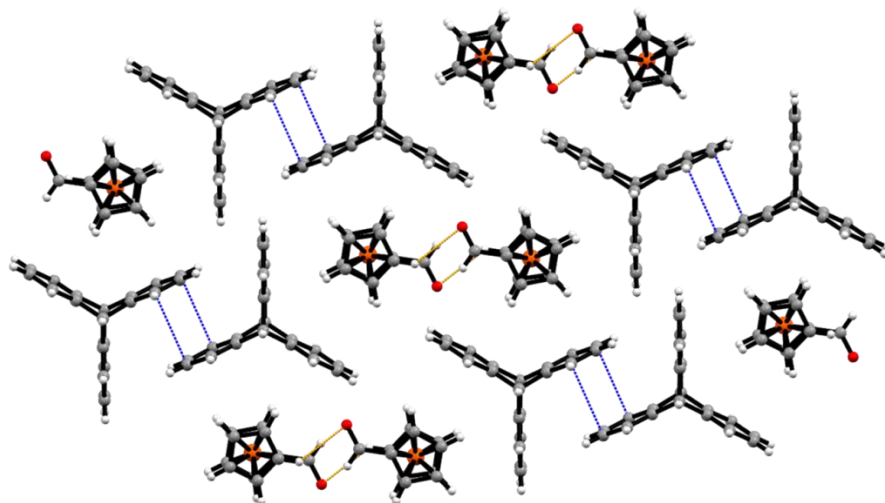


Figure 6.7. Note a π --- π stacking between two TripH molecules, so π --- π stacking in TripH is possible! (But not effective for TripH, itself packing), the cross-section view shows π --- π interactions with 3.508 Å (blue dotted lines).

In addition to O---H bonding between two FcCHO, the stacking π --- π interactions between two adjacent TripH Ph rings (3.508 Å) appear with a proper packing of FcCHO inside the grooves of TripH (**Figure 6.7**). This observation suggests a π --- π stacking in TripH is possible, but not realized in parent TripH since it does not comply with the geometrical requirements. Increased supramolecular functionality by CHO on FcH created a competition between Trip-H---Cp and O---H-Trip, it is surprising to note that the $H_{\text{bridgehead}}\text{---}\pi_{\text{Cp}}$ interaction is retained, whereas in case of I-C₂-I---Cp vs I-C₂-I---OAc-FcCp competition, the I---OAc was dominant over I---Cp.[45]

A further variation is brought by two FcH units which are connected not only by non-covalent bond but also by diacetylene bridge, due to which the distance between Fc units is increased to 6.611 Å. The FcC₂C₂Fc and TripH molecules are also organized in parallel chains of the one-dimensional strand in approximate *ab*-plane

to obtain a close packing in the form of a parallel chain. The nearest TripH---TripH separation is 3.04 Å along *b* axis. The TripH-TripH separation is increased on increasing the side arm of FcH. The FcC₂C₂Fc in adjacent is layer is 2.51 Å, and when triptycene is sandwiched between them, the distance becomes 10.24 Å (**Figure 6.8**).

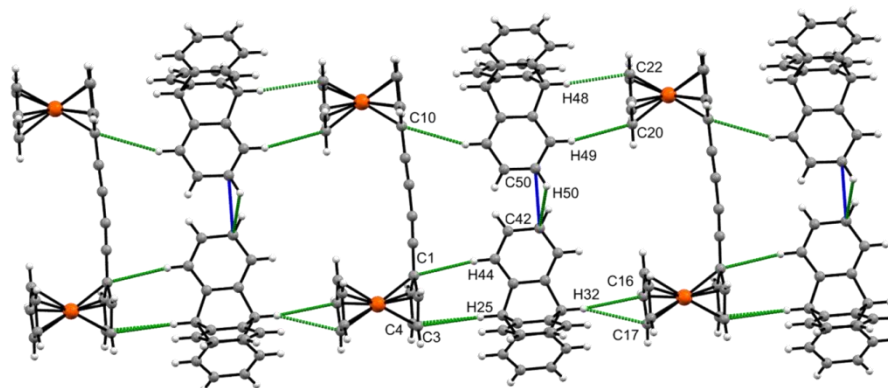


Figure 6.8. Fragment of the one-dimensional chain of Diferrocenyl diacetylene-TripH (**3**) with interactions having distance H49-C20 2.909 Å, H48-C22 2.801 Å, H52-C10 2.973 Å, H32-C16 2.851 Å, H32-C17 2.896 Å, H44-C1 2.925 Å, H25-C3 2.958 Å, H25-C4 2.989 Å, C42-C50 3.420 Å, and H50-C42 2.998 Å

Although the pattern of the slice changes accordingly to arrange the Fc-C₂-C₂-Fc and TripH units, yet the general arrangement of one Fc unit interacting with two different TripH moieties and C-H_{bridgehead}-- π_{Cp} assembled 2D chain pattern found in **1** is reproduced in **3** (**Figure 6.8**). Further, the cross-sectional view represents a better combination of closed packing and molecular recognition (**Figure 6.9**).

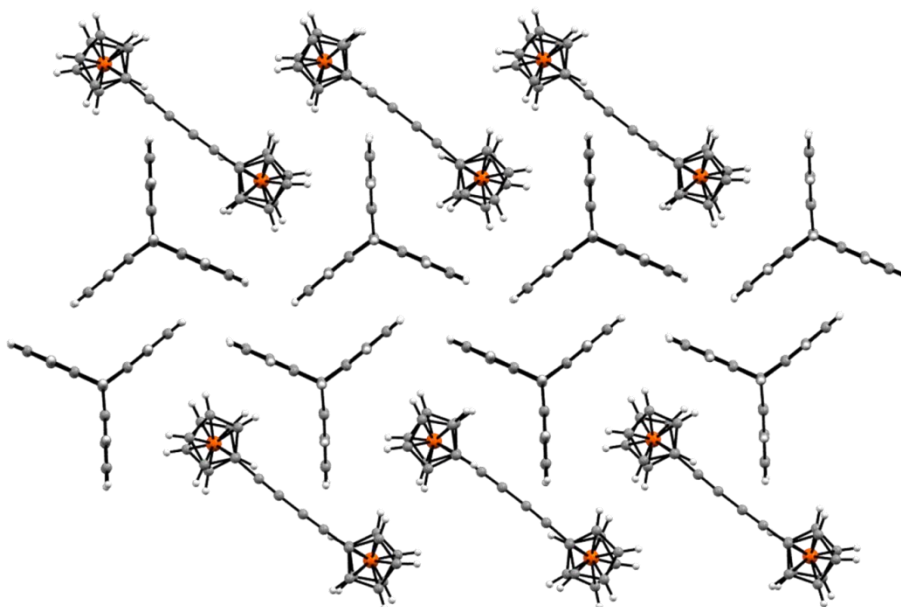


Figure 6.9. Beautiful case of closed packing and molecular recognition together in cocrystal **3**

A further complication is achieved by formal substitution of one Fc-C₂ fragment on the paracyclophane (PCP) moiety which changed the distance as well as the nature of cocrystal unit in **4**. The Fc-C₂-PCP and TripH molecules are organized in the one-dimensional strand in approximate *ac*-plane to obtain a close packing in the form of a chain. The nearest TripH---TripH separation is 4.00 Å along approximate *ab* axis. It can be observed that the TripH-TripH separation is further increased on increasing the side arm of FcH in **4** and is more than **1–3**. The Fc-C₂-PCP in the alternate layer is 10.13 Å (see **Figure 6.10**).

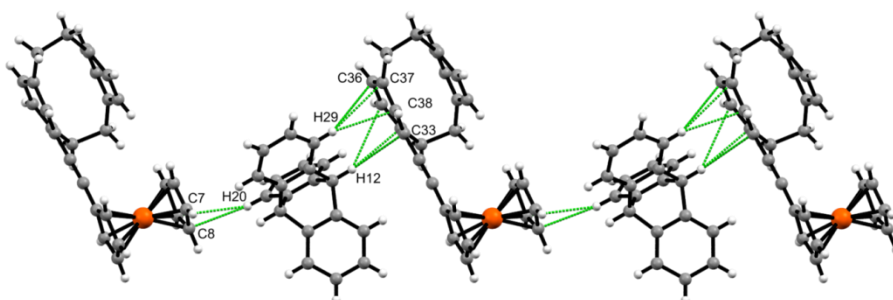


Figure 6.10. Fragment of the one-dimensional chain of PCP-Fc and TripH (**4**) with interactions having distance C7-H20 3.043 Å, C8-H20

2.824 Å, H12-C33 3.016 Å, H12-C34 2.731 Å, H12-C35 3.098 Å, C36-H29 3.054 Å, H29-C37 3.011 Å, and H29-C38 2.878 Å

Although distorted, we can still observe the same chains in **4**. In the cocrystal **4**, the bridgehead H and cp ring interactions are eliminated. Still, the C-H \cdots π interaction is present between the cp ring and non-bridged H of TripH. Instead of cp, the C-H \cdots π interactions between bridged and non-bridged H of TripH involves the pcp ring, which is responsible for the 1D chain (**Figure 6.10**).

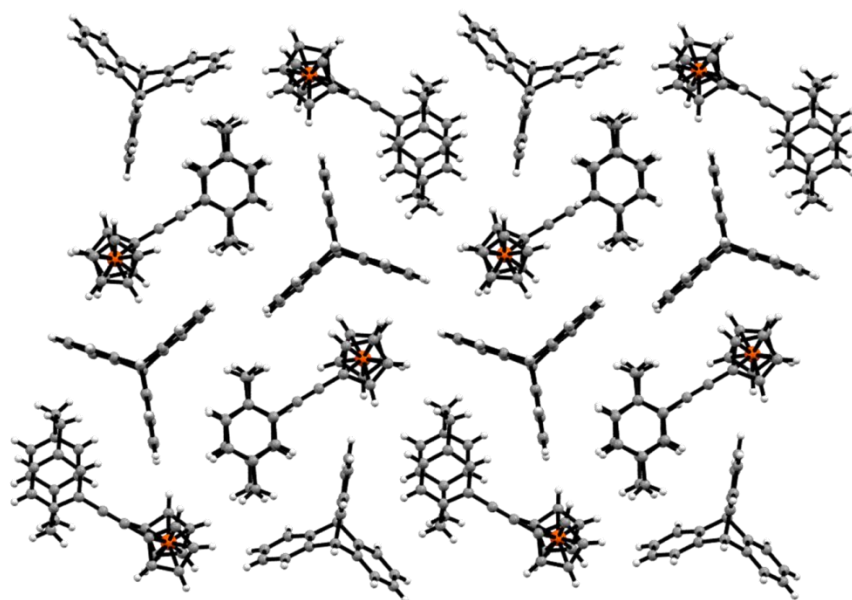


Figure 6.11. Zig-zag chain arrangement of PCP-Fc and TripH (**4**) (No π - π stacking between TripH units)

The cross-section view shows the zig-zag arrangement of PCP-Fc and TripH in **4** in approximate *bc* plane, due to the presence of C-H \cdots π interactions (**Figure 6.11**).

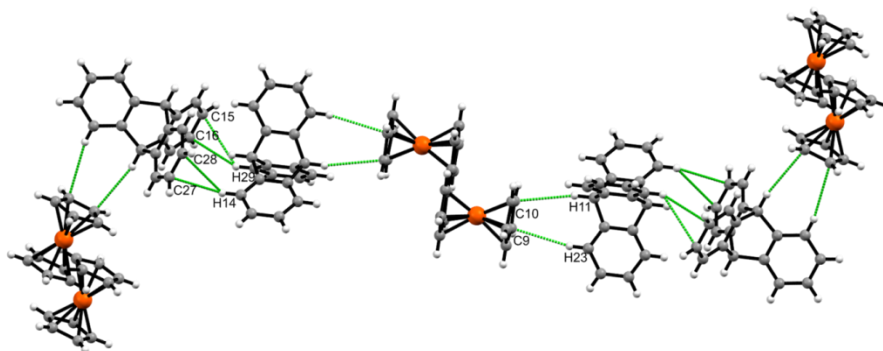


Figure 6.12. Fragment of the one-dimensional chain of Fc_2 - TripH with interaction having distance H29-C15 3.071 Å, H29-C16 2.834 Å, H14-C27 2.867 Å, H14-C28 3.086 Å, H11-C10 2.944 Å, and H23-C9 2.961 Å

Compounds **2** and **4** were crystallized successfully after various attempts, but despite several efforts, the crystal with good data set with the lower R index was not obtained. Till now the interplay of H---cp HBs and FcH-TripH close packing gave the similar results of HB 1D chains and orthogonal close-packed slices, but as soon as DiFc (Fc_2) system, is incorporated, it breaks the slice symmetry, yet the H---cp HBs are still possible, but chain expansion and arrangement is not possible anymore. Interestingly, the natural TripH close packing pattern re-appears to provide the effective packing (**Figure 6.12**). The cross-sectional view shows the reappearance of natural TripH packing pattern in the cocrystal **5** more clearly (**Figure 6.13** compare with **Figure 6.14**).

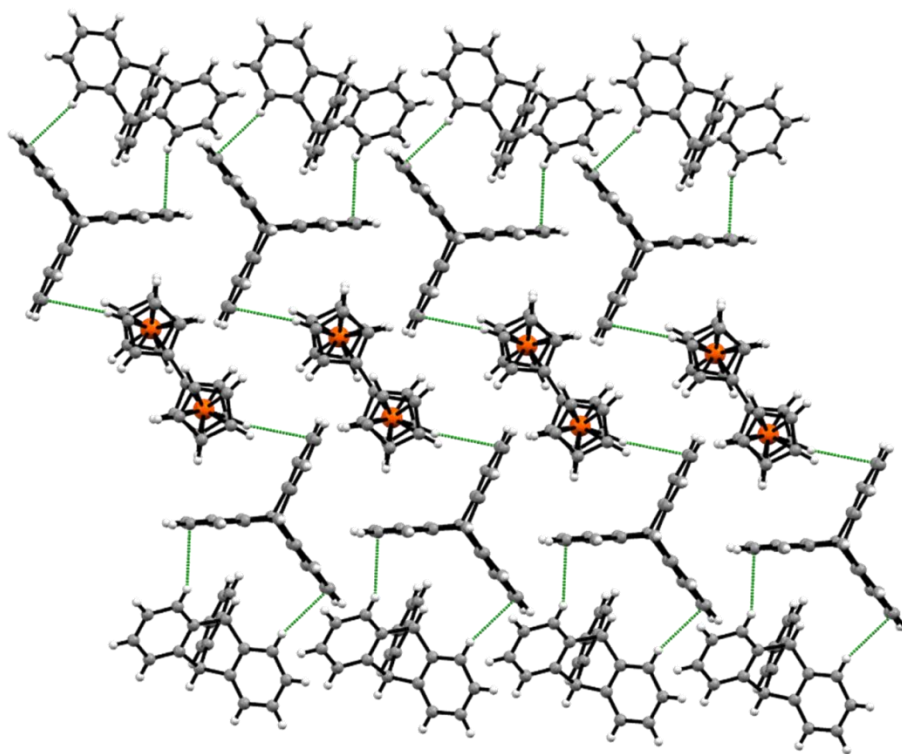


Figure 6.13. Re-appearance of natural TripH packing pattern in cocrystal **5** presents in tilted *ac* plane (Cross-sectional view)

The interactions present in **5** which are similar to the pure TripH rings interactions are solely due to the C-H... π interactions (**Figure 6.14**). (see CSD code TRIPCN03[5]).

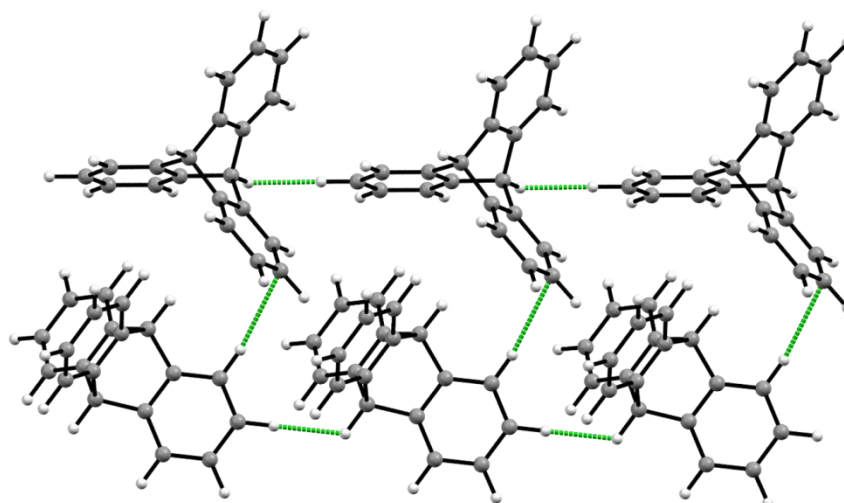


Figure 6.14. Natural packing pattern in TripH (from TRIPCN03)

Cp₂Ru which is not only a formal ruthenium congener of FcH but is also known to form mixed cocrystals with it,[46] did not give the cocrystal[47] with TripH under the same conditions as FcH. We have already noted before such supra-molecular inertness of Cp₂Ru compared to Cp₂Fe, despite the similar geometry in FcH---C₂I₂. [45] PCP molecule also failed to avail the hospitality of TripH, while PCP-C₂-Fc afforded the expected 1:1 cocrystal with TripH. This observation may indicate that FcH molecules are not just filling the voids to provide the efficient close packing, but there is specific Cp---H attractive interaction, which stabilizes the TripH---FcH assembly.

6.2.2 Energy Calculations

Taking into account quite a subjective nature of any supramolecular aggregates or structural patterns which can be identified in the solid state.[48-50] Hence, the objective requirement is the intermolecular energy calculation; therefore we used Crystal Explorer software[51] to simulate the intermolecular interaction energies in the **1–5** cocrystals and their ‘energy frameworks’.[52] The latter approach has also been used successfully before in several aspects of crystal engineering.[52-60]

In the natural Trip (TRIPCN03 *P2₁2₁2₁*) the strongest intermolecular contacts are stabilized by C_{sp³}-H---πPh (-28 kJ/mol) and C_{sp²}-H---πPh (18-19 kJ/mol) interactions (see **Figure 6.15** TRIPCN03). It is noteworthy that similar Trip (C_{sp³}-H---πPh) *o*-Me₂C₆H₄ 1D chain architecture was also observed in TripH - *o*-Me₂C₆H₄ - C₆₀ ternary cocrystal[61]

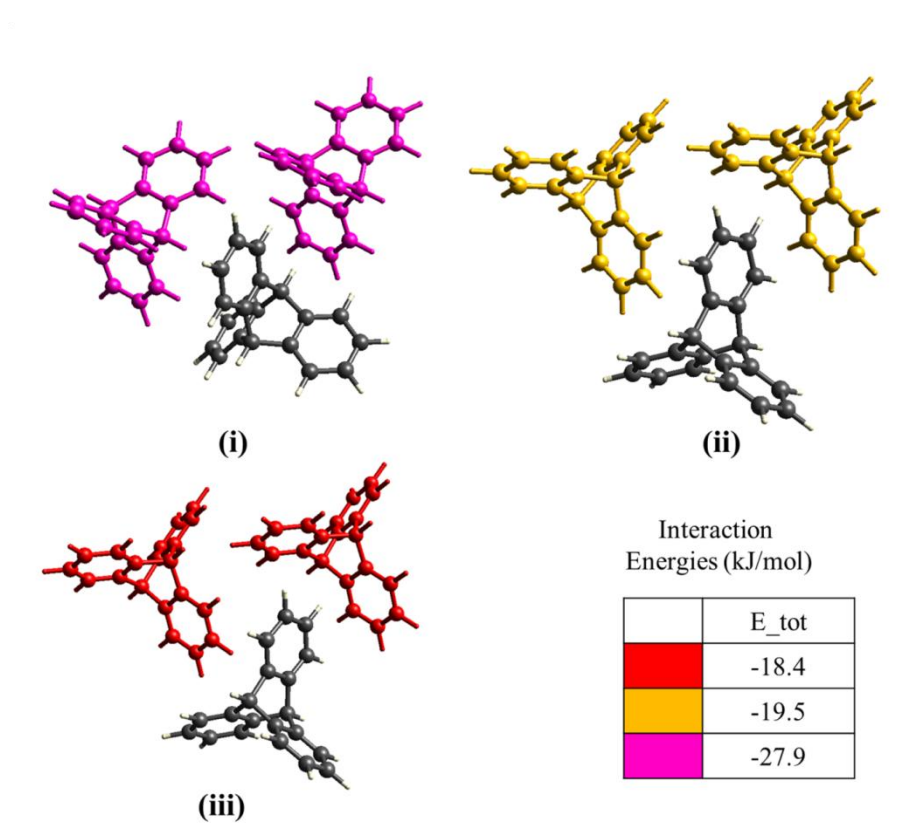


Figure 6.15. Trip-Trip interactions in TRIPCN03

Figure 6.16, 6.17 are showing the intermolecular interaction and total energy values present in cocystal **1** and **2**.

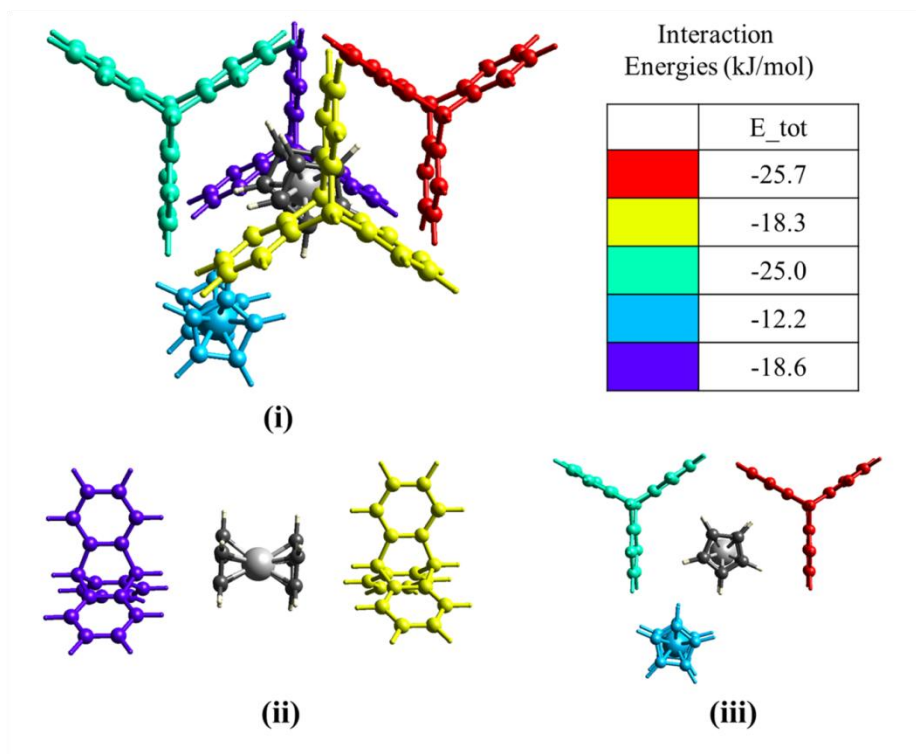


Figure 6.16. Interaction of FcH with TripH in cocrystal **1**[62]

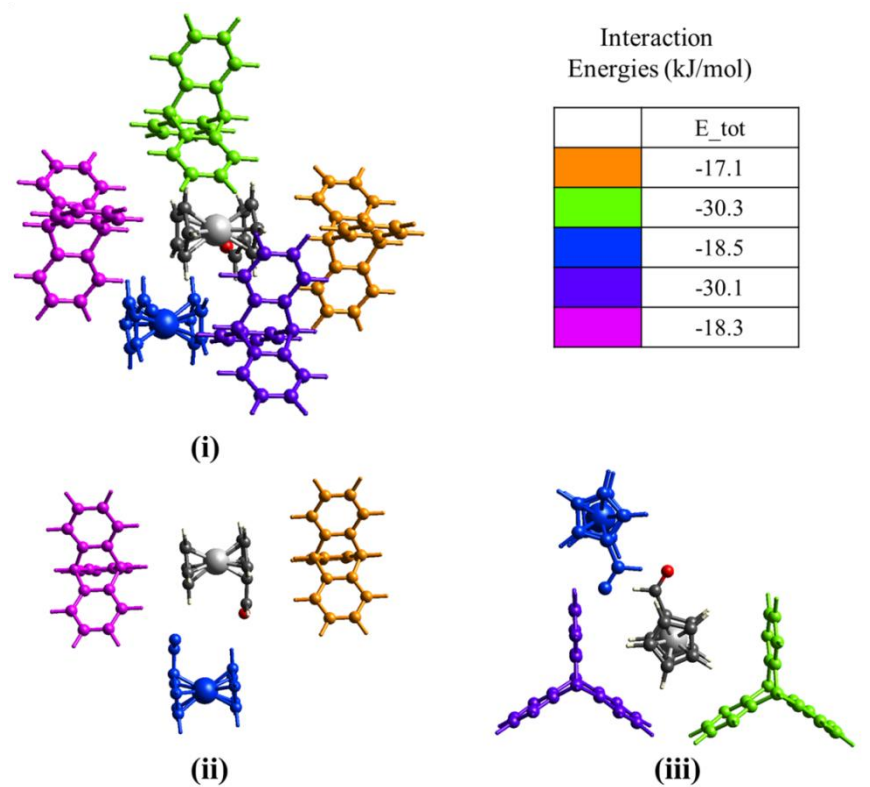


Figure 6.17. Interaction of FcCHO with TripH in cocrystal **2**[62]

The same energy and geometry of a couple of two strongest TripH-TripH $C_{sp^3}\text{-H} \cdots \pi_{Ph}$ and $C_{sp^2}\text{-H} \cdots \pi_{Ph}$ interactions (31.3 and 20.4 kJ/mol accordingly) as found in the packing of natural TripH is reproduced in its cocrystal Fc₂-TripH (-31.8 / -19.3 kJ/mol) (**Figure 6.18**).

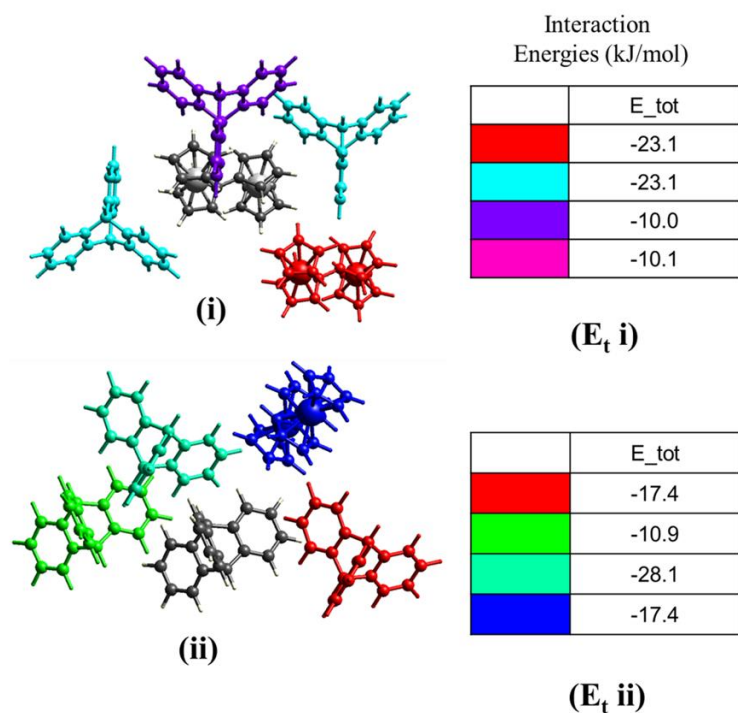


Figure 6.18. Interaction of Fc₂ with TripH in cocrystal **5**[62]

Fc₂ produce the strongest interaction with TripH filling the void between its Ph lobes, and its energy (-33 kJ/mol) is close to those found in FcH-TripH (-29 kJ/mol) (see **Figure 6.17**) as well as C_{sp3}-H--Cp interaction in Fc₂-TripH (-18.5 kJ/mol) is close to (-22.8 kJ/mol) in **1** (**Figure 6.18**).

In cocrystals **1**, **2** the honeycomb energy frameworks are observed, which are entirely in line with the strongest C_{sp3}-H--Cp intermolecular interactions, responsible for the 1D chain formation, and C_{sp2}-H--Ph close packing, filling the space between the Ph lobes of TripH and therefore inheriting its C₃ symmetry (**Figure 6.19**).

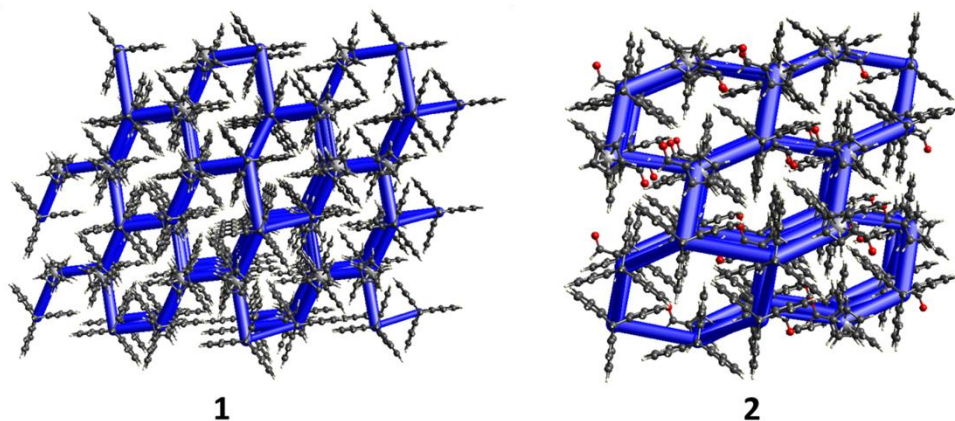
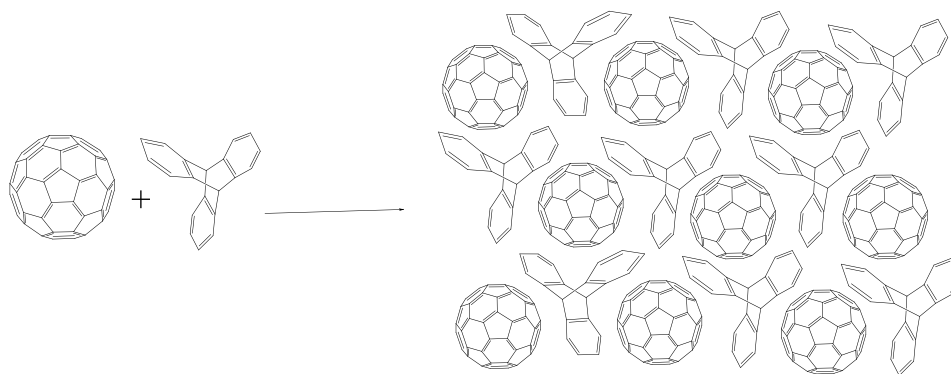


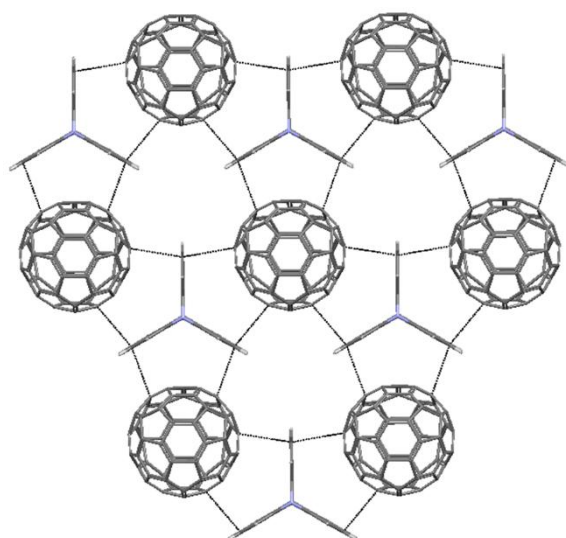
Figure 6.19. Energy framework in **1**, **2** (cut-off -11 kJ/mol)

FcH molecules in FcH-Trip are effectively isolated from one another by non-conducting TripH units, therefore measured electric conductivity of TripH -FcH cocrystals which is $10^{-9} \text{ S}\cdot\text{cm}^{-1}$, that is quite expectedly three orders less than that of parent FcH ($4\cdot 10^{-6} \text{ S}\cdot\text{cm}^{-1}$).[45]

Notably, the packing we observed in **1** (see **Figure 6.4**), resembles the pattern envisioned by Feringa *et al.*[61] (see **Scheme 6.2**).



(a)



(b)

Scheme 2. a) TripH-C₆₀ packing pattern expected in work
 b) packing pattern of aza-TripH---C₆₀ sheets

We can speculate, that apart from an enhanced electrostatic interaction between aza-Trip and C₆₀ mentioned in the aforementioned report,[61] the main reason for cocrystallization of azaTrip-C₆₀ and TripH-C₆₀, was the incorporation of xylene solvent molecules in TripH system represented by the ditopic C_{sp3}-H structure of TripH (**Figure 6.20**). Aza- Trip, in contrast, has only one C_{sp3}-H fragment capable of forming C_{sp3}-H---π_(xylene) contacts and therefore has no possibility for 1D chain extension.[1] This observation may mean that C_{sp3}-H---π_(arene, cp) is a strong heterosynthon in the structural chemistry and cocrystal design of triptycenes.

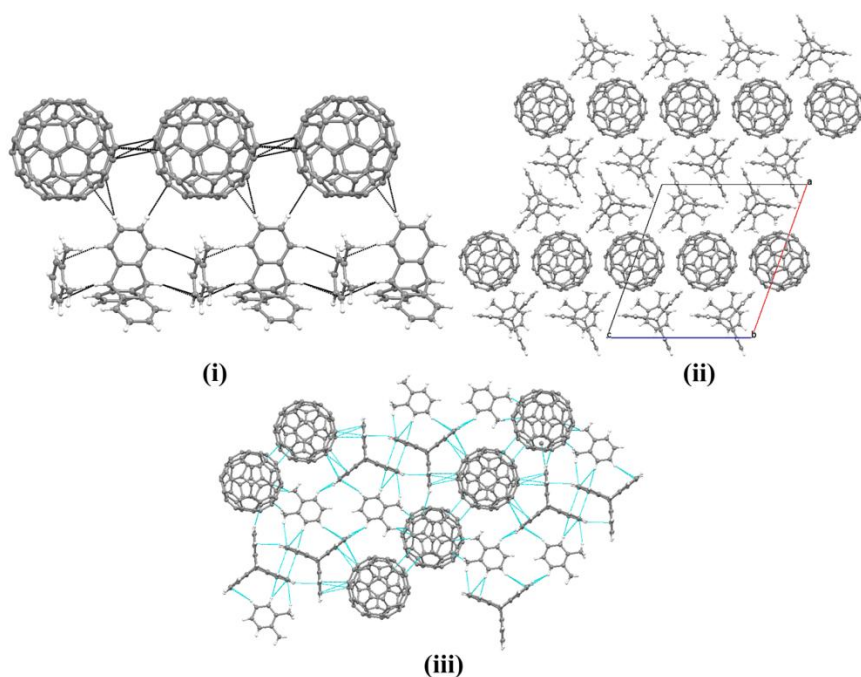


Figure 6.20. Chains and sheets C_{60} -TripH-*o*-xylene sheets in CEMNUD, Compare with TripH-FcH chains (see **Figure 6.4**) and FcC_2C_2Fc -TripH sheets (see **Figure 6.9**)

2D ($^{13}C/^1H$ HSQC) NMR studies in solution phase

However, the role of the solvent is more important for non-covalent assemblies than the covalent molecules. The balance between enthalpy and entropy is close in these aggregates. Small perturbations from solvation would, therefore, be expected to be much more important for them than for covalent compound.[63]

An advanced 2D heteronuclear single quantum correlation ($^{13}C/^1H$ HSQC) NMR characterization technique was used to find out the interaction present between ferrocene-triptycene adduct. Through this technique, the correlation between the π bond on ferrocene ring and hydrogen present on triptycene (benzene ring) could be observed. The chemical shift values did not change (**Table 6.1** and **Figure 6.21**), which indicates the interaction was not prevailed in the solution phase and get disturbed due to the incorporation of the solvent molecules in between the C_{sp^3} -H--- π interaction.

Table 6.1. $^{13}\text{C}/^1\text{H}$ NMR chemical shift values in solution phase of **1**

Entry No.	Assigned $^{13}\text{C}/^1\text{H}$	Triptycene $^{13}\text{C}/^1\text{H}$ (ppm)	Ferrocene $^{13}\text{C}/^1\text{H}$ (ppm)	Adduct $^{13}\text{C}/^1\text{H}$ (ppm)	$\Delta\delta = ^{13}\text{C}/^1\text{H}$ (ppm)
1	C_a/H_a	52.37/5.63	-	52.28/5.64	0.09/0.01
2	C_b/H_b	124.68/6.98	-	124.59/6.99	0.09/0.01
3	C_c/H_c	124.67/7.43	-	124.59/7.44	0.08/0.01
4	C_d/H_d	-	67.37/4.17	67.37/4.19	0/0.02

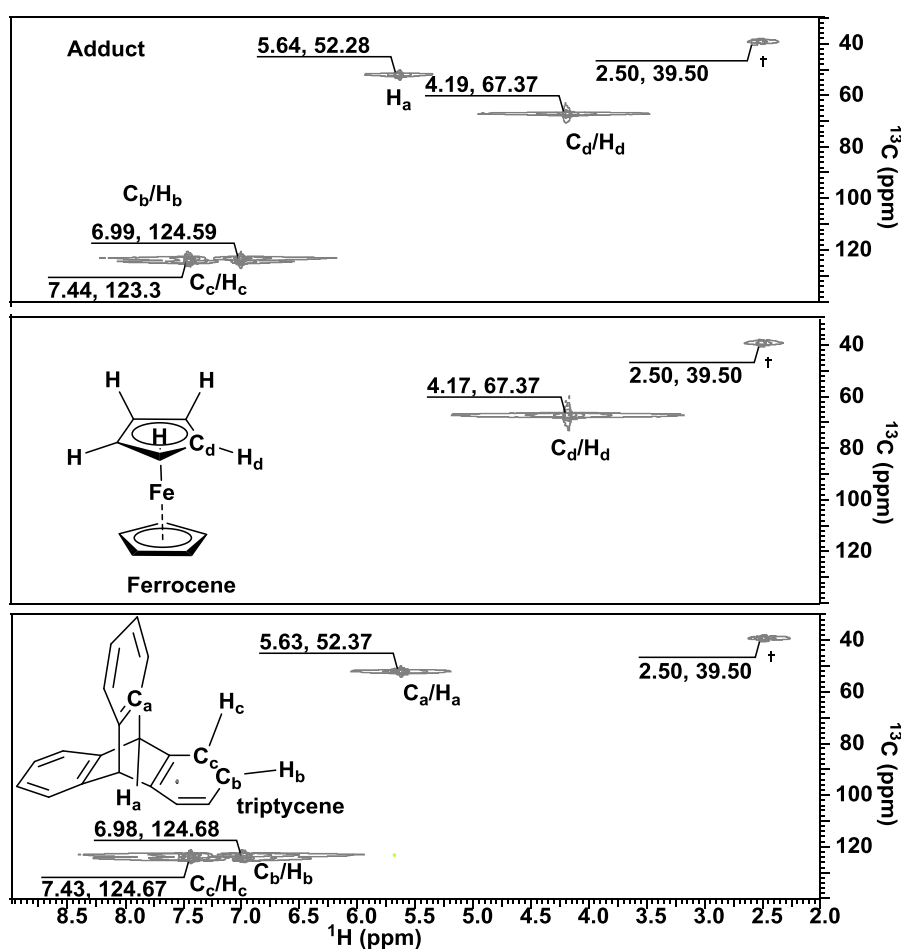


Figure 6.21. 2D HSQC NMR spectra of (a) triptycene, (b) ferrocene and (c) adduct triptycene-ferrocene. † signals indicate for the DMSO-d_6 solvent. All the spectra were recorded after dissolving ca. 1.0 mol samples in 0.7 mL deuterated DMSO solvent.

6.3 Conclusion

This report focuses on the structure of the triptycene-ferrocene derived cocrystals, featuring interplay between specific intermolecular $C_{sp^3}\text{-H}\cdots\pi_{cp}$ hydrogen bonding and close-packing requirements, providing a suitable model in an attempt to get a glance on early stages of crystallization. For the predominantly kinetic control of nucleation,[64] we can suppose that it starts when TripH and FcR molecules recognize each other via $C_{sp^3}\text{-H}\cdots\pi_{cp}$ hydrogen bonding interaction, so that the primary $C\text{-H}\cdots\pi_{cp}$ synthons assemble FcH---Trip molecules into the kinetically defined chain-like 1D oligomers. Further, they are packed in a parallel manner and stabilized by $C\text{-H}\cdots\pi_{ph}$ HBs which fit the geometry requirements (i.e. provides multiple hydrogen bonding), resulting in the balanced chain-sheets 3D structure. In some cases (Fc_2), when the close 3D packing of such chain oligomers could not be achieved, they form 2D ribbons, which are further packed closely by T-shaped secondary $C\text{-H}\cdots\pi_{ph}$ interaction and reproducing the geometry of top-ranking TripH---TripH interaction observed in the natural TripH crystal. Boldly expanding the genetics vocabulary use for crystal design, in addition to genotype/phenotype,[1] we can draw here the analogy with the dormant genes, which wake up at a particular condition, *i.e.* when the energy of a given intermolecular interaction in the cocrystal does not provide any considerable benefit in overall lattice energy as compared to the starting crystals.[65]

6.4 Experimental

TripH, FcH and its derivative were purchased from Sigma-Aldrich and were used without additional purification. PCP-Fc and Fc-C≡C-C≡C-Fc were prepared using C-C Suzuki coupling literature method. $(C_{10}H_9)_2Fe_2$ or DiFc (Fc_2) is prepared by using n-butyl lithium (dangerous chemical, please handle with care) and FcH reaction in a mixture of dried hexane and dried THF and oxidizing it with oxygen carefully. HPLC grade hexane, chloroform, and DCM were used without additional purification. Crystals were grown with the minor variation in the solvent according to the solubility of the molecules **1–5**.

6.4.1 Preparation of FcH/TripH (1)

37.2 mg (~0.2 mmol) of FcH and 51 mg (~0.2 mmol) of TripH were dissolved in a mixture of 1 mL of hexane and 1 mL of chloroform in a 2.5 mL tube under modest heating to ensure complete solubility of the starting materials. Then sonication was done for 5 min. The clear solution was covered using parafilm, and then left at room temperature for 24 h producing **1** as long orange crystals. Crystals were separated, and less un-crystallized white coloured TripH was removed manually, the crystals were not washed and using paraffin oil XRD measurement was performed, and other physical measurements have been carried out without additional purification. Yield: 79 mg (~90%)

6.4.2 Preparation of Cp_2FeCHO / TripH (2)

42.8 mg (~0.2 mmol) of Fc-carboxaldehyde (FcCHO) and 51 mg (~0.2 mmol) of TripH were dissolved in 1 mL of hexane and 1 mL of chloroform in a 2.5 mL tube under modest heating to ensure complete solubility of the starting materials. Then sonication was done for 5 min. The clear solution was covered with parafilm and then left at room temperature for 2 days producing **2** as dark red crystals. Crystals were separated, SC-XRD was done. Yield: 47 mg (50%)

6.4.3 Preparation of CpFeC₅H₄-C≡C-C≡C-C₅H₄FeCp/ TripH (3)

4.2 mg (~0.01 mmol) of Fc-C₂-C₂-Fc and 5.0 mg (~0.02 mmol) of TripH were dissolved in 0.5 ml of chloroform in a 1mL eppendorf and shake well to ensure complete solubility of the starting materials. The obtained orange solution was left at room temperature for two days in a closed eppendorf. Good quality orange crystalline molecules were separated and used for X-ray diffraction measurement without additional purification. Yield: 6 mg (65%)

6.4.4 Preparation of PCP-C≡C- Cp₂Fe/TripH (4)

8.3 mg (~0.02 mmol) of PCP-C≡C- Cp₂Fe and 5.1 mg (~0.02 mmol) of TripH were dissolved in 0.5 mL of hexane and 0.5 mL of chloroform in a 2.5 mL tube under average heating to ensure complete solubility of the starting materials. Then sonication was done for 5 min. The obtained clear solution was closed with a lid with one small hole and then left at room temperature for two days giving **4** as orange crystals. Crystals were separated, SC-XRD measurement was carried out. Yield: 8 mg (~60%)

6.4.5 Preparation of CpFeC₅H₄-C₅H₄FeCp/ TripH (5)

3.7mg (~0.01mmol) of diFc and 2.5 mg (~0.01mmol) of TripH were dissolved in 0.5ml of chloroform in a 1mL eppendorf and shake well to ensure complete mixing and solubility of the starting materials. The orange solution produced, was left at room temperature for two days with one pin hole on eppendorf. Orange crystalline molecules (**5**) were separated, followed by washing with 0.5 mL of cold hexane quickly and used for X-ray measurement without purification. Yield: 3 mg (~48%)

6.4.6 Computations

Intermolecular interactions energy and energy frameworks were calculated in CrystalExplorer 17.5 [TONTO, HF/3-21G, B3LYP/6-31G(d,p)][48,62] for all unique molecular pairs in the first

coordination sphere of a molecule ($\sim 3.8 \text{ \AA}$), using experimental crystal geometries. For the cocrystals, the above procedure has been performed for each conformer molecule centred cluster.[49]

6.4.7 Electrical conductivity measurements

The electrical conductivity was studied on a Z2000 impedance meter (LTD “Elins”) (operating frequencies range; 2 MHz–1 Hz) using C/solid electrolyte/C symmetrical cells. The external alternating signal amplitude has been 50–70 mV which depends on the impedance of the sample without any direct current polarization. The resistance frequency dependence has been analyzed by the graphical-analytical method. The samples have been prepared by pressing (10 atm) which produced the pellets of 0.7–1.2 mm thickness and 5 mm diameter and placed in the cells with nitrogen-atmosphere.

6.4.8 Crystal structure determination

Data were collected at 293 K using graphite-monochromated MoK α radiation ($\lambda = 0.71070 \text{ \AA}$) and CuK α radiation ($\lambda = 1.54184 \text{ \AA}$). The data collection strategy was interpreted by employing the CrysAlisPro software for **1–5**. The data has been collected through the standard omega scan technique and reduced by the SHELXL-97 software. Structures were solved by direct methods and refinement was carried out by full-matrix least squares against F^2 utilizing the SHELXL-97 software.[66] Non-hydrogen atoms have been refined with anisotropic thermal parameters. All hydrogen atoms have been geometrically fixed, and a riding model refinement is carried out. Olex2 software[67] was also used for labelling and refining of **1–5**.

Table 6.2. Crystal data and structure refinement for **1–3**

Identification code	1	2	3
Empirical formula	C ₃₀ H ₂₄ Fe	C ₃₁ H ₂₄ FeO	C ₆₄ H ₄₆ Fe ₂
Formula weight	440.34	468.35	926.71
Temperature/K	293(2)	293(2)	298

Crystal system	triclinic	triclinic	triclinic
Space group	<i>P</i> -1	<i>P</i> -1	<i>P</i> -1
a/Å	9.4217(5)	9.6767(12)	13.3320(15)
b/Å	10.3198(6)	10.3972(12)	13.4018(12)
c/Å	13.0913(6)	12.9455(15)	16.138(2)
α/°	67.835(5)	70.641(10)	95.029(9)
β/°	71.685(5)	71.847(11)	105.145(11)
γ/°	86.556(5)	89.794(10)	119.521(10)
Volume/Å³	1116.62(11)	1160.4(3)	2340.2(5)
Z	2	2	2
ρ_{calc}/cm³	1.31	1.34	1.315
μ/mm⁻¹	0.69	0.671	0.662
F(000)	460	488	964
Crystal size/mm³	0.45 × 0.38 × 0.30	0.40 × 0.36 × 0.33	0.34 × 0.32 × 0.28
Radiation	MoKα (λ = 0.71073)	MoKα (λ = 0.71073)	MoKα (λ = 0.71073)
2θ range for data collection/°	6.042 to 49.998	6.342 to 49.994	6.07 to 50
Index ranges	-8 ≤ h ≤ 11, -12 ≤ k ≤ 12, -15 ≤ l ≤ 15	-11 ≤ h ≤ 11, -12 ≤ k ≤ 12, -13 ≤ l ≤ 15	-15 ≤ h ≤ 15, -15 ≤ k ≤ 15, -19 ≤ l ≤ 19
Reflections collected	8587	9530	21024
Independent reflections	3924 [R _{int} = 0.0309, R _{sigma} = 0.0332]	4067 [R _{int} = 0.0898, R _{sigma} = 0.1012]	8192 [R _{int} = 0.1238, R _{sigma} = 0.1770]
Data/restraints/parameters	3924/0/280	4067/0/298	8192/0/595
Goodness-of-fit on F²	1.042	1.056	1.019
Final R indexes [I ≥ 2σ (I)]	R1 = 0.0447, wR2 = 0.1158	R1 = 0.1096, wR2 = 0.2850	R1 = 0.0915, wR2 = 0.1997
Final R indexes [all data]	R1 = 0.0496, wR2 = 0.1197	R1 = 0.1399, wR2 = 0.3190	R1 = 0.2107, wR2 = 0.2753
Largest diff. peak/hole / e Å⁻³	0.31/-0.36	1.37/-0.59	0.73/-0.38
CCDC No.	1586854	1586855	1839843

Table 6.3. Crystal data and structure refinement for **4–5**

Identification code	4	5
Empirical formula	C ₄₈ H ₃₈ Fe	C ₆₀ H ₄₆ Fe ₂

Formula weight	670.63	878.67
Temperature/K	293(2)	293(2)
Crystal system	monoclinic	monoclinic
Space group	<i>P2₁/c</i>	<i>P2₁/n</i>
a/Å	7.9500(4)	8.93360(10)
b/Å	28.507(2)	8.41050(10)
c/Å	15.5007(8)	28.5683(4)
α/°	90	90
β/°	104.262(5)	93.5820(10)
γ/°	90	90
Volume/Å³	3404.6(4)	2142.31(5)
Z	4	2
ρ_{calc}/cm³	1.308	1.362
μ/mm-1	3.8	5.734
F(000)	1408	916
Crystal size/mm³	0.4 × 0.34 × 0.33	0.38 × 0.33 × 0.28
Radiation	CuKα (λ = 1.54184)	CuKα (λ = 1.54184)
2θ range for data collection/°	11.018 to 144.248	6.2 to 142.574
Index ranges	-7 ≤ h ≤ 9, -34 ≤ k ≤ 34, -19 ≤ l ≤ 18	-10 ≤ h ≤ 10, -10 ≤ k ≤ 7, -35 ≤ l ≤ 33
Reflections collected	23737	13762
Independent reflections	6536 [Rint = 0.0946, Rsigma = 0.0811]	4112 [Rint = 0.0347, Rsigma = 0.0245]
Data/restraints/parameters	6536/0/442	4112/0/280
Goodness-of-fit on F²	1.027	1.044
Final R indexes [I ≥ 2σ (I)]	R1 = 0.1157, wR2 = 0.3069	R1 = 0.0438, wR2 = 0.1288
Final R indexes [all data]	R1 = 0.1746, wR2 = 0.3606	R1 = 0.0497, wR2 = 0.1398
Largest diff. peak/hole / e Å⁻³	1.03/-0.59	0.35/-0.54
CCDC No.	1586856	1586857

6.5 References

- [1] Mukherjee A. (2015), Building upon Supramolecular Synthons: Some Aspects of Crystal Engineering. *Cryst. Growth Des.*, 15(6), 3076-3085 doi:10.1021/acs.cgd.5b00242
- [2] Dunitz J. D. (2015), Intermolecular atom -- atom bonds in crystals? *IUCrJ*, 2(2), 157--158 doi:10.1107/S2052252515002006
- [3] Tejender S. Thakur R. D., Gautam R. Desiraju. (2015), Intermolecular atom -- atom bonds in crystals -- a chemical perspective. *IUCrJ*, 2(2), 159--160 doi:10.1107/S205225251500189X
- [4] Claude Lecomte E. E., Cherif F. Matta. (2015), On atom -- atom 'short contact' bonding interactions in crystals. *IUCrJ*, 2(2), 161--163 doi:10.1107/S2052252515002067
- [5] W. Fabiola Sanjuan-Szklarz A. A. H., Matthias Gutmann, Anders Østergaard Madsen and Krzysztof Woźniak. (2016), Yes, one can obtain better quality structures from routine X-ray data collection. *IUCrJ*, 3(1), 61--70 doi:10.1107/S2052252515020941
- [6] Gautam R. D. Supramolecular Synthons in Crystal Engineering—A New Organic Synthesis. *Angew. Chem. Int. Ed. Engl.*, 34(21), 2311-2327 doi:10.1002/anie.199523111
- [7] Dunitz J. D., Gavezzotti A. (2012), Supramolecular Synthons: Validation and Ranking of Intermolecular Interaction Energies. *Cryst. Growth Des.*, 12(12), 5873-5877 doi:10.1021/cg301293r
- [8] Saini A. K., Kumari P., Sharma V., Mathur P., Mobin S. M. (2016), Varying structural motifs in the salen based metal complexes of Co(ii), Ni(ii) and Cu(ii): synthesis, crystal

- structures, molecular dynamics and biological activities. *Dalton Trans.*, 45(47), 19096-19108 doi:10.1039/C6DT03573F
- [9] Desiraju G. R. (2013), Crystal Engineering: From Molecule to Crystal. *J. Am. Chem. Soc.*, 135(27), 9952-9967 doi:10.1021/ja403264c
- [10] Sakamoto R., Hoshiko K., Liu Q., Yagi T., Nagayama T., Kusaka S., . . . Nishihara H. (2015), A photofunctional bottom-up bis(dipyrinato)zinc(II) complex nanosheet. *Nat. Commun.*, 6, 6713 doi:10.1038/ncomms7713
- [11] Bauer T., Zheng Z., Renn A., Enning R., Stemmer A., Sakamoto J., Schlüter A. D. (2011), Synthesis of Free-Standing, Monolayered Organometallic Sheets at the Air/Water Interface. *Angew. Chem. Int. Ed.*, 50(34), 7879-7884 doi:10.1002/anie.201100669
- [12] Ciesielski A., Cadeddu A., Palma C.-A., Gorczynski A., Patroniak V., Cecchini M., Samori P. (2011), Self-templating 2D supramolecular networks: a new avenue to reach control over a bilayer formation. *Nanoscale*, 3(10), 4125-4129 doi:10.1039/C1NR10485C
- [13] Konarev D. V., Kuzmin A. V., Khasanov S. S., Batov M. S., Otsuka A., Yamochi H., . . . Lyubovskaya R. N. (2018), Salts with titanyl and vanadyl phthalocyanine radical anions. Molecular design and effect of cations on the structure and magnetic and optical properties. *CrystEngComm*, 20(4), 385-401 doi:10.1039/C7CE01918A
- [14] Novoselov K. S., Geim A. K., Morozov S. V., Jiang D., Katsnelson M. I., Grigorieva I. V., . . . Firsov A. A. (2005), Two-dimensional gas of massless Dirac fermions in graphene. *Nature*, 438, 197 doi:10.1038/nature04233

- [15] Williams J. R., DiCarlo L., Marcus C. M. (2007), Quantum Hall effect in a gate-controlled p-n junction of graphene. *Science*, 317(5838), 638-641 doi:10.1126/science.1144657
- [16] Wang F., Zhang Y., Tian C., Girit C., Zettl A., Crommie M., Shen Y. R. (2008), Gate-Variable Optical Transitions in Graphene. *Science*, 320(5873), 206-209 doi:10.1126/science.1152793
- [17] Chen C.-F. (2011), Novel triptycene-derived hosts: synthesis and their applications in supramolecular chemistry. *Chem. Commun.*, 47(6), 1674-1688 doi:10.1039/C0CC04852F
- [18] Kelly T. R. (2001), Progress toward a Rationally Designed Molecular Motor. *Acc. Chem. Res.*, 34(6), 514-522 doi:10.1021/ar000167x
- [19] Swager T. M. (2008), Iptycenes in the Design of High Performance Polymers. *Acc. Chem. Res.*, 41(9), 1181-1189 doi:10.1021/ar800107v
- [20] Tsui N. T., Paraskos A. J., Torun L., Swager T. M., Thomas E. L. (2006), Minimization of Internal Molecular Free Volume: A Mechanism for the Simultaneous Enhancement of Polymer Stiffness, Strength, and Ductility. *Macromolecules*, 39(9), 3350-3358 doi:10.1021/ma060047q
- [21] van Reenen A. J., Mathias L. J., Coetzee L. (2004), Polymerization of olefins with bulky substituents. 1. Homo- and copolymerization of 3-(1-adamantyl)propene. *Polymer*, 45(3), 799-804 doi:10.1016/j.polymer.2003.12.005
- [22] Peng L., Feng A., Huo M., Yuan J. (2014), Ferrocene-based supramolecular structures and their applications in electrochemical responsive systems. *Chem. Commun.*, 50(86), 13005-13014 doi:10.1039/C4CC05192K

- [23] Atencio R., Domasevitch K. V., Zaworotko M. J. (2000), Structural Conformation and Optical and Electrochemical Properties of Imidazolyl-Substituted Naphthalenediimide and Its HgII, CdII, and CuII Halide Complexes. *Cryst. Eng.*, 2000(3), 63 doi:10.5517/cc4rph1
- [24] Day M. W. M., A.J. Grubbs, R.H. (2002), CCDC 130854: Experimental Crystal Structure Determination. *CSD Communication* doi:10.5517/cc4d53s
- [25] Clyburne J. A. C., Hamilton, T., & Jenkins, H. A. (2001), *Acta Crystallogr., Sect. C: Cryst. Struct. Commun.*, 4, 1 doi:10.5517/cc57gqk
- [26] Batsanov A. S., Collings J. C., Marder T. B. (2006), *Acta Cryst. C*, 62, m229-m231
- [27] Olmstead M. M., Hao L., Balch A. L. (1999), Organometallic C70 chemistry. Preparation and crystallographic studies of $(\eta^2\text{-C}_{70})\text{Pd}(\text{PPh}_3)_2 \cdot \text{CH}_2\text{Cl}_2$ and $(\text{C}_{70}) \cdot 2\{(\eta^5\text{-C}_5\text{H}_5)_2\text{Fe}\}$. *J. Organomet. Chem.*, 578(1), 85-90 doi:10.1016/S0022-328X(98)01108-5
- [28] Crane J. D., Hitchcock P. B., Kroto H. W., Taylor R., Walton D. R. M. (1992), Preparation and characterisation of $\text{C}_{60}(\text{ferrocene})_2$. *J. Chem. Soc., Chem. Commun.*(24), 1764-1765 doi:10.1039/C39920001764
- [29] Tikhonova I. A., Dolgushin F. M., Tugashov K. I., Petrovskii P. V., Antipin M. Y., Shur V. B. (2004), Binding of ferrocene by cyclic trimeric perfluoro-o-phenylenemercury. Synthesis and structure of the first double-decker sandwich complex of a sandwich. *Russ. Chem. Bull.*, 53(12), 2871-2873 doi:10.1007/s11172-005-0205-8
- [30] Tsupreva V. N., Titov A. A., Filippov O. A., Bilyachenko A. N., Smol'yakov A. F., Dolgushin F. M., . . . Shubina E. S.

- (2011), Peculiarities of the Complexation of Copper and Silver Adducts of a 3,5-Bis(trifluoromethyl)pyrazolate Ligand with Organoiron Compounds. *Inorg. Chem.*, 50(8), 3325-3331 doi:10.1021/ic102132v
- [31] MacGillivray L. R., Spinney H. A., Reid J. L., Ripmeester J. A. (2000), Entrapment of ferrocenes within supramolecular, deep-cavity resorcin[4]arenes. *Chem. Commun.*(6), 517-518 doi:10.1039/A909745G
- [32] Wang Y.-J., Liu J.-L., Yang H.-M., Jia A.-Q., Zhang Q.-F. (2016), Inclusion of ferrocene within the deepened cavities formed from the hydrogen bonding self-assembly of calix[4]resorcinarenes with bis-pyridines. *J. Inclusion Phenom. Macrocyclic Chem.*, 85(1), 105-110 doi:10.1007/s10847-016-0609-0
- [33] Hardie M. J. (2002), Solid State Confinement of Ferrocene by Calixarenes. *Supramol. Chem.*, 14(1), 7-10 doi:10.1080/10610270290006529
- [34] Frišćić T., MacGillivray L. R. (2003), Double inclusion of ferrocene within a doubly interpenetrated three-dimensional framework based on a resorcin[4]arene. *J. Organomet. Chem.*, 666(1), 43-48 doi:10.1016/S0022-328X(02)02031-4
- [35] Mossine A. V., Kumari H., Fowler D. A., Shih A., Kline S. R., Barnes C. L., Atwood J. L. (2012), Ferrocene Species Included within a Pyrogallol[4]arene Tube. *Chem. - Eur. J.*, 18(33), 10258-10260 doi:10.1002/chem.201200263
- [36] Mossine A. V., Kumari H., Fowler D. A., Maerz A. K., Kline S. R., Barnes C. L., Atwood J. L. (2011), Ferrocene as a Hydrophobic Templating Agent with Pyrogallol[4]arenes. *Isr. J. Chem.*, 51(7), 840-842 doi:10.1002/ijch.201100068

- [37] Odagaki Y., Hirotsu K., Higuchi T., Harada A., Takahashi S. (1990), X-Ray structure of the α -cyclodextrin-ferrocene (2 : 1) inclusion compound. *J. Chem. Soc., Perkin Trans. 1*(4), 1230-1231 doi:10.1039/P19900001230
- [38] Liu Y., Zhong R.-Q., Zhang H.-Y., Song H.-B. (2005), A unique tetramer of 4 : 5 β -cyclodextrin-ferrocene in the solid state. *Chem. Commun.*(17), 2211-2213 doi:10.1039/B418220K
- [39] Jeon W. S., Moon K., Park S. H., Chun H., Ko Y. H., Lee J. Y., . . . Kim K. (2005), Complexation of Ferrocene Derivatives by the Cucurbit[7]uril Host: A Comparative Study of the Cucurbituril and Cyclodextrin Host Families. *J. Am. Chem. Soc.*, 127(37), 12984-12989 doi:10.1021/ja052912c
- [40] Adman E., Rosenblum M., Sullivan S., Margulis T. N. (1967), Structure of the ferrocene-tetracyanoethylene complex. *J. Am. Chem. Soc.*, 89(17), 4540-4542 doi:10.1021/ja00993a062
- [41] Hough E., Nicholson D. G. (1978), X-Ray crystallographic studies on ferrocene included in a thiourea host lattice. *J. Chem. Soc., Dalton Trans.*(1), 15-18 doi:10.1039/DT9780000015
- [42] Wei W., Wang G., Zhang Y., Jiang F., Wu M., Hong M. (2011), A Versatile Tripodal Host with Cylindrical Conformation: Solvatomorphism, Inclusion Behavior, and Separation of Guests. *Chem. - Eur. J.*, 17(7), 2189-2198 doi:10.1002/chem.201002246
- [43] Jiang J.-J., Yan C., Pan M., Wang Z., Deng H.-Y., He J.-R., . . . Su C.-Y. (2012), Structural Conformation and Optical and Electrochemical Properties of Imidazolyl-Substituted Naphthalenediimide and Its HgII, CdII, and CuII Halide Complexes. *Eur. J. Inorg. Chem.*, 2012(8), 1171-1179 doi:10.1002/ejic.201101181

- [44] Mendoza S., Davidov P. D., Kaifer A. E. (1998), Electrochemistry of Encapsulated Guests: Ferrocene inside Cram's Hemicarcerands. *Chem. - Eur. J.*, 4(5), 864-870 doi:10.1002/(SICI)1521-3765(19980515)4:5<864::AID-CHEM864>3.0.CO;2-W
- [45] Torubaev Y. V., Lyssenko K. A., Barzilovich P. Y., Saratov G. A., Shaikh M. M., Singh A., Mathur P. (2017), Self-assembly of conducting cocrystals via iodine $\cdots\pi$ (Cp) interactions. *CrystEngComm*, 19(34), 5114-5121 doi:10.1039/C7CE00857K
- [46] Miyamoto Y., Takamizawa S. (2015), Deformation twinning of ferrocene crystals assisted by the rotational mobility of cyclopentadienyl rings. *Dalton Trans.*, 44(12), 5688-5691 doi:10.1039/C4DT03922J
- [47] Clement R., Claude R., Mazieres C. (1974), Clathration of ferrocene and nickelocene in a thiourea host lattice. *J. Chem. Soc., Chem. Commun.*(16), 654-655 doi:10.1039/C39740000654
- [48] Aakeroy C. B., Salmon D. J. (2005), Building co-crystals with molecular sense and supramolecular sensibility. *CrystEngComm*, 7(72), 439-448 doi:10.1039/B505883J
- [49] Aakeröy Christer B., Desper J., Elisabeth E., Helfrich Brian A., Levin B., Urbina Joaquin F. (2005). Making reversible synthesis stick: competition and cooperation between intermolecular interactions. In *Zeitschrift für Kristallographie - Crystalline Materials* (Vol. 220, pp. 325).
- [50] Shishkin O. V., Medvediev V. V., Zubatyuk R. I. (2013), Supramolecular architecture of molecular crystals possessing shearing mechanical properties: columns versus layers. *CrystEngComm*, 15(1), 160-167 doi:10.1039/C2CE26126J

- [51] Turner M. J., McKinnon D. J. J., Wolff S. K., Grimwood D. J., Spackman P. R., Jayatilaka D., Spackman M. A. (CrystalExplorer17 (2017)), CrystalExplorer17.
- [52] Turner M. J., Thomas S. P., Shi M. W., Jayatilaka D., Spackman M. A. (2015), Front cover. *Chem. Commun.*, 51(18), 3691-3691 doi:10.1039/C5CC90086G
- [53] Shi M. W., Thomas S. P., Koutsantonis G. A., Spackman M. A. (2015), Supramolecular Recognition and Energy Frameworks in Host–Guest Complexes of 18-Crown-6 and Sulfonamides. *Cryst. Growth Des.*, 15(12), 5892-5900 doi:10.1021/acs.cgd.5b01316
- [54] Dey D., Bhandary S., Thomas S. P., Spackman M. A., Chopra D. (2016), Energy frameworks and a topological analysis of the supramolecular features in in situ cryocrystallized liquids: tuning the weak interaction landscape via fluorination. *PCCP*, 18(46), 31811-31820 doi:10.1039/C6CP05917A
- [55] Jha K. K., Dutta S., Kumar V., Munshi P. (2016), Isostructural polymorphs: qualitative insights from energy frameworks. *CrystEngComm*, 18(43), 8497-8505 doi:10.1039/C6CE01501H
- [56] Thomas Sajesh P., Shi Ming W., Koutsantonis George A., Jayatilaka D., Edwards Alison J., Spackman Mark A. (2017), The Elusive Structural Origin of Plastic Bending in Dimethyl Sulfone Crystals with Quasi-isotropic Crystal Packing. *Angew. Chem. Int. Ed.*, 56(29), 8468-8472 doi:10.1002/anie.201701972
- [57] Thomas Sajesh P., Shi Ming W., Jayatilaka D., Spackman Mark A. (2017), Quantitative approaches to crystal engineering: applications to mechanical properties. *Acta Crystallographica Section A*, 73(a2), C849 doi:10.1107/S2053273317087253

- [58] Wang C., Paul S., Wang K., Hu S., Sun C. C. (2017), Relationships among Crystal Structures, Mechanical Properties, and Tableting Performance Probed Using Four Salts of Diphenhydramine. *Cryst. Growth Des.*, 17(11), 6030-6040 doi:10.1021/acs.cgd.7b01153
- [59] Wang C., Sun C. C. (2018), Identifying Slip Planes in Organic Polymorphs by Combined Energy Framework Calculations and Topology Analysis. *Cryst. Growth Des.*, 18(3), 1909-1916 doi:10.1021/acs.cgd.8b00202
- [60] Bruce M. I., Head N. J., Skelton B. W., Spackman M. A., White A. H. (2018), Tetraiodoallene, $I_2C=C=CI_2$ – the missing link between $I_2C=CI_2$ and $I_2C=C=C=CI_2$ – and the oxidation product, 2,2-diiodoacrylic acid, $I_2C=CH(CO_2H)$. *Aust. J. Chem.*, 71(1), 70-73 doi:10.1071/CH17348
- [61] Marc Veen E., L. Feringa B., M. Postma P., T. Jonkman H., L. Spek A. (1999), Solid state organisation of C60 by inclusion crystallisation with triptycenes. *Chem. Commun.*(17), 1709-1710 doi:10.1039/A904457D
- [62] Campbell F Mackenzie ., Peter R. Spackman , Dylan Jayatilakaa , Spackman M. A. (2017), \it CrystalExplorer model energies and energy frameworks: extension to metal coordination compounds, organic salts, solvates and open-shell systems. *IUCrJ*, 4(5), 575-587 doi:10.1107/S205225251700848X
- [63] Whitesides G. M., Simanek E. E., Mathias J. P., Seto C. T., Chin D., Mammen M., Gordon D. M. (1995), Noncovalent Synthesis: Using Physical-Organic Chemistry To Make Aggregates. *Acc. Chem. Res.*, 28(1), 37-44 doi:10.1021/ar00049a006
- [64] Gavezzotti A. (1994), Are Crystal Structures Predictable? *Acc. Chem. Res.*, 27(10), 309-314 doi:10.1021/ar00046a004

- [65] Taylor C. R., Day G. M. (2018), Evaluating the Energetic Driving Force for Cocrystal Formation. *Cryst. Growth Des.*, 18(2), 892-904 doi:10.1021/acs.cgd.7b01375
- [66] Sheldrick G. M. (2015), Crystal structure refinement with SHELXL. *Acta Crystallogr., Sect. C: Struct. Chem.*, 71(Pt 1), 3-8 doi:10.1107/S2053229614024218
- [67] Dolomanov O. V., Bourhis L. J., Gildea R. J., Howard J. A. K., Puschmann H. (2009), OLEX2: a complete structure solution, refinement and analysis program. *J. Appl. Crystallogr.*, 42(2), 339-341 doi:10.1107/S0021889808042726

Chapter 7

Conclusions and Scope for Future Work

My thesis work mainly focusses on the synthesis and applications of an important class of organometallic compounds derived from $\text{Ru}_3(\text{CO})_{12}$ and ferrocene derivatives. First, the syntheses of tri-nuclear ruthenium clusters containing either pyridine alcohol or pyridine carboxylic acid bidentate ligands have been performed. They have revealed the catalytic efficiency for N-alkylation reactions and oxidation of alcohol to the carboxylic acid, respectively.

Later tetranuclear ruthenium pyridine methanol cluster was also synthesized and utilized for the water oxidation reaction.

Ferrocene-substituted bis(ethynyl)anthracene/anthraquinone, has been synthesized by C-C Coupling reactions and they have been shown to display anticancer properties. Five new supra-molecular synthons were prepared which shows $\text{C}_{\text{sp}3}\text{-H}_{\text{cp}}\text{---}\pi$ and $\text{C}_{\text{sp}2}\text{-H}_{\text{cp}}\text{---}\pi$ interactions, and their interaction energies were calculated too.

Overall present thesis work has revealed cluster synthesis and ferrocene unsaturated systems for homogeneous catalysis showing the crucial role of bidentate simple ligands and evaluation of biological activity of some derivatives. This work also discussed the supramolecular chemistry of triptycene and ferrocene.

The findings can be utilized to create new N/O-, N/P-, N/N-ligand based $\text{Ru}_3(\text{CO})_{12}$ clusters and use them for organic transformations. This work also gives an idea to create new ferrocene-based drugs for many biological activities. At last, the supramolecular chemistry of substituted triptycene and reported ferrocene and its derivatives can be easily used to create new supramolecules and study their interactions, and by using the idea from interactions, properties like electrical conductivity, redox properties etc. can be tuned feasibly.

Appendix A

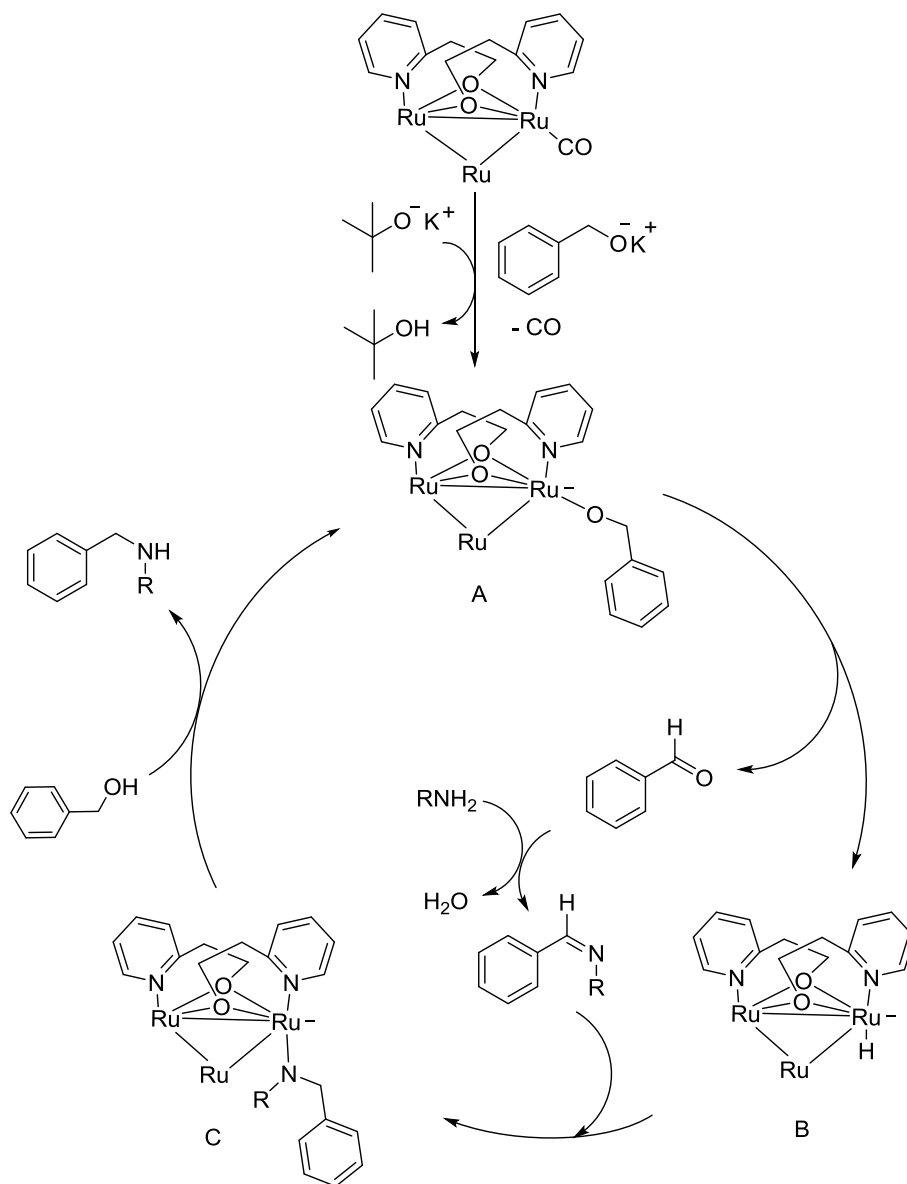


Figure 7.1. Proposed mechanism for the N-alkylation of primary amine to secondary amine using ruthenium cluster catalyst (Carbonyls are omitted for clarity).